1993

Strange bonding in a parallel world

Theresa Lynn Windus
Iowa State University

INFORMATION TO USERS

This manuscript has been reproduced from the microfilm master. UMI films the text directly from the original or copy submitted. Thus, some thesis and dissertation copies are in typewriter face, while others may be from any type of computer printer.

The quality of this reproduction is dependent upon the quality of the copy submitted. Broken or indistinct print, colored or poor quality illustrations and photographs, print bleedthrough, substandard margins, and improper alignment can adversely affect reproduction.

In the unlikely event that the author did not send UMI a complete manuscript and there are missing pages, these will be noted. Also, if unauthorized copyright material had to be removed, a note will indicate the deletion.

Oversize materials (e.g., maps, drawings, charts) are reproduced by sectioning the original, beginning at the upper left-hand corner and continuing from left to right in equal sections with small overlaps. Each original is also photographed in one exposure and is included in reduced form at the back of the book.

Photographs included in the original manuscript have been reproduced xerographically in this copy. Higher quality 6" x 9" black and white photographic prints are available for any photographs or illustrations appearing in this copy for an additional charge. Contact UMI directly to order.

U·M·I

University Microfilms International
A Bell & Howell Information Company
300 North Zeeb Road, Ann Arbor, MI 48106-1346 USA
313/761-4700 800/521-0600

Order Number 9414037

Strange bonding in a parallel world

Windus, Theresa Lynn, Ph.D.

Iowa State University, 1993

U·M·I
300 N. Zeeb Rd.
Ann Arbor, MI 48106

Strange bonding in a parallel world

by

Theresa Lynn Windus

A Dissertation Submitted to the

Graduate Faculty in Partial Fulfillment of the

Requirements for the Degree of

DOCTOR OF PHILOSOPHY

Department: Chemistry
Major: Physical Chemistry

Approved:

Members of the Committee:

Signature was redacted for privacy.

In Charge of Major Work

Signature was redacted for privacy.

For the Major Department

Signature was redacted for privacy.

Signature was redacted for privacy.

For the Graduate College

Iowa State University
Ames, Iowa

1993

DEDICATION

To my God, in the pursuit of wisdom.

"To know wisdom and instruction; to perceive the words of understanding;

To receive the instruction of wisdom, justice, and judgment, and equity;

To give wisdom to the simple, to the young man knowledge and discretion.

A wise man will hear, and will increase learning; and a man of understanding shall attain unto wise counsels;

To understand a proverb, and the interpretation; the words of the wise, and their dark sayings.

The fear of the Lord is the beginning of knowledge: but fools despise wisdom and instruction."

Proverbs 1:2-7

TABLE OF CONTENTS

LIST OF TABLES

PAPER 6

PAPER 7

PAPER 8

LIST OF FIGURES

ACKNOWLEDGEMENTS

There are so many people in my life that have contributed to the making of this thesis that it is hard to know where to begin. I suppose that means I should start at the beginning.

First, I would like to thank my Mom for her love and support. She taught me about hard work, optimism, and the importance of family. Thanks for getting me started on the right track. I would also like to acknowledge my brothers Randy and Warren. Even though I don't say it often enough, they have been very important in my life and I love them very much.

Next, I would like to thank all of the supportive teachers I have had throughout my elementary and secondary educations. Especially, I would like to thank Mrs. Thompson, who in second grade taught me the wonder and love of math; Mr. Strube, who in seventh grade taught me that curiosity is the key to learning; and to Dr. Leibelt, who in tenth grade fascinated me with physical science experiments.

I would also like to acknowledge all of the individual instruction and excellent support I received from the chemistry, math, and computer science divisions at Minot State University. There are so many wonderful teachers that I would surely miss any if I would try to name them all, so I would just like to thank two of them in particular. First, I

would like to thank Dr. Rand Rodewald for interesting me so much in chemistry that it became my primary major. Secondly, I would like to thank Dr. Dave Gano for his belief in my abilities.

Of course, no acknowledgement would be complete without thanking the major advisor. Thankfully, this is more than just lip service, since I have been lucky enough to have Dr. Mark Gordon for an advisor. Anyone who knows Mark knows how wonderful he is as a teacher and advisor. I can never do justice to the contributions he has made to my life and career. All I can do is hope that my career can be a testimony to all that he has done for me. Thanks so much!

I would also like to thank the members of Mark's research group. They have provided an enriching environment for learning and questioning. I have learned much from all of them. In particular, I would like to thank Dr. Mike Schmidt for ALL of his help and guidance. In many senses, Mike has been a second advisor to me and also a good friend.

Finally, I would like to thank my family. David, my wonderful and supportive husband, has been my rock. Without him, I would not have had the confidence (and probably the inclination) to pursue my education. Thanks for never doubting in me! I would also like to thank my children, Lacey, Amber, and Brandon, for keeping me grounded in reality. They have taught me that life really is a wonderful

trip, you just have to remember to look at it through the eyes of a child.

ABSTRACT

The doctoral research concentrates on novel bonding in several chemical systems and parallelization of ab initio codes. The specific chemical processes under consideration are the pseudorotation of pentacoordinated silicon anions of the form $SiH_nX_{5-n}^-$ where X = F or Cl and n=0-5, the pseudorotational potential energy surface of PH_4F, the π-bond strengths in $H_2X{=}YH_2$ where X = Ge or Sn and Y = C, Si, Ge, or Sn, and the geometries and proton affinities of a series of azaphosphatrane molecules of the form $ZP[NR(CH_2)_2]_3N$ where Z = unsubstituted, H^+, F^+, Cl^+, O, OH^+, NH, NH_2^+, CH_2, CH_3^+ and R = H, CH_3.

The azaphosphatrane studies are performed using the parallel version of the ab initio code GAMESS, showing that use of parallel codes allows theoreticians to produce results in a timely fashion and to facilitate communication and collaboration with experimentalists. The parallel research has produced parallel SCF (RHF, UHF, ROHF, and GVB) energies and gradients and new algorithms for the parallelization of SCF analytic hessians and GUGA MCSCF energies. The former is a small scale algorithm which sends different computational kernels to different subsets of processors. The latter includes a parallel transformation which requires no communication between processors and scales well when the

transformation and the diagonalization steps are the main bottlenecks for the MCSCF energy calculation.

INTRODUCTION

One of my interests during my graduate career has been the role of the S_N2 mechanism in organometallic compounds, specifically silicon containing compounds. This mechanism is particularly interesting because the transition state associated with carbon compounds turns out to be a stable minimum in the silicon compounds. Some of the questions we would like to answer are: "Why do silicon compounds form minima instead of transition states?", "What are the energetics of adding an anion to a neutral silicon molecule to obtain a pentacoordinated anion?", "How does energy transfer from the reaction coordinate into the molecule?", and "What type of products can be obtained from the reaction? (inversion or retention of stereochemistry)". To try and answer some of these questions, a systematic study of the pentacoordinated silicon anions was undertaken. The main focus has been to map out the different structures of these molecules (minima and maxima), to determine relative energies within a given system, and to determine the reaction paths between the isomers. Once these parts of the potential energy surface have been explored, some of the questions raised above can start to be answered.

One of my other interests is parallel processing. Parallel processing is the use of several (perhaps thousands!) of computers (or nodes) on one calculation. The

main idea is to be able to perform calculations that would otherwise not be possible or that would simply take an immense amount of time to be completed. As will be seen in this dissertation, parallel processing allows computational chemists to interact with experimentalists on a "realistic" time scale on relatively large problems.

Organization

This thesis has two main themes: novel bonding in several different chemical systems (Papers 1-6) and parallel processing (Papers 6-8). The first four papers deal with pentacoordinated bonding of silicon or phosphorus. Paper 5 deals with π-bonding of Ge and Sn with other Group IVA elements (C, Si, Ge, and Sn). Paper 6 briefly describes the method we use to parallelize the self-consistent field (SCF) calculations in GAMESS[1] (General Atomic and Molecular Structure System). Also in this paper is the application of the parallel processing to a system of azaphosphatrane bases which have unique transannular bonding. Paper 7 describes a small scale algorithm for the parallelization of analytic hessians. Paper 8 presents a parallel algorithm for GUGA MCSCF.

All of the papers in this thesis have been published in, have been submitted to, or will be submitted to peer review journals. In every paper except the first, I am the primary author. In the first paper, I performed all of the ab initio

calculations and was very involved in the interpretation of the data and the conclusions.

Each paper (or chapter) contains an introduction, results and discussion, and conclusion section. The general conclusions and the references for this general introduction follow the last paper. Since this is not an appropriate venue for a detailed description of ab initio methods, only a brief description of the methods used in the work will be presented here.

Theory

The ultimate goal of quantum chemistry is to solve the complete time-dependent Schrödinger equation[2]

$$-\frac{\hbar}{i}\frac{\partial\Psi(x,t)}{\partial t} = \mathrm{H}\Psi(x,t) \qquad 1$$

without any approximations. If this goal could be reached for any given molecular system, theoretically, we would have all of the information needed for that particular system. Usually, however, we are able to use the time-independent Schrödinger equation.[3]

$$\mathrm{H}\Psi(x) = E\Psi(x) \qquad 2$$

In practice, however, approximations must be made for all chemical systems except for the hydrogen atom.[4] In the

current work, one of the approximations made will be that relativistic effects are very small. However, this is something that must be taken into account when dealing with some (especially heavy atom) systems.

Another fundamental approximation is the Born-Oppenheimer approximation made for molecules.[5] This approximation assumes that the electrons move in a field of fixed nuclei. In general, this is a very good approximation since the nuclei are much heavier than the electrons and therefore, they move much slower than the electrons.

For multi-electron problems (in atoms or molecules), we are faced with trying to solve at least a three body problem. This does not have an exact solution so we generally make other approximations. The most common is the Hartree-Fock approximation. In this approximation, the Hamiltonian is replaced by an effective one-electron operator called the Fock operator (using the notation from Szabo and Ostlund[6])

$$f(i) = -\frac{1}{2}\nabla_i^2 - \sum_{A=1}^{M}\frac{Z_A}{r_{iA}} + v^{HF}(i) \qquad 3$$

where $v^{HF}(i)$ is the average potential experienced by electron i from the other electrons, ∇ is the Laplacian operator involving differentiation with respect to the electron coordinates, Z_A is the atomic number of nucleus A, and r_{iA} is the distance from the ith electron to nucleus A. The first

term on the right hand side of equation **3** represents the electronic kinetic energy and the second term represents the electron-nucleus attraction. The potential depends on the orbitals which are generally approximated by linear combinations of basis functions[7]:

$$\psi(i)=\sum_{\mu} C_{\mu i}\chi_{\mu} \qquad \textbf{4}$$

By making a guess at the initial orbitals, an iterative (self-consistent Hartree-Fock) method can be used to solve the eigenvalue problem

$$f(i)\psi(i)=\varepsilon_i\psi(i) \qquad \textbf{5}$$

This gives rise to the restricted Hartree-Fock (RHF)[8], unrestricted Hartree-Fock (UHF)[9], and restricted open-shell Hartree-Fock (ROHF)[10] methods.

Because Hartree-Fock wavefunctions do not account for the correlation of electrons and let the electrons come too close to one another, several methods have been developed to account for the correlation of electrons. One method that is used extensively in this dissertation is many body perturbation theory and specifically, the Moller-Plesset second order (MP2)[11] and fourth order (MP4)[12] methods.

In many chemical systems, especially those with biradical character, more than one electron configuration is important and it is necessary for the molecular wavefunction to reflect this. The multi-configurational self-consistent field (MCSCF) method,[13] which is a variational method for inclusion of electron correlation, is needed for these types of calculations. More concerning this method is described in Paper 8.

Other types of computational methods exist to account for electron correlation (such as coupled cluster[14] and density functional[15]), but those listed above are the ones used in this dissertation.

Another important aspect of this dissertation is the parallelization of ab initio computational codes, specifically the GAMESS code. The main concept of parallelization is to apply several central processing units (CPUs or commonly referred to as nodes) to perform a computational task.

Two main parallel hardware models are used: single-instruction multiple-data (SIMD) and multiple-instruction multiple-data (MIMD). The latter model is the one used in the current work. Another important aspect is whether there is shared memory between the nodes or if each node has its own local memory and must communicate through some sort of network. Since we have used the distributed memory model, we can run on both types of machines.

There are many ways to parallelize code: compiler directives, automated compilers, parallel languages (such as Linda), and portable codes (such as PVM and TCGMSG). We have chosen to use the TCGMSG code to perform the parallelization of GAMESS. This code was written by a chemist specifically for chemistry codes and therefore, has all of the features that are essential to the task.

More details of the methods used for parallelization are presented within the dissertation (Papers 6-9).

With this brief introduction, let the GAMESS begin!

PAPER 1: THEORETICAL STUDY OF PSEUDOROTATION OF PENTACOORDINATED SILICON ANIONS: THE PROTOTYPICAL SiH_5^-

Theoretical Study of Pseudorotation of Pentacoordinated Silicon Anions: The Prototypical SiH_5^-

Mark S. Gordon and Theresa L. Windus
Department of Chemistry
North Dakota State University
Fargo, North Dakota 58105

Larry W. Burggraf and Larry P. Davis
Directorate of Chemical and Atmospheric Sciences
Air Force Office of Scientific Research
Bolling AFB, Washington D.C. 20332

Reprinted with permission from
J. Am. Chem. Soc. **1990**, *112*, 7167-7171

ABSTRACT

Ab initio and semiempirical calculations are used to analyze the minimum energy path for the pseudorotation of SiH_5^-. Both AM1 and MP2/6-31++G(d,p) predict pseudorotation barriers of 2.4 kcal/mol. A decomposition of the projected vibrational frequencies along the path is used to assist in the interpretation of the process.

INTRODUCTION

Pentacoordinated silicon compounds preferentially bond in trigonal-bipyramidal (tbp) shapes rather than square-pyramidal (spy) or other geometries.[1] In the tbp geometry, the substituents can assume either one of the two axial positions or one of the three equatorial positions. Depending on the nature of the substituents, any or all of the possible permutations of the ligands may or may not be stable structures. For example, in the model compound SiX_4Y^-, two distinguishable isomers are predicted, one with Y axial and the other with Y equatorial. With a larger variety of substituents, there are a proportionately larger number of possible isomers of the pentacoordinated structure.

These stereoisomers of simple pentacoordinated silicon compounds are not experimentally separable at room temperature; rapid ligand exchange occurs between the axial and equatorial positions.[2] There has been a large body of work devoted to understanding these processes in the analogous pentacoordinated phosphorus compounds,[3-7] and studies of pentacoordinated silicon make use of this body of work as a base. Differences between the two systems will be strongly dictated by the more electropositive nature of the silicon atom as compared with phosphorus[8] and to the presence of a formal negative charge on silicon.

One possible mode for rapid ligand exchange is the process of pseudorotation. Strauss defines pseudorotation as an intramolecular motion of nuclei in a molecule in which conformers interchange to equivalent structures differing only by the number of the atoms.[9] In a broader sense, pseudorotation can also include the exchange of nonequivalent nuclei to produce a trigonal-bipyramidal stereoisomer of the original structure. Berry proposed a specific type of pseudorotation, now widely known as Berry pseudorotation, to explain fluxional behavior of phosphoranes.[10] This Berry pseudorotation process is now widely used to explain isomerization phenomena in 10-electron systems.[11] In this mechanism, shown in Figure 1, a single equatorial substituent (the pivot group) is held stationary, while the two axial ligands become equatorial and the two equatorial ligands become axial. At some intermediate point in the process, a square-pyramidal structure is formed with the four interconverting ligands forming basal positions in the pyramid and the pivot ligand occupying an apical position in the pyramid (see Figure 1). If all ligands are equivalent, the trigonal-bipyramidal structures have D_{3h} symmetry while the square-pyramidal structure has C_{4v} symmetry. In this case, the path joining the C_{4v} and D_{3h} structures will have C_{2v} symmetry. There are a number of other types of pseudorotations that are possible: see either Musher[12] or

Gillespie et al.[13] for discussion of all possible rearrangements of these systems.

The prototypical pentacoordinated silicon compound, SiH_5^-, anion has recently been observed in the gas phase.[14] A number of calculations have been done on this and related systems at both the semiempirical and ab initio levels of theory, as recently reviewed by Burggraf, Davis, and Gordon.[15] Predictions at all levels of theory confirm that the D_{3h} pentacoordinated trigonal-bipyramidal structure is a minimum on the potential surface and the C_{4v} tetragonal pyramid is higher in energy, but only a few studies have addressed the nature of the tetragonal structure as a transition state for Berry pseudorotation. Reed and Schleyer have done the most extensive characterization of the SiH_5^- system to date, showing that the tetragonal structure was indeed a transition state by a force constant analysis.[16] Wilhite and Spialter modeled systems of the type $SiH_{5-n}X_n^-$ (X more electronegative than H) in order to compare the energetics of various conformers of this series with regard to Berry pseudorotation. They concluded that Berry pseudorotation was more facile when the C_{4v} tetragonal-pyramid transition state had the more electropositive substituent in the apical position.[17] Deiters and Holmes have studied the Berry pseudorotation barriers in SiH_4X^- (X =

halogen) as part of a model explaining stereochemistry of nucleophilic attack on silicon compounds.[7]

Pentacoordinated species having structures which range from trigonal bipyramidal to square pyramidal along an expected generalized berry pseudorotational pathway have been found experimentally.[18] These observations lend some experimental credence to the Berry mechanism.

The purpose of this paper is to begin a systematic study of Berry pseudorotation processes in pentacoordinated silicon compounds, including characterizations of the potential energy surfaces, force constant analyses, and intrinsic reaction coordinate (IRC) calculations.[19] In many mixed-ligand systems, there are a number of stable isomers predicted, while in others there are only a very few. Only through a thorough systematic analysis of these structures can we understand trends in the behavior of these compounds. These pseudorotation processes may play a major role in determining the stereochemistry of a variety of reactions involving silicon compounds.[7b]

We have found that the use of semiempirical techniques to explore surfaces in a preliminary fashion and to extend results to large systems, combined with ab initio calculations to establish limits of accuracy of semiempirical methods and produce quantitative results for small- to medium-sized systems, has been exceedingly fruitful in studying these hypervalent silicon systems.[20-22] In this

initial paper, we lay the groundwork for this systematic study by considering in detail the Berry pseudorotation process in the prototypical SiH_5^- anion.

COMPUTATIONAL METHODS

All semiempirical calculations were performed with the MOPAC program.[23] Results were obtained for the MNDO,[24] AM1,[25] and PM3[26] Hamiltonians. In the case of MNDO, the silicon parameters were taken from a later publication by Dewar.[27]

All ab initio calculations were performed with a locally modified version of GAUSSIAN86.[28] Structures for all species were initially obtained at the restricted Hartree-Fock (RHF)/6-31G(d) level.[29] In addition, geometry optimizations were done at the second-order perturbation theory (MP2[30]) level with use of the 6-31G(d) and 6-31++G(d,p)[31] basis sets to assess the importance of correlation and diffuse functions in the basis set in predicting the geometries for these hypervalent species. Energies for all species were calculated at all levels of geometry optimization. In addition, energies were also calculated at the fourth-order perturbation theory level (MP4[32]) utilizing the 6-31++G(d,p) basis set. Zero-point vibrational energies were added to all electronic energies, making the differences more directly comparable to the semiempirical enthalpies. Mulliken population analyses were performed with RHF/6-31++G(d,p) wave functions.

All stationary points with all methods were verified by diagonalizing the Cartesian force constant matrices and

demonstrating that minima and transition states had zero and one negative eigenvalue, respectively. For the ab initio calculations, these normal-mode frequencies were calculated at all levels of geometry optimization. For all ab initio structures, the normal modes were analyzed in terms of their component internal coordinate contributions with the vibrational decomposition method developed by Boatz and Gordon.[33]

Intrinsic reaction coordinate (IRC) calculations at the ab initio level were done utilizing the fourth-order Runge-Kutta (RK4) method.[34] The initial quadratic step off the saddle point with a 10^{-6} $amu^{1/2}$·bohr step in the direction indicated by the imaginary normal mode was followed by RK4 steps of 0.0001-0.005 $amu^{1/2}$·bohr. The latter were adjusted so as to maximize the efficiency of the calculations, while maintaining the symmetry of the path. IRC calculations were performed at the semiempirical levels of theory with the approximate intrinsic reaction coordinate method developed by Stewart, Davis, and Burggraf[35] as implemented in MOPAC. Generalized normal-mode frequencies along the reaction path were obtained by projecting the 3N - 7 transverse normal modes in a space orthogonal to the reaction path, in the manner prescribed by Miller, Handy, and Adams.[36]

RESULTS AND DISCUSSION

Table I gives the complete set of optimized bond lengths for all levels of theory for the D_{3h} trigonal-bipyramidal structure of SiH_5^-. These results agree very well with previous calculations as discussed in our recent review paper.[15] Note that the semiempirical methods underestimate the Si-H bond lengths, with the recent PM3 method giving results closest to the ab initio results. There is very little change in geometry in improving the RHF/6-31G(d) optimization to include electron correlation at the MP2 level or diffuse functions in the basis set. Table II gives the analogous information for the C_{4v} tetragonal-pyramidal structure of SiH_5^-. Again, the semiempirical methods underestimate the Si-H bond lengths, and inclusion of electron correlation or diffuse basis set functions in the ab initio results makes little difference. A comparison of Tables I and II shows that all methods give the following trend in the lengths of the Si-H bonds: $R_{ax} > R_{bas} > R_{eq} > R_{ap}$. Tables I and II also give the Mulliken charges for each of the atoms for each structure according to each method. The trend in the charges on the hydrogen mimics the trends in the Si-H bonds; a higher negative charge on the hydrogen corresponds to a longer, and more ionic, Si-H bond. MNDO and AM1 tend to predict a higher positive charge on the silicon than does the ab initio calculation. This tendency has

previously been ascribed primarily to the hydrogens being predicted with too large a negative charge.[22] PM3 generally predicts a lower positive charge than does the ab initio calculation.

Differences in energy (and/or enthalpy) between the two SiH_5^- structures are given in Table III. All methods agree that the Berry pseudorotation barrier for SiH_5^- is about 2.0 kcal/mol. These results also agree with previous calculations on this system.[15] For example, Reed and Schleyer obtained an energy difference of 2.17 kcal/mol at the RMP4/6-31++G(d,p) level of theory corrected for zero-point energies obtained at the HF/6-31+G(d) level.[16] It is obvious that the Berry pseudorotation barrier is quite small in this system and that even simple levels of theory can account for it properly.

Cartesian force constant calculations along with harmonic normal-mode frequencies were calculated for both structures with all semiempirical methods and several ab initio levels of theory. These results are given for the D_{3h} minimum of SiH_5^- in Table IV.

We find general agreement among the various methods in these calculated frequencies. The semiempirical methods switch the lowest A'_2 vibration with the second E' pair, but all methods predict these sets of vibrations to be fairly close in frequency. PM3 also has the two highest frequency vibrations switched. All of the semiempirical methods tend

to overestimate the five highest vibrational frequencies, which are primarily Si-H stretching motions. There seems to be little difference among the ab initio results, except for the typical overestimation of frequencies at the SCF level.[37]

An analysis of these normal-mode motions shows that the five highest frequency modes are Si-H stretches, with ν_2 and ν_3 being primarily axial stretches and ν_1, ν_5, and ν_6 being primarily equatorial stretches.

This analysis is made more quantitative in Table V, where the MP2/6-31G(d) normal modes are decomposed into their internal coordinate contributions. It is also apparent from the table that ν_4, ν_7, ν_8, ν_{11}, and ν_{12}, are dominated by H_{ax}-Si-H_{eq} bending motions, whereas ν_9 and ν_{10} (as discussed in more detail below) correspond to the H_{eq}-Si-H_{eq} bend.

Mode ν_9, diagrammed in Figure 2, is one of the degenerate pair of the lowest frequency E' symmetry vibration, and it has the motion appropriate to carrying the molecule along a Berry pseudorotation pathway. Note that the two axial hydrogens move tangentially toward each other so as to close the H_{ax}-Si-H_{ax} angle, while two of the three equatorial hydrogens (H_1 and H_2) move tangentially away from each other so as to open the H_1-Si-H_2 angle. In this motion, H_3 is the pivotal hydrogen and the other two equatorial hydrogens become axial while the two axial hydrogens become equatorial. Compare the motion along this normal mode with the idealized Berry pseudorotation motion shown in Figure 1.

Providing additional support for the argument that this mode is indeed the one appropriate to a Berry pseudorotation pathway is the result obtained when an AM1 trajectory (DRC)[35] is computed starting in the direction of this mode with 5.0 kcal/mol of excess kinetic energy. The motion along the trajectory carries the molecule smoothly to the transition state for the Berry pseudorotation and then along to the equivalent isomer with H_1 and H_2 axial and the two axial hydrogen equatorial.

The normal-mode frequencies for the C_{4v} structure of SiH_5^- are given in Table VI. Again, we find general agreement among the various methods in these calculated frequencies. The decomposition of these normal-mode motions at the MP2/6-31G(d) level is given in Table VII. This analysis illustrates that the give highest frequency modes are Si-H stretches, with ν_1 containing a significant amount of the Si-H_{ap} stretch. Mode ν_6 (Table IV) has the required imaginary frequency that establishes the structure as the expected transition state; analysis of the atom motions (see also Table VII) confirms that this mode has the motion appropriate to a Berry pseudorotation transition state. The remaining normal modes are dominated by H-Si-H bending motions.

It is revealing to compare the calculated intrinsic frequencies with the trends in bond lengths (and implied bond

strengths) noted above. The MP2/6-31G(d) frequencies for the Si-H stretches are 2111, 1960, 1730, and 1590 cm^{-1}, respectively, for the apical (C_{4v}), equatorial (D_{3h}), basal (C_{4v}), and axial (D_{3h}) hydrogens. This is in complete agreement with the trend noted earlier and lends credence to the implied bond strengths.

Intrinsic reaction coordinate calculations were run starting at each of the semiempirical and MP2/6-31G(d) saddle points. These IRC's confirm that these transition states do indeed connect two trigonal-bipyramidal D_{3h} structures, each with a different pair of hydrogen atoms axial. A plot of the MP2/6-31G(d) energy along the IRC is given in Figure 3.

It is instructive to plot the generalized MP2/6-31G(d) normal-mode frequencies as a function of the distance along the C_{2v} path corresponding to the IRC. Figure 4 illustrates the variation of the a_1 and a_2 generalized normal-mode frequencies along the IRC, while Figure 5 contains the analogous curves for the b_1 and b_2 modes. To aid reading these figures, the correlation among C_{4v}, C_{2v}, and D_{3h} irreducible representations is given in Table VIII. Furthermore, note that only 3N - 7 modes are plotted, since the gradient (IRC) direction has been projected out to obtain proper normal modes.[36]

Vibrational analysis of the frequencies shown in Figures 4 and 5 reveals the detailed nature of these modes along the IRC. At the C_{4v} saddle point, the a_2 mode is an H_b-Si-H_b

bend (b = basal). As the structure moves to the D_{3h} minimum, the contribution from one of the H_b-Si-H_a (a = apical) bends increases and the two a_2 contributions become equivalent H_{eq}-Si-H_{eq} (eq = equatorial) bends. Similar comments apply to the other normal modes, with very little stretch-bend interaction throughout the IRC.

The variation of the intrinsic frequencies along the IRC is illustrated in Figure 6, with the internal coordinates described in Figure 7. At the saddle point, stretch 1 corresponds to an apical Si-H bond, while stretch 2 and stretch 3 are equivalent basal Si-H stretching motions. As the molecule moves down the IRC, stretches 1 and 3 become equivalent equatorial Si-H motions while stretch 2 transforms into one of the axial Si-H stretches. The bending motions evolve in a similar manner. At the transition state, bend 3 is an H_b-Si-H_b bend, while bend 1 and bend 2 are equivalent H_a-Si-H_b bending motions. Upon relaxation, bends 1 and 3 become equivalent H_{eq}-Si-H_{eq} bends while bend 2 transforms into the H_{ax}-Si-H_{ax} bend.

This completes our analysis of SiH_5^-. We have shown general agreement among these sets of calculations and previous calculations for structures and energetics of this prototype silicon pentacoordinated molecule. We have established a low barrier to Berry pseudorotation and completed a normal-coordinate analysis of both structures that are stationary points on the potential surface. We

have, for the first time, established (at this level of theory) that the C_{4v} square-pyramidal structure of SiH_5^- is the transition state for berry pseudorotation of one D_{3h} trigonal-bipyramidal structure into an equivalent bipyramidal structure. In future papers of this series, we will turn our attention to generalization of pseudorotation of anionic silicon pentacoordinated structure by considering halogen-substituted anions and by examining the details of the dynamics of the pseudorotation process.

ACKNOWLEDGMENT

This work was supported in part by grants (to M.S.G.) from the Air Force Office of Scientific Research (87-0049), the National Science Foundation (CHE86-40071), and the Petroleum Research Fund, administered by the American Chemical Society. The calculations were performed on the quantum chemistry VAX 8530, purchased with the assistance of DoD Grant 86-0237. We are also grateful to Dr. Jerry Boatz for his assistance with the vibrational analysis.

REFERENCES

1. Burdett, J.K. *Struct. Bonding (Berlin)* **1976**,*31*,67.

2. Carre,F.H.;Corriu,R.J.P.;Guerin,C.;Henner,B.J.L.;Wong Chi Man, W.W.C. *J. Organomet. Chem.* **1988**,*347*,C1-C4.

3. Rauk,A.;Allen,L.C.;Mislow,K. *J. Am. Chem. Soc.* **1972**, *94*,3035-3040.

4. Musher,J.I. *Angew. Chem.., Int. Ed. Engl.* **1969**,*8*,54.

5. Hoffman,R.;Howell,J.M.;Muetterties,E.L. *J. Am. Chem. Soc.* **1972**,*94*,3047.

6. Florey,J.B.;Cusachs,L.C. *J. Am. Chem. Soc.* **1972**,*94*,3040.

7. a. *Pentacoordinated Phosphorus-Structure and Spectroscopy*; ACS Monograph 175; American Chemical Society; Washington, DC, 1980; Vols. I and II.
b. Deiters,J.A.; Holmes,R.R. *J. Am. Chem. Soc.* **1987**,*109*, 1686-1692, 1692-1696.

8. Muetterties,E.L. *Acc. Chem. Res.* **1970**,*3*,226.

9. Strauss,H.L. *Annu. Rev. Phys. Chem.* **1983**,*34*,301-328.

10. Berry,R.S. *J. Chem. Phys.* **1960**,*32*,933-938.

11. Mislow,K. *Acc. Chem. Res.* **1970**,*3*,321.

12. Musher,J.I. *J. Chem. Educ.* **1974**,*51*,94-97.

13. Gillespie,P.;Hoffman,P.;Klusacek,H.;Marquarding,D.;Pfohl, S.;Ramirez,F.;Tsolis,E.A.;Ugi,I. *Angew. Chem., Int. Ed. Engl.* **1971**,*10*,687-715.

14. Hajdasz,D.J.;Squires,R.R. *J. Am. Chem. Soc.* **1986**, *108*,3139.

15. Burggraf,L.W.;Davis,L.P.;Gordon,M.S. *Topics Phys. Oganomet. Chem.* **1989**,*3*,75.

16. Reed,A.E.;Schleyer,P.R. *Chem. Phys. Lett.* **1987**,*133*,553-561.

17. Wilhite,D.L.;Spialter,L. *J. Am. Chem. Soc.* **1973**,*95*,2100-2104.

18. a. Birgi,H.B. *Angew. Chem., Int. Ed. Engl.* **1975**,*14*,460.

b. Mutterties,E.L.;Guggenberger,L.J. *J. Am. Chem. Soc.* **1974**, *96*,1748.
c. Holmes,R.R.;Day,R.O.;Chandrasekhar,V.;Holmes,J.M. *Inorg. Chem.* **1985**,*24*,2009.
d. Holmes,R.R.;Deiters,J.A. *J. Am. Chem. Soc.* **1977**, *99*,3318.

19. a. Garrett,B.C.;Redman,M.J.;Steckler,R.;Truhlar,D.G.; Baldridge,K.K.;Bartol,D.;Schmidt,M.W.;Gordon,M.S. *J. Phys. Chem.* **1988**, *92*,1476.
b. Reference 31 and references cited therein.

20. Davis,L.P.;Burggraf,L.W.;Baldridge,K.K.;Gordon,M.S. *J. Am. Chem. Soc.* **1985**,*107*,4415-4419.

21. Gordon,M.S.;Davis,L.P.;Burggraf,L.W.;Damrauer,R. *J. Am. Chem. Soc.* **1986**,*108*,7889-7893.

22. Davis,L.P.;Burggraf,L.W.;Gordon,M.S. *J. Am. Chem. Soc.* **1988**,*110*,3056-3062.

23. Stewart,J.J.P. *QCPE 455*.

24. Dewar,M.J.S.;Theil,W. *J. Am. Chem. Soc.* **1977**,*99*,4899-4907.

25. Dewar,M.J.S.;Zoebisch,E.G.;Healy,E.F.;Stewart,J.J.P. *J. Am. Chem. Soc.* **1985**,*107*,3902.

26. Stewart,J.J.P. *J. Comput. Chem.*, in press.

27. Dewar,M.J.S.;Healy,E. *Organometallics* **1982**,*1*,1705-1708.

28. Frish,M.J.;Binkley,J.S.;Schlegel,H.B.;Raghavachari,K.; Melius,C.F.;Martin,R.L.;Stewart,J.J.P.;Brobrowicz,F.W.; Rohlfing,C.M.;Kahn;DeFrees,D.J.;Seeger,R.;Whiteside,R.A.; Fox,D.J.;Fluder,E.M.;Topiol,S.;Pople,J.A. *GAUSSIAN86*; Carnegie-Mellon Quantum Chemistry Publishing Unit: Pittsburgh, PA 15213, 1986.

29. a. Hariharan,P.C.;Pople,J.A. *Theor. Chim. Acta* **1973**, *28*,213-222.
b. Francl,M.M.;Pietro,W.J.;Hehre,W.J.;Binkley,J.S.; Gordon, M.S.; DeFrees,D.J.;Pople,J.A. *J. Chem. Phys.* **1982**,77,3654-3665.
c. Gordon,M.S. *Chem. Phys. Lett.* **1980**,*76*,163-168.

30. Pople,J.A.;Binkley,J.S.;Seeger,R. *Int. J. Quantum Chem.* **1976**,*S10*,1-19.

31. Frisch,M.J.;Pople,J.A.;Binkley,J.S. *J. Chem. Phys.* **1984**,

80, 3265.

32. Krishnan,R.;Frisch,M.J.;Pople,J.A. *J. Chem. Phys.* **1980**, *72*, 4244.

33. Boatz,J.A;Gordon,M.S. *J. Phys. Chem.* **1989**,*93*,819.

34. Baldridge,K.K.;Gordon,M.S.;Steckler,R.;Truhlar,D.G. *J. Phys. Chem.*,**1989**,*93*,5107.

35. Stewart,J.J.P.;Davis,L.P.;Burggraf,L.W. *J. Comput. Chem.* **1987**,*8*,1117-1123.

36. Miller,W.H.;Handy,N.C.;Adams,J.E. *J. Chem. Phys.* **1980**, *72*,99.

37. Pople,J.A.;Luke,B.T.;Frisch,M.J.;Binkley,J.S. *J. Phys. Chem.* **1985**,*89*,2198.

Table I: [Trigonal Bipyramid SiH_5^- bond lengths (Å) and charges.]

	bond length (Å)		Si	H charge	
method	R(ax)	R(eq)	charge	ax	eq
MNDO	1.470	1.438	+1.872	-0.608	-0.552
AM1 1.524	1.496	+1.094	-0.499	-0.365	
PM3 1.571	1.534	+0.276	-0.360	-0.186	
RHF/6-31G(d)	1.622	1.531			
MP2/6-31G(d)	1.619	1.542			
MP2/6-31++G(d,p)	1.609	1.524	+0.617	-0.431	-0.252

Table II: [Tetragonal SiH_5^- bond lengths (Å) and charges.]

	bond length (Å)		A(ap)	Si	H charge	
method	R(ap)	R(bas)	(deg)	charge	ap	bas
MNDO	1.421	1.459	104.1	+1.879	-0.527	-0.588
AM1 1.478	1.515	104.0		+1.108	-0.293	-0.454
PM3 1.509	1.559	104.2		+0.288	-0.075	-0.303
RHF/6-31G(d)	1.514	1.579	101.7			
MP2/6-31G(d)	1.521	1.585	101.3			
MP2/6-31++G(d,p)	1.506	1.570	101.8	+0.631	-0.232	-0.350

Table III: Energy Differences Between D_{3h} and C_{4v} Structures of SiH_5^-.

method	$\Delta E'$ (kcal/mol)	$\Delta H'$[a] (kcal/mol)
MNDO		1.8
AM1	2.4	
PM3	3.3	
RHF/6-31G(d)	3.0	
MP2/6-31G(d)	2.5	2.2
MP2/6-31++G(d,p)	2.7	2.4
MP4/6-31++G(d,p)[b]	2.5	2.2

a. For the semiempirical methods, the enthalpy difference is calculated at 298 K. For the ab initio methods, the enthalpy difference is calculated at 0 K by making a zero-point correction to the energy difference.
b. Computed at the MP2/6-31++G(d,p) geometry.

Table IV: Harmonic Normal-Mode (cm^{-1}) for D_{3h} Structure of SiH_5^-

	ν_1	ν_2	ν_3	ν_4	ν_5, ν_6	ν_7, ν_8	ν_9, ν_{10}	ν_{11}, ν_{12}
symmetry	A_1'	A_1'	A_2'	A_2''	E'	E'	E'	E''
MNDO	2206	1802	1938	1146	2067	1092	510	1227
AM1	2149	1834	1986	953	2113	884	540	1091
PM3	1889	1718	1810	807	1904	748	567	943
RHF/6-31G(d)	2082	1414	1590	1089	2031	1136	583	1305
MP2/6-31G(d)	2014	1460	1608	1079	1986	1101	538	1257
MP2/6-31++G(d,p)	2052	1438	1594	1032	2031	1070	557	1243

Table V: Percentage Contribution of Internal Coordinates to Normal-Mode Frequencies: Trigonal-Bipyramidal Structure[a].

	Si-H_{ax}	Si-H_{eq}	H_{ax}-Si-H_{eq}	H_{eq}-Si-H_{eq}
ν_1	0.20	0.80	0.00	0.00
ν_2	0.80	0.20	0.00	0.00
ν_3	0.97	0.00	0.03	0.00
ν_4	0.03	0.00	0.97	0.00
ν_5, ν_6	0.00	1.00	0.00	0.00
ν_7, ν_8	0.00	0.00	0.88	0.12
ν_9, ν_{10}	0.00	0.00	0.12	0.87
ν_{11}, ν_{12}	0.00	0.00	1.00	0.00

a. H_{ax} = axial hydrogen, H_{eq} = equatorial hydrogen. The first two columns are stretching motions. The second two columns are bending motions.

Table VI: Harmonic Normal-Mode (cm^{-1}) for C_{4v} Structure of SiH_5^-.

	ν_1	ν_2	ν_3	ν_4	ν_5	ν_6	ν_7, ν_8	ν_9, ν_{10}	ν_{11}, ν_{12}
symmetry	A_1	A_1	A_1	B_1	B_2	B_2	E	E	E
MNDO	2218	2088	1073	1351	1785	389i	1981	1133	954
AM1	2219	2092	861	1204	1817	456i	2026	973	854
PM3	1987	1851	777	962	1712	541i	1836	855	740
RHF/6-31G(d)	2145	1956	1081	1425	1447	452i	1179	1222	1006
MP2/6-31G(d)	2114	1920	1009	1371	1475	412i	1760	1174	942
MP2/6-31++G(d,p)	2152	1951	1015	1356	1460	432i	1779	1143	957

Table VII: Percentage Contribution of Internal Coordinates to Normal-Mode Frequencies: Tetragonal Structure[a].

	Si-H_a	Si-H_b	H_a-Si-H_b	H_b-Si-H_b
ν_1	0.98	0.02	0.00	0.00
ν_2	0.02	0.98	0.00	0.00
ν_3	0.00	0.00	0.87	0.13
ν_4	0.00	0.00	0.00	1.00
ν_5	0.00	0.98	0.00	0.02
ν_6	0.00	0.02	0.98	0.00
ν_7, ν_8	0.00	0.98	0.00	0.00
ν_9, ν_{10}	0.00	0.02	0.00	0.98
ν_{11}, ν_{12}	0.00	0.00	1.00	0.00

a. H_a = apical hydrogen, H_b = basal hydrogen.

Table VIII: Correlation of Irreducible Representations.

C_{4v}	C_{2v}	D_{3h}
A_1, B_2	A_1	A_1', E'
B_1	A_2	E''
E	B_1	E', A_2'
E	B_2	E', A_2''

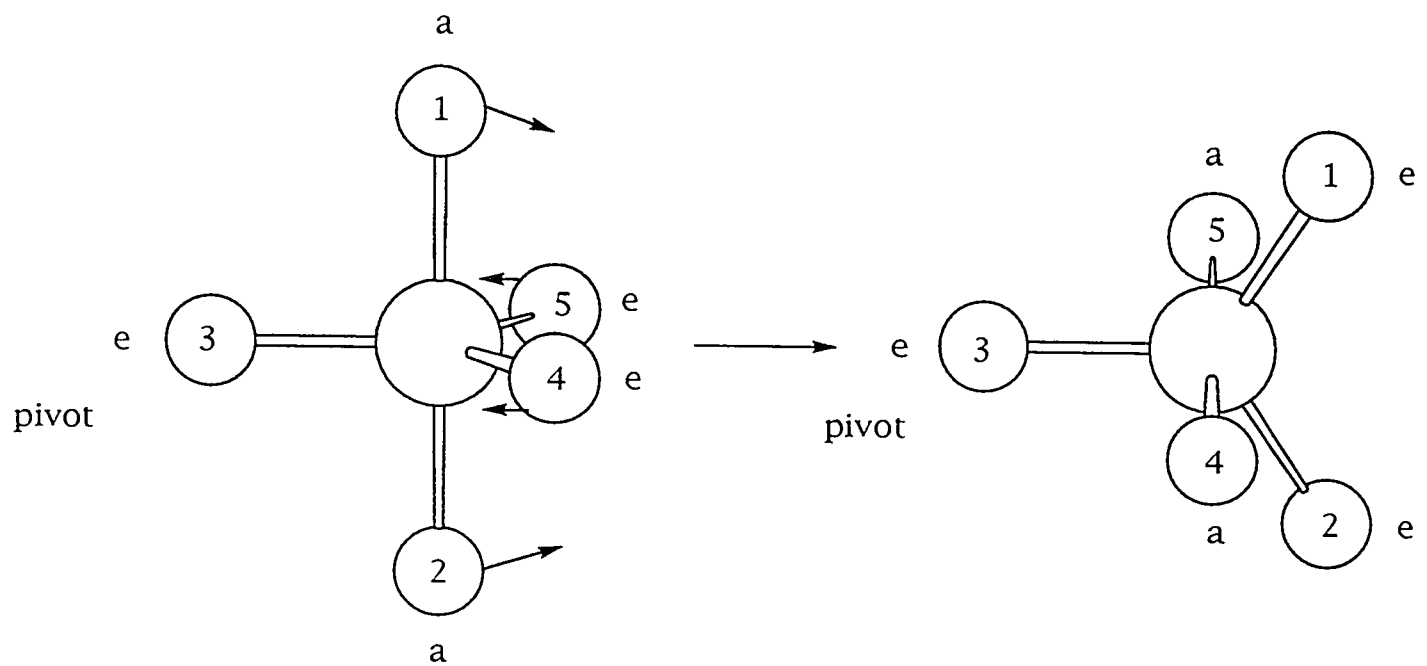

Figure 1: Illustration of Berry pseudorotation.

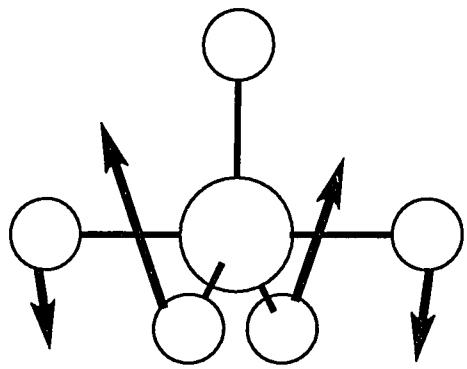

Figure 2: Illustration of normal-coordinate motion for mode ν_9, leading to pseudorotation.

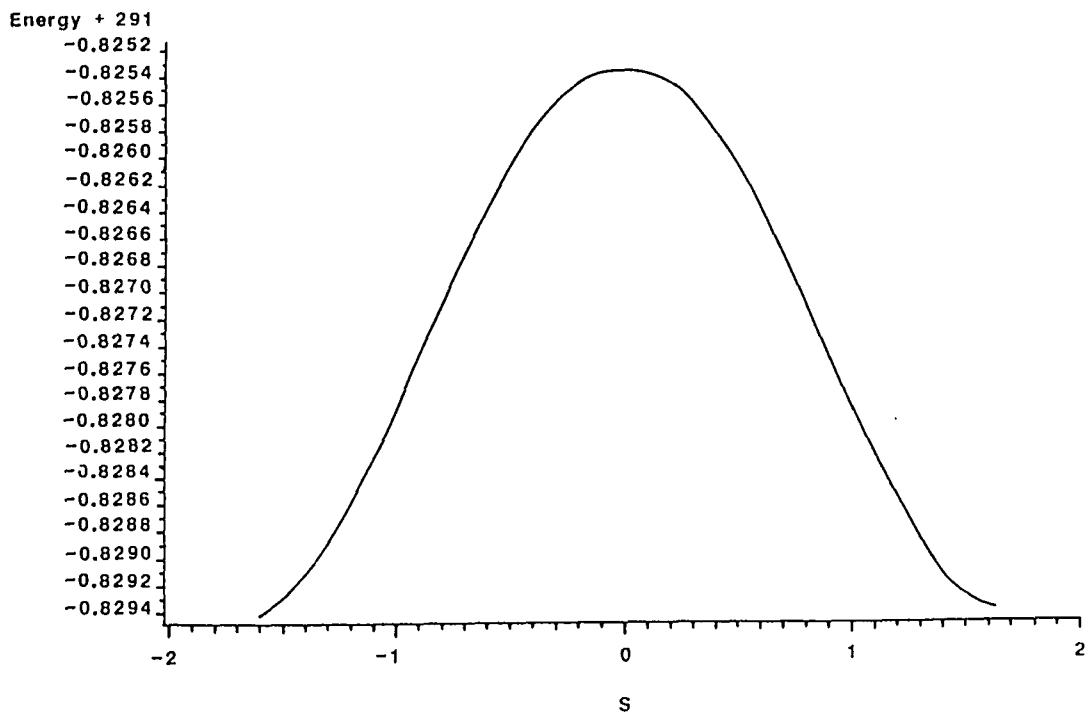

Figure 3: SiH_5^- MP2/6-31G(d) IRC (energy, hartrees; s, $amu^{1/2}$·bohr).

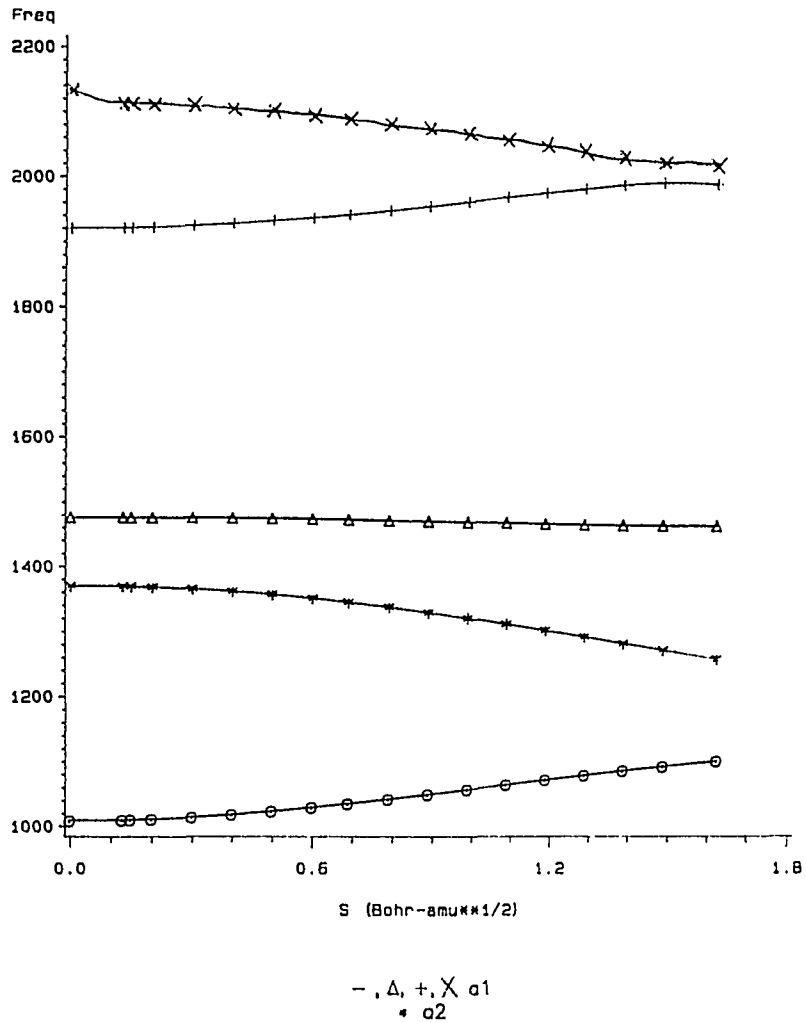

Figure 4: Plot of a_1 and a_2 generalized normal-mode frequencies (cm^{-1}) along the 6-31G(d) IRC.

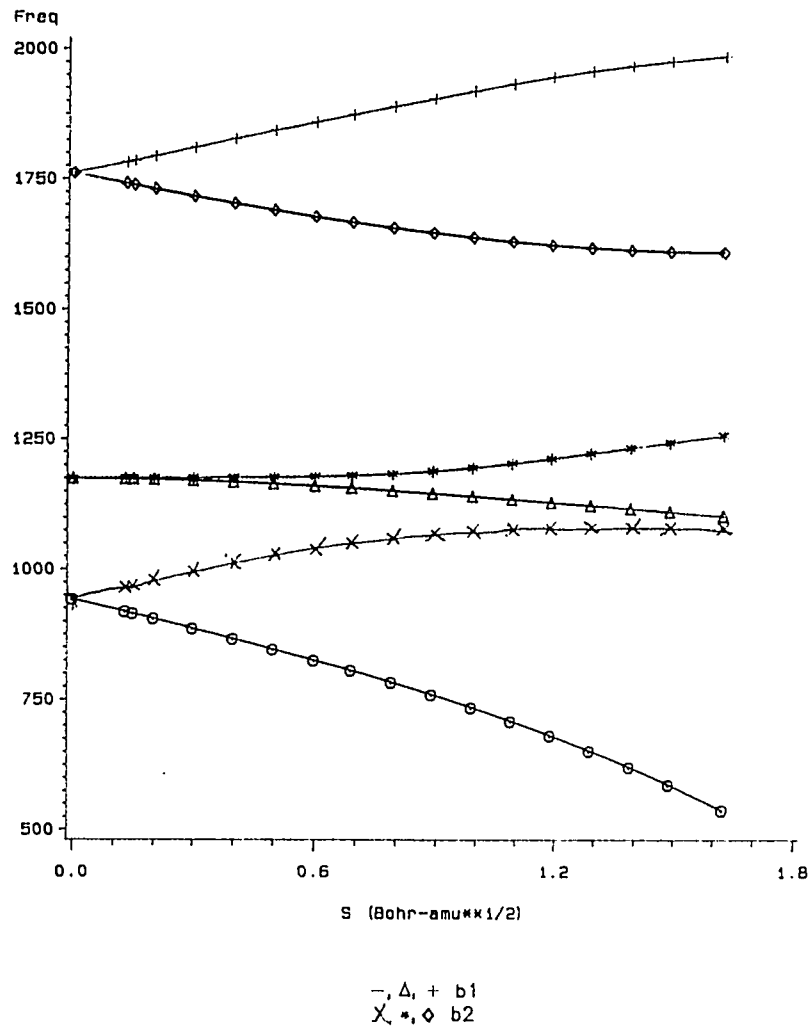

Figure 5: Plot of b_1 and b_2 generalized normal-mode frequencies (cm^{-1}) along the 6-31G(d) IRC.

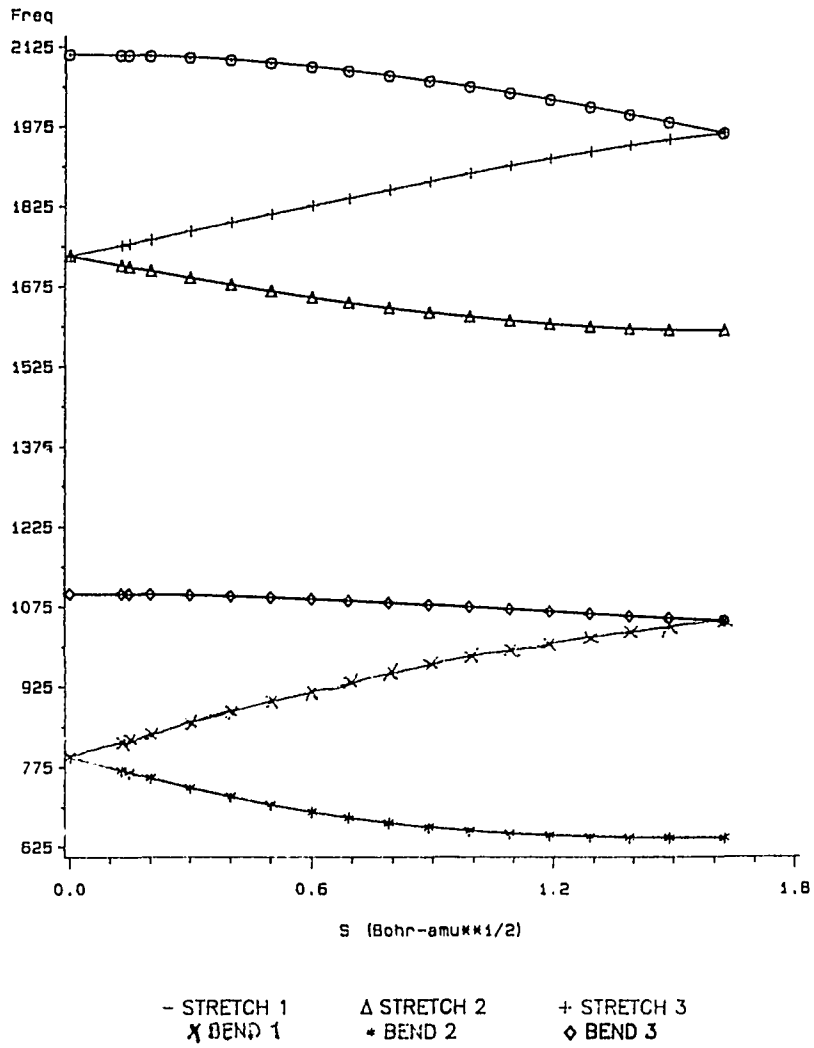

Figure 6: Generalized intrinsic frequencies (cm^{-1}) along the IRC.

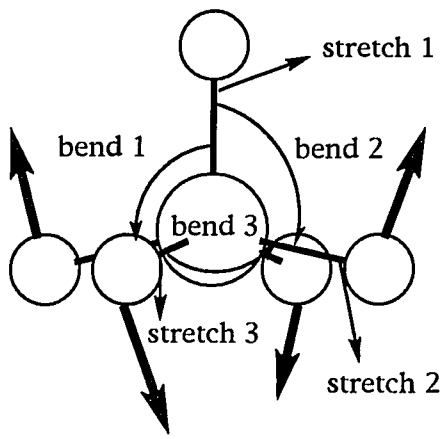

Figure 7: Schematic of internal coordinates for the pseudorotation motion.

PAPER 2: A NEW TWIST ON PSEUDOROTATION

A New Twist on Pseudorotation

Theresa L. Windus and Mark S. Gordon
North Dakota State University
Fargo, North Dakota 58105

Larry W. Burggraf
Directorate of Chemical and Atmospheric Sciences
Air Force Office of Scientific Research
Bolling AFB, D.C. 20332

Larry P. Davis
HQAFSC/XTR
Andrew AFB, D.C. 20334

Reprinted with permission from
J. Am. Chem. Soc. **1991**, *113*, 4356-4357

DISCUSSION

For pentacoordinated structures in a trigonal bipyramidal arrangement, Berry[1] proposed a "pseudorotation" mechanism whereby two such isomers can interconvert through a tetragonal transition state (TS). This Berry pseudorotation mechanism was demonstrated explicitly for SiH_5^- by following the MP2[2]/6-31G(d)[3] minimum energy path[4] (MEP).

In the Berry pseudorotation of SiH_4F^-, we expect two minima (trigonal bipyramids with F either axial, **1**, or equatorial, **2**) and two maxima (square pyramids with F either basal, **3**, or apical, **4**). Indeed, these are the results obtained by several investigators.[5-8] We report here that SiH_4F^- has only one minimum on its potential energy surface (PES) and therefore does not appear to follow the usual Berry pseudorotational model (**1** ⇔ **3** ⇔ **2** ⇔ **4**).

Optimized structures and hessians were calculated with use of restricted SCF (RHF) and Møller-Plesset perturbation theory (MP2)[2] wave functions with the 6-31G(d)[3] and 6-31++G(d,p)[9] basis sets. Final energies were determined at the full fourth order Møller-Plesset (MP4)[10] perturbation level. Calculations were performed with the GAUSSIAN86[11] program.

Relative energies of **1**-**4** are given in Table I. At the RHF/6-31G(d) level, we observe the four expected structures, but we also obtain an unexpected result. In the Berry model,

2 should pseudorotate to **1** with **3** as the TS. However, at all correlated levels **2** becomes *higher* in energy than **3**. This suggests that at higher computational levels the hessian of **2** will not be positive definite and that the usual Berry pseudorotation may not be taking place. Indeed, further investigation with the 6-31++G(d,p) basis set reveals that **2** and **3** coalesce into one C_{2V} TS with one imaginary frequency, even at the SCF level! The same result is found when the geometry is optimized at the MP2/6-31++G(d,p) level of theory. This finding, that SiH_4F^- has only one minimum on its PES, is contrary to common assumptions about such species.

The MP2/6-31++G(d,p) structures are shown in Figure 1 and Table II along with a depiction of the imaginary normal mode for each TS. The normal mode for **4** shows that this is the TS for the Berry pseudorotation connecting two equivalent equatorial structures (**2** $\rightarrow$**2**). But **2** is itself a TS connecting two equivalent axial minima. For example, the normal mode of **2** demonstrates that H_2 and F are moving into axial positions, giving isomer **1**. Therefore, the only stable SiH_4F^- isomer, **1**, can rotate through a non-Berry pseudorotational path to **2**, and **2** in turn can pseudorotate to **4**. A large basis set is needed to accurately define the stationary points on the SiH_4F^- surface.

To gain insight into the implications of the results reported here, consider the MEP leading from the highest

energy stationary point, **4**, downward. An MEP is a steepest descent path from a transition state and therefore follows the gradient downhill. Since the gradient preserves symmetry, the MEP does also. Thus, as the MEP follows the motion dictated by the imaginary normal mode of **4**, it moves downhill within C_{2v} symmetry to **2**, but since **2** is also a TS, a second imaginary frequency must have appeared along the MEP. The point at which this occurs is a bifurcation point which introduces a ridge in the PES. So in reality the molecule need not continue to follow the MEP. As discussed by Ruedenberg[12] and others,[13] the downhill path from **4** can proceed to **1** without passing through **2**. In other words, the adiabatic motion must depart the MEP at the bifurcation point in some manner: possibly in the direction of the second imaginary mode; possibly in some composite direction of the two imaginary modes, but *not* along the steepest descent path. A more complete probe of the PES and analysis of the associated dynamics will be necessary to fully understand this complex motion.

Preliminary ab initio calculations on more complex pentacoordinated species (e.g., $SiH_3F_2^-$) suggest that the results reported here are not unique. Also, unusual non-Berry adiabatic motion has been discovered with AM1 in $SiF_2H_2Cl^-$.[14] In a later paper, the results of calculations on $SiH_mX_{5-m}^-$(X = F, Cl; m = 0-4), including PESs, will be reported.

ACKNOWLEDGMENT

This work was supported by grants from the Air Force Office of Scientific Research (90-0052) and the National Science Foundation (CHE89-11911). The calculations reported here were performed on the CRAY Y-MP computer at the San Diego Supercomputer Center and on the IBM 3090/200E computer at North Dakota State University Computer Center, obtained in part with a joint study agreement with IBM. We appreciate stimulating discussions with Dr. M. W. Schmidt.

REFERENCES

1. Berry, R.S.;*J.Chem.Phys.*,**1960**,*32*,933-938.
   Mislow,K.;*Acc.Chem.Res.*,**1970**,*3*,321.

2. Pople,J.A.;Binkley,J.S.;Seeger,R.;*Int.J. Quantum Chem.*, **1976**,*S10*,1-19.

3. Hariharan,P.C.;Pople,J.A.;*Theor.Chem.Acta*,**1973**,*28*,213-222.
   Francl,M.M.;Pietro,W.J.;Hehre,W.J.;Binkley,J.S.;Gordon,M.S.;DeFrees,D.J.;Pople,J.A.;*J.Chem.Phys.*,**1982**,*77*,3654-4665.
   Gordon,M.S.;*Chem.Phys.Lett.*,**1980**,*76*,163-168.

4. Gordon,M.S.;Windus,T.L.;Burggraf,L.W.;Davis,L.P.;*J.Am. Chem. Soc.*,**1990**,*112*,7167-7171.

5. Wilhite,D.L.;Spialter,L.;*J.Am.Chem.Soc.*,**1973**,*95*,2100-2104.

6. Deiters,J.A.;Holmes,R.R.;*J.Am.Chem.Soc.*,**1990**,*112*,7197-7202.
   Deiters,J.A.;Holmes,R.R.;*J.Am.Chem.Soc.*,**1987**,*109*,1686-1692, 1692-1696.

7. Gronert,S.;Glaser,R.;Streitwieser,A.;*J.Am.Chem.Soc.*,**1989**, *111*,3111-3117.

8. Gordon,M.S.;Davis,L.P.;Burggraf,L.W.;Damrauer,R.A.;*J.Am. Chem.Soc.*,**1986**,*108*,7889-7893.

9. Frisch,M.J.;Pople,J.A.;Binkley,J.S.;*J.Chem.Phys.*,**1984**,*80*, 4244.

10. Krishnan,R.;Frisch,M.J.;Pople,J.A.;*J.Chem..Phys.*,**1980**,*72*, 4244-4245.

11. Frisch,M.J.;Binkley,J.S.;Schlegel,H.B.;Raghavachari,K.; Melius,C.F.;Martin,R.L.;Stewart,J.J.P.;Bobrowicz,F.W.; Rohlfing,C.M.;Kahn,L.R.;DeFress,D.J.;Seeger,R.;Whiteside, R.A.;Fox,D.J.;Fleuder,E.M.;Pople,J.A.;Carnegie-Mellon Quantum Chemistry Publishing Unit,Pittsburgh, PA 15213.

12. Hoffman,D.K.;Nord,R.S.;Ruedenberg,K.;*Theor.Chim.Acta*, **1986**,*69*,265-279.
    Valtazanos,P.;Ruedenberg,K.;*Theor.Chim.Acta*, **1986**,*69*, 281,307.

13. Kraus,W.A.;DePristo,A.E.;*Theor.Chim.Acta*,**1986**,*69*,309-322.
Baker,J.;Gill,P.M.W.;*J.Comp.Chem.*,**1988**,*9*,465-475.
Shida,N.;Almlöf,J.E.;Barbara,P.F.;*Theor.Chim.Acta*,**1989**,
76,7-31.

14. Davis,L.P.;Burggraf,L.W.;unpublished results.

TableI: Relative Energies[a]

structure	MP4/6-31++G(d,p)// RHF/6-31G(d)[b]	MP4/6-31++G(d,p)// RHF/6-31++G(d,p)[b]	MP4/6-31++G(d,p)// MP2/6-31++G(d,p)[b]
1	0.0 (0.0)	0.0 (0.0)	0.0 (0.0)
2	7.7 (7.4)	8.1 (7.5)[c]	7.7 (7.2)[c]
3	7.1 (6.6)		
4	22.2 (21.3)	23.2 (22.1)	23.2 (22.0)

a. Energies are in kcal/mol. Values in parentheses include zero point energies where the RHF frequencies are scaled by 0.89. b. The notation level2/basis2//level1/basis1 denotes an energy for level 2 using basis 2 at the geometry from basis 1 at level 1. c. This is the energy of the coalesced structure of **2** and **3**. See **2** in Figure 1.

Table II: MP2/6-31++G(d,p) Structures[a]

structure	Si-F	Si-H_1	Si-H_2	Si-H_3	Si-H_4	F-Si-H_1	F-Si-H_2	F-Si-H_3	F-Si-H_4
1	1.813	1.503	1.575	1.503	1.503	88.4	180.0	88.4	88.4
2	1.764	1.526	1.526	1.541	1.541	127.5	127.5	83.7	83.7
3	1.692	1.562	1.562	1.562	1.562	101.4	101.4	101.4	101.4

a. Bond lengths are in angstroms and angles in degrees.

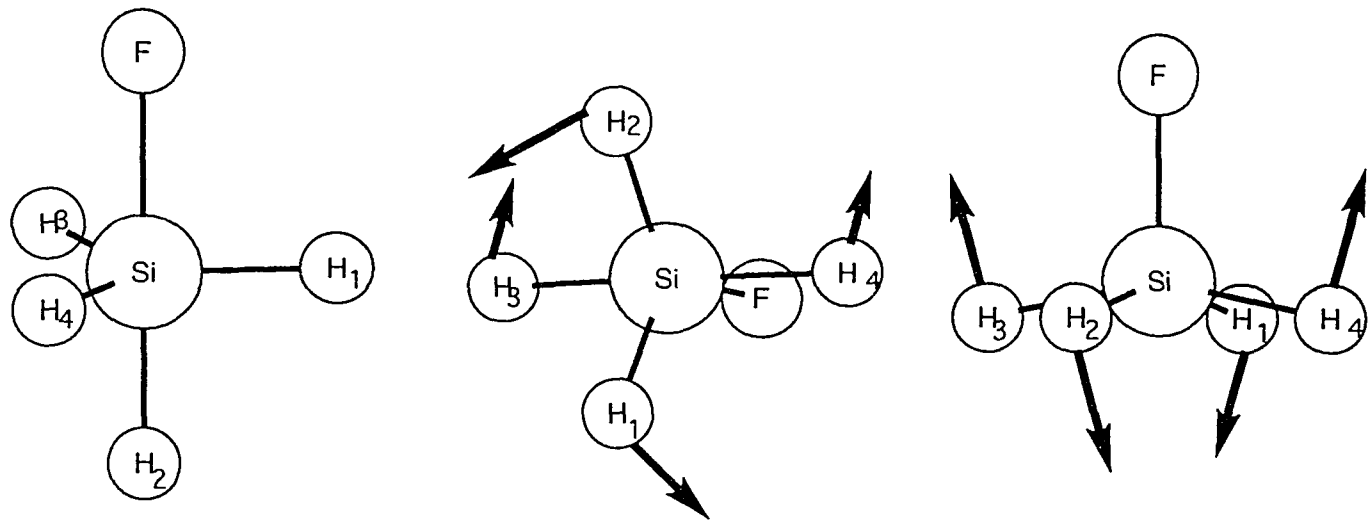

1

C_{3V}

2

C_{2V}, 194.9i

4

C_{4V}, 797.2i

Figure 1: MP2/6-31++G(d,p) structures. Imaginary frequencies in cm^{-1} are given for transition states.

PAPER 3: A DETAILED ANALYSIS OF PSEUDOROTATION IN PH_4F

A DETAILED ANALYSIS OF PSEUDOROTATION IN PH_4F

Theresa L. Windus and Mark S. Gordon

Department of Chemistry
North Dakota State University
Fargo, ND 58105

Reprinted with permission from
Theor. Chim. Acta **1992**, *83*, 21-30

ABSTRACT

Pentacoordinated molecules are thought to undergo intramolecular isomerization by the widely accepted Berry pseudorotation mechanism. Through our investigations, we have found that the actual pseudorotation for the PH_4F system is more complex than that envisioned by Berry. The potential energy surface of PH_4F is mapped out at the RHF/6-311G(d,p) level. According to the Berry mechanism, this system is expected to have two minima and two maxima; however, the system actually has two transition states and one global minimum. The minimum energy path from the highest transition state is followed to the second transition state, which in turn has a minimum energy path leading to the global minimum. Along the path between the two transition states there is a branching region. This portion of the potential energy surface is probed extensively.

I. INTRODUCTION

The reactivity of pentacoordinated compounds, particularly those with silicon or phosphorus centers, is profoundly influenced by the orientational preferences and motions about the central atom. For pentacoordinated compounds with a trigonal bipyramidal structure, Berry [1] proposed that conformational changes occur via a square pyramidal transition state, as illustrated in Figure 1. This mechanism, termed Berry pseudorotation, was explicitly demonstrated for SiH_5^- by tracing the minimum energy path (MEP) connecting the two equivalent trigonal bipyramidal minima [2].

When the central atom is surrounded by two or more **different** ligands, it is generally accepted that several minima exist, such that each ligand can be placed in either an axial or an equatorial position. Thus, for a compound AH_4X, one expects to find four stationary points: two minima with X either axial (**1**) or equatorial (**2**) and two square pyramidal transition states with X either basal (**3**) or apical (**4**). However, it has already been demonstrated [3] that in the case of SiH_4F^-, structures **2** and **3** merge into a single transition state, leaving only one minimum (**1**) on the conformational potential energy surface, if an adequate level of theory is used (i.e. RHF/6-31++G(d,p)). Since the minimum energy, steepest descent path leading from **4** (F apical) to **2**

(F equatorial) connects two transition states (i.e., two structures, each of which has one imaginary frequency corresponding to a downhill motion), it was suggested that (a) the pseudorotational "mechanism" in compounds such as SiH_4F^- can be more complex than that envisioned in the Berry mechanism and (b) a bifurcation is to be expected along the MEP.

The molecule PH_4F is isoelectronic with SiH_4F^- and is a simple pentacoordinated phosphorus compound which is expected to have two minimum energy structures (**1** and **2**) on its ground state conformational potential energy surface (PES). In the present paper, the conformational PES of PH_4F is explored in detail in an attempt to understand the complex nature of its pseudorotational mechanism.

While PH_4F is as yet unknown experimentally, there have been several ab initio studies of the species suggesting that PH_4F is a minimum on the PES. Several of these investigations [4] were limited to the structure with F in the axial position. Stritch and Veillard [5], using idealized geometries, predicted the equatorial (**2**) and square pyramidal (**3**) structures to be 15.8 and 7.9 kcal/mol above the axial structure (**1**). Keil and Kutzelnigg [6], using constrained geometry optimizations, found the equatorial structure to be 23 kcal/mol above axial. McDowell and Streitweiser [7] performed geometry optimizations and predicted equatorial PH_4F to be 7.5 kcal/mol above axial, but

no Hessians were evaluated to assess the nature of the stationary points. Most recently, Wang etal. [8] carried out full geometry optimizations for the axial, equatorial, and square pyramidal structures for several PH_4X compounds. For X = F, these authors found the equatorial structure to be a transition state 8.0 kcal/mol above axial. The square pyramidal structure with F in the apical position (**4**) was predicted to be 33.5 kcal/mol above axial. While the reactions $PH_4F \rightarrow PH_3 + HF$ and $PH_4F \rightarrow PH_2F + H_2$ are exothermic (16.2 and 4.1 kcal/mol, respectively, at the MP2/6-311G(d,p)//MP2/6-311G(d,p) level of theory), it is nonetheless a minimum on the potential energy surface and therefore of interest from the point of view of pseudorotation.

II. COMPUTATIONAL APPROACH

In order to determine the dependence of the calculated energetics and stationary points on the level of theory, the structures of all stationary points were determined at several levels. The simplest level of theory used (referred to as Level A) is the self-consistent field (SCF) method with the 6-31G(d) [9] basis set. In Level B, the structures are again determined with SCF wavefunctions, but with the larger 6-311G(d,p) [10] basis set. Finally, in Level C the 6-311G(d,p) basis is used in conjunction with second order Moller-Plesset perturbation theory [11]. All stationary points were characterized as minima or transition states by calculating and diagonalizing the matrix of energy second derivatives (Hessian) to determine the number of negative force constants (0 for minima, 1 for transition states).

To follow each minimum energy path (MEP), the fourth order Runge-Kutta (RK4) and the Euler with stabilization (ES2) algorithms, developed in this laboratory [12], were used with step sizes varying from 0.0001 - 0.05 bohr-amu$^{1/2}$ depending on the convergence of the paths. All MEP's were calculated at Level B.

The projection method of Miller, Handy, and Adams [13], which projects out the translations, rotations and gradient at non-stationary points, was used to analyze the frequencies along the MEP's. In addition, the purification method

developed in this laboratory [14] was used to obtain qualitative information about the frequencies associated with the reaction path (See Appendix). The purification method removes the rotations and translations from the vibrations. This method provides only qualitative results, since the gradient is not projected out. So, the eigenvalues of this purified but unprojected Hessian can be used to obtain frequencies only when the gradient is small.

All calculations were performed using the electronic structure theory code GAMESS [15] and a locally modified version of GAUSSIAN86 [16].

III. RESULTS AND DISCUSSION

A. Structures and Energetics

At all levels of theory used in this work, only three stationary points are found on the PH_4F PES. The axial structure **1** is predicted to be a minimum, while the equatorial (**2**) and apical (**4**) structures are found to be transition states. Thus, in analogy with the previous calculations on SiH_4F^- [3], the basal structure **3** merges with **2**, and there is a minimum energy path connecting two transition states **2** and **4**. An important difference between PH_4F and SiH_4F^- is that in the former molecule the equatorial structure is clearly a transition state even at the SCF/6-31G(d) level of theory. The imaginary frequency in the equatorial structure is calculated to be 261i, 324i, and 298i cm^{-1} according to Levels A, B, and C, respectively. The corresponding values for the apical structure are 1067i, 1031i, and 1084i cm^{-1}, respectively.

The structures of the three stationary points are illustrated in Figure 2, and the energetics are summarized in Table I. The structures follow the generally expected trends. The axial bonds are somewhat longer than the equatorial bonds for both ligands, since the axial atoms are bound by a three-center, four-electron bond. The apical PF bond is even shorter than that in the equatorial structure. The effects of both basis set and correlation on the

calculated geometries are small, with the largest change being the 0.03Å increase in the equatorial PF bond length upon the addition of correlation.

Improving the basis set from 6-31G(d) to 6-311G(d,p) decreases the axial-equatorial energy difference (Table I) by 1.7 kcal/mol and increases the axial-apical energy difference by 1.4 kcal/mol. Both of these energy differences are somewhat larger than those found for SiH_4F^-. The addition of correlation has virtually no effect on the calculated relative energies. The addition of zero point vibrational energies changes the results in Table I by less than 1 kcal/mol in all cases.

The normal modes for the transition states (TS's) are shown in Figure 2. The normal mode for **4** shows this to be the TS for the Berry pseudorotation connecting two equivalent equatorial structures (**2** → **2**). However, **2** is itself a TS which connects two equivalent axial structures (**1** → **1**). To illustrate, the normal mode of **2** demonstrates that H_2 and F are moving into axial positions and H_1, H_3, and H_4 are moving into equatorial positions, giving isomer **1**. Indeed, the mode shown for **2** in Figure 2 is strikingly similar (although not identical) to the turnstile TS discussed by several authors [17]. The difference is that one does not expect the turnstile TS to occur at what is essentially the equatorial structure. Therefore, it is of interest to explore the MEP's that connect the stationary structures to determine the

nature of the potential energy surface.

When two TS's are connected by a MEP, either a bifurcation or a branching region must occur, because a second imaginary frequency associated with the lower energy TS is building in somewhere along the path. This second imaginary frequency (which indicates that the molecule may follow a motion not dictated by the MEP) is not "recognized" by the MEP. This is because the MEP by definition follows the steepest descent (gradient) path and therefore may not break symmetry. A bifurcation is identified by two imaginary frequencies, one associated with each TS, in the same region. In a branching region, the first imaginary frequency (associated with the higher energy TS) becomes real before the second imaginary frequency (associated with the lower energy TS) builds in. In either case (bifurcation or branching), a molecule not constrained by symmetry may move away from the MEP when it encounters a new imaginary mode. As will be discussed below, a branching region occurs in the PH_4F pseudorotation reaction.

B. MEP's and Branching Region

To examine this surface, the MEP's from **4** and **2** were calculated using the methods mentioned in Section II. The MEP's that connect structures **4** and **2** and structures **2** and **1** are displayed in Figures 3 and 4, respectively. These will be referred to as MEP4→2 and MEP2→1, respectively. MEP2→1

is relatively flat at the beginning. This prompted the use of very small step sizes to obtain path convergence. This is in contrast to MEP4→2 where the surface is not very flat and larger step sizes could be used.

Since a MEP follows the gradient and the gradient is totally symmetric in both cases, the MEP retains the symmetry of the molecule. So, MEP4→2 is a C_{2V} path and therefore leads directly to **2**. However, since there must be a bifurcation or branching somewhere on the MEP, the molecule need not be constrained to C_{2V} symmetry; that is, it may leave the original MEP.

To discover the point on MEP4→2 at which the new imaginary mode first appears, force fields were calculated at several points along this path. Figure 5 is a plot of the projected normal modes along MEP4→2. The lowest A_1 frequency (the one associated with MEP4→2) is projected to zero by the projection scheme and therefore the data for this frequency is obtained through the purification method. The frequency for the lowest A_1 mode goes from imaginary at small s to 0 between s = 0.952 and s = 1.052 bohr-amu$^{1/2}$ to positive for large s. Also, by examining the lowest B_2 mode (this is the mode initially followed for MEP2→1), the associated frequency goes from positive at small s to 0 between s = 1.962 and s = 1.963 bohr-amu$^{1/2}$ to imaginary for large s. By comparing the s values at which the two frequencies become zero, we see that the A_1 frequency becomes zero (has an inflection point)

before the B_2 frequency becomes imaginary. At the point that the B_2 frequency becomes zero there is a branching point. As discussed by Ruedenberg [18] and others [19], the downhill path from **4** can proceed to **1** without passing through **2**. In other words, the reaction could continue to follow MEP4→2, follow the direction associated with the B_2 mode, or some composite of the two. In reality, the amount of energy available to the system (e.g., the temperature) will play a role in the actual **motion**.

In an attempt to further explore the branching region between s = 1.962 and s = 2.298, "jumps" were taken off of MEP4→2 in the direction dictated by the B_2 mode for several points in this region, and then the gradient was followed to the minimum structure, **1**. For clarity, these jumping off points will be referred to as "path initiation points" (PIP's) and the MEP's from the PIP's will be referred to as "branching paths" (BP's). The resulting plots of energy vs. reaction coordinate for s = 1.963, 1.985, 2.086, and 2.286 bohr-amu$^{1/2}$ are given in Figures 6, 7, 8, and 9, respectively. The projected B_2 frequencies associated with these points are 15.3i, 82.0i, 149.1i, and 259.7i cm^{-1}, respectively. The magnitudes of these frequencies suggest that the surface associated with the B_2 mode starts out rather flat and gradually gains more curvature as the molecule progresses farther along the branching region.

Several comments need to be made about Figures 6-9. First , these plots have an unusual shape at the top of the BP. This can be explained in the following manner. The initial step from the PIP's were taken such that the energy would decrease by less than $1x10^{-5}$ au. In cases where the surface is very flat this first step can still be quite large. The large step with small energy decrease accounts for the singularities at s' = 0.0 in Figures 6, 7, and 8 [20]. Also, the resulting gradient of the initial step from the PIP is only slightly changed from the gradient of the PIP. As the molecule follows the BP, the gradient is changing from a gradient similar to MEP4→2 to that of a gradient similar to MEP2→1; until finally, the gradient is essentially that of MEP2→1. This change in the nature of the gradient, and therefore the potential energy surface, is directly seen in Figures 6, 7, and 8. The initial points along the BP (those following a gradient similar to MEP4→2) are following a faster changing portion of the surface than are the points after the gradient has changed to that of MEP2→1. Therefore, we see a characteristic change in the curvature of the plots.

Second, since the molecules tend to have gradients similar to MEP4→2 at the beginning of the BP and to have gradients similar to MEP2→1 after only a drop of less than one kcal/mol, the molecule must stay in a reaction swath that is rather narrow. The fact that the branching point is close

to **2** also suggests that the branching region of the surface must span a small volume near MEP4→2 and MEP2→1. This implies that while the reaction may not go exactly through **2**, it will come close to **2**. This could have interesting effects on the dynamics of this system.

As a final point, the "bump" in the BP's starts to become smaller and flatten out as we start at PIP's farther along MEP4→2, until at PIP's close to **2** it is essentially gone. Figure 9, which is a BP from a structure close to that of **2**, bears this out. This trend is to be expected. The further along MEP4→2 the molecule is before it takes its "jump", the more the gradient of the molecule is going to resemble that of MEP2→1. In other words, at the initial step from s=1.963 bohr-amu$^{1/2}$ the gradient is more like that of MEP4→2 than the initial step from s=1.985 bohr-amu$^{1/2}$. The latter is more of a composite of the gradients for MEP4→2 and MEP2→1. Also, if the molecule is starting at a lower energy on MEP4→2 it has less of the reaction swath to follow than if it had "jumped" from a point of higher energy.

IV. CONCLUSIONS

The results reported here have shown that the simple Berry pseudorotational model is not followed in the case of PH_4F. In fact, we obtain two maxima and one minimum as opposed to the two maxima and two minima that are expected. The pseudorotational path is that of **1** ⇔ **2** ⇔ **4** with a branching region occurring between **2** and **4**. In the narrow branching region, the molecule can proceed from **4** to **1** without going through **2**. As shown by the BP's from this region, the molecule will stay close to MEP4→2 and MEP2→1, but does not necessarily need to be on these paths. While these results are interesting in their own right, an analysis of the dynamics of this system is needed to fully understand this complex reaction. This will be reported in a later paper.

V. ACKNOWLEDGEMENTS

This work was supported by grants from the Air Force Office of Scientific Research (90-0052) and the Petroleum Research Fund, administered by the American Chemical Society. Calculations were performed on a DECstation 3100 and an IBM RS 6000/530, both obtained with the assistance of grants from AFOSR. Many helpful discussions with Drs. Michael Schmidt, Larry Davis, and Larry Burggraf are gratefully acknowledged.

VI. APPENDIX

To convert from cartesian coordinate space to internal coordinate space one uses a **B** matrix such that

$$r_i = \sum_j B_{ij} x_j .$$

This **B** matrix is formally defined as a m x 3N (m = 3N - 6 for nonlinear or 3N-5 for linear molecules) matrix where N is the number of atoms in the system. In practice, however, **B** is a square matrix [21]. This allows **B** to be inverted so we can also convert from internal coordinate space to cartesian coordinate space. Therefore, a cartesian Hessian matrix is converted to an internal Hessian matrix using

$$h_r = (B^{-1})^t h_x B^{-1}$$

and also an internal Hessian matrix is converted to a cartesian Hessian matrix using

$$B^t h_r B = h_x .$$

Formally, the internal Hessian matrix should be m x m, but in practice, because the **B** matrix is square, the internal Hessian matrix is 3N x 3N. The extra elements in the matrix are associated with the rotations and translations, and should be exactly zero, but quite often are not. In the purification method, these very small non-zero elements are made to be exactly zero. Then, when the internal Hessian matrix is converted back to the cartesian Hessian matrix, the five or six frequencies associated with the rotations and

translations are zero. In effect, the purification separates the rotations and translations from the vibrations.

REFERENCES

1. Berry RS (1960) J.Chem.Phys. 32:933
   Mislow K (1970) Acc.Chem.Res. 3:321

2. Gordon MS, Windus TL, Burggraf LW, Davis LP (1990) J.Am. Chem. Soc. 112:7167

3. Windus TL, Gordon MS, Burggraf LW, Davis LP J.Am.Chem. Soc. accepted

4. Deiters JA, Holmes RR (1990) J.Am.Chem.Soc. 112:7197
   Magnusson E (1990) J.Am.Chem.Soc. 112:7940
   Breidung J, Thiel W, Kormornicki A (1988) J.Phys.Chem. 9 2:5603

5. Strich A, Veillard A (1973) J.Am.Chem.Soc. 95:5574

6. Keil F, Kutzelnigg W (1975) J.Am.Chem.Soc. 97:3623

7. McDowell RS, Streitwieser A, Jr. (1985) J.Am.Chem.Soc. 107: 5849

8. Wang P, Zhang Y, Glaser R, Reed AE, Schleyer PvR, Streitwieser A (1991) J.Am.Chem.Soc. 113:55

9. Francl MM, Pietro WJ, Hehre WJ, Binkley JS, Gordon MS, DeFrees DJ, Pople JA (1982) J.Chem.Phys. 77:3654
   Hehre WJ, Ditchfield R, Pople JA (1972) J.Chem.Phys. 56: 2257
   Ditchfield R, Hehre WJ, Pople JA (1971) J.Chem.Phys. 54: 724
   Hariharan PC, Pople JA (1973) Theoret.Chim.Acta 28:213

10. Krishnan R, Binkley JS, Seeger R, Pople JA (1980) J.Chem. Phys. 72:650
    McLean AD, Chandler GS (1980) J.Chem.Phys. 72:5639

11. Pople JA, Binkley JS, Seeger R (1976) Int.J. Quantum Chem. S10:1

12. Baldridge KK, Gordon MS, Steckler R, Truhlar DG (1989) J.Phys.Chem. 93:5107

13. Miller WH, Handy NC, Adams JE (1980) J.Chem.Phys. 72:99

14. Boatz JA, Schmidt MW implemented in GAMESS in 1986. See reference 15.

15. Schmidt MW, Baldridge KK, Boatz JA, Jensen JH, Koseki S,

Gordon MS, Nguyen KA, Windus TL, Elbert ST (1990) QCPE Bulletin 10:52

16. Frisch MJ, Binkley JS, Schlegel HB, Raghavachari K, Melius CF, Martin RL, Stewart JJP, Bobrowicz FW, Rohlfing CM, Kahn LR, DeFrees DJ, Seeger R, Whiteside RA, Fox DJ, Fleuder EM, Pople JA Carnegie Mellon Quantum Chemistry Publishing Unit Pittsburgh PA 15213

17. Ugi I, Ramirez F (1972) Chem.Br. 8:198
Kutzelnigg W, Wasilewski J (1982) J.Am.Chem.Soc. 104:953
Wang P, Agrafiotis DK, Streitwieser A, Schleyer PvR (1990) J.Chem.Soc.,Chem.Comm. 201

18. Hoffman DK, Nord RS, Ruedenberg K (1986) Theor.Chim.Acta 69:265
Valtazanos P, Ruedenberg K (1986) Theor.Chim.Acta 69:281

19. Kraus WA, DePristo AE (1986) Theor.Chim.Acta 69:309
Baker J, Gill PMW (1988) J.Comp.Chem. 9:465
Shida N, Almlöf JE, Barbara PF (1989) Theor.Chim.Acta 76:7

20. One of the reviewers has noted that an alternative explaination is "that the BP's, being non-symmetric, follow neither the downhill B_2 or A_1 modes per se, but must first jump over a small region of hypersurface which is higher in energy. Depending on the PIP, this may be a small or a large first step.

21. Wilson EB, Jr., Decius JC, Cross PC (1955) Molecular Vibrations, McGraw-Hill Book Company, Inc. New York Toronto London

TABLE I: Total (hartree) and Relative[a] Energies (kcal/mol) for PH_4F Isomers.

Level	Axial	Equatorial	Apical
A	-442.43020 (0.0)	-442.41264 (11.0)	-442.37744 (33.1)
B	-442.49316 (0.0)	-442.47829 (9.3)	-442.43822 (34.5)
C	-442.91968 (0.0)	-442.90455 (9.5)	-442.86447 (34.6)

a. Energies relative to the axial isomer are given in parentheses.

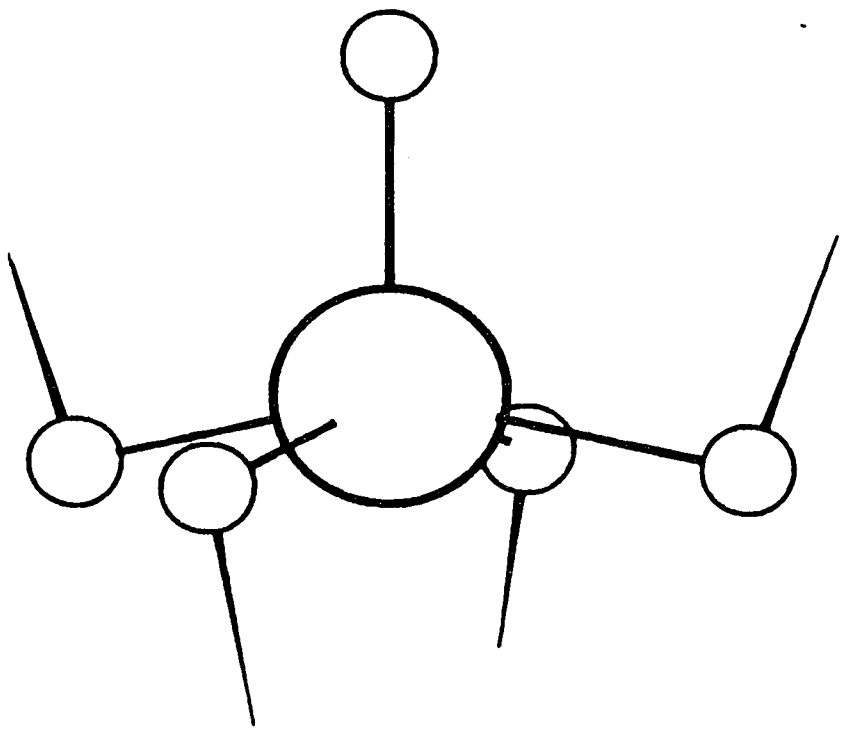

Figure 1: Imaginary normal mode for square pyramidal SiH_5^-.

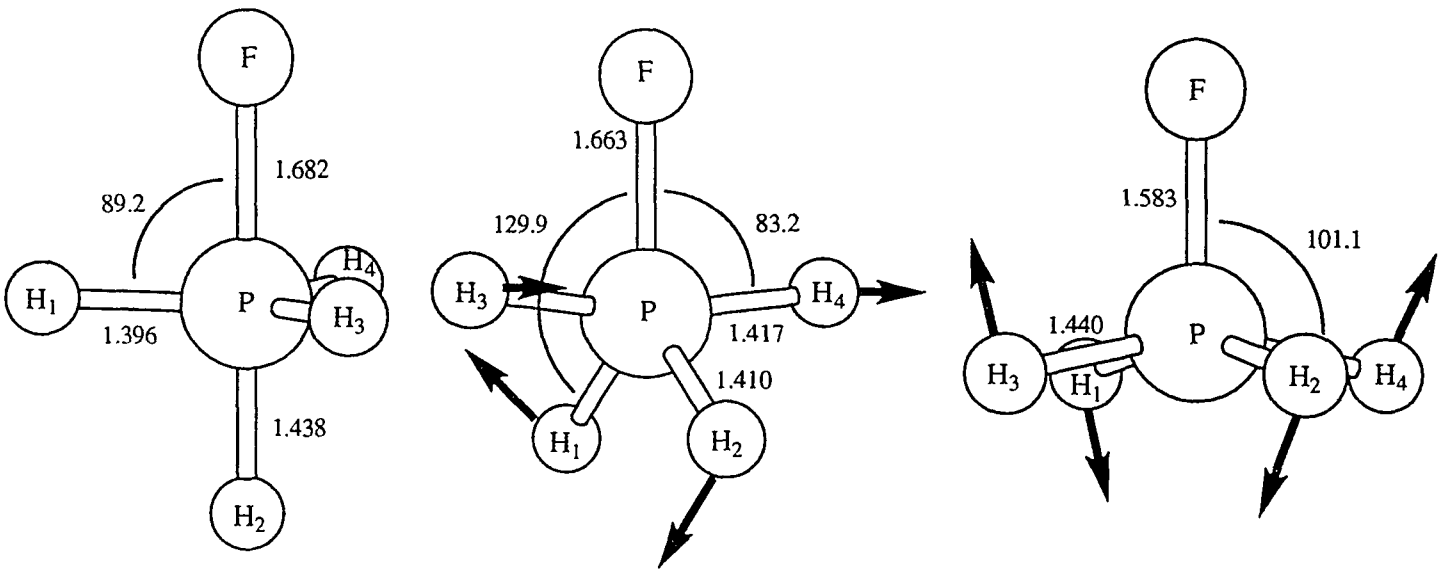

1
C_{3v}

2
C_{2v}, 298i

4
C_{4v}, 1084i

Figure 2: MP2/6-311G(d,p) structures. Imaginary frequencies in cm^{-1} are given for transition states. Bond lengths are in Angstroms and bond angles are in degrees.

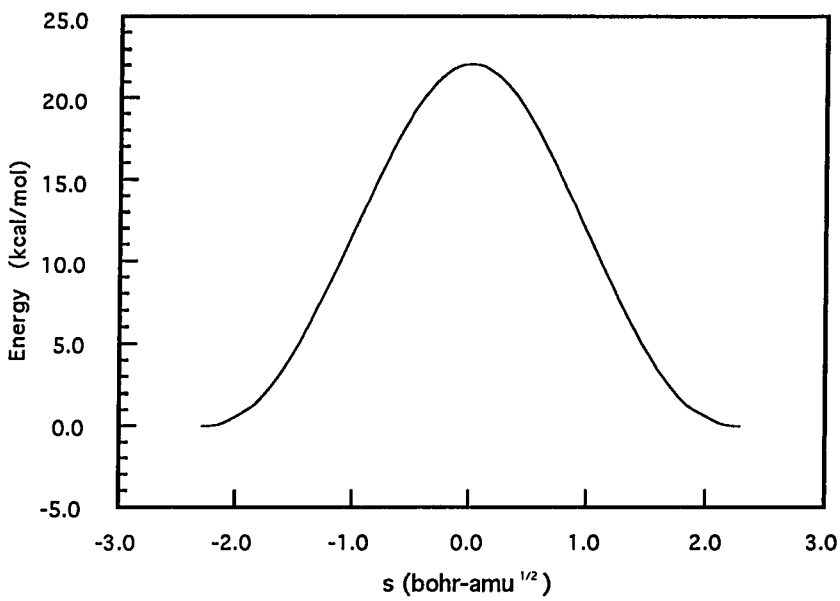

Figure 3: PH_4F IRC from F apical, tetragonal energy vs. reaction coordinate, energy is relative to structure 2; energy unit is kcal/mol.

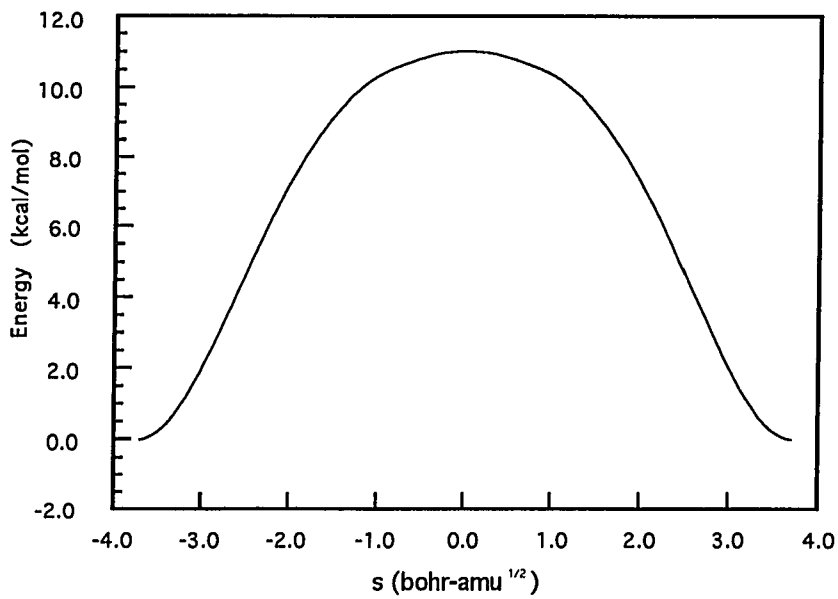

Figure 4: PH_4F IRC from F equatorial, trigonal bipyramidal energy vs. reaction coordinate; energy unit is kcal/mol.

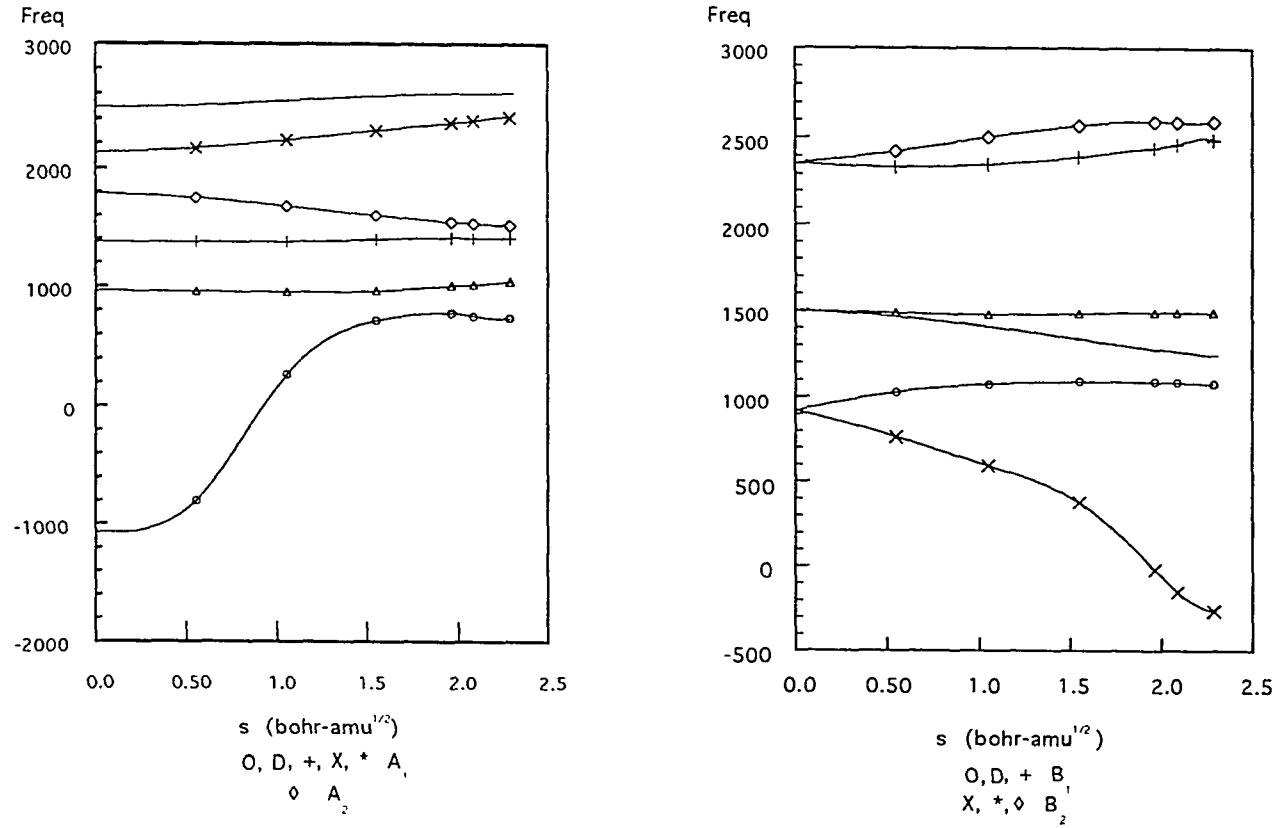

Figure 5: a. PH_4F pseudorotation from C_{4v} structure generalized harmonic frequencies - A_1 and A_2 generalized normal modes; b. PH_4F pseudorotation from C_{4v} structure generalized harmonic frequencies - B_1 and B_2 generalized normal modes.

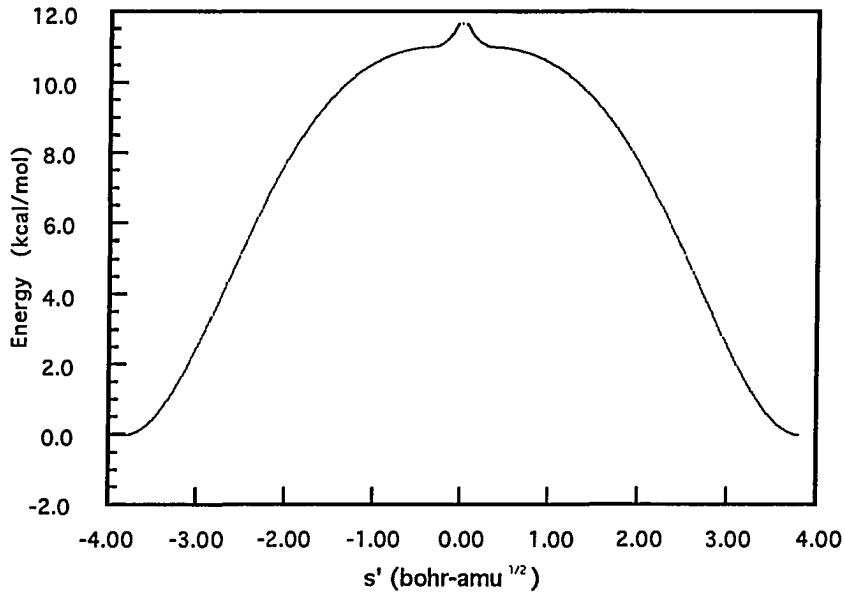

Figure 6: PH_4F IRC from s=1.963 bohr-amu$^{1/2}$, energy vs. reaction coordinate; energy unit is kcal/mol.

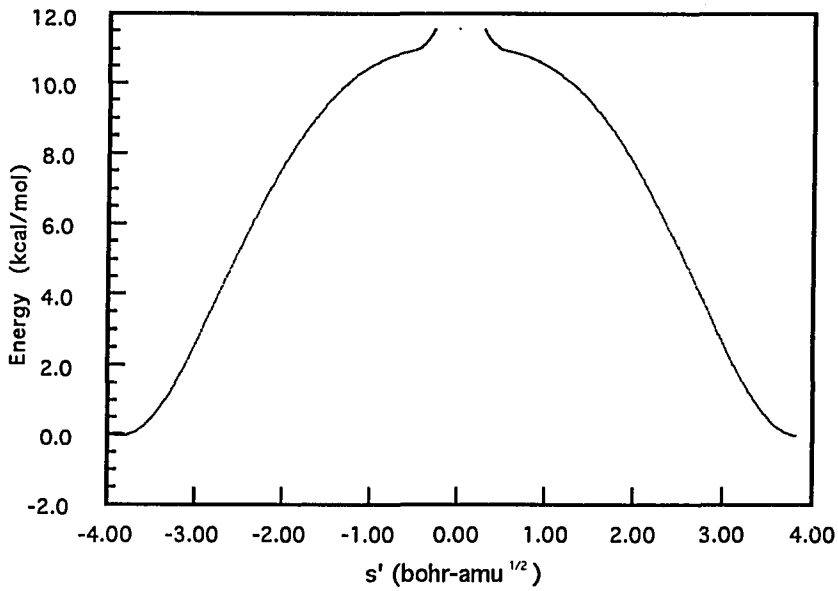

Figure 7: PH_4F IRC from s=1.985 bohr-amu$^{1/2}$, energy vs. reaction coordinate; energy unit is kcal/mol.

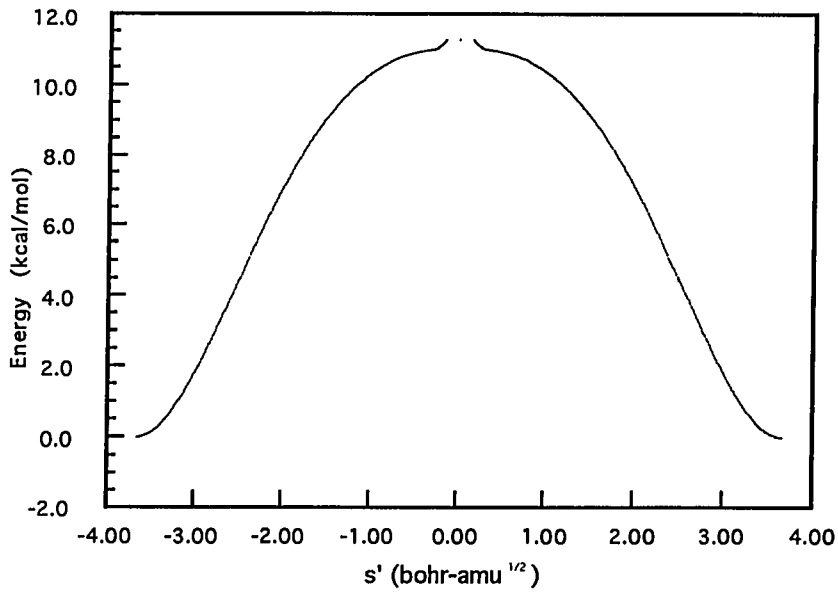

Figure 8: PH_4F IRC from s=2.086 bohr-amu$^{1/2}$, energy vs. reaction coordinate; energy unit is kcal/mol.

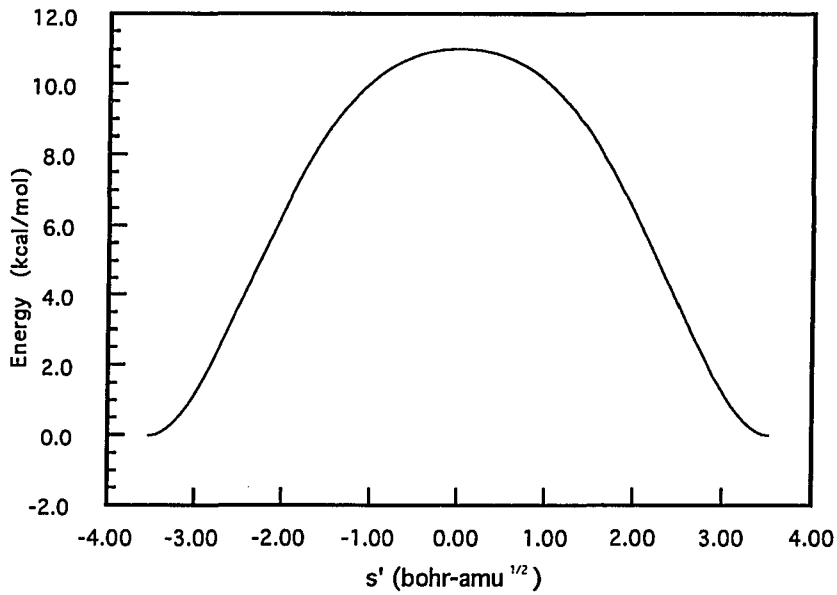

Figure 9: PH_4F IRC from s=2.286 bohr-amu$^{1/2}$, energy vs. reaction coordinate; energy unit is kcal/mol.

PAPER 4: THEORETICAL STUDY OF PSEUDOROTATION OF PENTACOORDINATED SILICON ANIONS: $SiH_{5-n}X_n^-$ (X= F, Cl)

Theoretical Study of Pseudorotation of Pentacoordinated Silicon Anions: $SiH_{5-n}X_n^-$ (X = F, Cl)

Theresa L. Windus, Mark S. Gordon
Department of Chemistry
Iowa State University
Ames, IA 50011

Larry P. Davis
Air Force Office of Scientific Research
Bolling AFB, DC 20332

Larry W. Burggraf
Air Force Institute of Technology
Engineering Physics Department
Wright-Patterson Air Force Base, Ohio 45433

submitted to *J. Am. Chem. Soc.*

ABSTRACT

A thorough *ab initio* investigation of the pseudorotation of the pentacoordinated silicon anions $SiH_{5-n}X_n^-$ (X = F, Cl; n = 0-5) is reported. The minima and maxima of each of the systems under consideration are characterized and intrinsic reaction coordinate (IRC) calculations are performed to connect the maxima with corresponding minima. These systems are compared to the Berry pseudorotation mechanism and earlier calculations on these systems.

INTRODUCTION

The existence and stabilities of pentacoordinated silicon anions of the type $SiX_nY_{5-n}^-$ play a major role in the mechanism for nucleophilic displacement reactions occurring at silicon and the resulting stereochemistry of these displacements.[1] We have been investigating these issues for the last several years[2-4] at both the semi-empirical and *ab initio* levels, and our previous work has been quite successful in predicting which pentacoordinated species should be present in gas-phase reactions of this type[2b].

In this paper we systematically explore the trends in the relative energetics for the various stationary points (both stable and otherwise) on the potential energy surfaces of the series $SiH_nX_{5-n}^-$, X = F or Cl. In particular, we compare our results with the early *ab initio* work of Willhite and Spialter[5] (WS) who conducted studies on the $SiH_nX_{5-n}^-$ series that modeled the electronegative atom "X" by increasing the hydrogen nuclear charge. Our results, coupled with previous theoretical and experimental work, offer new insights into stereochemical structure of pentacoordinated silicon compounds. This in turn will have a strong impact on silicon-centered nucleophilic substitution reactions based on the nature of the Berry pseudorotational[6] potential energy surfaces of the pentacoordinated silicon intermediates.

The rest of the paper is organized in the following

manner. First the computational methods used will be discussed. Then, the results and discussion for each individual system will be presented, followed by the conclusions.

COMPUTATIONAL METHODS

All *ab initio* structure, energy and frequency calculations were performed with locally modified versions of GAUSSIAN88,[7] GAUSSIAN90[8] or the San Diego Supercomputer Center version of GAUSSIAN92[9]. Structures were obtained at the restricted Hartree-Fock RHF/6-31G(d)[10] (level A), the RHF/6-31++G(d,p)[11](level B), and the second-order Moller-Plesset[12] perturbation MP2/6-31++G(d,p) (level C) levels of theory. Level A was used to probe the surface of the species in question. Levels B and C were used to explore the importance of using diffuse functions and correlation to determine the structures of these species. As will be discussed later, several of these species require the use of the higher levels of theory to obtain even qualitatively correct results.

Energy information was obtained at each of the optimization levels. In addition, fourth-order Moller-Plesset[13] perturbation (MP4) energies were calculated at each of the optimization levels using the 6-31++G(d,p) basis set.

Second derivatives of the energy with respect to the nuclear coordinates were calculated at each stationary point at all levels of theory used for geometry determination. The Cartesian force constant matrix (hessian) was diagonalized to determine frequencies and zero point energies and to verify that minima and transition states had zero and one imaginary

frequency, respectively.

Intrinsic reaction coordinate[14] (IRC) calculations were performed with the GAMESS[15] *ab initio* program to "connect" maxima with corresponding minima. The specific methods used were Euler with stabilization (ES2),[16] fourth order Runge-Kutta (RK4),[17] and second order Gonzalez-Schlegel (GS2).[18] ES2 and RK4 were used before the new addition of GS2 to GAMESS. We have found that the GS2 method is much more cost effective than the other two methods for IRCs, since larger step sizes can be used while still having an IRC that is converged. All IRCs are calculated at level B unless otherwise specified.

The notation level2/basis2//level1/basis1 is used throughout this paper to represent energetics calculated at level2 using basis2 at the structure optimized at level1 using basis1.

RESULTS AND DISCUSSION

Reactants

All of the reactants of the reaction

$$SiX_nY_{4-n} + Y^- \rightarrow SiX_nY_{5-n}^- \qquad (1),$$

where X, Y = H, F, or Cl, have been optimized within the appropriate point group symmetry at the C level of theory. The geometric information for these structures are available as supplementary information. The energetics for these systems at the MP4/6-31++G(d,p)//MP2/6-31++G(d,p) level are given in Table I.

Interestingly, the exothermicities for these reactions are, in general, quite large. Indeed, it was demonstrated in a previous paper that many of the pentacoordinated species that are predicted to be quite stable can be detected in flowing afterglow.[2b]

Investigations are currently in progress to determine the extent that the energy gained upon formation of the pentacoordinated anion can be transferred into the pseudorotational motion.[19] Most of the pentacoordinated isomers are below the dissociation limits calculated here; however, a few of them are not. These particular systems will be discussed in the sections to follow.

SiH_5^-

We have previously reported[3] our results for this system. The structures in Figure 1 and energetics in Table

II are included for completeness. As reported in our previous study, the results agree well with those of other workers.[5,20] This system follows the typical Berry pseudorotational process[6] which is shown in Scheme 1.

Scheme 1 for SiX_5^-:

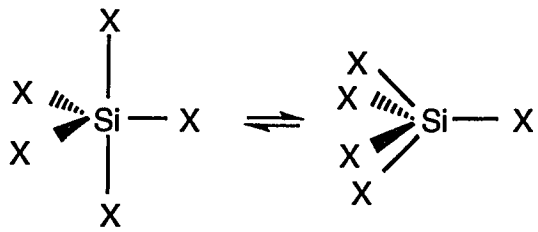

1 **2**

The (local minimum) trigonal bipyramid (TB), **1**, will pseudorotate to an equivalent structure (assuming that all ligands are equivalent) through the square pyramidal (SPY) transition state (TS), **2**. This is accomplished by "freezing" one of the equatorial ligands as the pivot atom. Then the other two equatorial ligands move away from each other to become axial and the axial ligands move toward each other to become equatorial.

The IRC for this system has been calculated to definitively prove the reaction pathway. The RK4 method was used at the MP2/6-31G(d) level for this purpose.[3] Since the reaction of $SiH_4 + H^-$ produces 15.8 kcal/mol of energy, we

are currently investigating through the use of semi-classical trajectories how much of this energy can be transferred into the pseudorotational motion and if there is any mode-specificity in the reaction.

SiH_4F^-

We have also previously reported[4] our results on the SiH_4F^- system. The structures in Figure 2, geometries in Table III, and energetics in Table II are included here for completeness. This system, unlike the SiH_5^- system, displays characteristics that are much different from that of the "typical" Berry pseudorotation. Scheme 2 represents the expected Berry pseudorotation mechanism for a monosubstituted system.

Scheme 2 for SiH_4X^-:

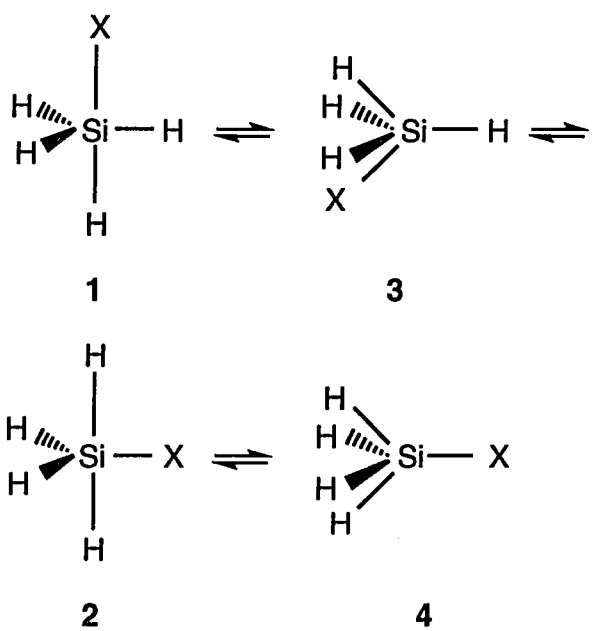

Our previous work showed that at levels B and C the structures corresponding to the F equatorial in the TB (**2**) and the F basal in the SPY (**3**) have coalesced into one structure: a TS (**2**).[4] The pseudorotational process is therefore much different than would be expected.

This type of system has been further explored on the PH_4F surface which displays the same type of topology.[21] The IRCs calculated for the PH_4F system show that the IRC for TS structure **4** leads to the second TS **2**. The IRC starting from TS **2** leads to the minimum structure **1**. The net effect of this overall pathway is to interconvert two equivalent structures **1** without passing through any other minima.

Several others have explored some of the structures of SiH_4F^-.[2b-c,5,22] Deiter and Holmes[22a-b] (DH) have used RHF/6-31+G(d) to study the two TB structures in the "ideal" Berry mechanism. The minimum structure **1** was optimized at the RHF/6-31+G(d) level. The largest difference with our results is an 0.047 Å longer Si-F distance. All other parameters are very similar to those reported here, but no hessians were calculated. In another study[22c], DH have constrained the angles of the TB "minima" to the idealized angles. Using this method, they found a structure corresponding to the idealized minimum structure **2** which we have characterized as a TS. Again, no hessians were calculated.

Gronert and coworkers[22d] calculated geometries at the RHF/3-21G(d) level for the two TB "minima". The structure for **1** is again very similar to the one reported here, except that the Si-F bond length is longer by 0.063 Å in the present work. There is a reported structure for the "minimum" **2**, however no hessians were calculated. The relative energies of the two isomers were calculated to be 0 and 8 kcal/mol for **1** and **2**, respectively. This is similar to our results of 0.0 and 7.2 kcal/mol for **1** and **2**, respectively.

Gordon and coworkers[2a-b] have also calculated the geometries and energetics of the two "minimum" structures. These were calculated at our level A and, therefore, agree well with our level A results. However, as we have shown[4], a larger basis set and/or correlation must be used for this system in order to characterize the stationary points correctly. The dissociation limits relative to structure **1** are very similar to those obtained in our previous study.

The studies of Wilhite and Spialter (WS[5]) are compared with our results in Figure 3.a. The predictions of WS were obtained using a model in which the electronegative element is modeled by forcing a hydrogen nuclear charge to be +1.1. This gives the hydrogen an electronegativity of 2.9 on the Pauling scale.[23] This is not the electronegativity of hydrogen, fluorine or chlorine (H=2.20, F=3.98, and Cl=3.16). However, it was intended to give a reasonable, qualitative

representation of the electronegativity effects (or inductive effects) of a model X.

The plots in Figure 3 are intended to be qualitative. The curvatures shown are obtained using a smoothing algorithm between the points, so they should not be used to infer any actual curvature information. To understand the nature of each structure (i.e. whether it is a minimum or TS), the reader is referred to the figure corresponding to each individual compound.

Our results for SiH_4F^- differ from those of WS (Figure 3.a.). Nevertheless, using the simple WS model, **3** and **2** are predicted to be quite close in energy and **4** is the highest energy conformer. So, even for this complex system, the WS results provide qualitatively correct information.

SiH_4Cl^-

Structures for this system are given in Figure 4 and the energetics are listed in Table II. Only two of the four possible geometrical isomers were found on this surface. As has been noted in earlier research,[2b,24] chlorine favors an axial or apical position in these pentacoordinated systems. When chlorine is placed in the equatorial or basal positions, the geometry optimization leads either to dissociation of the chlorine from the rest of the molecule or to one of the known structures.

For structure **1**, the Si-Cl bond length is quite long

(3.271 Å) compared to that in the SiH_3Cl molecule (2.062 Å). This isomer is bound by a charge-dipole interaction, rather than by strong covalent forces. The Mulliken charge on Cl is -0.9 showing that most of the negative charge lies with Cl. Structure **1** is only 4.6 kcal/mol more stable than $SiH_4 + Cl^-$ and 57.3 kcal/mol more stable than $SiH_3Cl + H^-$, as seen in Table I.

The TS structure **2** is quite high in energy. At the MP4/6-31++G(d,p)//MP2/6-31++G(d,p) level it is 32.1 kcal/mol relative to structure **1** (Table II). While structure **2** appears to be the typical Berry TS connecting two equivalent Cl equatorial TB's (see Scheme 2), following the IRC from this TS leads to dissociation of the chlorine anion. This, again, is related to the resistance of chlorine to occupying an equatorial position in the TB structure and is not surprising given that only 4.6 kcal/mol is needed to dissociate Cl^- from structure **1**.

Only a few studies have been performed for the pseudorotation of this system.[2b,5,22] DH have performed optimizations for the two idealized minima by constraining the angles to those of the idealized molecule.[22c] In this fashion, they found a minimum corresponding to the chlorine equatorial in the TB. However, no hessians were performed. Gordon and coworkers[2b] performed level A optimizations for structure **1** and found results that are similar to those in this work with the molecule being described as a charge-

dipole complex. They did not find a structure with the chlorine equatorial.

Although SiH_4Cl^- is included in Figure 3a, a comparison of the present work with that of WS is not revealing since two of the necessary structures are not found in the present study.

$SiH_3F_2^-$

The ideal Berry pseudorotation for disubstituted systems is shown in Scheme 3.

Scheme 3 for $SiH_3X_2^-$:

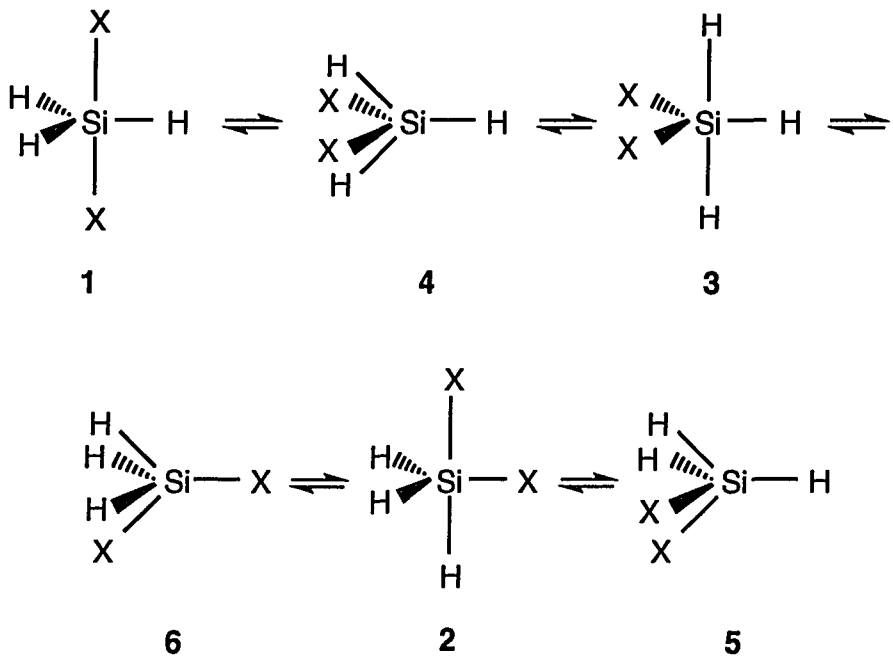

Structures for this system are given in Figure 5 and Table IV and relative energetics are given in Table II. All of the structural data is at the C level except that of structure **4**. Despite extensive searches at theory levels B and C, this structure was only found at theory level A. By examining the energetic and geometric differences between **3** and **4**, it is quite easy to see that structures **3** and **4** have coalesced to a distorted minimum at higher levels of theory. As an example, the H_1-Si-H_2 angle for structure **3** is 93.5° at level C and the same angle for structure **4** is 94.9° at level A. Also, at MP4/6-31++G(d,p)//RHF/6-31G(d), **3** and **4** have virtually the same energy. The distortions caused by the fluorines seem to cause some structures (**3** and **4** in this case) to coalesce. This is analogous to the results of the SiH_4F^- system. However, this time the coalesced structure is a minimum on the surface instead of a transition state.

Since structures **3** and **4** have coalesced to a minimum, there is a question about how structure **1**, the lowest minimum on this part of the potential energy surface (PES), can isomerize to structure **3**. The most likely possibilities are (a) the existence of a high energy (non-dissociative) route, possibly through a higher order saddle point or (b) the lack of a non-dissociative route from **1** to **3**.

It is interesting that **5**, with two adjacent fluorines in the base, is only at +11 kcal/mol relative to **1**, whereas in SiH_4F^-, **4** is +22 kcal/mol relative to its minimum. Also, it

is interesting that **6**, which can be thought of as a hybrid between **4** in SiH_4F^- and **5** in $SiH_3F_2^-$ is approximately halfway (16 kcal/mol) between the two in energy. So, F seems to prefer the basal to the apical position when given the choice, but prefers TB to SPY even more (i.e. the two coalesce when possible).

All of the previous work for this system has been restricted to the minimum energy structures(**1-3**).[2b,5,22a,25] Most of these studies concentrated on the lowest energy minimum structure, **1**. Exceptions are the DH study that constrained the isomers to ideal TB angles[22a], the Fujimoto and coworkers study[25b-c], and the WS results. As mentioned previously, the DH study included no hessians. Fujimoto and coworkers obtained geometries at our level B and MP4/6-31++G(d,p) energies for structures **1** and **2**. Their geometries and energetics are very similar to the level C calculations presented in this work. All of the calculations relating to structure **1** agree fairly well with the results presented here.

As can be seen in Figure 3.b., the model WS results follow our qualitative trends very well. Interestingly, the WS results again show that structures **4** and **3** are very close in energy where the present results show structure **4** to be "missing". This is similar to the WS results for the SiH_4F^- system.

$SiH_3Cl_2^-$

Structures for this system are given in Figure 6 and Table IV and relative energetics are given in Table II. All of the structural data is at the C level except that of structure **4** which is at level A. The $Si-Cl_1$ distance of **4** is very long (3.559 Å) and this structure was only found when the C_{2V} symmetry normally associated with this TS was relaxed. This structure did not survive further exploration at levels B and C.

It should be noted that the structure with both chlorines equatorial (**3**) was not found, as would be expected due to the preference of chlorine to bond axially.[24] Optimization of **3** led to **1** with no barrier. The same apical preference very likely explains the absence of structure **4**.

Interestingly, structure **2** disappears at level B but not at levels A and C. Geometry optimizations at level B were performed starting at the optimized structures from both A and C. In each case, Cl_2 (here the subscript refers to atom numbering in Figure 6) tended to dissociate. Even at level C, the $Si-Cl_2$ bond length is quite large (3.170 Å). Still, it is stable to dissociation of Cl^- by 7.2 kcal/mol. The charge on Cl is -0.9, suggesting that **2** is an ion-dipole complex.

By examining the hydrogen bond lengths in the two $SiH_3X_2^-$ sytems (Table IV), it is quite clear that the

hydrogen bonds in the fluorine substituted systems are longer than those in the analogous chlorine systems. One explanation for this is that since the flourines tend to bind more tightly to the silicon than do the chlorines, and since the five bonds in these compounds are formed using just eight electrons (four pairs), the hydrogens must bind less tightly (and therefore, lengthen the bond) to compensate. This trend can also be seen in the SiH_4X^- system, but the comparison is not as clear here, since the chlorine system is missing two of the structures, the minimum (**1**) is a charge dipole complex, and the transition state structure (**4**) is above the Cl^- dissociation limit.

The energy of the TS structure **6** relative to **1** is above the limit for Cl^- dissociation from **1** by about 1 kcal/mol. The IRCs for this structure show that **6** is indeed a TS associated with structure **2** in one direction (this is the direction shown in Figure 6). However, in the other direction (that would lead to structure **3** in the classical Berry pseudorotation: see Scheme 3) the IRC instead leads to dissociation of Cl^-. This clearly illustrates the instability of chlorine when it is equatorial. This also suggests that there may be a slight barrier of 1.0 kcal/mol for the more or less on edge attack of Cl^- on SiH_3Cl.

Transition state structure **5** is only slightly below the Cl^- dissociation limit from **1** (1.8 kcal/mol). An IRC calculation shows that **5** is the transition state structure

connecting two equivalent **2**s. However, even this result is slightly different from that proposed by Berry. There is large "precessional motion" of H_2 and Si (refer to Figure 6) that is not generally associated with Berry pseudorotation. This "motion" is largely associated with the closing (or opening in the direction opposite to that shown) of the H_2-Si-H_1 angle. However, the end results are the same. Further examples of this behavior are presented below.

The only previous calculations known for this system were performed on the three minima.[2b,22a] The study by DH again assumes ideal angles for the TB structures. This works well for structure **1**, but is obviously not correct for structures **2** and **3**. The study of Damrauer and coworkers[2b] are at our theory level A and only for structure **1**. The limit for dissociation of Cl^- is essentially identical to the results presented here.

The results of WS (in Figure 3.b.) again follow the trend of the present results with the exception of structures **3** and **4**. One might expect that the behavior predicted by the WS model would be closer to our chlorine predictions than those of fluorine, since the electronegativity of the WS model (2.9) is much closer to that of chlorine than fluorine. However, chlorine is much larger than fluorine and therefore should show appreciable steric effects. This is, no doubt, the reason for chlorine not having many of the typical isomers of these systems. Another contributing factor is

that the Si-F bond is also much stronger than the Si-Cl bond, so Si-Cl is floppier and easier to dissociate.

$SiH_2F_3^-$

The ideal Berry pseudorotation pathway for trisubstituted systems is given in Scheme 4.

Scheme 4 for $SiH_2X_3^-$:

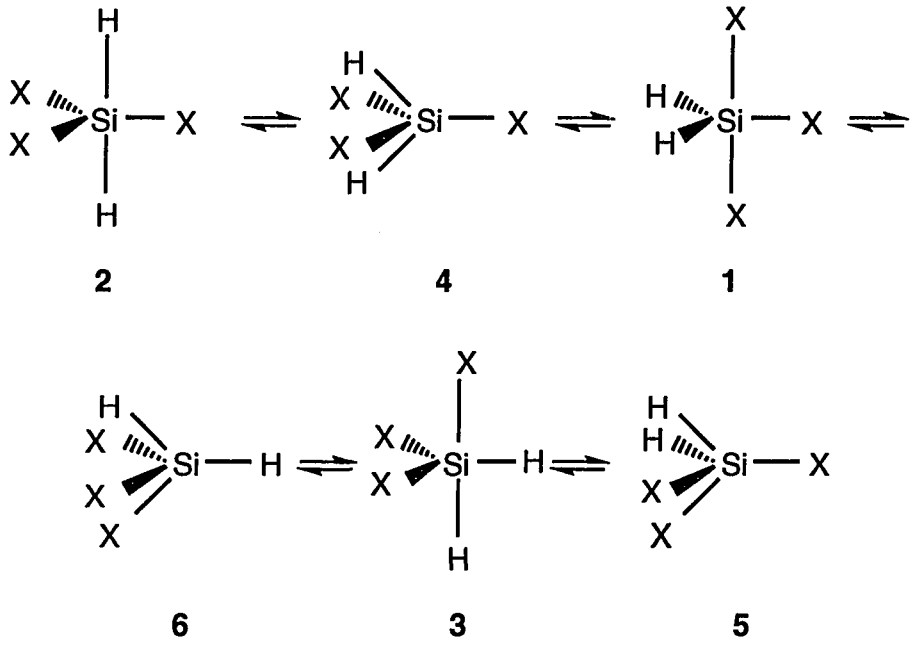

Geometries for this system are given in Figure 7 and Table V and relative energetics are given in Table II. All of the structural data is at the C level. This is the first system (other than SiH_5^-) where all of the classically expected structures are found at the highest level of theory.

All of the geometric parameters are fairly normal with no great surprises. This may account for finding all six of the structures at level C. However, note that at the highest level of theory, including zero point vibrational energies, the energy of **4**, the TS connecting **1** and **2**, is identical to that of **2**, so these two structures could well coelesce at even higher levels of theory. The same may be said for **6** and **3**.

IRCs from the TSs verify that the Berry pseudorotation mechanism is indeed followed for this system. As was seen in the $SiH_3Cl_2^-$ system, the normal modes for **5** and **6** show a "precessional motion" where the F_2 for **5** and H_2 for **6** are involved in decreasing (or increasing) bond angles. Even, the silicon centers of these molecules participate in this "motion".

The energies of all $SiH_2F_3^-$ isomers are much lower relative to **1** than are those in the SiH_4F^- system. They are also lower in energy relative to **1** than are the isomers in $SiH_3F_2^-$ relative to its lowest isomer. Indeed, the energies seem to cluster closer together with increasing heavy atom substitution.

The only previous calculations for $SiH_2F_3^-$ were performed by DH[22a-b] and WS. DH examined only the minima (**1-3**) and since the TB structures are not very distorted from the ideal, the DH model of constraining the angles works fairly well for this system. Their relative energies are

within 1 kcal/mol of those presented here. In another study, DH have minimized structure **1**,[22a] and those predictions agree well with the current results (bond lengths agree to within 0.04 Å and angles agree to within 1°).

The predictions of the WS model (Figure 3.c.) are in reasonably good qualitative agreement with the more accurate calculations presented here. The main difference is the relative energetics of structures **6**, **3**, and **5** compared to **2** and **4**. It appears that the qualitative model is unable to reproduce the effects of moderate distortions, such as those predicted for structures of **6**, **3**, and **5** in the present work.

$SiH_2Cl_3^-$

Geometries for this system are given in Figure 8 and Table V and relative energetics are given in Table II. All of the structural data is at the C level. Interestingly, all of the classically expected structures for this system are found, and there are no long Si-Cl bonds as in the SiH_4Cl^- and $SiH_3Cl_2^-$ systems. Another interesting trend (shown in Table V) is that the angles in $SiH_2Cl_3^-$ are very similar to those in $SiH_2F_3^-$. The largest discrepancies are for the **1** isomers. There is quite a bit of distortion of the axial chlorines from linear (Cl_2-Si-Cl_2 = 171.6°). This can be atributed to the large size of the chlorines. As in $SiH_3X_2^-$, the hydrogen bonds of the flourine substituted system are longer than those of the analogous chlorine system.

The relative energies of all six structures are fairly low and are much lower than the Cl^- dissociation limit relative to **1**. As already noted for $SiH_2F_3^-$, structures **2** and **4** and structures **3** and **6** are very similar in energy and therefore each pair may ultimately coelesce. This is very easy to understand since the geometries are also very similar. The energetics are also clustering closer together for this system than those for the $SiH_3Cl_2^-$ and SiH_4Cl^- systems. This is the same trend seen for the flourine substituted systems.

IRC calculations confirm that the Berry pseudorotation mechanism is essentially followed in $SiH_2Cl_3^-$. Interestingly, the normal modes for **5** and **6** show large "motions" of Cl_2 (**5**), H_2 (**6**) and Si. These are the same type of "motions" that are seen in structures **5** and **6** of $SiH_2F_3^-$.

The only previous calculations on this system are those of DH[22a] and WS. Because the minima are not distorted very much from the ideal TB structure, the constrained results of DH give good relative energetics for the three minima, agreeing with the fully optimized results to within 2 kcal/mol for structure **2** and ~0 kcal/mol for structure **3**.

The comparison of the present work with that of WS is given in Figure 3.c. Our chlorine results suggest an even bigger differential between the energies of structures **6**, **3**, and **5** relative to those of structures **2** and **4** than is found for fluorine. As noted above, this is due to steric effects

of the chlorine and the different strengths of Si-F and Si-Cl bonds.

$SiHF_4^-$

The idealized Berry pseudorotation for tetrasubstituted systems is given in Scheme 5.

Scheme 5 for $SiHX_4^-$:

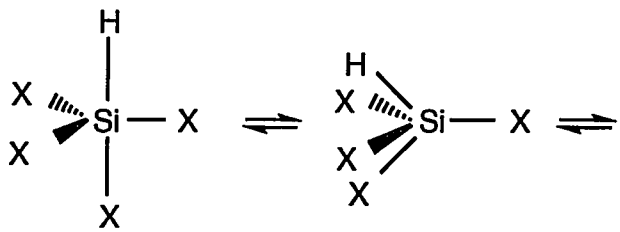

2 **4**

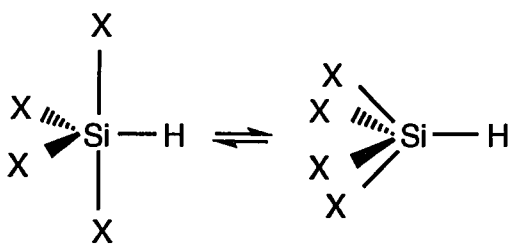

1 **3**

Structures for this system, which is the inverse of SiH_4F^-, are given in Figure 9 and Table VI and relative energetics are given in Table II. All of the structural data is at the C level. The four structures are not distorted very much from their "ideal" structures. Relative energies

are even smaller and more tightly clustered in this system than the previous fluorine substituted systems.

IRC calculations verify the Berry pseudorotation mechanism for this system. However, there is again additional "motion" in **4** that is not predicted by the Berry mechanism.

DH[22b] and WS provide the only previous calculations for $SiHF_4^-$. The relative energetics of the DH study are in excellent agreement with ours (differing by 0.1 kcal/mol) for the two minima.

The comparison with the WS results in Figure 3.d. show good relative agreement between the two methods. Our results for **3** are high energetically compared to the WS results, but the overall relative energies generally compare well. Also, note that in all cases, the WS model predicts less energy variation than is actually found until $SiHX_4^-$.

$SiHCl_4^-$

Structures for this system are given in Figure 10 and Table VI and relative energetics are given in Table II. All of the structural data is at the C level. As in the $SiH_2Cl_3^-$, there are no long Si-Cl bonds. The angles for this system are very close to those of the associated $SiHF_4^-$ system. Again, the largest difference occurs for the X_2-Si-X_2 angles which are ideally linear in the structures numbered **1**. Also, the hydrogen bond distances in $SiH_2F_3^-$ are consistently longer than those associated with $SiH_2Cl_3^-$.

The Berry pseudorotational mechanism is followed for this compound. Again, there is additional "motion" of Cl_2 and Si associated with **4** that is not predicted by the Berry mechanism. This has been a common thread among the species that are not fully substituted by the same ligand. Therefore, we propose a fine-tuning of the Berry mechanism in those cases for which the basal ligands are not the same. Then there is additional "motion" of the apical ligand in the SPY TS and possibly the central atom (silicon in this case). This does not occur, of course, when such motions are precluded by symmetry. Indeed the Berry mechanism presumes a degree of symmetry that precludes this "precessing" motion.

DH[22b] and WS provide the only previous computational results for $SiHCl_4^-$. DH predict **2** to be 2.2 kcal/mol higher in energy than we do.

Again, the comparison with the WS results (Figure 3.d.) appear to be fairly good. The one major difference is the relative energy of **3**. This may be related to the distortion of Cl_3 from the "ideal" structure. The bond length of $Si-Cl_3$ of 2.162Å is about 0.04Å longer than that of $Si-Cl_1$ and the $Cl_2-Si-Cl_3$ bond angle is about 8° smaller than that of $Cl_2-Si-Cl_1$.

SiF_5^-

Structures for this system are given in Figure 11 and relative energetics are given in Table II. All of the structural data is at the C level. The results are similar

to those discussed earlier for SiH_5^- (Scheme 1). Even the energetics of the two systems are similar, with an energy barrier of 2.2 kcal/mol for the SiH_5^- and 2.9 kcal/mol for the SiF_5^- pseudorotational mechanism. The trends in bond lengths are also similar for the two systems with $Si\text{-}X_{axial} > Si\text{-}X_{apical} > Si\text{-}X_{basal} > Si\text{-}X_{equatorial}$. One of the major differences between the two systems is the X^- dissociation limit. The addition of F^- to SiF_4 is exothermic by 72.3 kcal/mol (Table I), whereas the addition of H^- to SiH_4 is exothermic by only 15.8 kcal/mol.

An IRC calculation tracking the path from **2** to **1** verifies the Berry pseudorotational mechanism.

Many experimental studies have been performed on this SiF_5^- anion,[26] with several of them relating to the exchange mechanism of F^- in several different solutions.[26a-d] The anion has been observed in ion cyclotron resonance (ICR) experiments[26e-i] in small quantities. The F^- dissociation is estimated to be 60 ± 4 kcal/mol relative to **1**. This is approximately 12 kcal/mol less than the dissociation limit predicted in this study. IR and Raman studies have been performed in an argon matrix[26j-k] and in aqueous solution.[26l-m] The heat of formation has been determined to be less than or equal to -583 kcal/mol[26n] and relaxation times as a function of temperature have been determined.[26e] One X-ray structure has been determined for the $[(phenyl)CH_2N(methyl)_3][SiF_5]$ salt.[26o] The largest deviation

from TB for the anion was the F_{eq}-Si-F_{eq} angle (117.5°). Thermally corrected values of the bond lengths are 1.660 and 1.622Å for Si-F_{ax} and Si-F_{eq}, respectively. These correspond to the MP2/6-31++G(d,p) bond lengths of 1.694 and 1.657 Å for the Si-F_2 and Si-F_1 bond lengths of the free anion. This agreement is very good considering the amount of distortion observed in the crystal structure.

Several theoretical studies have been performed that relate to SiF_5^-.[5,22a,27] The ionization potential (IP) has been calculated using X_α theory;[27a-b] the dissociation of F^- has been studied by several workers;[27c-e] and the reaction $SiF_5^- + F^- \rightarrow SiF_6^{2-}$ has been studied using coupled Hartree-Fock perturbation theory (CHFPT) with a near Hartree-Fock limit basis set[27f] and using RHF/6-31++G(d,p) theory.[2b] Each of these studies only examined the minimum structure (**1**). All of the studies produced geometries that were 0.03-0.04 Å different in the bond lengths than those presented here. WS predicted a pseudorotation barrier of 2.94 kcal/mol which is in excellent agreement with our results. The calculated F^- dissociation energies agree to within 6 kcal/mol of our results. Interestingly, all the other calculated dissociation energies were higher than those presented here, even though the estimated experimental dissociation energy is approximately 12 kcal/mol lower than that predicted here.

$SiCl_5^-$

Structures for this system are given in Figure 12 and

relative energetics are given in Table II. All of the structural data is at the C level.

Most of the comments regarding SiF_5^- apply to this system as well. The same trend is found in bond lengths and energetics: the largest difference between this system and SiH_5^- and SiF_5^- is the dissociation energy. The exothermicity of Cl^- reacting with $SiCl_4$ (21.9 kcal/mol) is much closer to that of SiH_5^- (15.8 kcal/mol) than SiF_5^-(72.3 kcal/mol). This reflects the relative strengths of Si-Cl vs. Si-F bonds in these complexes.

An IRC calculation verifies the Berry mechanism for this system. Interestingly, the trend from monosubstitution to pentasubstitution of heavy atoms seems to be a stabilizing one. The more heavy elements (compared to H) that are present the more likely the system is to have all of the isomers predicted by the Berry model and the smaller the relative energetics are compared to the local minimum.

Several experiments have succeeded in finding evidence of $SiCl_5^-$. [28a,c] The compound has been observed spectroscopically in a solution of $(CH_3)NO_2$.[28a] It has also been investigated in an electron attachment study of tetrachlorosilane.[28c] Two groups have performed ICR experiments in an attempt to find evidence for the $SiCl_5^-$ anion with no success.[28b,26g] In the study by Sheldon and coworkers[28b], an SCF/6-21G optimization and hessian was performed, verifying that the TB structure was a minimum.

Using these results, they had hoped to successfully produce the anion, but their attempts were not successful.

The only other theoretical studies of $SiCl_5^-$ were X_α calculations of the electron attachment of $SiCl_5$,[27a-b] and the WS paper. The structure used for **1** in the X_a studies had bond lengths of 2.13 and 2.08 Å for the $Si-Cl_2$ and $Si-Cl_1$ bond distances respectively. The $Si-Cl_2$ distance is quite different from that predicted in our work (2.216Å). As mentioned in the SiF_5^- section, the WS relative energies are very similar to those presented here (0.3 kcal/mol difference for the relative energy of **2**).

SUMMARY OF ENERGETICS

Addition of F^- to silane is exothermic by more than 30 kcal/mol, while the addition of a chloride ion only reduces the energy by 4.6 kcal/mol. This reflects the fact that SiH_4F^- is a true trigonal bipyramidal structure, whereas SiH_4Cl^- is a weakly bound ion-dipole complex. Because a second Cl (in $SiH_3Cl_2^-$) occupies an axial position opposite the first Cl, the lowest energy arrangement of $SiH_3Cl_2^-$ is much more stable relative to $SiH_3Cl + Cl^-$, than is SiH_4Cl^- relative to dissociation of Cl^-. Interestingly, the dissociation of $SiH_nCl_{5-n}^- \rightarrow SiH_nCl_{4-n} + Cl^-$ is nearly constant for $n \leq 3$, as shown in Table 1. In contrast, the corresponding dissociations of $SiH_nF_{5-n}^-$ become monotonically more endothermic as n decreases.

Relative to X^- dissociation (X = H, F, Cl), the pseudorotation PES is much less demanding energetically for SiH_5^-, $SiH_3F_2^-$, $SiH_2X_3^-$, $SiHX_4^-$, and SiX_5^-. Indeed, the pseudorotation barriers for SiH_5^-, SiF_5^- and $SiCl_5^-$ are all $\leq$ 3 kcal/mol.

CONCLUSIONS

There are several general conclusions that can be drawn from this work.

1) There seems to be a trend that the more heavy elements (compared to H) that are substituted on the silicon the closer the potential energy surface is to an idealized Berry surface; that is the highly substituted structures do not distort very much from the ideal TB or SPY configuration. Also, structures that are expected in the Berry model tend to be found in highly substituted systems.

The highly substituted systems also seem to have lower relative energies that are clustered closer together than the less substituted systems. Therefore, they have lower pseudorotational barriers, and all of the minima on the surface should be easily accessible. They also have isomers and pseudorotation barriers that are much lower in energy than the dissociation limits.

2) The simple electronegativity model proposed by Wilhite and Spialter gives generally good results when compared to the accurate calculations presented here. The greatest differences arise for those structures that have large distortions (generally associated with size) from the "ideal" Berry model. This agreement is remarkable considering the time at which the WS calculations were performed and their simplified nature.

3) The systems that have all of the same ligands (i.e. SiX_5^-) have bond lengths that follow the trend $Si\text{-}X_{axial} > Si\text{-}X_{apical} > Si\text{-}X_{basal} > Si\text{-}X_{equatorial}$.

4) The hydrogen bond distances in a particular $SiH_{5-n}X_n$ (n=1-4) system are consistently longer in the fluorine substituted systems than in the analogous chlorine systems. This is believed to be related to the tighter binding of the fluorines to the silicon which in turn induces a "loosening" of the hydrogen binding and therefore lengthens the hydrogen bond.

5) Much of the information presented here may be useful in determining S_N2 reaction mechanisms. However, since most of the structures lie below the X^- dissociation limits, only dynamics calculations will be able to determine how much energy for the initial $SiY_{4-n}X_n + X^-$ reaction can be transferred in the pseudorotational motion.

6) We have calculated IRCs for the transition states to verify the minima associated with them. In many cases these led to the expected minima on the Berry pseudorotational path, but occasionally these led to dissociation. Where there is asymmetry in the ligands of a TS, we have found a "precessional motion" that is not expected in the traditional Berry mechanism and suggest that this type of motion be used as a "fine-tuning" of the mechanism.

ACKNOWLEDGMENT

The calculations in this work were performed on an IBM 3090/200E computer at North Dakota State University Computer Center, obtained in part with a joint study agreement with IBM, the Cray Y-MP at the San Diego Supercomputer Center, and RS/6000s provided by Iowa State University. Funding was provided from the Air Force Office of Scientific Research (92-0226) and a GAANN fellowship from the Department of Education to TLW.

SUPPLEMENTARY MATERIAL

Structural information for the reactants, Mulliken populations, and frequencies are available (5 pages). Ordering information is given on any current masthead page.

Geometric information for the reactants at the MP2/6-31++G(d,p) level:

SiH_4 (T_d) : Si-H = 1.475 Å; H-Si-H = 109.5°
SiH_3F (C_{3v}) : Si-H = 1.471 Å; Si-F = 1.639 Å; H-Si-F = 107.9°; H-Si-H = 111.0°
SiH_3Cl (C_{3v}) : Si-H = 1.471 Å; Si-Cl = 2.062 Å; H-Si-Cl = 108.5°; H-Si-H = 110.4°
SiH_2F_2 (C_{2v}) : Si-H = 1.463 Å; Si-F = 1.622 Å; H-Si-F = 108.4°; H-Si-H = 115.1°; F-Si-F = 107.8°
SiH_2Cl_2 (C_{2v}) : Si-H = 1.466 Å; Si-Cl = 2.047 Å; H-Si-Cl = 108.4°; H-Si-H = 112.8°; Cl-Si-Cl = 110.3°
$SiHF_3$ (C_{3v}) : Si-H = 1.451 Å; Si-F = 1.606 Å; H-Si-F = 110.8°; F-Si-F = 108.1°
$SiHCl_3$ (C_{3v}) : Si-H = 1.461 Å; Si-Cl = 2.035 Å; H-Si-Cl = 109.4°; Cl-Si-Cl = 109.6°
SiF_4 (T_d) : Si-F = 1.593 Å; F-Si-F = 109.5°
$SiCl_4$ (T_d) : Si-Cl = 2.028 Å; Cl-Si-Cl = 109.5°

Mulliken populations and frequencies (in cm^{-1}) for the pentacoordinated anions are given at the MP2/6-31++G(d,p) level unless otherwise specified. The numbering scheme is that of the figures in the paper:

SiH_5^-:
1 : Populations : Si = 0.6; H_1 = -0.3; H_2 = -0.4
Frequencies : E' : 556.8, 1069.9, 2030.9; A_2'' : 1032.1, 1594.2; E'' : 1242.6; A_1' : 1438.4, 2052.4
2 : Populations : Si = 0.6; H_1 = -0.3; H_2 = -0.2
Frequencies : B_2 : -432.3, 1459.9; E : 956.8, 1143.4, 1778.8; A_1 : 1015.4, 1951.0, 2152.0; B_1 = 1356.4

SiH_4F^-:
1 : Populations : Si = 0.6; H_1 = -0.2; H_2 = -0.3; F = -0.5
Frequencies : A_1 : 497.5, 1058.2, 1751.6, 2139.2; E : 510.9, 892.7, 1187.4, 2147.2
2 : Populations : Si = 0.7; H_1 = -0.2; H_2 = -0.3; F = -0.5
Frequencies : B_1 : -194.9, 988.9, 2028.9; A_1 : 528.1, 847.4, 1118.7, 1828.8, 2086.1; B_2 : 836.7, 1188.6, 1940.4; A_2 : 1195.3
4 : Populations : Si = 1.0; H_1 = -0.4; F = -0.5
Frequencies : B_2 : -797.2, 1501.4; E : 700.0, 1157.0, 1824.2; A_1 : 730.4, 1088.2, 1990.2; B_1 : 1400.0

SiH_4Cl^-:

1 : Populations : Si = 0.5; H_1 = -0.1; H_2 = -0.2; Cl = -0.9
Frequencies : A_1 : 84.0, 918.9, 2176.5, 2348.3; E : 244.7, 943.2, 1031.9, 2370.8

4 : Populations : Si = 0.7; H_1 = -0.3; Cl = -0.5
Frequencies : B_2 : -741.5, 1565.4; A_1 : 455.1, 1050.7, 2013.4; E : 635.7, 1150.9, 1867.4; B_1 : 1394.7

$SiH_3F_2^-$:

1 : Populations : Si = 0.9; H_1 = -0.3; F_2 = -0.5
Frequencies : E' : 279.9, 890.5, 2204.2; A_1' : 463.6, 2194.8; A_2'' : 629.7, 1140.8; E'' : 1040.3

2 : Populations : Si = 0.9; H_1 = -0.2; H_2 = -0.3; F_1 = -0.5; F_2 = -0.5
Frequencies : A'' : 322.4, 805.5, 1205.0, 2142.3; A' : 348.5, 559.6, 655.9, 782.2, 991.9, 1172.7, 1873.2, 2146.6

3 : Populations : Si = 0.9; H_1 = -0.3; H_2 = -0.3; F_1 = -0.5
Frequencies : A' : 110.9, 592.2, 689.0, 1048.4, 1251.0, 1908.7, 2035.4, 2085.4; A'' : 449.7, 747.5, 1008.4, 1100.2

4 : This is at the RHF/6-31G(d) level.
Populations : Si = 1.0; H_1 = -0.3; H_2 = -0.3; F_1 = -0.6
Frequencies : A_1 : -64.3, 651.2, 1041.5, 1882.4, 2114.5; B_1 : 689.0, 1236.7, 1964.7; B_2 : 697.6, 884.1, 1211.2; A_2 : 1143.7

5 : Populations : Si = 0.8; H_1 = -0.3; H_2 = -0.2; F_1 = -0.5
Frequencies : A'' : -314.5, 583.4, 922.3, 995.7, 1885.3; A' : 390.6, 694.4, 799.4, 1035.4, 1276.6, 2034.4, 2207.8

6 : Populations : Si = 1.0; H_1 = -0.3; H_2 = -0.3; F_1 = -0.5; F_2 = -0.5
Frequencies : A' : -362.8, 369.6, 636.5, 745.4, 1031.2, 1140.1, 1759.8, 2056.9; A'' : 728.4, 829.9, 1338.6, 2047.1

$SiH_3Cl_2^-$:

1 : Populations : Si = 0.6; H_1 = -0.1; Cl_2 = -0.6
Frequencies : E' : 179.0, 878.9, 2354.1; A_1' : 239.5, 2305.2; A_2'' : 267.0, 1011.9; E'' : 929.0

2 : Populations : Si = 0.6; H_1 = -0.1; H_2 = -0.2; Cl_1 = -0.3; Cl_2 = -0.9
Frequencies : A' : 47.6, 118.5, 539.8, 651.6, 917.9, 1002.9, 2214.8, 2388.4; A'' : 307.1, 651.8, 1048.8, 2420.5

4 : At the RHF/6-31G(d) level.
Populations : Si = 0.5; H_1 = -0.0; H_2 -0.1; Cl_1 = -1.0; Cl_2 = -0.4
Frequencies : A' : -62.1, 79.7, 512.4, 691.4, 950.8, 1028.3, 2318.8, 2475.3; A'' : 199.3, 709.2, 1071.3, 2509.3

5 : Populations : Si = 0.7; H_1 = -0.2; H_2 = -0.3; Cl_1 = -0.6; Cl_2 = -0.4
Frequencies : A' : -315.2, 176.0, 400.0, 475.2, 984.9, 1078.0, 1871.4, 2140.5; A'' : 616.9, 789.5, 1313.2, 2186.6

6 : Populations : Si = 0.7; H_1 = -0.2; H_2 = -0.3; Cl_1 = -0.6; Cl_2 = -0.4
Frequencies : A' : -315.2, 176.0, 400.0, 475.2, 984.9, 1078.0, 1871.4, 2140.5; A'' : 616.9, 789.5, 1313.2, 2186.6

$SiH_2F_3^-$:

1 : Populations : Si = 1.1; H_1 = -0.3; F_1 = -0.5; F_2 = -0.5
Frequencies : A' : 251.6, 371.8, 494.8, 698.8, 731.4, 898.4, 1144.4, 2219.2; A'' : 278.5, 663.3, 1078.3, 2236.2

2 : Populations : Si = 1.1; H_2 = -0.3; F_1 = -0.5
Frequencies : E' : 109.9, 742.0, 1056.1; A_2'' : 504.8, 2169.9; A_1' : 535.5, 2128.3; E'' : 993.7

3 : Populations : Si = 1.1; H_1 = -0.2; H_2 = -0.3; F_1 = -0.5; F_2 = -0.5
Frequencies : A' : 108.6, 429.9, 584.1, 712.5, 853.0, 1200.3, 2005.8, 2168.3; A'' : 335.9, 627.9, 821.2, 1083.7

4 : Populations : Si = 1.1; H_1 = -0.3; F_1 = -0.5; F_2 = -0.5
Frequencies : A_1 : -103.0, 525.7, 751.8, 978.6, 2135.1; B_2 : 201.4, 727.5, 1124.0; B_1 : 500.1, 885.6, 2179.8; A_2 : 1075.1

5 : Populations : Si = 1.2; H_1 = -0.3; F_1 = -0.5; F_2 = -0.5;
Frequencies : A' : 345.5, 483.3, 772.0, 821.8, 1020.6, 1343.7, 2101.7; A'' : -240.5, 499.4, 691.5, 1011.8, 1917.1

6 : Populations : Si = 1.0; H_1 = -0.3; H_2 = -0.2; F_1 = -0.5; F_2 = -0.5
Frequencies : A' : -105.1, 420.1, 552.5, 711.8, 793.9, 1124.5, 2053.2, 2208.6; A'' : 380.7, 708.8, 836.5, 1132.3

$SiH_2Cl_3^-$:

1 : Populations : Si = 0.6; H_1 = -0.1; Cl_1 = -0.3; Cl_2 = -0.6
Frequencies : A_1 : 135.0, 250.5, 499.0, 809.9, 2311.9; B_2 : 199.9, 317.7, 1041.1; B_1 : 216.4, 573.1, 2369.4; A_2 : 995.0

2 : Populations : Si = 0.7; H_2 = -0.1; Cl_1 = -0.5
Frequencies : E' : 62.8, 435.1, 960.4; A_1' : 295.9, 2217.2; A_2'' : 322.5, 2308.9; E'' : 931.2

3 : Populations : Si = 0.5; H_1 = -0.1; H_2 = -0.2; Cl_1 = -0.4; Cl_2 = -0.5
Frequencies : A' : 60.9, 250.7, 286.3, 433.0, 753.4, 1164.7, 2137.7, 2245.7; A'' : 204.7, 444.9, 661.5, 1060.1

4 : Populations : Si = 0.6; H_1 = -0.1; Cl_1 = -0.5; Cl_2 = -0.4
Frequencies : A_1 : -60.8, 282.6, 470.5, 898.9, 2227.7; B_2 : 108.6, 397.4, 1032.7; B_1 : 318.3, 842.7, 2320.0; A_2 : 994.2

5 : Populations : Si = 0.7; H_1 = -0.2; Cl_1 = -0.5; Cl_2 = -0.4
Frequencies : A' : 183.8, 254.6, 433.1, 501.9, 923.3, 1266.0, 2186.0; A'' : -175.7, 221.2, 499.2, 912.5, 2099.5

6 : Populations : Si = 0.5; H_1 = -0.2; H_2 = -0.1; Cl_1 = -0.4; Cl_2 = -0.5
Frequencies : A' : -60.8, 249.8, 291.2, 423.6, 708.5, 1119.9, 2165.1, 2264.7; A'' : 220.4, 441.2, 715.9, 1093.6

$SiHF_4^-$:

1 : Populations : Si = 1.2; H = -0.2; F_1 = -0.5; F_2 = -0.5
Frequencies : A_1 : 152.1, 445.9, 524.0, 753.4, 2261.2; B_1 : 256.5, 688.0, 877.4; A_2 : 371.4; B_2 : 420.4, 761.4, 1136.3

2 : Populations : Si = 1.3; H = -0.3; F_1 = -0.5; F_2 = -0.5
Frequencies : E : 129.2, 402.8, 810.5, 1034.7; A_1 : 462.4, 558.2, 740.5, 2151.9

3 : Populations : Si = 1.3; H = -0.3; F_1 = -0.5
Frequencies : B_2 : -110.0, 500.2; E : 401.5, 799.9, 944.9; B_1 : 429.6; A_1 : 477.4, 684.8, 2316.6

4 : Populations : Si = 1.3; H = -0.3; F_1 = -0.5; F_2 = -0.5; F_3 = -0.5
Frequencies : A' : -115.9, 360.4, 458.4, 543.3, 749.9, 798.8, 893.5, 2171.1; A'' : 246.2, 431.8, 791.9, 1144.7

$SiHCl_4^-$:

1 : Populations : Si = 0.4; H = -0.0; Cl_1 = -0.2; Cl_2 = -0.5
Frequencies : A_1 : 96.5, 245.9, 269.4, 476.3, 2329.5; B_1 : 157.3, 498.9, 670.1; A_2 : 208.8; B_2 : 243.0, 371.9, 1078.7

2 : Populations: Si = 0.6; H = -0.1; Cl_1 = -0.4; Cl_2 = -0.4
Frequencies : E : 78.2, 233.7, 501.0, 988.8; A_1 : 266.8, 296.3, 433.8, 2230.3

3 : Populations : Si = 0.4; H = 0.0; Cl_1 = -0.3
Frequencies : B_2 : -72.6, 240.1; E : 248.2, 474.1, 882.1; B_1 : 258.5; A_1 : 293.9, 406.5, 2343.2

4 : Populations : Si = 0.6; H = -0.3; Cl_1 = -0.4; Cl_2 = -0.3; Cl_3 = -0.4
Frequencies : A' : -73.2, 206.6, 259.5, 281.8, 452.4, 516.8, 810.3, 2257.4; A'' : 144.1, 251.0, 444.2, 1111.8

SiF_5^-:

1 : Populations : Si = 1.3; F_1 = -0.5; F_2 = -0.5
Frequencies : E' : 137.8, 429.5, 875.6; E'' : 393.7; A_2'' : 456.5, 829.3; A_1' : 529.8, 678.6

2 : Populations : Si = 1.3; F_1 = -0.4; F_2 = -0.5
Frequencies : B_2 : -99.5, 524.7; E : 289.0, 453.1, 853.5; A_1 : 424.6, 674.1, 865.6; B_1 : 443.5

$SiCl_5^-$:

1 : Populations : Si = 0.6; Cl_1 = -0.2; Cl_2 = -0.4
Frequencies :

2 : Populations : Si = 0.6; Cl_1 = -0.3; Cl_2 = -0.3
Frequencies : B_2 : -58.8, 244.8; E : 167.6, 272.3, 496.1; A_1 : 251.3, 366.2, 546.6; B_1 : 265.7

REFERENCES

1.a. Corriu,R.J.P.;Guerin,C. *J. Organomet. Chem.*, **1980**, *198*, 231.
b. Corriu,R.J.P.;Guerin,C. *Adv. Organomet. Chem.*, **1982**, *20*, 265.
c. Eisch,J.J.;Chiu,C.S. *J. Organomet. Chem.*, **1988**, *358*, C1-C5.
d. Mislow,K. *Acc. Chem. Res.*, **1970**, *3*, 321-331.

2.a. Gordon,M.S.;Davis,L.P.;Burggraf,L.W.;Damrauer,R. *J. Am. Chem. Soc.*, **1986**, *108*, 7889-93.
b. Damrauer,R.;Burggraf,L.W.;Davis,L.P.;Gordon,M.S. *J. Am. Chem. Soc.*, **1988**, *110*, 6601-6606.
c. Davis,L.P.;Burggraf,L.W.;Gordon,M.S. *J. Am. Chem. Soc.*, **1988**, *110*, 3056-3062.
d. Davis,L.P.;Burggraf,L.W.;Gordon,M.S. *Int. J. Quantum Chem.*, **1992**, *44*, 691-698.
e. Gordon,M.S.;Carroll,M.T.;Davis,L.P.;Burggraf,L.W. *Comp. Mat. Sci.*, **1993**,*1*, 161-168.

3. Gordon,M.S.;Windus,T.L.;Burggraf,L.W.;Davis,L.P. *J. Am. Chem. Soc.*, **1990**, *112*, 7167-7171.

4. Windus,T.L.;Gordon,M.S.;Burggraf,L.W.;Davis,L.P. *J. Am. Chem. Soc.*, **1991**, 4356-4357.

5. Willhite, D.L.; Spialter, L. *J. Am. Chem. Soc.* **1973**, *95*, 2100-04.

6.a. Berry, R.S. *J. Chem. Phys.* **1960**,*32*, 933-938.
b. Mislow,K. *Acc. Chem. Res.* **1970**, *3*, 321.

7. Frisch,M.J.;Head-Gordon,M.;Schlegel,H.B.;Raghavachari, K.;Binkley,J.S.;Gonzalez,C.;DeFrees,D.J.;Fox,D.J.; Whiteside,R.A.;Seeger,R.;Melius,C.F.,Baker,J.;Martin,R. L.;Kahn,L.R.;Stewart,J.J.P.;Fluder,E.M.;Topiol,S.;Pople, J.A. Gaussian, Inc., Pittsburgh PA.

8. M. J. Frisch, M. Head-Gordon, G. W. Trucks, J. B. Foresman, H. B. Schlegel, K. Raghavachari, M. Robb, J. S. Binkley, C. Gonzalez, D. J. Defrees, D. J. Fox, R. A. Whiteside, R. Seeger, C. F. Melius, J. Baker, R. L. Martin, L. R. Kahn, J. J. P. Stewart, S. Topiol, and J. A. Pople, Gaussian, Inc., Pittsburgh PA, 1990.

9. M. J. Frisch, G. W. Trucks, M. Head-Gordon, P. M. W. Gill, M. W. Wong, J. B. Foresman, B. G. Johnson, H. B. Schlegel, M. A. Robb, E. S. Replogle, R. Gomperts, J. L. Andres, K. Raghavachari, J. S. Binkley, C. Gonzalez, R.

L. Martin, D. J. Fox, D. J. Defrees, J. Baker, J. J. P. Stewart, and J. A. Pople, Gaussian, Inc., Pittsburgh PA, 1992.

10.a. Hehre,W.J. Ditchfield,R. Pople,J.A. *J. Chem. Phys.*, **1972**, *56*, 2257-2261.
b. Francl,M.M.;Pietro,W.J.;Hehre,W.J.;Binkley,J.S. Gordon,M.S.;DeFrees,D.J.; Popel,J.A. *J.Chem.Phys.* **1982**,*77*,3654-3665.
c. Gordon,M.S. *Chem.Phys.Lett.* **1980**,*76*,163-168.
d. Ditchfield,R.;Hehre,W.J.;Pople,J.A. *J. Chem. Phys.*, **1971**, *54*, 724-728.
e. Hariharan,P.C.;Pople,J.A. *Theor. Chim. Acta*, **1973**, *28*, 213-222.

11. Frisch,M.J.;Pople,J.A.;Binkley,J.S. *J.Chem.Phys.* **1984**,*80*,3265.

12.a. Carsky,P.;Hess,B.A.;Schaad,L.J. *J. Comp. Chem.*, **1984**, *5*, 280-287.
b. Pople,J.A.;Binkley,J.S.;Seeger,R. *Int.J.Quantum Chem.* **1976**,*S10*,1-19

13. Krishnan,R.;Frisch.M.J.;Pople,J.A. *J.Chem.Phys.* **1980**,*72*,4244.

14. Fukui,K. *Acc. Chem. Res.*, **1981**, *14*, 363.

15. Schmidt,M.W.;Baldridge,K.K.;Boatz,J.A.;Elber,S.T.; Gordon,M.S.;Jensen,J.H.;Koseki,S.;Matsunaga,N.;Nguyen,K. A.;Su,S.;Windus,T.L.;Dupuis,M.;Montgomery,J.A. Jr. accepted *J. Comp. Chem.*

16.a. Ishida,K.;Morokuma,K.;Kormornicki,A. *J. Chem. Phys.*, **1977**, *66*, 2153.
b. Schmidt,M.W.;Gordon,M.S.;Dupuis,M. *J. Am. Chem. Soc.*, **1985**, *107*, 2585.

17. Baldridge,K.K.;Gordon,M.S.;Steckler,R.;Truhlar,D.G. *J. Phys. Chem.*, **1989**, *93*, 5107.

18.a. Gonzalez,C.;Schlegel,H.B. *J. Phys. Chem.*, **1990**, *94*, 5523.
b. Gonzalez,C.;Schlegel,H.B. *J. Phys. Chem.*, **1991**, *95*, 5853.

19. Bintz,K.;Thompson,D.L.;Windus,T.L.;Gordon,M.S. in progress

20.a. Burggraf,L.W.; Davis,L.P.;Gordon,M.S. *Topics Phys. Organomet. Chem.* **1989**, *3*, 75

b. Reed,A.E.;Schleyer,P.R. *Chem. Phys. Lett.*, **1987**, *133*, 553-561.
c. Frolov,Y.L.;Shevchenko,S.G.;Voronkov,M.G. *J. Organomet. Chem.* **1985**, *292*, 159-166.
d. Vitkovskaya,N.M.;Mantsivoda,V.B.;Moskovkaya,T.E.; Voronkov, M.G. *Int. J. Quantum Chem.*, **1980**, *17*, 299-305.
e. Keil,F.;Ahlrichs,R. *Chem. Phys.*, **1975**, *8*, 384-390.

21. Windus,T.L.;Gordon,M.S. *Theor. Chim. Acta*, **1992**, *83*, 21-30.

22.a. Deiters,J.A.;Holmes,R.R. *J. Am. Chem. Soc.*, **1990**, *112*, 7197-7202.
b. Deiters,J.A.;Holmes,R.R. *J. Am. Chem. Soc.*, **1987**, *109*, 1686-1692.
c. Deiters,J.A.;Holmes,R.R.;Holmes,J.M. *J. Am. Chem. Soc.*, **1988**, *110*, 7672-7681
d. Gronert,S.;Glaser,R.;Streitwieser,A. *J. Am. Chem. Soc.*, **1989**, *111*, 3111-3117.

23.a. Cottrell,T.L.;Sutton,L.E. *Proc. Roy. Soc., Ser. A*, **1951**, *207*, 48.
b. Hurley,A.C. *Proc. Roy. Soc., Ser. A*, **1953**, *218*, 333.

24. Holmes,R.R. *Pentacoordinated Phosphorus-Structure and Spectroscopy*, American Chemical Society: Washington, D.C., 1980; Vol I, ACS Monograph No. 175.

25.a. Magnusson,E. *J. Am. Chem. Soc.*, **1993**, *115*, 1051-1061.
b. Fujimoto,H.; Yabuki,T.;Tamao,K.;Fukei,K.; *Theochem*, **1992**, *92*, 47-61.
c. Fujimoto,H.;Arita,N.;Tamao,K. *Organometallics*, **1992**, *11*, 3035-3041.

26.a. Gel'mbol'dt,V.O. *Koord. Khim.*, **1989**, *15*, 1501-1503.
b. Marat,R.K.;Janzen, A.F. *Can. J. Chem.*, **1977**, *55*, 3845-3849.
c. Gibson,J.A.;Ibbott,D.G.;Janzen,A.F. *Can. J. Chem.*, **1973**, *51*, 3203-3210.
d. Parpiev,N.A.;Maslennikov,I.A. *Usb. Khim. Zh.*, **1968**, *12*, 6-9.
e. Reynhardt,E.C.;Froneman,S. *J. Magn. Reson.*, **1988**, *80*, 268-279.
f. Saes,L.H.;Brongersma,H.H.;Van d'Hart,W.J. *Symp. Proc. - Int. Symp. Plasma Chem, 7th,* Volume 4,**1985**, ed. Timmermans,C.J.; Eindhoven, pp. 1355-1359.
g. Larsen,J.W.;McMahon,T.B. *J. Am. Chem. Soc.*, **1985**, *107*, 766.
h. Larsen,J.W.;McMahon,T.B. *J. Am. Chem. Soc.*, **1983**, *105*,

2944.
i. Larsen,J.W.;McMahon,T.B. *J. Am. Chem. Soc.*, **1982**, *104*, 5848.
j. Jacox,M.E. *J. Phys. Chem. Ref. Data*, **1984**, *13*, 945-1068.
k. Ault,B.S. *Inorg. Chem.*, **1979**, *18*, 3339.
l. Kleboth,K. *Montash. Chem.*, **1970**, *101*, 357-361.
m. Kleboth,K. *Montash. Chem.*, **1968**, *99*. 1177-1185.
n. Thynne,J.C.J.;MacNeil,K.A.G. *Inorg. Chem.*, **1970**, *9*, 1946-1947.
o. Schomburg,D.;Krebs,R. *Inorg. Chem.*, **1984**, *23*, 1378.

27.a. Gutsev,G.L.;Boldyrev,A.I. *Zh. Neorg. Khim.*, **1981**, *26*, 2353-2357.
b. Gutsev,G.L.;Boldyrev,A.I. *Chem. Phys.*, **1981**, *56*, 277-283.
c. Sliznev,V.V.;Solomonik,V.G. *Mol. Strukt.*, **1990**, 38-47.
d. Gel'mbol'dt,V.O. *Zh. Neorg. Khim.*, **1989**, *34*, 231-232.
e. O'Keefe,M. *J. Am. Chem. Soc.*, **1986**, *108*, 4341-3.
f. Kleboth,K.;Rode,B.M. *Montash. Chem.*, **1974**, *105*, 815-821.
g. Tossell,J.A.;Lazzeretti,P. *J. Chem. Phys.*, **1986**, *84*, 369-374.
h. Gutsev, G.L.; *J. Chem. Phys.*, **1993**, *99*, 3906-3912

28.a. Beattie,I.R.;Livingston,K.M.S. *J. Chem. Soc. A*, **1969**, *5*, 859-860.
b. Sheldon,J.C.; Hayes,R.N.;Bowie,J.H. *J. Am. Chem. Soc.*, **1984**, *106*, 7711-7715.
c. Moylan,C.R.;Christopher,R.;Green,S.B.;Brauman,J.I. *Int. J. Mass Spectrom. Ion Processes*, **1990**, *96*, 299-307.

Table I: MP4/6-31++G(d,p)//MP2/6-31++G(d,p) energetics of the $SiX_nY_{4-n} + Y^- \rightarrow SiX_nY_{5-n}^-$ reactions in kcal/mol.

	ΔE	ΔH[a]
$\underline{SiH_5}^-$		
$SiH_4 + H^-$	-18.1	-15.8
$\underline{SiH_4F}^-$		
$SiH_4 + F^-$	-31.5	-30.6
$SiH_3F + H^-$	-46.0	-42.5
$\underline{SiH_4Cl}^-$		
$SiH_4 + Cl^-$	-5.2	-4.6
$SiH_3Cl + H^-$	-61.2	-57.3
$\underline{SiH_3F_2}^-$		
$SiH_3F + F^-$	-52.1	-51.0
$SiH_2F_2 + H^-$	-61.3	-57.2
$\underline{SiH_3Cl_2}^-$		
$SiH_3Cl + Cl^-$	-22.4	-21.7
$SiH_2Cl_2 + H^-$	-76.9	-72.4
$\underline{SiH_2F_3}^-$		
$SiH_2F_2 + F^-$	-58.9	-54.4
$SiHF_3 + H^-$	-67.1	-62.7
$\underline{SiH_2Cl_3}^-$		
$SiH_2Cl_2 + Cl^-$	-23.4	-22.9
$SiHCl_3 + H^-$	-77.7	-73.0
$\underline{SiHF_4}^-$		
$SiHF_3 + F^-$	-65.2	-64.3
$SiF_4 + H^-$	-78.3	-73.7
$\underline{SiHCl_4}^-$		
$SiHCl_3 + Cl^-$	-22.8	-22.5
$SiCl_4 + H^-$	-78.1	-76.4
$\underline{SiF_5}^-$		
$SiF_4 + F^-$	-73.4	-72.3
$\underline{SiCl_5}^-$		
$SiCl_4 + Cl^-$	-22.2	-21.9

a. Includes zero point vibrational energy corrections.

Table II: Relative energies in kcal/mol. Values in parenthesis include zero point energies where the RHF frequencies are scaled by 0.89.

Structure	MP4/6-31++G(d,p)//RHF/6-31G(d)[a]		MP4/6-31++G(d,p)//RHF/6-31++G(d,p)[a]		MP4/6-31++G(d,p)//MP2/6-31++G(d,p)[a]	
SiH_5^-						
1					0.0	(0.0)
2					2.5	(2.2)
SiH_4F^-						
1	0.0	(0.0)	0.0	(0.0)	0.0	(0.0)
2	7.7	(7.4)	8.1	(7.5)	7.7	(7.2)
3	7.1	(6.6)				
4	22.2	(21.3)	23.2	(22.1)	23.2	(22.0)
SiH_4Cl^-						
1	0.0	(0.0)	0.0	(0.0)	0.0	(0.0)
4	33.4	(32.2)	33.2	(31.9)	33.4	(32.1)
$SiH_3F_2^-$						
1	0.0	(0.0)	0.0	(0.0)	0.0	(0.0)
2	9.0	(8.7)	9.5	(9.0)	9.2	(8.9)
3	11.6	(11.3)	13.2	(12.7)	12.8	(12.5)
4	11.1	(10.7)				
5	11.2	(10.6)	11.9	(11.2)	11.7	(11.1)
6	16.2	(15.5)	16.9	(16.0)	16.7	(15.9)
$SiH_3Cl_2^-$						
1	0.0	(0.0)	0.0	(0.0)	0.0	(0.0)
2	14.9	(14.5)			14.8	(14.5)
3						
4	14.4	(13.9)				
5	20.3	(19.8)	20.2	(19.7)	20.4	(19.9)
6	23.3	(22.7)	23.2	(22.6)	23.4	(22.7)
$SiH_2F_3^-$						
1	0.0	(0.0)	0.0	(0.0)	0.0	(0.0)
2	6.1	(6.2)	5.7	(5.8)	5.6	(5.7)
3	7.3	(7.1)	7.4	(7.1)	7.1	(6.9)
4	6.1	(6.1)	5.8	(5.9)	5.7	(5.7)
5	11.3	(10.7)	11.1	(10.4)	10.9	(10.3)
6	6.7	(6.5)	7.1	(6.9)	7.1	(6.8)
$SiH_2Cl_3^-$						
1	0.0	(0.0)	0.0	(0.0)	0.0	(0.0)
2	3.6	(3.9)	3.5	(3.9)	3.6	(3.9)
3	10.4	(10.3)	10.4	(10.4)	10.5	(10.4)
4	3.7	(4.0)	3.6	(3.9)	3.8	(4.0)
5	14.2	(13.8)	14.1	(13.8)	14.3	(14.0)
6	10.3	(10.2)	10.2	(10.2)	10.5	(10.4)

Table II: (cont.)

$SiHF_4^-$								
1	0.0	(0.0)	0.0	(0.0)	0.0	(0.0)		
2	4.3	(4.3)	4.1	(4.1)	4.0	(4.0)		
3	4.0	(4.1)	4.1	(4.1)	4.0	(4.1)		
4	5.0	(4.9)	4.9	(4.8)	4.9	(4.8)		
$SiHCl_4^-$								
1	0.0	(0.0)	0.0	(0.0)	0.0	(0.0)		
2	2.6	(2.8)	2.5	(2.8)	2.7	(2.9)		
3	6.5	(6.6)	6.4	(6.5)	6.6	(6.7)		
4	3.7	(3.8)	3.6	(3.8)	3.8	(4.0)		
SiF_5^-								
1	0.0	(0.0)	0.0	(0.0)	0.0	(0.0)		
2	3.0	(2.9)	3.0	(2.9)	3.0	(2.9)		
$SiCl_5^-$								
1	0.0	(0.0)	0.0	(0.0)	0.0	(0.0)		
2	3.2	(3.1)	3.1	(3.1)	3.2	(3.2)		

a. The notation level2/basis2//level1/basis1 denotes an energy for level 2 using basis2 at the geometry from basis1 at level1.

Table III: SiH_4F^- MP2/6-31++G(d,p) geometries. Bond lengths in angstroms and angles in degrees.

Structure	**1**	**2**	**4**
Si-F	1.813	1.764	1.692
Si-H_1	1.503	1.526	1.562
Si-H_2	1.575	1.541	
F-Si-H_1	88.4	127.5	101.4
F-Si-H_2	180.0	83.7	
H_1-Si-H_1	119.9	105.0	87.8
H_1-Si-H_2	91.6	93.8	
H_2-Si-H_2		192.6	

Table IV: $SiH_3X_2^-$ MP2/6-31++G(d,p) geometries. Bond lengths in Angstroms and angles in degrees.

	$SiH_3F_2^-$						$SiH_3Cl_2^-$				
Structure	**1**	**2**	**3**	**4**[a]	**5**	**6**	**1**	**2**	**4**[a]	**5**	**6**
Si-X_1		1.703	1.725	1.673	1.730	1.736		2.081	3.559	2.245	2.306
Si-X_2	1.784	1.764				1.685	2.333	3.170	2.118		2.144
Si-H_1	1.493	1.504	1.529	1.545	1.535	1.521	1.468	1.462	1.459	1.513	1.495
Si-H_2		1.549	1.523	1.527	1.494	1.561		1.496	1.488	1.484	1.547
X_1-Si-X_1			119.9	132.7	87.2					89.1	
X_1-Si-X_2		87.5				106.7		89.7	126.4		110.4
X_1-Si-H_1		121.1	120.0	88.1	86.2	87.3		111.6	60.2	85.1	86.9
X_1-Si-H_2		88.0	88.3	113.6	104.2	149.4		101.5	130.3	102.7	147.8
X_2-Si-X_2	180.0						180.0				
X_2-Si-H_1	90.0	89.0				99.4	90.0	69.5	107.2		99.0
X_2-Si-H_2		175.5				104.0		168.8	103.3		101.8
H_1-Si-H_1	120.0	117.6		170.3	86.2	161.1	120.0	118.8	120.4	88.6	161.9
H_1-Si-H_2		93.4	93.5	94.9	103.1	87.7		105.8	108.7	103.9	88.2
H_2-Si-H_2			173.0								

a. This structure is given at the RHF/6-31G(d) level: see text.

Table V: $SiH_2X_3^-$ MP2/6-31++G(d,p) geometries. Bond lengths in Angstroms and angles in degrees.

	$SiH_2F_3^-$						$SiH_2Cl_3^-$					
Structure	**1**	**2**	**3**	**4**	**5**	**6**	**1**	**2**	**3**	**4**	**5**	**6**
Si-X_1	1.674	1.714	1.695	1.728	1.717	1.712	2.099	2.198	2.158	2.232	2.230	2.183
Si-X_2	1.749		1.728	1.691	1.667	1.717	2.291		2.271	2.149	2.114	2.239
Si-H_1	1.487		1.501	1.497	1.521	1.516	1.465		1.485	1.472	1.498	1.492
Si-H_2		1.498	1.523			1.493		1.473	1.497			1.483
X_1-Si-X_1		120.0	123.8	135.5	86.0	137.5		120.0	125.4	133.7	87.0	134.3
X_1-Si-X_2	90.9		88.1	112.2	101.6	87.0	94.2		89.0	113.2	102.8	88.5
X_1-Si-H_1	116.9		118.0	88.1	85.7	87.3	114.9		117.2	87.8	84.5	87.0
X_1-Si-H_2		90.0	88.9			111.2		90.0	88.5			112.8
X_2-Si-X_2	179.2						171.6					
X_2-Si-H_1	89.6		89.8	95.0	103.2	164.4	88.2		87.9	95.5	102.1	168.4
X_2-Si-H_2			173.8			94.7			174.4			91.4
H_1-Si-H_1	126.1			170.0	92.1		130.3			169.0	93.4	
H_1-Si-H_2			96.3			100.9			97.7			100.2
H_2-Si-H_2		180.0						180.0				

Table VI: $SiHX_4^-$ MP2/6-31++G(d,p) geometries. Bond lengths in Angstroms and angles in degrees.

	$SiHF_4^-$				$SiHCl_4^-$			
Structure	**1**	**2**	**3**	**4**	**1**	**2**	**3**	**4**
Si-X_1	1.664	1.683	1.699	1.703	2.100	2.151	2.185	2.204
Si-X_2	1.720	1.699		1.659	2.254	2.194		2.107
Si-X_3				1.691				2.162
Si-H	1.481	1.498	1.473	1.495	1.466	1.479	1.468	1.474
X_1-Si-X_1	115.3	120.0	86.8	144.3	114.6	120.0	87.4	145.7
X_1-Si-X_2	90.3	89.2		107.8	91.7	90.6		107.1
X_1-Si-X_3				87.2				88.8
X_1-Si-H	122.4	90.8	103.8	87.7	122.7	89.4	102.4	85.8
X_2-Si-X_2	179.0				173.6			
X_2-Si-X_3				96.7				99.0
X_2-Si-H	89.5	180.0		99.7	86.8	180.0		99.6
X_3-Si-H				163.6				161.5

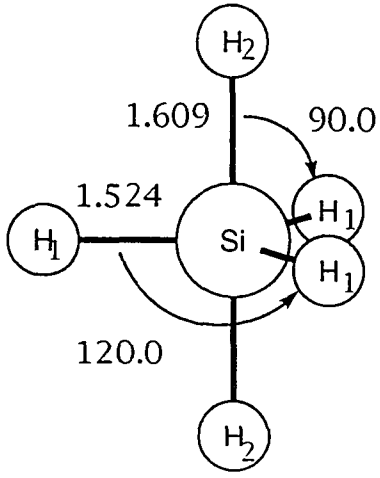

1

D_{3h}

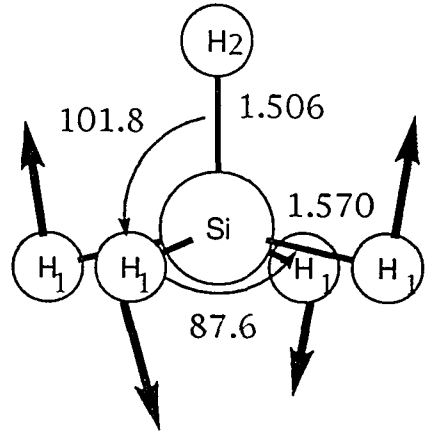

2

C_{4V}, 432i

Figure 1: SiH_5^- MP2/6-31++G(d,p) Structures. The imaginary frequency in cm^{-1} is given for the transition state.

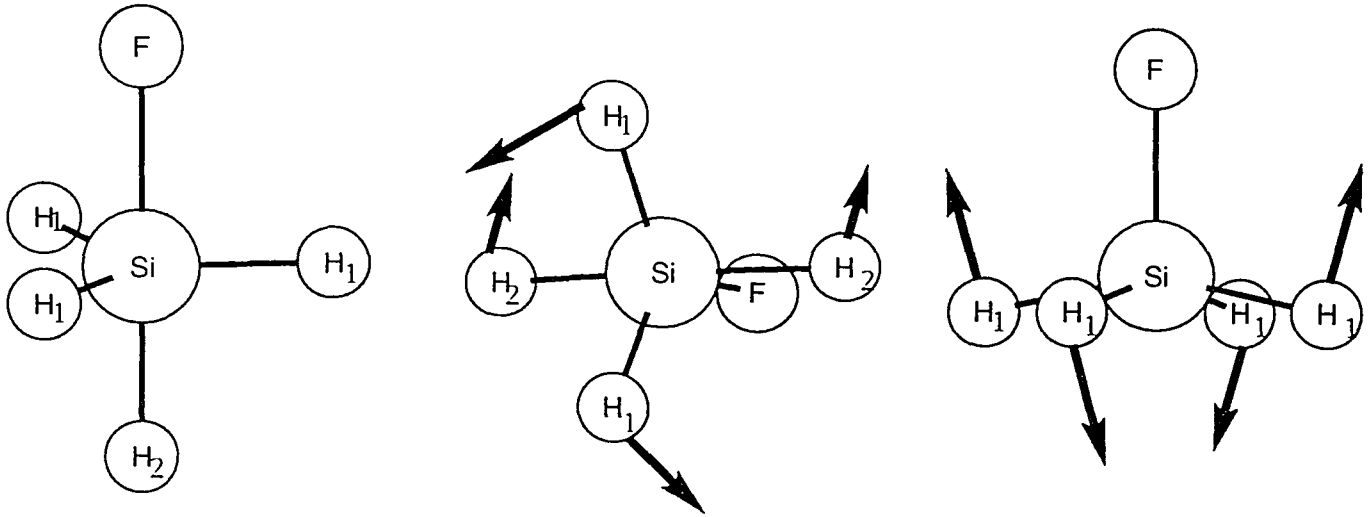

1

C_{3V}

2

C_{2V}, 194.9i

4

C_{4V}, 797.2i

Figure 2: SiH_4F^- MP2/6-31++G(d,p) Structures. Imaginary frequencies in cm^{-1} are given for transition states.

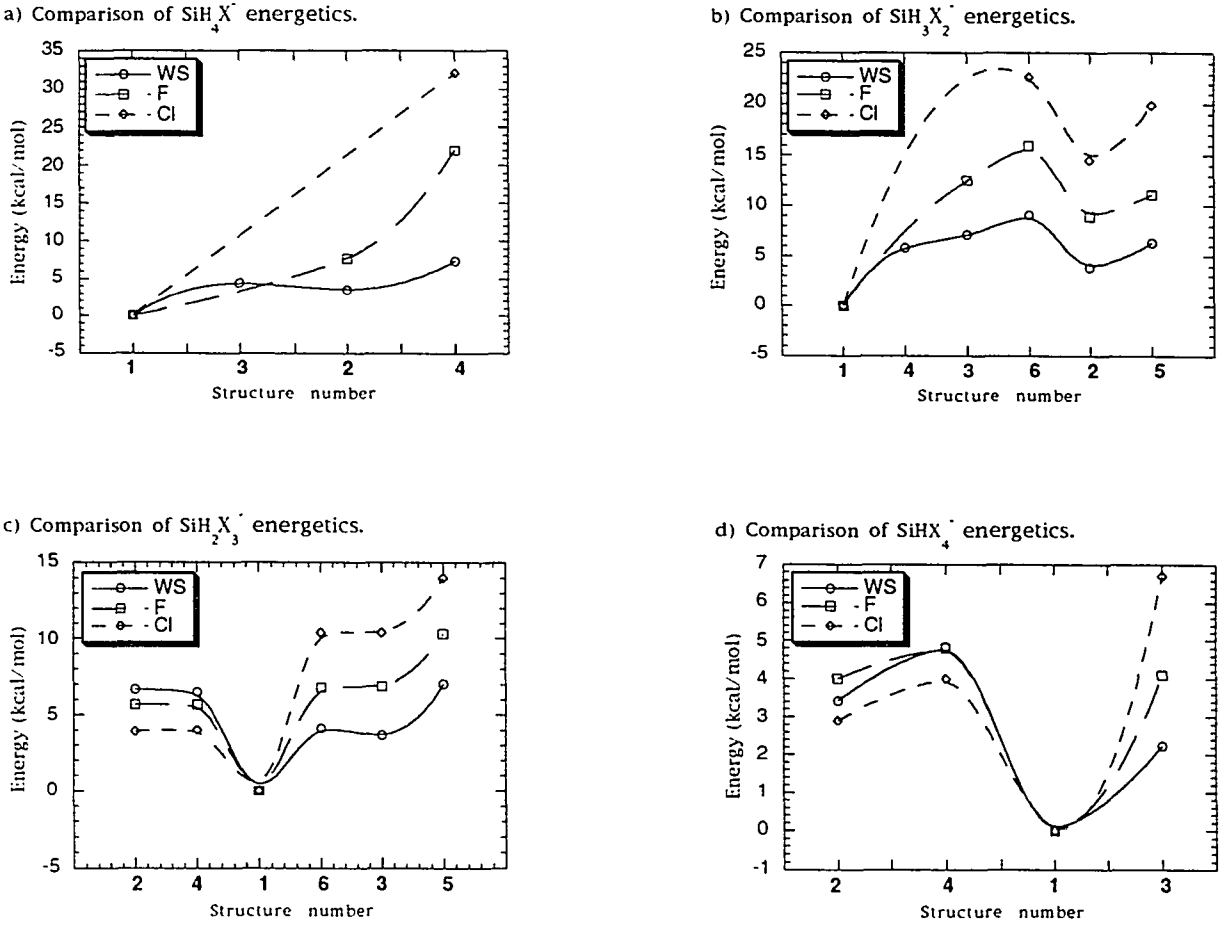

Figure 3: Comparisons of energetics between the present work and WS.

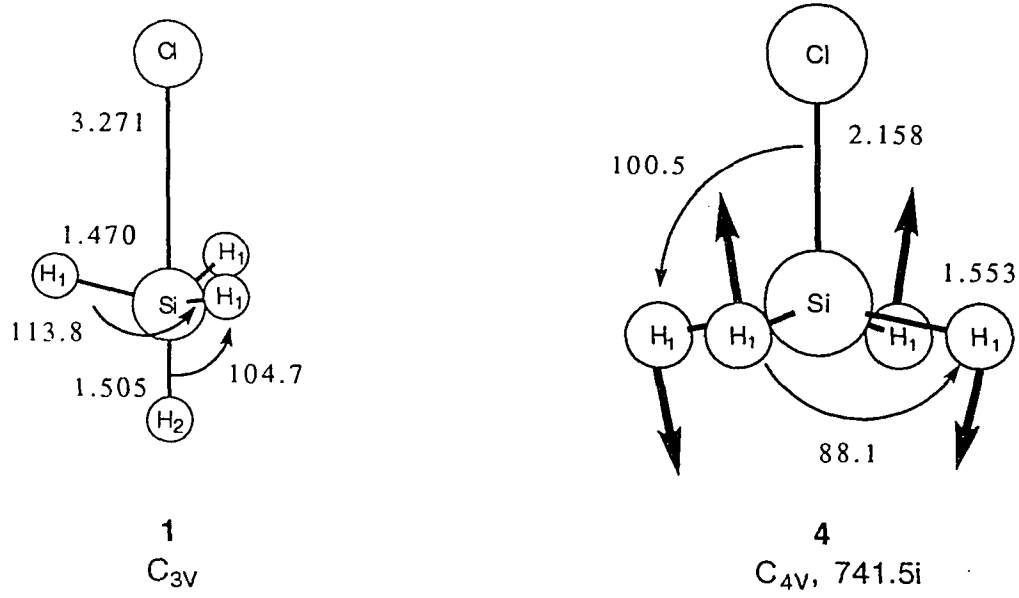

Figure 4: SiH_4Cl^- MP2/6-31++G(d,p) structures. The imaginary frequency in cm^{-1} is given for the transition state. Bond lengths in Angstroms and angles in degrees.

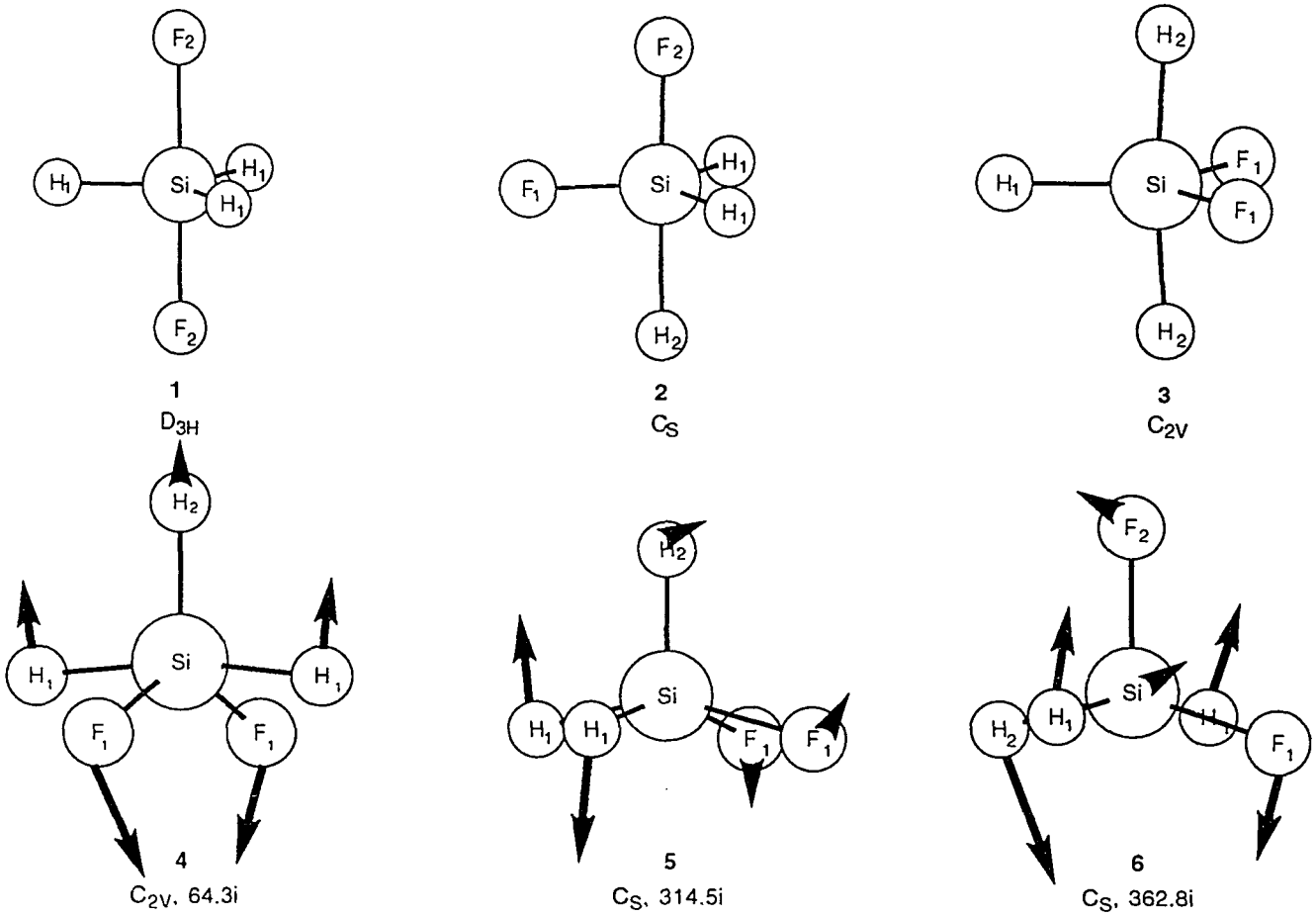

Figure 5: SiH_2F_2 MP2/6-31++G(d,p) Structures. Imaginary frequencies in cm^{-1} are given for transition states. Structure **4** is optimized at the RHF/6-31G(d) level (see text).

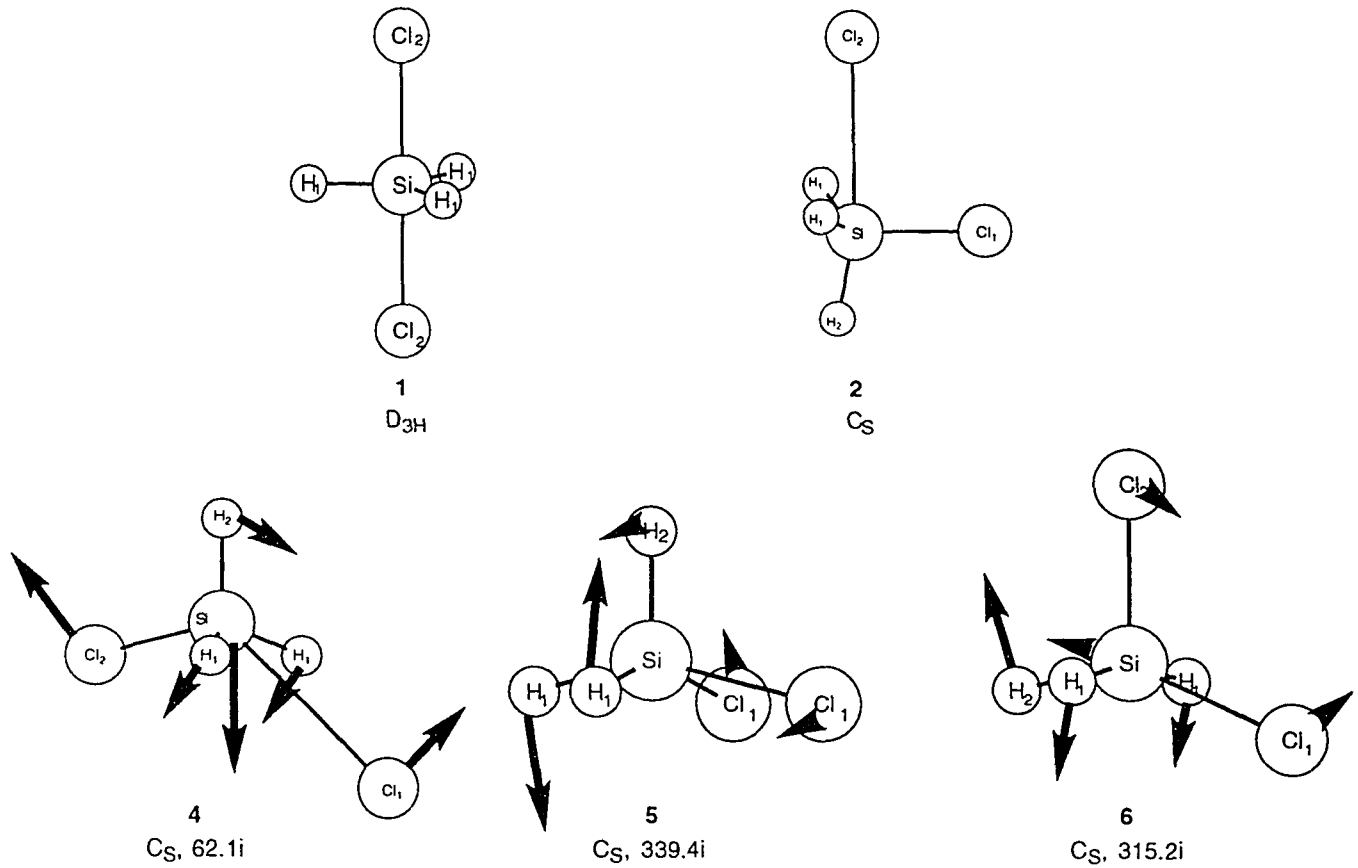

Figure 6: $SiH_3Cl_2^-$ MP2/6-31++G(d,p) Structures. Imaginary frequencies in cm^{-1} are given for transition states. Structure **4** is optimized at the RHF/6-31G(d) level (see text).

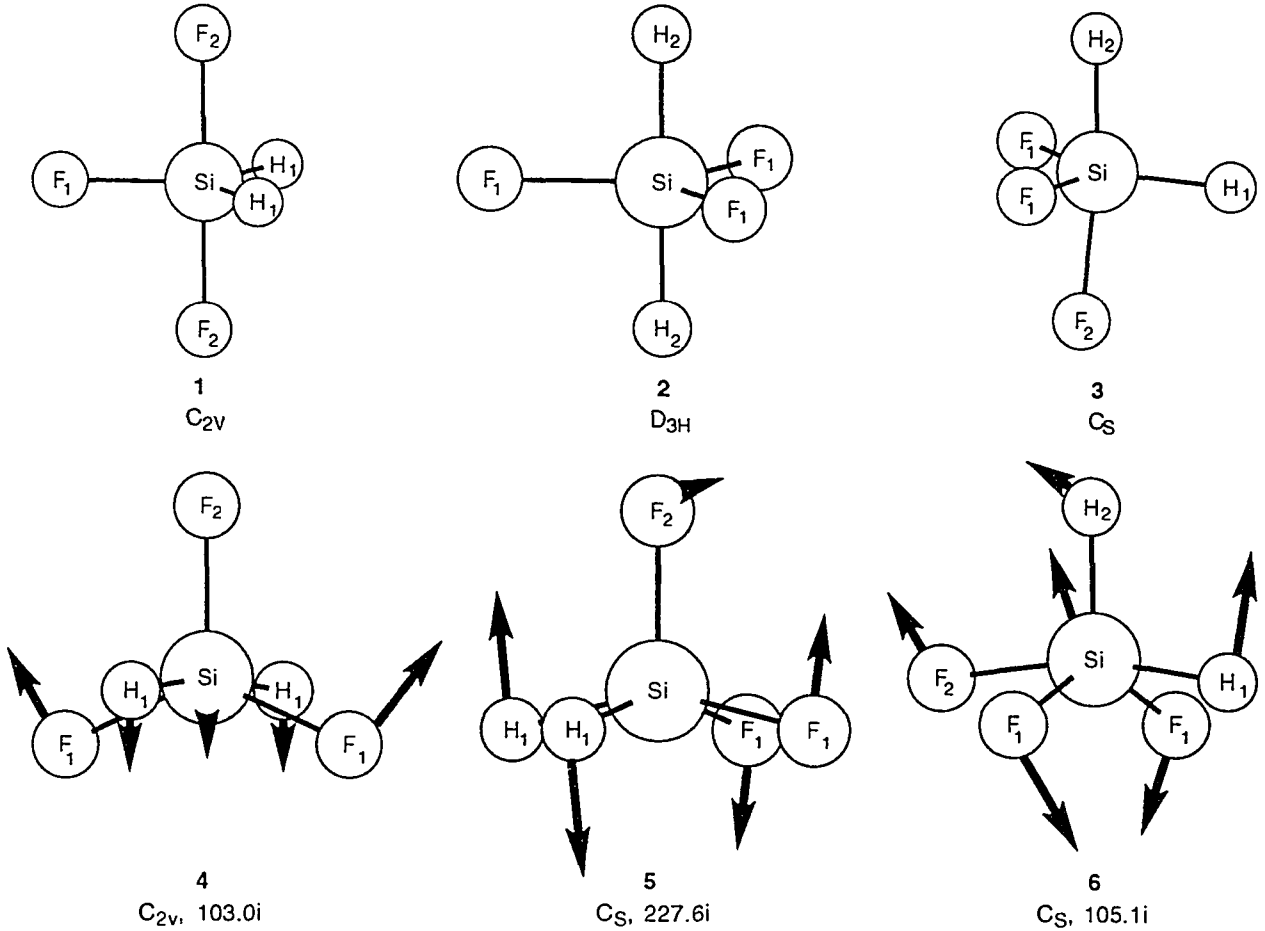

Figure 7: $SiH_2F_3^-$ MP2/6-31++G(d,p) Structures. Imaginary frequencies in cm^{-1} are given for transition states.

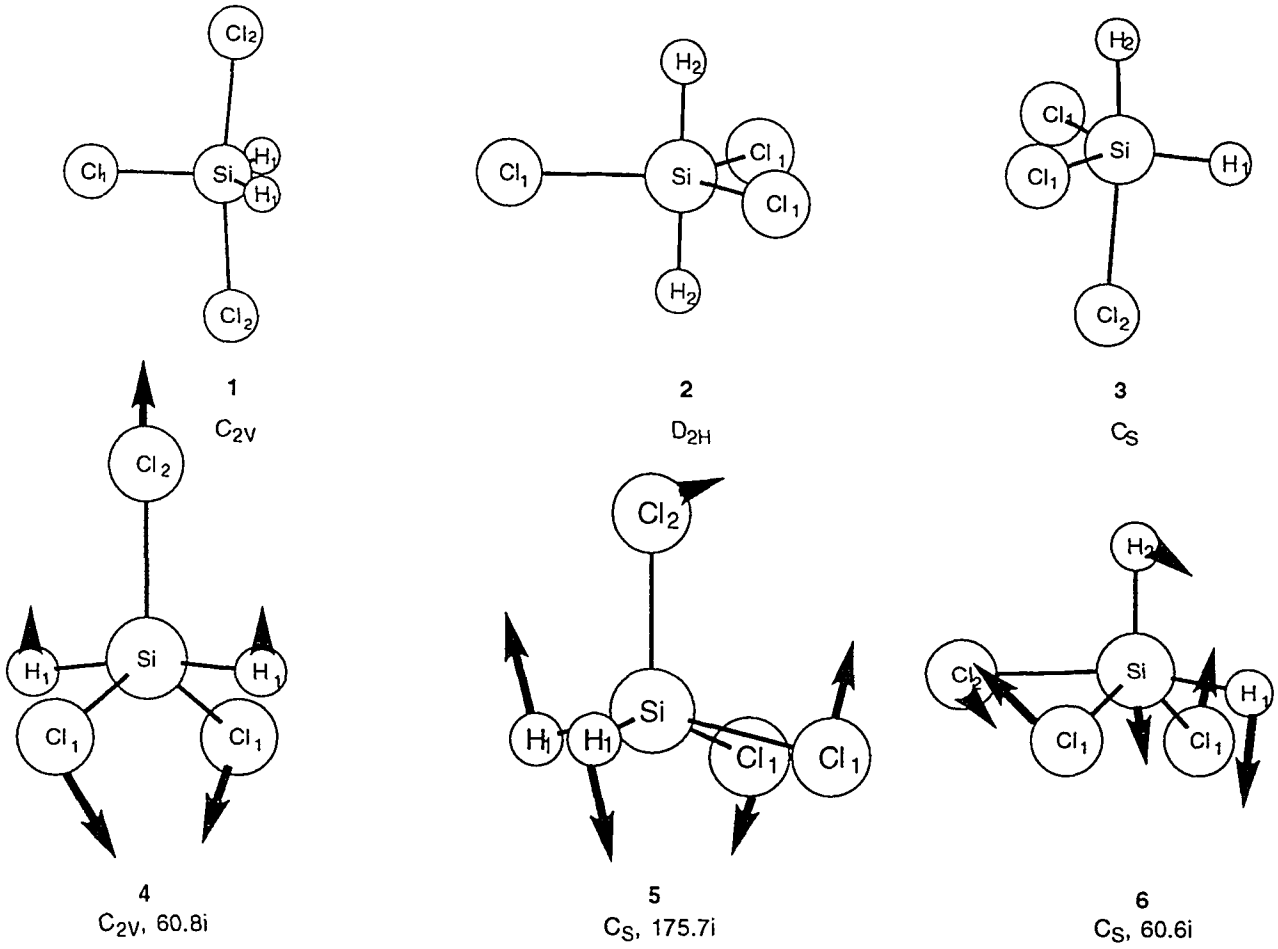

Figure 8: $SiH_2Cl_3^-$ MP2/6-31++G(d,p) Structures. Imaginary frequencies in cm^{-1} are given for transition states.

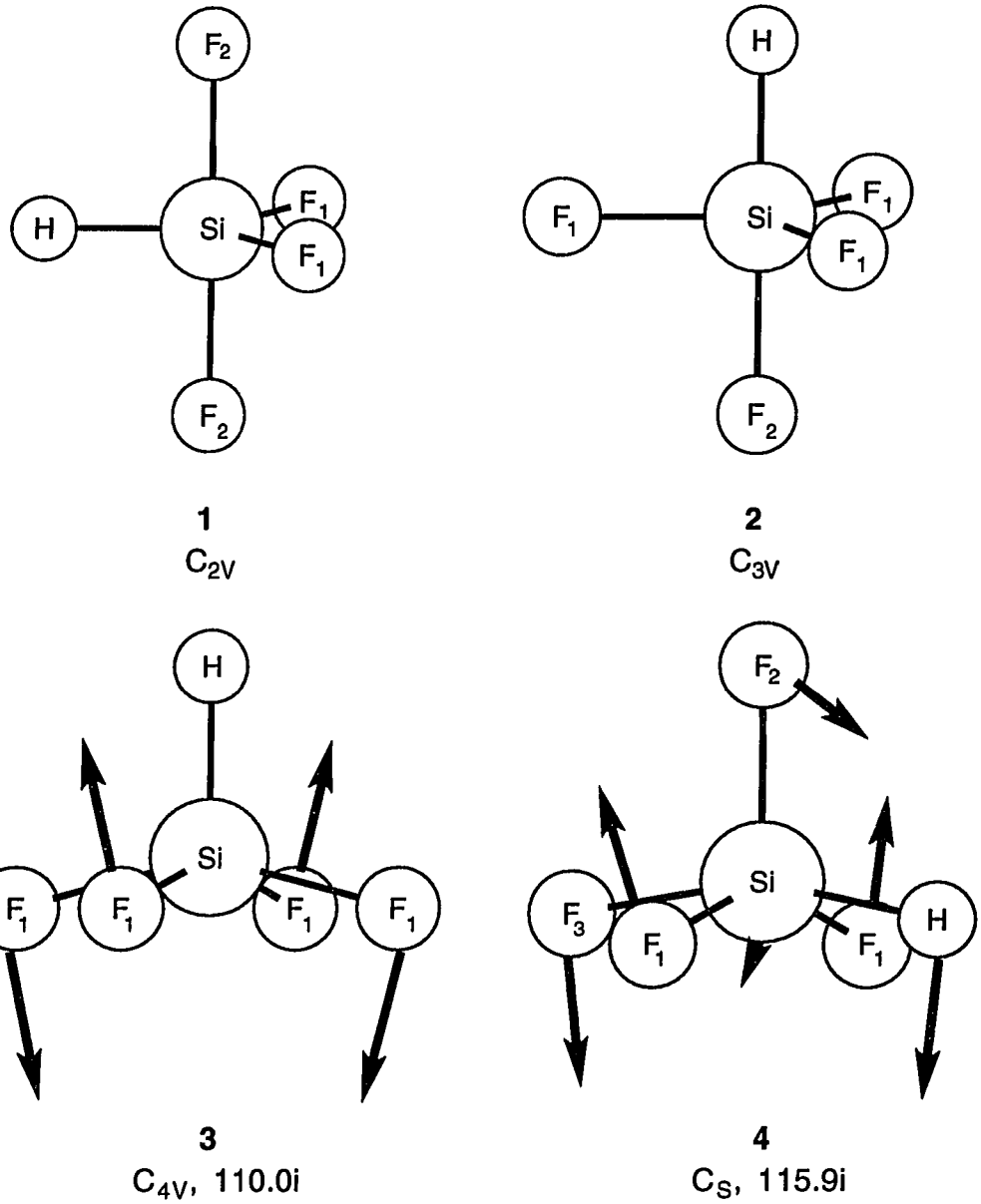

Figure 9: $SiHF_4^-$ MP2/6-31++G(d,p) Structures. Imaginary frequencies in cm^{-1} are given for transition states.

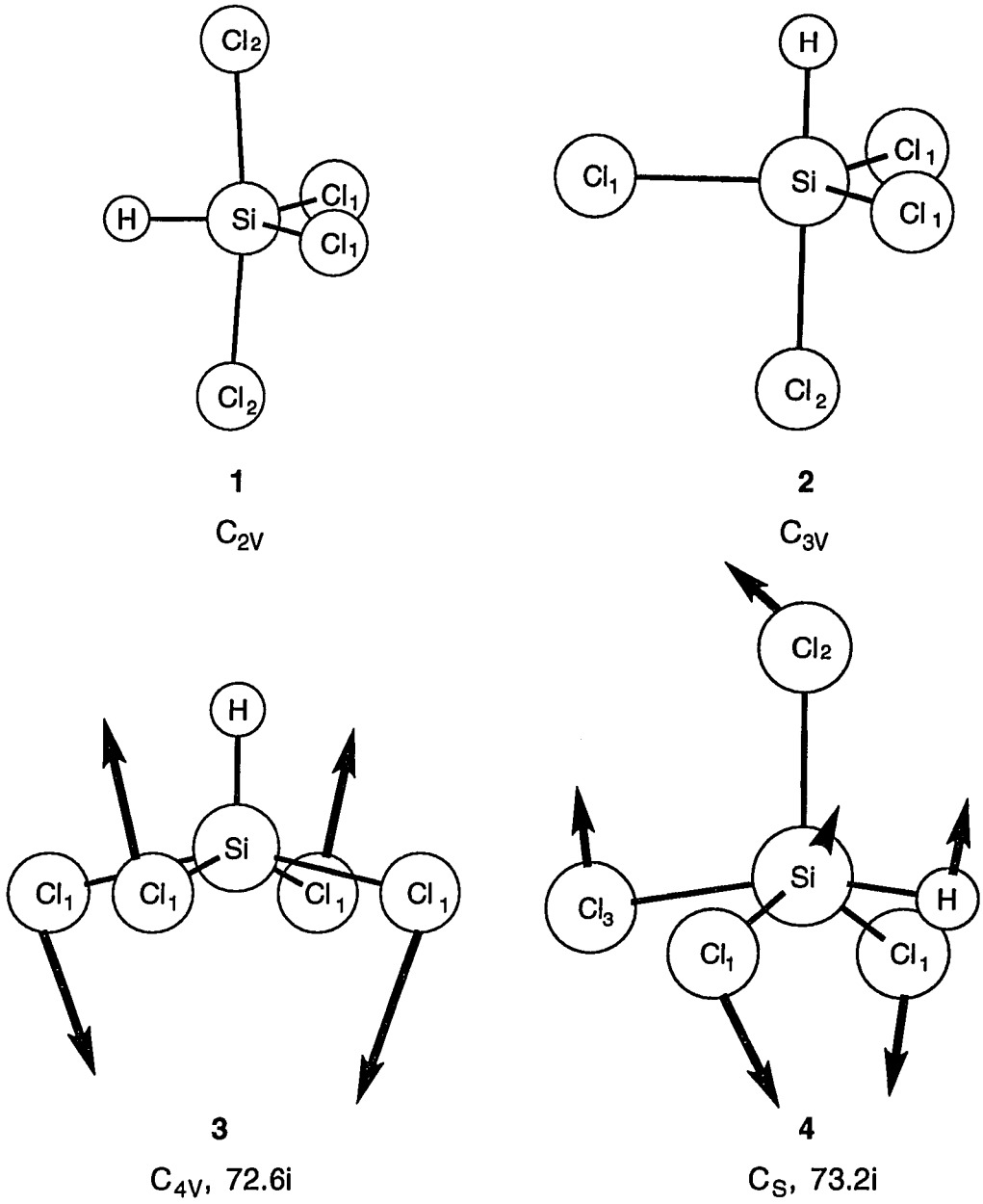

Figure 10: $SiHCl_4^-$ MP2/6-31++G(d,p) Structures. Imaginary frequencies in cm^{-1} are given for transition states.

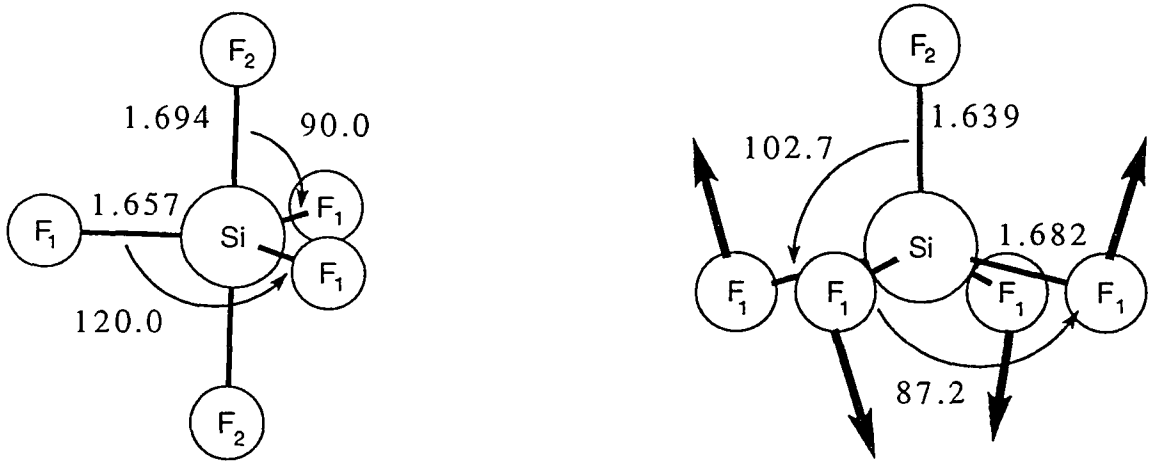

Figure 11: SiF_5^- MP2/6-31++G(d,p) structures. The imaginary frequency in cm^{-1} is given for the transition state. Bond lengths in Angstroms and angles in degrees.

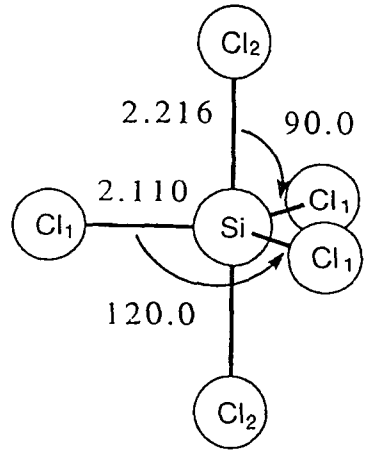

1

D_{3H}

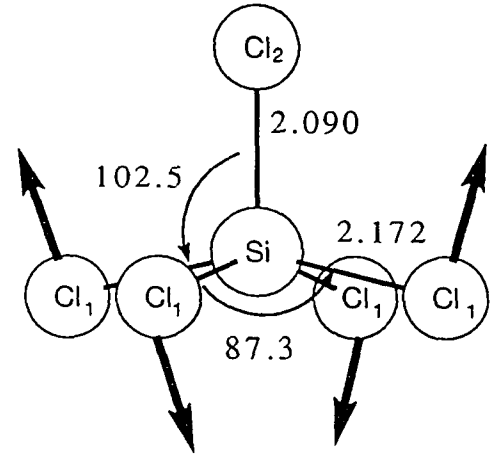

2

C_{4V}, 58.8i

Figure 12: $SiCl_5^-$ MP2/6-31++G(d,p) structures. The imaginary frequency in cm^{-1} is given for the transition state. Bond lengths in Angstroms and angles in degrees.

PAPER 5: π-BOND STRENGTHS OF $H_2X{=}YH_2$: X=Ge, Sn AND Y=C, Si, Ge, Sn

π-Bond Strengths of $H_2X{=}YH_2$: X=Ge,Sn and Y=C,Si,Ge,Sn

Theresa L. Windus[a] and Mark S. Gordon[a]
Department of Chemistry
North Dakota State University
Fargo, North Dakota 58105

Reprinted with permission from
J. Am. Chem. Soc. **1992**, *114*, 9559-9568

a) Current address: Department of Chemistry, Iowa State University, Ames, Iowa 50011

ABSTRACT

The molecular structures and π-bond strengths are determined using both MP2 and MCSCF + CI energies for a series of $H_2X{=}YH_2$ compounds, where X = Ge or Sn and Y = C, Si, Ge, or Sn. These strengths are estimated both by evaluating the rotation barriers and investigating the appropriate thermochemical cycles. The results show that C > Si ~ Ge > Sn in their ability to form π-bonds.

I. INTRODUCTION

Recently, there has been considerable interest in the molecular and electronic structure and reactivity of compounds containing a double bond between Group IVA elements. But, while the double bonds in ethylene, disilene and silaethylene have been well characterized by both experiment and theory (see, for instance, Ref. 1-5), the double bonds formed with germanium and tin have only recently been examined. Several reviews have been written on the subject of Ge and Sn double bonds[6]. Many of the species which contain double bonds to these elements are transient reactive intermediates. However, some have been isolated.

Through the use of large, bulky groups for steric and electronic stabilization, three germenes ($R_2Ge{=}CR'_2$) were isolated in 1987[7,8]. (Until then, germenes had been seen only as transient species[9-12].) At that time, Berndt and coworkers[7] synthesized germenes **1a** and **1b**.

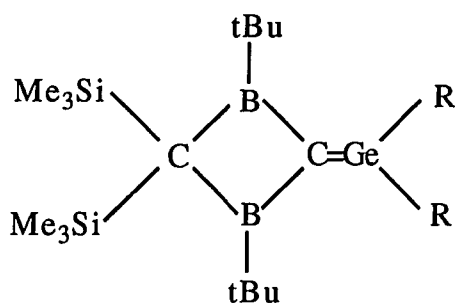

1a,b

a, R = $N(SiMe_3)_2$

b, R, R = $NtBu(SiMe_2)NtBu$

These stable germenes were characterized by both NMR and X-ray diffraction techniques. The Ge=C bond length was determined to be 1.827Å, with an average twist angle of 36° about the GeC bond. In addition, the local structure about the Ge and C atoms is nonplanar. Thus, the dihedrals at the Ge and C ends were determined to be 1.7° and 4.8°, respectively. The phenomenon of trans bending in heavier homologs of ethylene has been discussed by several authors[13,14].

Couret and coworkers[8] synthesized the germene **2**.

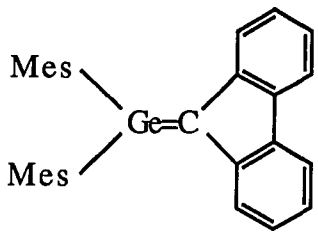

2

This molecule was characterized through selected reactions, as well as by NMR and X-ray diffraction. The Ge=C bond length was determined to be 1.801Å with an average twist angle of 5.9° about the bond. However, the molecule was found to be essentially planar about Ge and C.

Recently, four new germenes, **3a-d**, have been synthesized[15], and identified through the use of NMR.

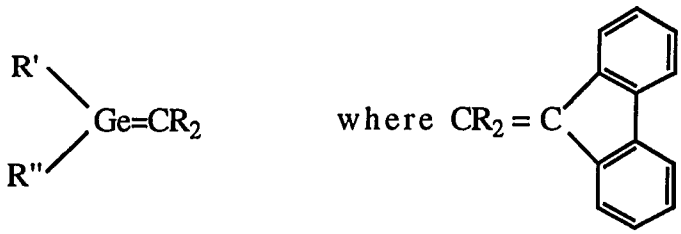

3a, R'=R"=CHR_2; **3b**, R'=CHR_2, R"=tBu; **3c**, R'=R"=Bis; **3d**, R'=Bis,R"=Mes

The parent germene, $H_2Ge=CH_2$, while not known experimentally, has been examined in several theoretical studies.[16-18] Both MNDO[16] and *ab initio*[17,18] calculations (at the self-consistent field (SCF) level using 3-21G*, pseudopotentials with double-zeta (DZ) valence, and DZ basis sets) predict germene to be planar, with a Ge-C bond distance of 1.717Å predicted by MNDO and 1.71 to 1.81Å calculated by the *ab initio* methods. *Ab initio* studies have also predicted methylgermylene to be more stable than germene by 22.7[17a] and 15.0[17b] kcal/mol. However, experience with Si[19] suggests that as the level of theory is improved, the double bond species will preferentially decrease in energy.

In 1987, the only isolated stannene **4** was synthesized.[7b,20] This stannene was thoroughly identified through NMR and X-ray diffraction studies. The Sn=C bond length was determined to be 2.025Å with an average twist angle of 61° about the bond. As in the case of GeC, the

local structure at Sn and C is found to be nonplanar, with dihedrals at the Sn and C ends of 5° and 16°, respectively.

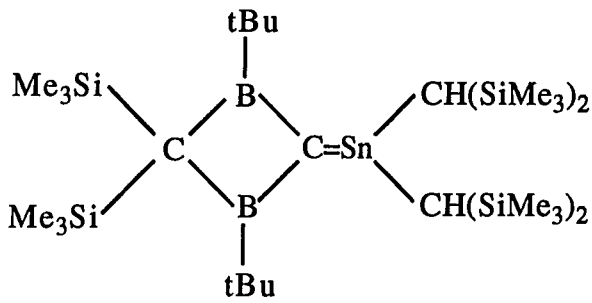

4

Theoretical investigations of the stannenes are as scarce as experimental work. Dewar and coworkers[21] performed MNDO and UMNDO calculations on the lowest singlet and triplet states of stannene ($H_2Sn=CH_2$). Since the energy difference between these two states was determined to be small (the triplet being lower in energy than the singlet by 1.1 kcal/mol), they concluded that tin does not form π-bonds. This is in agreement with the conclusions of Pauling.[14] Dobbs and Hehre[18] performed calculations at the UHF/3-21G(d)[45] level and found stannene to be a planar structure with a weak π-bond of 19 kcal/mol and a Sn=C bond length of 1.982Å. These authors determined the π-bond strength by calculating the rotation barrier (this method for finding the π-bond energy will be discussed in more detail later in the

paper) and by calculating the energies of disproportionation of the products of hydrogen atom addition.

No germasilenes are known as stable species. However, Baines and Cooke[22] have found evidence of the tetramesitylgermasilene reactive intermediate.

The only theoretical study is that of Grev and coworkers[23] on germasilene ($H_2Ge=SiH_2$) at the configuration interaction with single and double excitations (CISD) level of theory using basis sets of DZ plus polarization (DZP) quality. This method predicts a Ge=Si bond length of 2.211Å and out-of-plane bend angles of 31.2 and 33.5° at the Ge and Si, respectively. By calculating the rotation barrier, they predict a π-bond energy of 25 kcal/mol. However, the twisted triplet state was used instead of the twisted singlet state and should lead to a π-bond energy that is too low. (Refer to Section IV of this paper for more details of this method.) These authors also find silylgermylene, $H_3Si-GeH$, to be 7.5 kcal/mol more stable than germasilene.

To our knowledge, no stannasilenes are known as transient species or stable compounds.

Even though several transient digermenes have been identified (see for instance Ref. 24 - 27), only five stable digermenes have been reported. The parent digermene, $H_2Ge=GeH_2$, has been found in nitrogen and argon matrices at 5K and studied using Raman and IR spectroscopy.[28] Three digermenes have been isolated in crystal form, **5**[29], **6**[30] and

7[31], while another digermene, 8[32], has been found to be stable in solution.

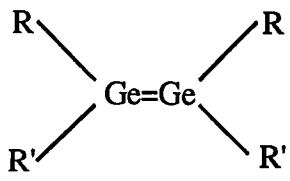

5, R,R'=$HC(SiMe_3)_2$; **6**, R,R'= 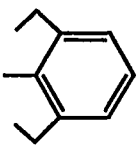 ;

7, R = 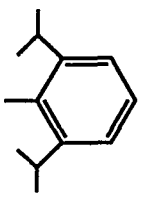 , R' = Mes; **8**, R,R' = 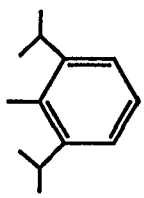

Compound **5** was identified through the use of Raman and X-ray spectra, **6** using X-ray spectra and chemical reactivity, **7** using X-ray and NMR spectra, and **8** with NMR, UV, mass spectra, and chemical reactivity. The X-ray structures show that **5** has a Ge=Ge bond length of 2.347Å, a twist angle of 0° about the bond and an out-of-plane angle of 32°. The corresponding data for **6** are 2.213Å, 11°, and 15°, respectively, and for **7** are 2.313Å, 7°, and 36°, respectively.

The parent digermene, $H_2Ge=GeH_2$, has been studied by several theoretical methods.[29c,33-38] The methods used included MNDO, RHF with pseudopotentials + DZ (and DZP)

valence basis sets, all electron DZ and DZP basis sets, and RHF plus CI with pseudopotentials + DZP valence basis set. The predicted Ge=Ge bond distances range from 2.259 to 2.325Å and the out-of-plane angle leading to a trans bent structure is predicted to be 34 to 40°. At the SCF with DZ basis set level of theory[36] germylgermylene is predicted to be 9.5 kcal/mol more stable than digermene. However, when CI is used[35], digermene is predicted to be 5 kcal/mol more stable than germylgermylene. Again, this suggests that as the level of theory is improved, the double bond species will preferentially decrease in energy.

The only distannene isolated to date, **9**, is that synthesized by Lappert and coworkers.[39,29a,29c,34]

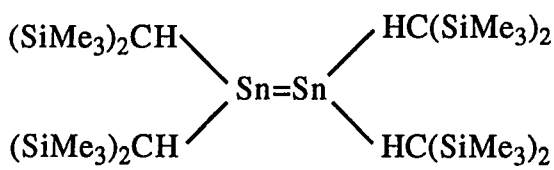

9

This molecule has been thoroughly identified through the use of X-ray diffraction and NMR studies. The X-ray structures show a Sn=Sn bond length of 2.768Å, a twist angle of 0° about the bond and an out-of-plane angle of 41°.

Another distannene, **10**, has been found to be stable in solution by Masamune and Sita.[40]

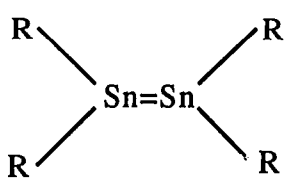

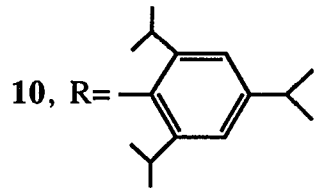

The parent distannene, $H_2Sn=SnH_2$, has been examined in several theoretical studies.[20,29c,34,37,38,41,42] The methods used included MNDO, RHF with pseudopotentials + DZ valence and all electron DZ basis sets, MP2 with pseudopotentials + DZ valence basis set, and RHF plus CI with pseudopotentials + DZP valence basis set. These methods predict Sn=Sn bond distances ranging from 2.70 to 2.72Å and an out-of-plane angle of 41 to 49°. Márquez and coworkers[42] also predict stannilstannilene, SnH_3SnH, to be more stable than trans-bent $H_2Sn=SnH_2$ by 1.4 kcal/mol using energies at the two-reference single and double excitation CI (TRSDCI) level using pseudopotentials + DZP basis set.

No experimental or theoretical studies of germastannenes, $R_2Ge=SnR'_2$, have been reported to our knowledge.

Several methods have been used to determine π-bond strengths. One of these is to rotate one end of the molecule by 90°. Since this rotation breaks the π-bond, the π-bond strength, D_π, may be estimated as the energy difference

between the rotated and singlet ground state forms. An alternative method for determining D_π is to use thermochemical cycles. One such method, presented by Schleyer and Kost[43], uses isodesmic reactions and bond dissociation energies. All of these methods have been found to predict similar π-bond strengths for most compounds.[1,43,44] A different method based on hydrogenation will be used in this paper. Both the rotation and hydrogenation methods are described in further detail below. This paper is a continuation[1,44] of our interest in the structure, bonding, and π-bond strengths of unsaturated compounds containing Group IV elements.

The remainder of this paper is organized in the following manner: The computational methods used are summarized in Section II. Some preliminary considerations are discussed in Section III. The results of the computations are presented in Section IV. Section V contains a comprehensive discussion of the results, and the conclusions from this work are summarized in Section VI.

II. COMPUTATIONAL METHODS

The 3-21G[45] basis set augmented by d functions on all heavy atoms is used throughout this work. The d polarization exponents used are: C, 0.80; Si, 0.395; Ge, 0.246; and Sn, 0.183. Based on the level of agreement between experiment and theory in earlier work[1], this basis set, together with methods that include electron correlation, should provide reliable structures. The tin isotope ^{120}Sn is used for all frequency calculations.

When planar or nearly planar π bonded X=Y is rotated to a perpendicular form, the π-bond is broken, and a biradical is produced, generally with singlet and triplet states that are very close in energy. A realistic[1,2] description of this rotational surface is provided by a four-electron, four-orbital full optimized reaction space (FORS)[46] MCSCF wavefunction. This wavefunction allows the four electrons in the X=Y bonds to be distributed in all possible ways among the σ, π, π^*, and σ^* orbitals and allows for breaking of the π-bond, as well as correlation changes in the σ-bond due to its lengthening during the rotation. The resultant wavefunction consists of 20 electronic configurations. Geometry optimizations using analytical gradients and numerical energy second derivative matrices at the optimized structures were calculated at the MCSCF level. Energies were determined using second order CI (SOCI), in which all single and double

excitations from the 20 MCSCF reference configurations into the MCSCF virtual orbitals are allowed.

The MC/LMO/CI analysis is used to gain qualitative understanding of the valence bond-like "resonance" structures (configurations) that contribute most to the wavefunction. This analysis has been described elsewhere[44,46,47], so only a brief description of the three steps will be included here. The first step is to perform the MCSCF calculation described in the previous paragraph. In the second step, the MCSCF natural orbitals are localized using the technique developed by Pipek and Mezey[48]. In the final step, a CI calculation in C_1 symmetry using only the MCSCF active space is performed to generate all configurations that contribute to the double bond.

The MCSCF and SOCI calculations were performed using the North Dakota State University version of the GAMESS[49] electronic structure package.

The thermochemical cycle, which will be discussed in more detail in Section IV, requires the calculation of $H_2X{=}YH_2$ and H_3XYH_3 energies. Since these structures are closed shell, restricted SCF (RHF) and second order Møller-Plesset perturbation theory (MP2)[50] wavefunctions were used to determine geometries and energy second derivatives. Final energies were determined at the full fourth order Møller-Plesset perturbation theory level (MP4)[51] for all stationary

points. Only the valence electrons (excluding inner d's for Ge and Sn) were correlated in the MP4 energy calculations. All calculations for this method were performed using the GAUSSIAN86[52] and GAUSSIAN88[53] programs.

III. PRELIMINARY CONSIDERATIONS

Before the details of the results are discussed, it is useful to consider some of the qualitative aspects of the π-bonds of these systems. The MCSCF natural orbital occupation numbers of the σ, π, π*, and σ* orbitals given in Table I provide some insight into the amount of biradical character in these molecules. The corresponding information for the C-C, C-Si, and Si-Si molecules are included for completeness. As will be discussed in Section IV, the only π-bond structures that are planar are the C-C, C-Si, and C-Ge molecules. As may be seen in Table I, the σ and σ* occupation numbers are nearly 2.0 and 0.0, respectively, so the σ-bond is well described by a single configuration, Hartree-Fock wavefunction. There is more configurational mixing in the π space. In particular, the nonplanar molecules have a significantly higher π* occupation number than the planar structures, suggesting that the non-planar molecules have some biradical character.

The results of the MC/LMO/CI analysis are collected into Table II. The localization results in orbitals that resemble a p_z (contributing to the σ-bond) and a p_y (contributing to the π-bond)

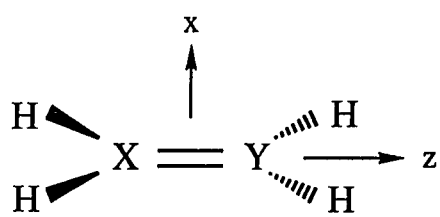

on each end of the π-bond (referred to as σ_X, π_X, π_Y, and σ_Y, where X and Y are the heavy atoms in the molecule). Each configuration |ijkl> resulting from the CI represents i electrons in a σ_X LMO, j electrons in a π_X LMO, k electrons in a π_Y LMO, and l electrons in a σ_Y LMO. Only those configurations that are chemically sensible (i.e. configurations resulting in two electron bonds) are included in Table II, since the other contributions have vanishingly small coefficients. The following nomenclature is used in Figure 1. The lower line or arrow corresponds to the σ-bond, while the upper line or arrow corresponds to the π-bond. A line with no head means the bond is covalent; e.g., |1jk1> signifies a covalent σ-bond. An arrow X→Y signifies a dative bond in which X donates a pair of electrons to Y. In the case of |1111>, there are two spin couplings which give a singlet state, so there are two such configurations. Figure 2 depicts the resonance structures that correlate with the major configurations with the |2020>, |1111>, and |0202> configurations (⇄ , = , and ⇄ , respectively) representing a charge balanced configuration, the |2110>, |1201>, and |2200> configurations (→ , ⇉ , and ⇉ , respectively) representing an electrophilic Y, and the |0112>, |1021>, and |0022> configurations (← , ⇇ , and ⇄ respectively) representing a nucleophilic Y.

The first noticeable trend in Table II is that the charge balanced configurations (covalent, σ dative + π backbond, π dative + σ backbond) comprise the majority of the wavefunction for all species. Indeed, there are only minor variations in the contributions from the individual resonance structures, with the covalent contribution being approximately 50% in each case. This is qualitatively the same as the results obtained by Trinquier and Malrieu[13c] using their valence bond analysis. Also, as expected from electronegativity arguments, when carbon is part of the double bond it is a nucleophilic center. The differences in the electrophilic contribution and the nucleophilic contribution for the other species are too small for any meaningful conclusions to be made. For most of the compounds, the configurations listed in Table II contribute 88% or more of the total wavefunction. The ten configurations omitted from Table II each contribute less that 5% to the total wavefunction in <u>all</u> cases. For H_2SnSiH_2, there are several of these excluded configurations that contribute approximately 5%. As a result, the primary configurations listed in Table II contribute only 80% of the total wavefunction.

IV. RESULTS

Structures

Both planar and ground state structures were examined for the XYH_4 species. The planar structures at the MCSCF/3-21G(d) level are given in Table III along with the lowest frequency associated with each species. The only planar structure that is a minimum on its surface is $GeCH_4$. It is particularly interesting that H_2SnCH_2 is not planar at the MCSCF level of computation. This is contrary to the SCF/3-21G(d) results of Dobbs and Hehre[18]. The imaginary frequency of the planar molecule is, however, only 176i (Table III) suggesting that the surface for this molecule is quite flat.

The fully optimized ground state XYH_4 geometries at each level of theory are given in Table IV. It is interesting to note that the flap angles X-Y-H-H and Y-X-H-H are generally largest in the MCSCF geometry and smallest in the RHF geometry. Thus, RHF and MP2 predict $SnCH_4$ to be planar, whereas MCSCF predicts this compound to be trans bent. In general, the MP2 and RHF geometries agree to within 0.04 Å for bond lengths and 3° for bond angles. It is interesting that the MP2 X=Y distances are <u>not</u> consistently longer than those predicted at the RHF level. The predicted MCSCF X=Y bond lengths are generally longer than those predicted by either RHF or MP2. Also, the lengthening of R(X=Y) predicted by MCSCF upon relaxation of planarity is generally in the

range of 0.07 - 0.10Å. The difference in flap angles is less than 2.8° for all structures except for $GeSiH_4$ where the difference is 5.6° for GeSiHH and 6.2° for SiGeHH.

The geometries of the XYH_6 molecules at the RHF/3-21G(d) and MP2/3-21G(d) levels in the staggered configuration are given in Table V. Notice again that the RHF and MP2 geometries agree quite well: within 0.04Å for bond lengths and 0.3° for angles. The major difference between the RHF and MP2 geometries is the X-Y bond length, all other parameters being essentially the same for the two methods. Also, it is interesting to note that the X-Y-H and Y-X-H angles are approximately 110° for all X and Y. Likewise, the H-X-H and H-Y-H angles are all approximately 108°.

For ease of comparison, the double and single bond lengths for each X-Y are collected into Table VI. Known experimental values are also given in this table. The experimental bond lengths for the single bond structures are quoted for the fully hydrogenated compound, except for that of Sn-Sn, and are therefore directly comparable with experiment. The experimental bond lengths for compounds containing double bonds are those discussed in the Introduction.

The four experimental single bond distances are within 0.035Å of the MP2/3-21G(d) values. The MP2 distances are consistently too long, suggesting that larger basis sets are

needed to bring the theoretical values into closer agreement with experiment. The exception here is for the Sn-Sn bond where the experimental value is from a substituted system.

For the double bond structures, the RHF distances, as expected, are shorter than experiment; varying from 0.04 to 0.07Å from the first listed experimental values. In each case, the first experimental value quoted is the one that is least hindered by bulky substituents. However, where possible, a second experimental value is listed to illustrate the rather large variability that can occur in the bond length with change in substituents. Surprisingly, even the MP2 bond lengths are shorter than the experimental values. The error varies from 0.02 to 0.08Å. The MCSCF values are within 0.04Å, with the theoretical values being longer except in $GeCH_4$.

Generally, the calculated X=Y bond lengths are 0.12 - 0.21Å shorter than the corresponding X-Y bond lengths. This difference tends to decrease as the participating Group IVA elements become heavier, suggesting a weaker π interaction for those elements.

Frequencies

The frequencies for the X-Y stretches are listed in Table VII at all three theoretical levels. The values for C-C, Si-C, and Si-Si single and double bond structures are from Reference 1. Also, experimental values are given when possible. It should be noted that several of the heavy atom

(X = Ge or Sn) experimental frequencies are from heavily substituted molecules.

Note that four of the systems, Ge-Ge, Sn-Si, Sn-Ge, and Sn-Sn, have larger frequencies for the single bond structures than for the double bond structures at the RHF level. Comparison with the MP2 frequencies show that the double bond frequencies at the RHF level are significantly lower than the MP2 frequencies for these four species, whereas the single bond frequencies are nearly identical. This suggests that RHF frequencies for these four double bond species are unreliable.

The MP2 and MCSCF frequencies follow the generally expected trend. The heavier the elements involved in the X-Y stretch, the lower the associated stretching frequency. As an example, consider the sequence of the single bond stretches for the Ge-Y molecules at the MP2/3-21G(d) level: Ge-C (609 cm^{-1}) > Ge-Si (379 cm^{-1}) > Ge-Ge (286 cm^{-1}) > Ge-Sn (237 cm^{-1}).

The experimentally known frequencies for the heavy atom single bond structures are lower than the MP2 frequencies by an amount ranging from 11 cm^{-1} to 73 cm^{-1}. The two experimentally known frequencies for the heavy atom double bond structures are both larger than the MP2 frequencies: by 93 cm^{-1} for Ge=Ge and 161 cm^{-1} for Ge=C. This is reasonable agreement for the level of theory being used, however, larger basis sets would probably improve these results.

Torsional Barriers

This method of determining the π-bond strength involves the twisting of one end of the molecule by 90° to break the π-bond. The energy required to reach the perpendicular singlet transition state from the ground state is considered to be the energy D_π for breaking the π-bond. Of course, this is an approximation, because other factors are also involved, such as lengthening of the X-Y σ-bond. However, the D_π obtained in this manner corresponds to the most common experimental method for determining D_π. The triplet twisted biradical is a minimum on its surface and its energy tends to be lower than that of the singlet. This leads to the following qualitative energy diagram:

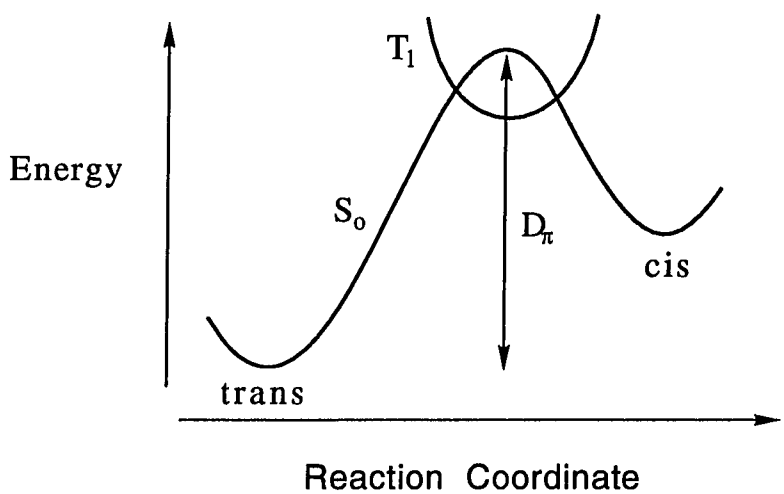

Since the singlet and triplet twisted structures tend to have similar geometries, an efficient method for finding the singlet structure is to optimize the triplet structure and

then perform the saddle point search for the singlet starting from the triplet geometry.

The structures of the singlet and triplet twisted molecules are given in Figure 2. The difference between the singlet and triplet geometries is small, differing by less that 0.01Å for bond lengths and 2° for angles. The other structures required to evaluate the rotation barrier have already been given in Tables III and IV. Generally, the X-Y bond lengths in the twisted structures are similar to the single bond lengths listed in Table VI.

MCSCF and SOCI total energies of these molecules are given in Table VIII, and the relative energies are given in Table IX. As mentioned earlier, the $SnCH_4$ is rather floppy, requiring only 0.6 kcal/mol to become planar. The other molecules require 3.5 to 8.7 kcal/mol to make them planar.

Table IX also shows that the π-bond strengths (singlet excited state energy relative to the ground state energy) decrease in the following order: Ge-C > Ge-Si ~ Ge-Ge > Sn-C ~ Sn-Si ~ Sn-Ge > Sn-Sn. However, it should be noted that the last four species differ by only two kcal/mol. This general trend parallels that noted earlier for X=Y vs. X-Y bond lengths.

In general, the twisted triplet minimum is, as expected, 2 - 3 kcal/mol lower in energy than the twisted singlet transition state. Contrary to the earlier MNDO

predictions,[21] singlet stannene is predicted to be 19.1 kcal/mol lower in energy than the lowest triplet state.

Hydrogenation Reactions

An alternative method for determining D_π is to use the following thermochemical cycle:

$H_3X\text{-}YH_3$	$\rightarrow H_2\dot{X}\text{-}YH_3 + \dot{H}$	D(X-H)
$H_2\dot{X}\text{-}YH_3$	$\rightarrow H_2\dot{X}\text{-}\dot{Y}H_2 + \dot{H}$	D(Y-H)
$H_2\dot{X}\text{-}\dot{Y}H_2$	$\rightarrow H_2X{=}YH_2$	$-D_\pi$
$2\dot{H}$	$\rightarrow H_2$	-D(H-H)
$H_3X\text{-}YH_3$	$\rightarrow H_2X{=}YH_2 + H_2$	$\Delta H°(0\ K)$

This allows D_π to be calculated by the equation

$$D_\pi = D(X\text{-}H) + D(Y\text{-}H) - D(H\text{-}H) - \Delta H°(0\ K) \quad (1)$$

D(H-H) is known to be 103.3 kcal/mol[67]. With the exception of D(Ge-H) in $CGeH_6$, the experimental values of D(X-H) and D(Y-H) are, unfortunately, not available for the compounds of interest. Therefore, estimates of the bond dissociation energies must be used instead. The values of the bond dissociation energies used for this paper can be found in the Appendix.

D_π could be determined entirely by experiment if the $\Delta H°$ (0 K) are known experimentally. Unfortunately, this is not the case, so computed values will be used in this paper. Combining experimental D(X-H) and D(H-H) with computed $\Delta H°$ affords a semi-theoretical estimate of D_π from equation (1).

All of the necessary structures are given in Tables IV and V. The total energies along with the zero point energies

(ZPE) are given in Table X. RHF, MP2, and MP4 energies are given at both the RHF and MP2 geometries. The ΔH° values, which are determined by combining the MP4/3-21G(d)//MP2/3-21G(d) energies and the ZPE's from the MP2/3-21G(d) geometries, are given in Table XI. Also shown in this table are the D(X-H), D(Y-H) and the calculated D_{π} values.

V. DISCUSSION

The D_π energies from both methods are gathered into Table XII. Other theoretical values and two experimental values are also included for comparison. The thermochemical and rotational results from this work are in quite good agreement. The difference between the π-bond strengths obtained from the two methods is less than 1 kcal/mol in all cases except those of Ge-Ge (a difference of 2.6 kcal/mol) and Ge-Sn (a difference of 1.4 kcal/mol). This excellent agreement between the two methods is gratifying and lends some credibility to the calculated π-bond strengths. In addition, the agreement suggests that the configurational mixing presented in Table I does not have a significant effect on the thermochemical π-bond energies.

The calculated π-bond strengths presented in this work are in good agreement with the other theoretical values. The only exception to this is the value of the Ge-C π-bond energy of 26.9 kcal/mol obtained by Trinquier and coworkers[17b]. These workers used an SCF wavefunction to obtain geometries and CI energies. As mentioned earlier, the biradical nature of the excited singlet and triplet states require the use of MCSCF wavefunctions. This is believed to be the main cause of the discrepancy between their results and the results of this work.

The π-bond energies estimated from experiment are in disagreement with the rotationally determined values by 3.2 kcal/mol for Ge-Ge, 11 kcal/mol for Ge-C and 24 kcal/mol for Sn-C. Part of the discrepancy for the last two experimental values could arise from the methyl substituents on the Ge and the Sn in the experimentally measured compounds. However, the experimentally determined numbers were, as noted by the authors, not consistent with the π-bond strengths in silicon compounds. The authors also comment that the values were not reliable as they were based on thermochemical data that was subject to large errors. It is likely that the calculated π-bond energies reported here are more accurate.

The data from Table XII also shows that Sn forms much weaker π-bonds than does Ge. This follows the generally accepted order of C>Si~Ge>Sn in effectiveness of forming π-bonds. Also of interest, is that the Sn molecules all have π-bond energies within two kcal/mol of each other. This reflects the inefficiency of Sn in forming π-bonds, even with "good" π-bonding atoms such as carbon.

Another way to judge the π-bond capability of an atom is to define the π-bonding energy of atom X as

$$E_\pi(X) = (1/2)D_\pi(X=X).$$

Using the D_π values from calculated rotation barriers and listed in Table XI, one obtains E_π of 12.7 kcal/mol for Ge and 9.9 kcal/mol for Sn. E_π for C and Si have previously

been reported to be 32.5 and 12.5 kcal/mol, respectively.[1] For mixed bonds X=Y one can evaluate which of the two atoms (X or Y) dominates the π-bond by using

$$E_\pi(X) = D_\pi(X=Y) - E_\pi(Y).$$

Averaging over the two different values (Y = Ge and Sn) gives 15.3 and 12.3 kcal/mol for C and Si, respectively. This again agrees with the order of C > Si ~ Ge > Sn. Note that while E_π(Si) is unchanged, E_π(C) is much lower than that reported by Schmidt and coworkers[1], again reflecting the ineffectiveness of the heavier atoms to form π-bonds. This supports the notion expressed by others.[69]

VI. CONCLUSIONS

The results from this work show that the order of ability to form π-bonds is C > Si ~ Ge > Sn. Sn in particular seems to form compounds of approximately the same π-bond strength independent of the Group IVA element to which it is bonded.

Interestingly, compounds containing Ge-Ge double bonds have been synthesized, but not compounds containing Ge-Si double bonds, even though these two are predicted to have approximately the same π-bond strength. The same can be said about the known Sn=Sn compounds and their as yet experimentally unknown Sn=Ge and Sn=Si analogues. This work suggests that the experimentally unknown compounds should be thermodynamically stable. All five of the aforementioned π-bonds have similar amounts of π diradical character (see Table I). At least by this measure, their kinetic stability should be similar as well, so the eventual synthesis of Ge=Si, Sn=Ge, and Sn=Si π-bond containing compounds does not seem to be out of the question, unless these compounds are highly unstable to isomerizations.

VII. ACKNOWLEDGEMENT

This work was supported by a grant from the National Science Foundation (CHE-8911911). The calculations were performed on the IBM 3090-200E/VF at the North Dakota State University Computer Center, obtained in part by a Joint Study Agreement with IBM, an IBM RS/6000-530 workstation, obtained with the aid of grants from the National Science Foundation, the CrayY-MP at the San Diego Supercomputer Center, and an Ardent Titan which was made available to us by Stardent. The authors thank Dr. Michael W. Schmidt (MSM) for his helpful insight and discussions.

VIII. APPENDIX

Only one of the necessary experimental D(A-H) BDE's is known. Therefore, the rest of the BDE's were estimated by finding the closest analogue to the system of interest and using that BDE for the calculations. This, of course, can be a major source of error. The following gives the choices made for the BDE's.

CH: The CH BDE's of several molecules have been determined[70]. However, Me_3Si-CH_3[71] (BDE of 99.2 kcal/mol) is the most similar to the present systems. Therefore, the value of 99 kcal/mol is used for all CH BDE's.

SiH: The closest analogue to the systems of interest is the $H_3Si-SiH_3$ molecule which has a BDE of 86.3 kcal/mol[71]. The value of 86 kcal/mol is used for all SiH BDE's.

GeH: The BDE of Ge-H for CH_3GeH_3 is 83 kcal/mol[72]. The BDE for GeH_4 is given as 84[73] and 89[72] kcal/mol by different experimental researchers. Also, a theoretical value of 84.8 has been determined by Binning and Curtiss[74]. The BDE for Me_3GeH has been determined to be 82 kcal/mol. The value of 82 kcal/mol is chosen for all Ge-H BDE's except that of CH_3GeH_3 since the electronegativity of Si, Ge, and Sn should have similar effects as that of the bulky methyl groups of Me_3GeH.

SnH: The BDE of SnH_4 is 71.6 kcal/mol[75]. The value for Me_3Sn-H[76,77] and Bu_3Sn-H[78] is 74 kcal/mol. Therefore, the value of 74 kcal/mol is used for all Sn-H BDE's.

REFERENCES

1. Schmidt,M.W.;Truong,P.N.;Gordon,M.S.; *J.Am.Chem.Soc.*, **1987**,*109*, 5217-5227

2. Schmidt,M.W.;Gordon,M.S.;Dupuis,M.; *J.Am.Chem.Soc.*, **1985**,*107*, 2585-2589

3. Harmony,M.D.;Laurie,V.W.;Kuczkowski,R.L.;Schwendeman, R.H.;Ramsay,D.A.; Lovas,F.J.;Lafferty,W.J.;Maki,A.G. *J.Phys.Chem.Ref.Data*, **1979**, *8*, 619-721

4.a. Wiberg,N.;Wagner,G.;Muller,G.; *Angew.Chem.,Int.Ed. Engl.*, **1985**, *24*, 229-230
b. Brook,A.G.;Abdesaken,F.;Gutekunst,B.;Gutekunst,G.; Kallury,R.K.; *J.Chem.Soc.,Chem.Commun.*, **1981**, 191-192
c. Allison,C.E.;McMahon,T.B.; *J.Am.Chem.Soc.*, **1990**, *112*, 1672-1677

5.a. Fink,M.J.;Michalczyk,M.J.;Haller,K.J.;West,R.;Michl,J.; *J.Chem.Soc.,Chem.Commun.*, **1983** , 1010-1011
b. West,R.;Fink,M.J.;Michl,J.; *Science* , **1981**, *214*, 1343-1344
c. Masamune,S.;Hanzawa,Y.;Murakami,S.;Bally,T.;Blount, J.F.; *J.Am.Chem.Soc.*, **1982**, *104*, 1150-1153
d. Boudjouk,P.;Han,B.;Anderson,K.R.; *J.Am.Chem.Soc.*, **1982**,*104*, 4992-4993

6.a. Satgé,J.; *Adv.Organomet.Chem.*, **1982**, *21*, 241-287
b. Cowley,A.H.; *Polyhedron*, **1984**, *3*, 389-432
c. Cowley,A.H.; *Acc.Chem.Res.*, **1984**, *17*, 386-392
d. Barrau,J.;Escudié,J.;Satgé,J.; *Chem.Rev.*, **1990**, *90*, 283-319
e. Tsumuraya,T.;Batcheller,S.A.;Masamune,S.; *Angew.Chem. Int.Ed.Engl.*, **1991**, *30*, 902-930

7.a. Meyer,H.;Baum,G.;Massa,W.;Berndt,A.; *Angew.Chem.Int.Ed. Engl.*, **1987**, *26*, 798-799
b. Berndt,A.;Meyer,H.;Baum,G.;Massa,W.;Berger,S.; *Pure & Appl.Chem.*, **1987**, *59*, 1011-1014

8.a. Couret,C.;Escudie,J.;Satge´,J.;Lazraq,M.; *J.Am.Chem. Soc.*; **1987**,*109*, 4411-4412
b. Lazraq,M.;Escudie,J.;Couret,C.;Satge´,J.;Drager,M.; Dammel,R.;*Angew.Chem.Int.Ed.Engl.*, **1988**, *27*, 828-829

9. Barton,T.J.;Kline,E.A.;Garvey,P.M.; *J.Am.Chem.Soc.*; **1973**,*95*, 3078

10.a. Barton,T.J.; *Pure Appl.Chem.*, **1980**, *52*, 615

b. Barton,T.J.;Hoekman,S.K.; *J.Am.Chem.Soc.*; **1980**, *102*, 1584-1591
c. Norsoph,E.B.;Coleman,B.;Jones,M.,Jr.; *J.Am.Chem.Soc.*; **1978**,*100*, 994-995

11. Riviere,P.;Castel,A.;Satge´,J.; *J.Am.Chem.Soc.*; **1980**, *102*, 5413-5415

12. Wiberg,N.; *J.Organomet.Chem.*, **1984**, *273*, 141-177

13.a. Trinquier,G.;Malrieu,J.P.;*J.Am.Chem.Soc.*,**1987**,*109*, 5303-5315
b. Malrieu,J.P.;Trinquier,G.;*J.Am.Chem.Soc.*,**1989**,*111*, 5916-5921
c. Trinquier,G.;Malrieu,J.P.;*J.Phys.Chem.*,**1990**,*94*,6184-6196

14. Pauling,L.; *Proc.Natl.Acad.Sci. U.S.A.*, **1983**, *80*, 3871

15.a. Anseleme,G.;Escudié,J.;Couret,C.;Satgé,J.;*J.Organomet. Chem.*, **1991**, *403*, 93 - 100
b. Lazraq,M.;Couret,C.;Escudié,J.;Satgé,J.;Soufiaoui,M.; *Polyhedron*, **1991**, *10*, 1153-1161

16. Dewar,M.J.S.;Grady,G.L.;Healy,E.F.; *Organometallics*, **1987**, *6*, 186-189

17.a. Kudo,T.;Nagase,S.; *Chem.Phys,Lett.*, **1981**, *84*, 375-379
b. Trinquier.G.;Barthelat,J.;Satge´,J.; *J.Am.Chem.Soc.*; **1982**, *104*, 5931-5936
c. Nagase,S.;Kudo,T.; *Organomettalics*, **1984**, *3*, 324-325

18. Dobbs,K.D.;Hehre,W.J.; *Organometallics*, **1986**, *5*, 2057-2061

19. Gordon, M.S.;Truong,T.N.;Bonderson,E.K.; *J.Am.Chem. Soc.*; **1986**; *108*, 1421-1427

20. Meyer,H.;Baum,G.;Massa,W.;Berger,S.;Berndt,A.; *Angew. Chem.Int.Ed.Engl.*, **1987**, *26*, 546-548

21. Dewar,M.J.S.;Grady,G.L.;Kuhn,D.R.;Merz,K.M.,Jr.; *J.Am. Chem.Soc.*; **1984**, *106*, 6773-6777

22. Baines,K.M.;Cooke,J.A.; *Organomet.*, **1991**, *10*, 3419-3421

23. Grev,R.S.;Schaefer,H.F.,III;Baines,K.M.; *J.Am.Chem. Soc.*; **1990**, *112*, 9458-9467

24.a. Satge´,J.; *Adv.Organomet.Chem.*, **1982**, *21*, 241-287

b. Barrau,J.;Escudie´,J.;Satge´,J.; *Chem.Rev.*, **1990**, *90*, 283-319

25. Riviere,P.;Castel,A.;Satge´,J.; *J.Organmet.Chem.*, **1981**, *212*, 351-367

26. Sakuri,H.;Nakadaira,Y.;Tobita,H.; *Chem.Lett.*, **1982**, 1855-1858

27. Masamune,S.;Hanzawa,Y.;Williams,D.J.; *J.Am.Chem.Soc.*, **1982**, *104*, 6136-6137

28.a. Bleckman,P.;Minkwitz,R.;Neumann,W.P.;Schriewer,M.; Thibud,M.;Watta,B.; *Tetrahedron Lett.*, **1984**, *25*, 2467-2470
b. Bleckmann,P.;Thibud,M.;Trippe,H.-D.; *J.Mol.Struct.*, **1986**, *142*, 303-306

29.a. Davidson,P.J.;Harris,D.H.;Lappert,M.F.; *J.Chem.Soc., Dalton Trans.*, **1976**, 2268-2274
b. Hitchcock,P.B.;Lappert,M.F.;Miles,S.T.;Thorne,A.J.; *J.Chem Soc.,Chem.Comm.*, **1984**, 480-482
c. Goldberg,D.E.;Hitchcock,P.B.;Lappert,M.F.;Thomas,K.M.; Thorne,A.J.;Fjeldberg,T.;Haaland,A.;Schilling.B.E.R.; *J.Chem.Soc.,Dalton Trans.*, **1986**, 2387-2394

30.a. Snow,J.T.;Marakami,S.;Masamune,S.;Williams,D.J.; *Tetrahedron Letters*, **1984**, *25*, 4191-4194
b. Snow,J.T.;Masamune,S.; *Organomet.Synth.*, **1986**, 557
c. Collins,S.;Marakami,S.;Snow,J.T.;Masamune,S.; *Tetrahedron Letters*, **1985**, *26*, 1281-1284

31. Batcheller,S.A.;Tsumuraya,T.;Tempkin,O.;Davis,W.M.; Masamune,S.; *J.Am.Chem.Soc.*, **1990**, *112*, 9394-9395

32. Park,J.;Batcheller,S.A.;Masamune,S.; *J.Organomet.Chem.*, **1989**, *367*, 39-45

33. Dewar,M.J.S.;Grady,G.L.;Healy,E.J.; *Organomettalics*, **1987**, *6*, 186-189

34. Fjeldberg,T.;Haaland,A.;Lappert,M.F.;Schilling,B.E.R.; Seip,R.;Thorne,A.J.; *J.Chem.Soc.,Chem.Comm,*, **1982**, 1407-1408

35. Trinquier,G.;Malrieu,J.-P.;Rivière,P.; *J.Am.Chem.Soc.*, **1982**, *104*, 4529-4533

36. Nagase,S.;Kudo,T.; *J.Mol.Struct.*, **1983**, *103*, 35-44

37. Liang,C.;Allen,L.C.; *J.Am.Chem.Soc.*, **1990**, *112*, 1039-

1041

38. Trinquier,G.; *J.Am.Chem.Soc.*, **1990**, *112*, 2130-2137

39.a. Gorldberg,D.E.;Harris,D.H.;Lappert,M.F.;Thomas,K.M.;*J. Chem.Soc.,Chem.Comm.*, **1976**, 261-262
b. Zilm,K.W.;Lawless,G.A.;Merrill,R.M.;Millar,J.M.;Webb, G.G.; *J.Am.Chem.Soc.*, **1987**, *109*, 7236-7238

40. Masamune,S.;Sita,L.R.; *J.Am.Chem.Soc.*, **1985**, *107*, 6390-6391

41. Fjeldberg,T.;Haaland,A.;Schilling,B.E.R;Volden,H.V.; Lappert,M.J.;Thorne,A.J.; *J.Organomet.Chem.*, **1984**, *276*, C1-C4

42. Márquez,A.;Gonzalez,G.G.;Fenandezsanz,J.; *Chem.Phys.*, **1989**, *138*, 99-104

43. Schleyer,P.v.R.;Kost,D.; *J.Am.Chem.Soc.*, **1988**, *110*, 2105-2109

44. Cundari,T.; Gordon,M.S.; *J.Am.Chem.Soc.*, **1991**, *113*, 5231-5243

45.a. Binkley,J.S.;Pople,J.A.;Hehre,W.J.; *J.Am.Chem.Soc.*; **1980**,*102*, 939-947
b. Gordon,M.S.;Binkley,J.S.;Pople,J.A.;Pietro,W.J.;Hehre, W.J.; *J.Am.Chem.Soc.*, **1982**, *104*, 2797-2803
c. Pietro,W.J.;Francl,M.M.;Hehre,W.J.;DeFrees,D.J.;Pople, J.A.;Binkley,J.S.; *J.Am.Chem.Soc.* , **1982** , *104*, 5039-5048
d. Dobbs,K.D.;Hehre,W.J.; *J.Comput.Chem.*, **1986**, 7, 359-378

46.a. Ruedenberg,K.;Schmidt,M.W.;Gilbert,M.M.;Elbert,S.T.; *Chem.Phys.*, **1982**, *71*, 41-49
b. Ruedenberg,K.;Schmidt,M.W.;Gilbert,M.M.; *Chem.Phys.*, **1982**, *71*, 51-64
c. Ruedenberg,K.;Schmidt,M.W.;Gilbert,M.M.;Elbert,S.T.; *Chem.Phys.*, **1982**, *71*, 65-78

47. Lam,B.;Schmidt,M.W.;Ruedenberg,K.; *J.Phys.Chem.*, **1985**, *89*, 2221-2235

48. Pipek,J.;Mezey,P.Z.; *J.Chem.Phys.*, **1989**, *90*, 4916-4926

49. Schmidt,M.W.;Baldridge,K.K.;Boatz,J.A.;Jensen,J.H.; Koseki,S.;Gordon,M.S.;Nguyen,K.A.;Windus,T.L.;Elbert, S.T.; QCPE Bulletin 10, **1990**, 52

50. Pople,J.A.;Binkley,J.S.;Seeger,R.; *Int.J. Quantum Chem.*, **1976**, *S10*, 1-19

51. Krishnan,R.;Frisch,M.J.;Pople,J.A.; *J.Chem.Phys.*, **1980**, *72*, 4244-4245

52. Frisch,M.J.;Binkley,J.S.;Schlegel,H.B.;Raghavachari,K.; Melius,C.F.;Martin,R.L.;Stewart,J.J.P.;Bobrowicz,F.W.; Rohlfing,C.M.;Kahn,L.R.;DeFrees,D.J.;Seeger,R.; Whiteside, R.A.;Fox,D.J.;Fleuder,E.M.;Pople,J.A.; Carnegie-Mellon Quantum Chemistry Publishing Unit, Pittsburgh, PA 15213

53. Frisch,M.J.;Head-Gordon,M.;Schlegel,H.B.;Raghavachari, K.; Binkley,J.S.;Gonzalez,C.;DeFrees,D.J.;Fox,D.J.; Whiteside,R.A.;Seeger,R.;Melius,C.F.;Baker,J.; Martin,R.; Kahn,L.R.;Stewart,J.J.P.;Fluder,E.M.;Topiol, S.;Pople, J.A.;Gaussian, Inc., Pittburgh, PA, 1988

54. Private communication from Michael W. Schmidt.

55. Laurie,V.W.; *J.Chem.Phys.*, **1959**, *30*, 1210-1214

56. Cox,A.P.;Varma,R.; *J.Chem.Phys.*, **1967**, *46*, 2007-2008

57. Pauling,L.;Laubengayer,A.W.;Hoard,J.L.;*J.Am.Chem.Soc.*, **1938**, *60*, 1605-1607

58. Lide,D.R.; *J.Chem.Phys.*, **1951**, *19*, 1605-1606

59. Puff,H.;Breuer,B.;Gehrke-Brinkmann,G.;Kind,P.;Reuter, H.; Schuh,W.;Wald,W.;Weidenbrück,G.; *J.Organomet.Chem.*, **1989**,*363*, 265-280

60.a. Shimanouchi,T.; *Natl.Stand.Ref. Data Ser., U.S. Natl.Bur.Stand.*, **1972**, *39*

b. Shimanouchi,T.; *J.Phys.Chem.Ref. Data*, **1977**, *6*, 993-1102

61. Maier,G.;Mihm,G.;Reisenauer,H.P.; *Angew.Chem.,Int.Ed. Engl.*, **1981**,*20*, 597-598

62. Durig,J.R.;Church,J.S.; *J.Chem.Phys.*, **1980**, *73*, 4784-4797

63. Marchand,A.;Gerval,P.;Duboudin,F.;Joanny,M.;Mazerolles, P.; *J.Organomet.Chem.*, **1984**, *267*, 93-106

64. Mohan,S.;Prabakaran,A.R.;Payami,F.;*J.Raman Spectrosc.*, **1989**, *20*, 119-121

65. Kimmel,H.;Dillard,C.R.; *Spectrosc.*, **1968**, *24A*, 909-912

66. Adams,S.;Dräger,M.;*J.Organomet.Chem.*, **1985**, *288*, 395-404

67. Huber,K.P.;Herzberg,G.; *Constants of Diatomic Molecules*; Van Nostrand reinhold; New York, 1979

68. Pietro,W.J.;Hehre,W.J.; *J.Am.Chem.Soc.*, **1982**, *104*, 4329-4332

69. Kutzelnigg,W.;*Angew.Chem.Int.Ed.Engl.*, **1984**, *23*, 272-295

70. See for instance
a. Benson,S.W.;O'Neal,H.E.; *Kinetic Data on Gas Phase Unimolecular Reactions*, U.S. Dept. of Commerce, National Bureau of Standards, NSRDS-NMD 21, February 1970
b. Shum,L.G.S.;Benson,S.W.; *Int.J.Chem.Kinet.*, **1985**, *17*, 277-292

71. Walsh,R.; *Acc.Chem.Res.*, **1981**, *14*, 246-252

72. Austin,E.R.;Lampe.F.W.; *J.Phys.Chem.*, **1977**, *81*, 1546-1549

73. Noble,P.N.;Walsh,R.; *Int.J.Chem.Kin.*, **1983**, *15*, 547-560

74. Binning,R.C.;Curtiss,L.A.; *J.Chem.Phys.*, **1990**, *92*, 1860-1864

75. Ruscic,B.;Swarz,M.;Berkowitz,J.; *J.Chem.Phys.*, **1990**, *92*, 1865-1875

76. Jackson,R.A.; *J.Organomet.Chem.*, **1979**, *166*, 17-19

77. Griller,D.;Kanabus-Kaminska,J.M.;Maccoll,A.; *J.Mol. Struct.(Theochem)*, **1988**, *163*, 125-131

78. Burkey,T.J.;Majewski,M.;Griller,D.; *J.Am.Chem.Soc.*, **1986**,*108*, 2218-2221

Table I: MCSCF natural orbital occupation numbers for $H_2X{=}YH_2$.

X	Y	σ	π	π*	σ*
C	C[a]	1.98	1.92	0.08	0.02
C	Si[a]	1.97	1.90	0.10	0.03
Ge	C	1.97	1.89	0.11	0.03
Si	Si[a]	1.98	1.84	0.16	0.02
Ge	Si	1.98	1.83	0.17	0.02
Ge	Ge	1.98	1.82	0.18	0.02
Sn	C	1.97	1.81	0.19	0.03
Sn	Si	1.98	1.79	0.21	0.02
Sn	Ge	1.98	1.80	0.20	0.02
Sn	Sn	1.98	1.78	0.22	0.02

a. Reference 54.

Table II: Primary resonance contributions from MC/LMO/CI for $H_2X{=}YH_2$. Values are the configuration coefficients squared.

config.[a]	GeC	GeSi	GeGe	SnC	SnSi	SnGe	SnSn
|2020>	0.052	0.030	0.037	0.029	0.020	0.035	0.034
|1111>[b]	0.417	0.408	0.415	0.438	0.391	0.412	0.427
|0202>	0.049	0.040	0.037	0.040	0.030	0.030	0.034
|2110>	0.120	0.155	0.152	0.101	0.136	0.139	0.153
|1201>	0.062	0.061	0.053	0.046	0.038	0.040	0.044
|2200>	0.009	0.013	0.010	0.006	0.009	0.007	0.008
|0022>	0.023	0.010	0.010	0.016	0.008	0.010	0.008
|1021>	0.097	0.046	0.053	0.063	0.038	0.052	0.044
|0112>	0.171	0.141	0.152	0.188	0.134	0.158	0.153
neut[c]	0.518	0.478	0.489	0.507	0.441	0.477	0.495
elec[d]	0.191	0.229	0.215	0.153	0.183	0.186	0.205
nucl[e]	0.291	0.197	0.215	0.267	0.180	0.220	0.205
total[f]	1.000	0.904	0.919	0.927	0.804	0.883	0.905

a. Each configuration |ijkl> represents i electrons in a σ_X LMO, j electrons in a π_X LMO, k electrons in a π_Y LMO, and l electrons in a σ_Y LMO, for an X=Y bond.

b. This configuration actually consists of two |1111> singlet configurations that differ in spin coupling.

c. Configurations |2020> + |1111> + |0202> correspond to a neutral charge distribution between center X and Y.

d. Configurations |2110> + |1201> + |2200> correspond to Y as an electrophilic center.

e. Configurations |0022> + |1021> + |0112> correspond to Y as a nucleophilic center.

f. Total of listed configurations.

Table III: Planar MCSCF structures for XYH_4. Bond lengths in Å and angles in degrees.

X	Y	X=Y	X-H	Y-H	X-Y-H	Y-X-H	H-X-H	H-Y-H	Lowest frequency
Ge	C	1.814	1.536	1.076	121.4	122.9	114.3	117.2	266
Ge	Si	2.222	1.535	1.471	122.1	122.6	114.8	115.7	355i
Ge	Ge	2.270	1.534	1.534	122.4	122.4	115.3	115.3	390i
Sn	C	2.041	1.734	1.077	121.5	123.5	113.0	117.0	176i
Sn	Si	2.428	1.733	1.471	122.4	123.0	114.0	115.2	370i
Sn	Ge	2.466	1.732	1.536	122.7	123.0	114.1	114.7	390i
Sn	Sn	2.662	1.733	1.733	123.2	123.2	113.6	113.6	379i

Table IV: MCSCF, RHF, and MP2 structures for XYH_4. Bond lengths in Å and angles in degrees. RHF structures are in parenthesis. MP2 structures are in brackets.

X	Y	X=Y	X-H	Y-H	X-Y-H	Y-X-H	H-X-H	H-Y-H	X-Y-H-H	Y-X-H-H
Ge	C	1.814	1.536	1.076	121.4	122.9	114.3	117.2	0.0	0.0
		(1.761)	(1.536)	(1.077)	(121.9)	(123.1)	(113.8)	(116.3)	(0.0)	(0.0)
		[1.784]	[1.543]	[1.085]	[121.3]	[122.6]	[114.8]	[117.4]	[0.0]	[0.0]
Ge	Si	2.284	1.547	1.480	116.0	116.7	109.8	110.2	40.1	38.7
		(2.193)	(1.541)	(1.474)	(119.7)	(120.2)	(112.0)	(112.6)	(26.8)	(25.9)
		[2.208]	[1.550]	[1.484]	[118.0]	[118.4]	[111.6]	[112.3]	[32.4]	[32.1]
Ge	Ge	2.341	1.550	1.550	115.4	115.4	109.0	109.0	42.4	42.4
		(2.275)	(1.547)	(1.547)	(117.6)	(117.6)	(109.5)	(109.5)	(36.6)	(36.6)
		[2.270]	[1.554]	[1.554]	[116.9]	[116.9]	[110.4]	[110.4]	[37.5]	[37.5]
Sn	C	2.063	1.740	1.079	120.5	120.0	111.8	115.5	17.9	26.8
		(1.976)	(1.734)	(1.077)	(122.1)	(123.9)	(112.2)	(115.8)	(0.0)	(0.0)
		[2.007]	[1.741]	[1.085]	[121.5]	[123.3]	[113.4]	[117.1]	[0.0]	[0.0]
Sn	Si	2.511	1.749	1.482	114.5	115.9	107.7	108.4	44.7	42.2
		(2.436)	(1.747)	(1.481)	(116.5)	(118.9)	(107.8)	(108.9)	(39.9)	(34.9)
		[2.429]	[1.753]	[1.488]	[115.8]	[118.1]	[108.6]	[109.9]	[40.7]	[36.1]
Sn	Ge	2.555	1.752	1.554	114.1	115.3	107.4	107.5	46.3	43.7
		(2.504)	(1.751)	(1.555)	(114.8)	(117.6)	(106.0)	(106.8)	(45.3)	(39.7)
		[2.479]	[1.756]	[1.560]	[114.2]	[117.7]	[107.4]	[108.2]	[45.5]	[38.3]
Sn	Sn	2.769	1.754	1.754	114.1	114.1	106.2	106.2	47.1	47.1
		(2.728)	(1.756)	(1.756)	(115.4)	(115.4)	(104.7)	(104.7)	(45.4)	(45.4)
		[2.690]	[1.760]	[1.760]	[115.5]	[115.5]	[106.3]	[106.3]	[44.2]	[44.2]

Table V: RHF and MP2 structures for staggered XYH_6. Bond lengths in Å and angles in degrees. MP2 structures are in parenthesis.

X	Y	X-Y	X-H	Y-H	X-Y-H	Y-X-H	H-X-H	H-Y-H
Ge	C	1.976	1.551	1.087	110.5	110.4	108.5	108.5
		(1.966)	(1.556)	(1.092)	(110.2)	(110.5)	(108.4)	(108.7)
Ge	Si	2.400	1.550	1.481	110.2	110.5	108.4	108.7
		(2.374)	(1.555)	(1.488)	(110.2)	(110.6)	(108.4)	(108.8)
Ge	Ge	2.443	1.550	1.550	110.3	110.3	108.6	108.6
		(2.415)	(1.555)	(1.555)	(110.3)	(110.3)	(108.6)	(108.6)
Sn	C	2.188	1.750	1.087	110.5	110.3	108.6	108.4
		(2.178)	(1.756)	(1.092)	(110.3)	(110.4)	(108.5)	(108.6)
Sn	Si	2.610	1.748	1.481	110.4	110.5	108.4	108.5
		(2.585)	(1.754)	(1.488)	(110.4)	(110.5)	(108.4)	(108.6)
Sn	Ge	2.642	1.748	1.550	110.6	110.3	108.6	108.4
		(2.611)	(1.753)	(1.556)	(110.7)	(110.4)	(108.5)	(108.3)
Sn	Sn	2.845	1.748	1.748	110.6	110.6	108.3	108.3
		(2.813)	(1.754)	(1.754)	(110.7)	(110.7)	(108.2)	(108.2)

Table VI: MCSCF, RHF, MP2, and experimental X-Y double and single bond lengths in Å. RHF lengths are in parenthesis. MP2 lengths are in brackets.

		X=Y		X-Y	
X	Y	theory	exp	theory	exp
Ge	C	1.814	1.80[a]		
		(1.761)	1.827[b]	(1.976)	1.945[g]
		[1.784]		[1.966]	
Ge	Si	2.284			
		(2.193)		(2.400)	2.357[h]
		[2.208]		[2.374]	
Ge	Ge	2.341	2.347[c]		
		(2.275)	2.213[d]	(2.443)	2.41[i]
		[2.270]		[2.415]	
Sn	C	2.063	2.025[e]		
		(1.976)		(2.188)	2.143[j]
		[2.007]		[2.178]	
Sn	Si	2.511			
		(2.436)		(2.188)	
		[2.429]		[2.585]	
Sn	Ge	2.555			
		(2.504)		(2.642)	
		[2.479]		[2.611]	
Sn	Sn	2.769	2.768[f]		
		(2.728)		(2.845)	2.823[k]
		[2.690]		[2.813]	

a. From **2**[8].
b. From **1**[7] and **3**[15].
c. From **5**[29a].
d. From **6**[30a].
e. From **4**[7b].
f. From **8**[29a].
g. From $GeCH_6$[55].
h. From $GeSiH_6$[56].
i. From Ge_2H_6[57].
j. From $SnCH_6$[58].
k. From Bz_6Sn_2[59].

Table VII: RHF, MP2, MCSCF and experimental frequencies for X-Y double and single bond structures. Units are cm^{-1}.

	RHF	MP2	MCSCF	exp
C-C	1046			995[a]
C=C	1853			1623[a]
Si-C	736			700[a]
Si=C	1080			985[b]
Si-Si	466			432[c]
Si=Si	653			630[d]
Ge-C	613	609		
Ge=C	904	827	785	988[e]
Ge-Si	377	379		320[f]
Ge=Si	526	497	371	
Ge-Ge	282	286		275[g]
Ge=Ge	272	311	285	404[g]
Sn-C	552	546		527[h]
Sn=C	755	737	660	
Sn-Si	323	324		
Sn=Si	295	378	314	
Sn-Ge	234	237		
Sn=Ge	222	259	233	
Sn-Sn	189	192		119[i]
Sn=Sn	172	204	184	

a. From C_2H_6, C_2H_4, and $SiCH_6$[60].
b. From $SiCH_6$[61].
c. From Si_2H_6[62].
d. From $Si_2(CH_3)_4$[63].
e. From **2**[28b].
f. From $GeSiH_6$[64].
g. From $Ge_2(CH_3)_6$ and $Ge_2(CH_3)_4$[28b].
h. From $SnCH_6$[65].
i. From $I(tBu_2Sn)_4I$[66].

Table VIII: Total energies in hartrees at the MCSCF/3-21G(d) geometries.[a]

molecule	ZPE MCSCF	Total energies MCSCF	SOCI
$H_2Ge=CH_2$			
gs	0.04022	-2105.50258	-2105.53125
sing	0.03779	-2105.44849	-2105.47745
trip	0.03840	-2105.45118	-2105.48065
$H_2Ge=SiH_2$			
gs	0.03171	-2355.28861	-2355.32016
pl	0.03109	-2355.28359	-2355.31395
sing	0.03094	-2355.24963	-2355.27847
trip	0.03157	-2355.25352	-2355.28317
$H_2Ge=GeH_2$			
gs	0.03018	-4133.34776	-4133.37773
pl	0.02967	-4133.34019	-4133.36878
sing	0.02913	-4133.30825	-4133.33618
trip	0.03017	-4133.31251	-4133.34132
$H_2Sn=CH_2$			
gs	0.03743	-6036.71807	-6036.74488
pl	0.03704	-6036.71752	-6036.74350
sing	0.03560	-6036.68273	-6036.70980
trip	0.03606	-6036.68570	-6036.71313
$H_2Sn=SiH_2$			
gs	0.02949	-6286.51939	-6286.54903
pl	0.02889	-6286.51152	-6286.53946
sing	0.02859	-6286.48710	-6286.51382
trip	0.02970	-6286.49117	-6286.51865
$H_2Sn=GeH_2$			
gs	0.02800	-8064.58155	-8064.60967
pl	0.02753	-8064.57140	-8064.59818
sing	0.02709	-8064.54789	-8064.57428
trip	0.02758	-8064.55223	-8064.57941
$H_2Sn=SnH_2$			
gs	0.02595	-11995.81786	-11995.84499
pl	0.02555	-11995.80578	-11995.83066
sing	0.02518	-11995.78815	-11995.81274
trip	0.02558	-11995.79257	-11995.81804

a.gs = equilibrium groun state structure; pl = planar structure;
sing = singlet twisted structure; trip = triplet twisted structure

Table IX: Relative energies in kcal/mol using 3-21G(d) basis set.[a]

molecule	Relative enthalpies MCSCF	SOCI
	$H_2Ge=CH_2$	
gs	0.0	0.0
sing	32.4	32.2
trip	30.7	30.2
	$H_2Ge=SiH_2$	
gs	0.0	0.0
pl	2.8	3.5
sing	24.0	25.7
trip	21.9	23.1
	$H_2Ge=GeH_2$	
gs	0.0	0.0
pl	4.4	5.3
sing	24.1	25.4
trip	22.1	22.8
	$H_2Sn=CH_2$	
gs	0.0	0.0
pl	0.1	0.6
sing	21.0	20.9
trip	19.5	19.1
	$H_2Sn=SiH_2$	
gs	0.0	0.0
pl	4.6	5.6
sing	19.7	21.5
trip	17.8	19.2
	$H_2Sn=GeH_2$	
gs	0.0	0.0
pl	6.1	6.9
sing	20.5	21.6
trip	18.1	18.7
	$H_2Sn=SnH_2$	
gs	0.0	0.0
pl	7.3	8.7
sing	18.1	19.7
trip	15.6	16.7

a.gs = equilibrium ground state structure; pl = planar structure;
sing = singlet twisted structure; trip = triplet twisted structure

Table X: Energies at the RHF and MP2 optimized structures with energies from the MP2 structures in parenthesis. Energies in hartrees.

molecule	ZPE	Total energies RHF	MP2	MP4
$GeCH_6$	0.06275	-2106.67874	-2106.89164	-2106.93180
	(0.06094)	(-2106.67863)	(-2106.89174)	(-2106.93200)
$GeCH_4$	0.04139	-2105.44880	-2105.66279	-2105.69959
	(0.03949)	(-2105.44831)	(-2105.66344)	(-2105.70065)
$GeSiH_6$	0.05058	-2356.46429	-2356.62865	-2356.67324
	(0.04897)	(-2356.46408)	(-2356.62876)	(-2356.67346)
$GeSiH_4$	0.03208	-2355.24811	-2355.41440	-2355.45680
	(0.03092)	(-2355.24781)	(-2355.41480)	(-2355.45769)
Ge_2H_6	0.04835	-4134.51328	-4134.67567	-4134.72003
	(0.04678	(-4134.51306)	(-4134.67572)	(-4134.72016)
Ge_2H_4	0.03037	-4133.30737	-4133.47137	-4133.51364
	(0.02937)	(-4133.30723)	(-4133.47149)	(-4133.51386)
$SnCH_6$	0.05892	-6037.89777	-6038.10044	-6038.14016
	(0.05715)	(-6037.89767)	(-6038.10052)	(-6038.14034)
$SnCH_4$	0.03839	-6036.65772	-6036.86674	-6036.90382
	(0.03662)	(-6036.65708)	(-6036.86764)	(-6036.90522)
$SnSiH_6$	0.04718	-6287.68747	-6287.84071	-6287.88498
	(0.04561)	(-6287.68728)	(-6287.84080)	(-6287.88518)
$SnSiH_4$	0.02968	-6286.47810	-6286.63438	-6286.67759
	(0.02872)	(-6286.47794)	(-6286.63449)	(-6286.67781)
$SnGeH_6$	0.04497	-8065.73881	-8065.89031	-8065.93437
	(0.04344)	(-8065.73859)	(-8065.89034)	(-8065.93450)
$SnGeH_4$	0.02799	-8064.54223	-8064.69544	-8064.73803
	(0.02717)	(-8064.54202)	(-8064.69549)	(-8064.73797)
Sn_2H_6	0.04174	-11996.96598	-11997.10625	-11997.15005
	(0.04023)	(-11996.96577)	(-11997.10626)	(-11997.15016)
Sn_2H_4	0.02584	-11995.78069	-11995.92223	-11995.96488
	(0.02511)	(-11995.78041)	(-11995.92230)	(-11995.96483)

Table XI: Thermochemical D_π for XYH_4. Energies in kcal/mol.

X	Y	$\Delta H°$	D(X-H)	D(Y-H)	D_π
Ge	C	45.9	83	99	33
Ge	Si	38.3	82	86	26
Ge	Ge	32.7	82	82	28
Sn	C	48.9	74	99	21
Sn	Si	33.7	72	86	21
Sn	Ge	27.3	72	82	23
Sn	Sn	21.0	72	72	20

Table XII: XYH_4 π-bond strengths. Energies in kcal/mol.

X	Y	thermo. cycle	rotation	other theor.	exp
Ge	C	33	32.2	31[a], 26.9[b]	43[c]
Ge	Si	26	25.7	25[d]	
Ge	Ge	28	25.4	25[d]	22.2[e]
Sn	C	21	20.9	19[a]	45[c]
Sn	Si	21	21.5		
Sn	Ge	23	21.6		
Sn	Sn	20	19.7		

a. Reference 18.
b. Reference 17b.
c. Reference 68.
d. Reference 24.
e. Reference 31.

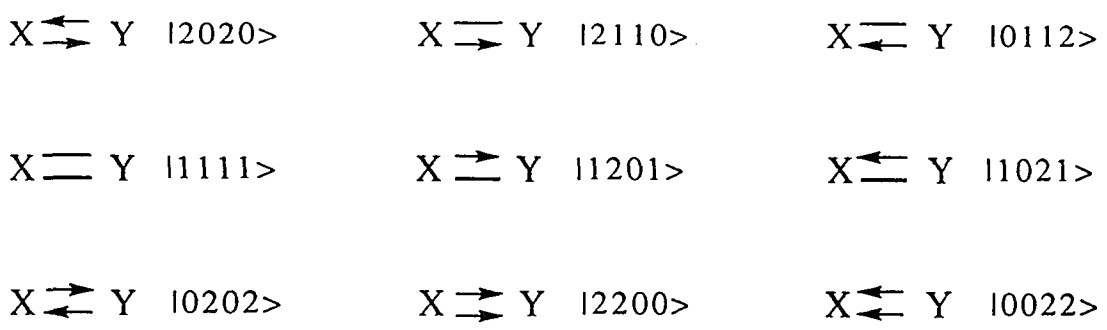

Figure 1: Primary Resonance Structures.

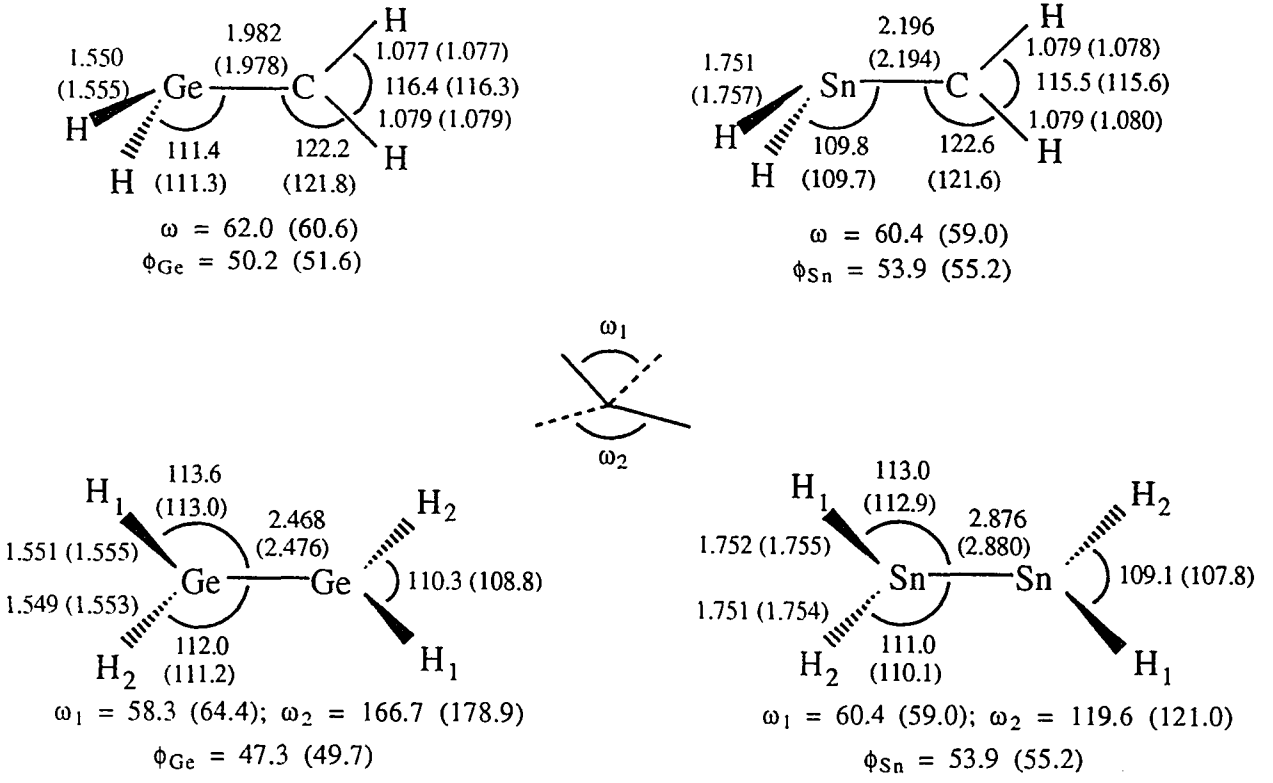

Figure 2: Structures for the twisted singlet and triplet structures. Bond lengths are in Angstroms and angles are in degrees. Triplet values are in parenthesis. ω is the dihedral angle HXYH and ϕ_Y is the flap angle between bond XY and plane YH_2 at pyramidal atom Y.

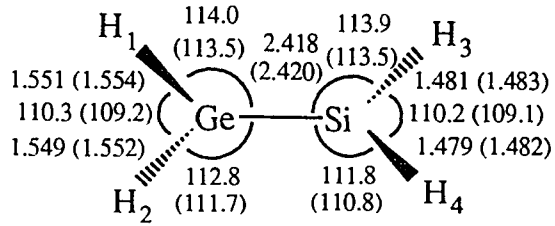

ω_1 = 55.5 (61.1); ω_2 = 163.0 (173.8)

ϕ_{Ge} = 46.0 (48.3); ϕ_{Si} = 47.3 (49.3)

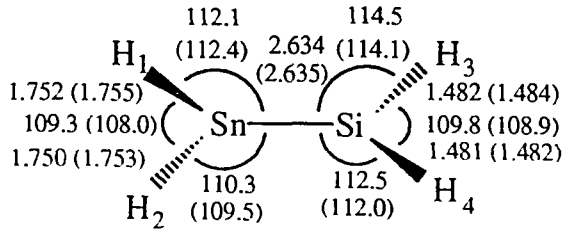

ω_1 = 60.2 (64.0); ω_2 = 171.9 (179.7)

ϕ_{Sn} = 51.3 (52.4); ϕ_{Si} = 46.1 (47.7)

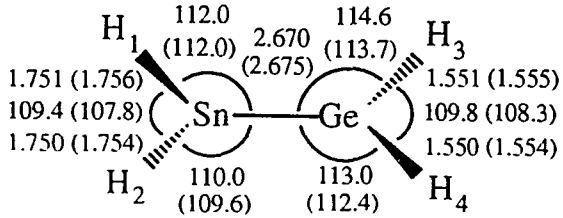

ω_1 = 62.9 (64.2); ω_2 = 174.3 (179.0)

ϕ_{Sn} = 51.7 (52.9); ϕ_{Ge} = 45.4 (47.9)

Figure 2: (continued)

PAPER 6: THEORETICAL INVESTIGATION OF AZAPHOSPHATRANE BASES

Theoretical Investigation of Azaphosphatrane Bases

Theresa L. Windus
Michael W. Schmidt
Mark S. Gordon

Department of Chemistry
Iowa State University
Ames, Iowa 50011

to be submitted

ABSTRACT

A series of azaphosphatrane molecules of the form $ZP[NH(CH_2)_2]_3N$, where Z = H^+, F^+, Cl^+, CH_2, CH_3^+, NH, NH_2^+, O, or OH^+ are compared with the unsubstituted compound. The proton affinities of the base molecules are determined and predictions of their relative base strengths are given. The dramatic change in the P-N transannular distance upon addition of Z and the nature of the P-N bond is investigated for these molecules. The cationic species are shown to have some dative bonding. An estimate of the solvent effects on the acid-base relationships of these molecules is also given.

INTRODUCTION

In the past several years, our group has been interested in the nature of the bonding in polycyclic and cage compounds, such as bicyclobutanes, propellanes, and silatranes.[1] In this paper, we extend our interest in transannular bonding to the unique azaphosphatrane molecules synthesized by Verkade and coworkers.[2] The prototype azaphosphatrane, **1**, (top view and side view shown below) {P[N(CH$_3$)(CH$_2$)$_2$]$_3$N} has

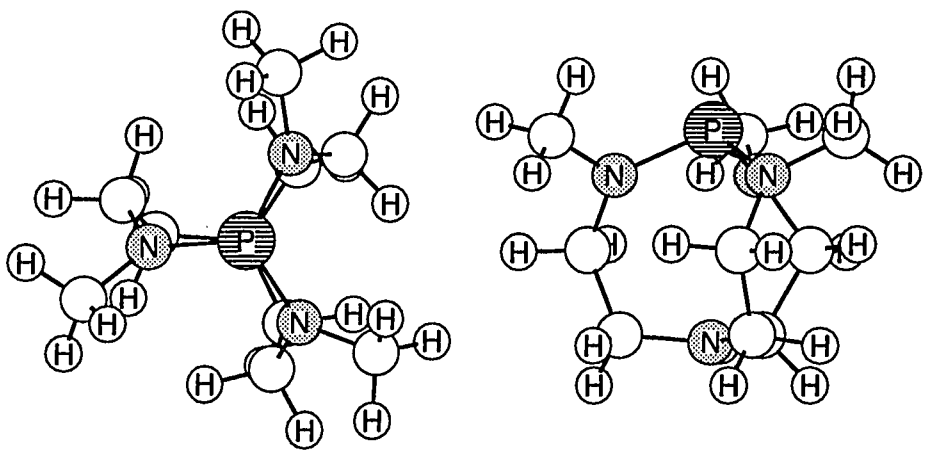

1

been shown to be useful as a non-ionic base and as a catalyst in the synthesis of triaryl isocyanurates which are used in the synthesis of nylon-6. **1** is a very strong base whose

conjugate acid, **2**, (again shown with top and side views) has a pK_a of 27 in dimethylsulfoxide (DMSO).

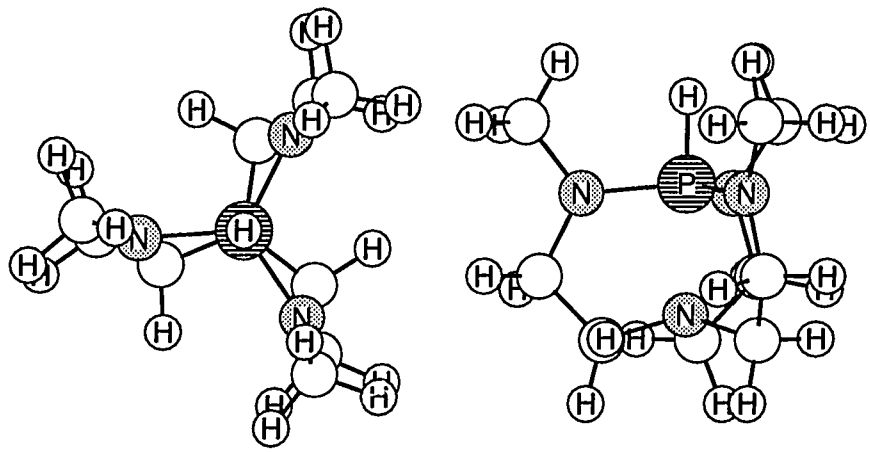

2

This makes **1** a stronger base than any phosphine base known. The transannular P-N distance is quite short in **2** (1.976 Å from crystallographic data[2.d.]) suggesting some dative bonding, and it is very much shorter than in **1** as found in the coordination compound cis-$PtCl_2$(**1**)$_2$ (3.33 Å[2.c.]). The latter distance is very close to the sum of the van der Waals radii (3.35 Å).

Another interesting feature of the azaphosphatrane is the drastic change that can be made in the transannular P-N bond by varying the substituent Z on the phosphorus. X-ray structures have shown that the P-N distance can vary from

about 2.0 to 3.4 Å depending on Z^2. This large change is amazing!

In this paper, we investigate substitution effects of Z = unsubstituted, H^+, F^+, Cl^+, CH_2, CH_3^+, NH, NH_2^+, O, or OH^+ on the proton affinities of the neutrals and the nature of the transannular bond. For simplicity, this paper will concentrate on azaphosphatranes with a hydrogen on the nitrogens alpha to the phosphorus. The experimentally known compounds normally have methyl groups at this location. Using the Onsager reaction field method,[3] we will also qualitatively assess the effects of solvent on the proton affinities and dipoles of these molecules.

This work is organized in the following manner: first the computational methods used will be discussed, then the results and discussion will be presented and, finally, the conclusions will be formulated.

COMPUTATIONAL METHODS

Geometries and energetics were calculated at the RHF[4]/6-31G(d)[5] level of theory. For those cases in which it was appropriate, C_3 symmetry was used in the optimization procedure. All geometries were converged so that the root mean square of the gradient was less than 0.0001 and the maximum component of the gradient was less than 0.00003.

Numerical second derivatives of the energy with respect to the nuclear coordinates (hessians) were only calculated for the two smallest molecules of the series {$P[NH(CH_2)_2]_3N$ and $HP[NH(CH_2)_2]_3N^+$} because of the prohibitive cost of these calculations. Both of the calculated hessians were positive definite.

Because of the large number of basis functions (from 199 to 220), the parallel version of the electronic structure code GAMESS[6] was used for these calculations. All calculations were performed on the Touchstone Delta using the parallel implementation. Typical runs employed 128 or 256 nodes. Since the description of parallel GAMESS is presented elsewhere,[6,7] only a brief discussion will be included here.

Parallelization of GAMESS is accomplished through the use of the message passing toolkit, TCGMSG.[8] This package allows for the best communication of the particular parallel architecture to be used. It runs on distributed memory machines (such as the Touchstone Delta), shared memory

machines (such as the Alliant) and an Ethernetwork of UNIX machines (potentially of different platforms).

A distributed memory, single program multi-data (SPMD) model is used, where all of the nodes have all of the necessary information for the calculation. Energies and gradients for self-consistent field (SCF) wavefunctions have been parallelized. Since the gradients are parallelized, optimizations, transition state searches, intrinsic reaction coordinate (IRC) following and numerical hessians all work in parallel. Recently, a small scale method of analytic hessian parallelization has been implemented.[7]

Load balancing is accomplished through two different methods. One is based on static load balancing and is best used when the nodes are of similar speed and load. This method splits the work between the nodes without using any communication. As an example, approximately equal numbers of integrals are assigned to each processor by splitting off different shells of integrals to different processors. This is the method that is used on the Delta and therefore, in this work.

The second type of load balancing is a dynamic load balancing technique. This method has a shared counter (handled by TCGMSG) that allows each processor to get more work when it is finished with its current batch of work. This method uses communication (for the shared counter) and

is intended for machines that are not of the same speed and/or work load.

The density analysis of Bader and coworkers[9] is used to investigate the nature of the P-N bonding. As previously reported, an extra d function needs to be added to the basis set to eliminate spurious behavior of the density. Only one additional RHF/6-31G(2d) energy calculation is performed to obtain the input and wavefunction needed for the AIMPAC program of Bader and coworkers.[9]

Since the density analysis has been described elsewhere, only a brief description of the points needed for this paper will be presented. A bond critical point is a "saddle point" in the electron density between two atoms. At this point, the hessian of the density has one positive eigenvalue along the bond and two negative eigenvalues along the axes orthogonal to the bond. A bond critical point *implies* a bond between the two atoms of interest. The other type of critical point found in this work is a ring critical point. The hessian of the density at such a point has one negative eigenvalue and two positive eigenvalues.

The Onsager reaction field[3] is used to obtain qualitative information about solvent effects. Since the azaphosphatranes are nearly spherical in nature, the spherical approximation used in this theory is well met. The dielectric constant is chosen to be that of DMSO, ϵ = 45.0.

The basicity experiments for **1** were performed in DMSO, and it is one of the common solvents used with these molecules.

RESULTS AND DISCUSSION

Figure 1 shows the top view (looking down the P-N transannular "bond") of the molecules involved in this study. Full geometric information is available as supplementary information. For the rest of this paper N_a will be used to represent the N in the transannular position (in a pseudo-axial position when a transannular bond exists) and N_e will be used to represent the N alpha to the phosphorus (in a pseudo-equatorial position).

As can be seen in Figure 1, the structure of the side rings are similar for all of the molecules. However, N_e does not eclipse the carbon adjacent to N_a in the cations as it does in the neutral molecules. This tends to be one of the largest differences between the cations and neutrals, in addition to the large changes in the P-N_a and P-Z distances.

Table I shows the energetics and changes in P-N_a, P-N_e, and P-Y distances associated with the series of reactions $YP[NH(CH_2)_2]_3N + X^+ \rightarrow XYP[NH(CH_2)_2]_3N^+$, where Y = unsubstituted, CH_2, NH or O and X = H, F, or Cl.

An interesting feature shown in Table I is the dramatic change in the P-N_a distance. For reactions with direct attachment of X^+ onto the phosphorus atom, the change is more than 1 Å. For systems in which the addition is to Y and not directly onto the phosphorus, the change in the P-N_a distance is not quite as large (about 0.75 Å). The cation P-N_a

distances for Y = CH_2 and NH are longer than those in the other four cations by about 0.2 Å.

It is useful to look at the Mulliken populations for these molecules to obtain quantitative information about where the charges reside. In all of these molecules (including the cations), N_a and N_e have negative charges of -0.7 to -0.8 for N_a and -0.9 for N_e. For the cations in which there is direct attachment of the "cation" on N_a, the "cation", X, has a negative charge (-0.1 for X=H, -0.4 for X=Cl, and -0.5 for X=F). The positive charge resides mostly on the phosphorus (+1.5 to +1.8). However, even for the neutrals where there is extra coordination on the phosphorus, the phosphorus has a large positive charge (+1.5 to 1.6). Therefore, it appears to be the additional ligand that makes phosphorus highly positive, rather than the overall charge of the molecule. By analyzing the charges on the rest of the molecule, the positive charge of the cations is found to be spread throughout the molecule onto the carbons (which become less negative) and the hydrogens (which become more positive).

To understand the bonding in these species, we start by looking at the length of P-N_a, since this distance suggests that some bonding is present in the cationic species. Based on an RHF/6-31G(d) calculation of PH_2NH_2 (an analogue of hydrazine), a single P-N bond length is about 1.7 Å. This is about 0.3-0.6 Å shorter than the cationic P-N_a distances

found here. Also, congruent with the decrease in the P-N_a bond is a lengthening of the P-Y bond. This is exactly what would be expected if some bonding interaction is occurring across the transannular P-N_a space. The change in the P-N_e bond lengths is relatively small for these reactions. However, the trend is to decrease the P-N_e bond length as the P-N_a bond length decreases. Interestingly, the P-N_e distance for all species is similar to the normal P-N distance in PH_2NH_2.

Figure 2 shows the variation of the P-N_a distance vs. the N_e-P-N_e angle. As would be expected, the shorter P-N_a, the closer the N_e-P-N_e angle is to 120°. This reflects the trend of the phosphorus to become truly pentacoordinated in a trigonal bipyramidal structure as P-N_a decreases. The same trend is seen by Verkade and coworkers in a series of X-ray structures of $ZP[N(CH_3)(CH_2)_2]_3N$ molecules.[2]

To further explore whether or not there is a transannular bond in these molecules, we have performed a Bader analysis on each of the species involved. The densities ρ_c at the critical points are given in Table II. The neutral species are at the top of the table, cations are in the middle of the table, and the average ρ_c for all of the P-N_e bonds is at the bottom of the table.

Two of the neutrals (Z = CH_2 and NH) have ring critical points instead of bond critical points, suggesting that there is not a P-N_a bond in these two species. The P-N_a densities

ρ_c in the cations are 4-8 times larger than those in the neutrals, and in turn, the average P-N_e ρ_c is 2-3 times larger than the P-N_a ρ_c in the cations. This suggests that the cations have at least some P-N_a dative bonding since the ρ_c associated with the cations are closer to the ρ_c(P-N_e) than they are to ρ_c(P-N_a) in the neutral compounds.

To emphasize this last point, the total densities for the parent base and its conjugate acid are plotted in Figure 3. The plots definitely show that the acid has significant density between P and N_a, whereas the base has very little density between P and N_a.

As can be seen in Table I, the calculated P-N_a distance in $HP[NH(CH_2)_2]_3N^+$ is very close to the distance found in the crystal structure obtained by Laramay and Verkade.[2.d.] This agreement could be fortuitous, since crystal forces could make the P-N_a distance shorter than would be expected in the gas phase. A measure of how important crystal forces are is provided by the energy required to decrease the P-N_a distance. To explore this facet of the problem, we have performed constrained optimizations (constraining only the P-N_a distance) for the neutral base and its conjugate acid at several points on either side of the equilibrium P-N_a distance. Plots of the data are shown in Figure 4.

As can be seen in Figure 4, the azaphosphatrane base, 1.a. in Figure 1, is rather floppy energetically with respect

to changing the P-N_a distance. Only about 6.5 kcal/mol is needed to compress the P-N_a distance by 0.5Å. On the other hand, to compress P-N_a in the conjugate acid, 1.b., by the same amount requires 33.4 kcal/mol. To compress the P-N_a distance to that of the PH_2NH_2 distance (a decrease of 0.3 Å) requires 8 kcal/mol. Of course, when the acid is compressed by 0.5 Å, the P-N_a distance is only 1.5 Å. This is shorter than our calculated P-N single bond distance of 1.7 Å in PH_2NH_2. Nuclear repulsion is clearly playing a role in the energy increase. This large change in the energy upon compression is evidence that the agreement between the calculated and experimental P-N_a distance is not fortuitous.

To lengthen the P-N_a distance requires about the same amount of energy for both the base and the acid (5.4 and 6.7 kcal/mol respectively for a stretch of 0.5 Å). Thus, the energy plot shown in Figure 4 for the base is fairly symmetric, while the plot shown in Figure 4 for the acid is very asymmetric. This is related to both the the nuclear repulsion upon compression of the acid and the weakness of the P-N_a interaction in the base.

By fitting a parabola to the lowest three points energetically on both plots, an estimate of the force constant associated with P-N_a can be made. This leads to estimated force constants of 0.09 hartrees/bohr^2 for the base and 0.31 hartrees/bohr^2 for the acid. Furthermore, from the hessian calculations for the two molecules, the internal P-N_a

force constant for the base is 0.11 hartrees/bohr^2 and for the acid 0.38 hartree/bohr^2. For comparison the N-P_e force constant for the base is 0.30 hartree/bohr^2 and for the acid is 0.45 hartree/bohr^2. Also, the internal force constant calculated for P-N in H_2PNH_2 is 0.32. This clearly illustrates that there is stronger P-N_a bonding in the acid than in the base, and that in the acid this bond is at least similar to ordinary P-N single bonds.

Since we have thoroughly explored the question of a transannular bond in these molecules, we now turn our attention to the energetics and therefore, the proton affinities of these molecules, given in Table I.

One of the most interesting points is that the ylide type structure, $CH_2P[NH(CH_2)_2]_3N$, is predicted to have the largest proton affinity, and is therefore, the strongest base of this series of molecules. Even the molecule with Y = NH is predicted to be a stronger base than the parent molecule. On the other hand, the molecule with Y = O is predicted to be a weaker base than the parent base. Our predictions have prompted further experimental investigation by the Verkade group into the ylide base.[10]

Because these bases are used in solution experimentally, we have used the Onsager reaction field model with a dielectric constant of 45.0 (representing DMSO) to obtain a qualitative measure of the solvent effect on the proton affinities. Since this solvent approximation requires a

cavity radius, we have also explored the effect of cavity radius on the energies of the molecules.

The cavity diameters were chosen to be equal to the sum of the largest internuclear distance in the molecule plus the van der Waals radii of the two atoms involved. These two atoms were always hydrogen, so the van der Waals radius was taken to be 1.2 Å. The cavity radius of 4.00 Å was derived from $HP[NH(CH_2)_2]_3N^+$ and the cavity radius of 4.60 Å was derived from $CH_2P[NH(CH_2)_2]_3N$. Based on the molar volume, V_m, from crystal data[10] and the formula $r^3 = (3V_m)/(4\pi N)$ (where N is Avagodro's number), the experimental radius of the parent acid is 4.4 Å. Therefore, the calculated and experimental radii are in reasonable agreement.

The solvation data is presented in Table III. The changes in energy and dipole are given for each of the base-acid pairs for the gas phase, the solvent using a cavity radius of 4.60 Å, and the solvent using a cavity radius of 4.00 Å all at the gas phase geometry. All dipoles are given relative to the center of mass.

The trends in the reaction energies as a function of Y are the same for all three calculations (Tables III and IV) so the trends in the basicities are expected to be unchanged by solvation. However, the differences in relative energies between gas phase and the two different cavity radii for a given system are as large as 3 kcal/mol. This can have a significant effect on the pK_a expected for the acid in

question. A complete investigation of this requires a determination of the Gibbs free energies of the molecules. Determining the Gibbs free energies would require hessians for all of the species.

Changes in dipoles are also included in Table III since the solvent model changes the dipole of the molecule. Not surprisingly, molecules with the largest dipole are affected the most by the reaction field. The dipole moments do not change significantly for molecules with a small dipole (an example is the unsubstituted molecule) and do change quite a bit for molecules with a large dipole (an example is the molecule with Y = O).

From the energetics given in Table IV, the solvent modifies the proton affinity trends by only about 3 kcal/mol. However, these energies were calculated at the gas phase geometry. The effect of the solvent model on the geometry of the molecules was explored for a solvent cavity radius of 4.30 Å. The results for a few of the geometric parameters and energetics for the acid-base pairs are given in Table V.

In general, the trends observed in the gas phase are also observed in the solvent model. The proton affinities are very similar to those in Table III for the gas phase geometry. The "bond" distances given in Table V are also very similar to those in gase phase (Table I). So, overall, performing single point solvent energies at the gas phase

geometries appear to be adequate to determine qualitative solvent effects for these types of molecules.

CONCLUSIONS

This study has explored the effects of different substituents Z in the azaphosphatrane series $ZP[NH(CH_2)_2]_3N$ where Z = unsubstituted, H^+, F^+, Cl^+, CH_2, CH_3^+, NH, NH_2^+, O or OH^+. Based on the $P\text{-}N_a$ distances, Bader analyses, and constrained geometry optimizations, there is clear evidence for transannular dative bonding in the cationic species.

We have also found two molecules (Z = CH_2 and NH) that are predicted to be stronger bases than the parent base. Using the Onsager reaction field method, we have shown that the basicity trends that are found in the gas phase are also expected in a solvent.

One of the effects we have not explored is the effect of the methylation at N_e. In this study, we have replaced the methyl normally found in the experimental studies with a hydrogen for simplicity. We are currently exploring what differences that these methyls might make in the basicities of these molecules.

ACKNOWLEDGMENT

The calculations were performed on the Touchstone Delta and on RS/6000s purchased by Iowa State University. This work was supported by a grant from the Air Force Office of Scientific Research (93-1-0105), a Department of Energy GAANN fellowhsip to TLW and with the assistance of the Advanced Research Projects Agency. The authors would like to thank the Delta personnel for their help and patience and Dr. John Verkade for inspiring this work and for illuminating discussions.

SUPPLEMENTARY INFORMATION

Cartesian coordinates for the azaphosphatranes are available (6 pages). Ordering information is given on any current masthead page.

Cartesian Coordinates for $P[NH(CH_2)_2]_3N$:

N	0.0000000000	0.0000000000	-2.6551521626
C	0.5606275652	1.3238275902	-2.6664308636
C	-1.4267821060	-0.1763960816	-2.6664308636
C	0.8661545408	-1.1474315086	-2.6664308636
C	1.2751292934	1.6873688833	-1.3682966391
C	-2.0988689652	0.2606099195	-1.3682966391
C	0.8237396718	-1.9479788028	-1.3682966391
N	0.4188465226	1.5069417582	-0.2045913749
N	-1.5144731059	-0.3907391502	-0.2045913749
N	1.0956265833	-1.1162026080	-0.2045913749
H	0.6598071793	2.1435570335	0.5252106787
H	-2.1862784351	-0.5003687379	0.5252106787
H	1.5264712558	-1.6431882956	0.5252106787
P	0.0000000000	0.0000000000	0.4965450791
H	1.2620375541	1.4423456972	-3.4944760516
H	-1.8801267919	0.3717837338	-3.4944760516
H	0.6180892378	-1.8141294310	-3.4944760516
H	-0.2447729038	2.0299681171	-2.8325499781
H	-1.6356175064	-1.2269636114	-2.8325499781
H	1.8803904102	-0.8030045057	-2.8325499781
H	2.1882291104	1.1042846282	-1.2805288493
H	-2.0504530962	1.3429196848	-1.2805288493
H	-0.1377760142	-2.4472043130	-1.2805288493
H	1.5652457986	2.7335499691	-1.4109382837
H	-3.1499466151	-0.0112323598	-1.4109382837
H	1.5847008165	-2.7223176093	-1.4109382837

Cartesian coordinates $HP[NH(CH_2)_2]_3N^+$:

N	0.0000000000	0.0000000000	-2.1268849339
C	0.4967401236	1.3313373762	-2.5282044514
C	-1.4013420506	-0.2354791220	-2.5282044514
C	0.9046019270	-1.0958582542	-2.5282044514
C	1.4910793469	1.7721341941	-1.4651149920
C	-2.2802529045	0.4052454965	-1.4651149920
C	0.7891735575	-2.1773796905	-1.4651149920
N	0.9150518655	1.3661795208	-0.1975154612
N	-1.6406721039	0.1093684009	-0.1975154612
N	0.7256202384	-1.4755479217	-0.1975154612
H	1.3556698507	1.7128340464	0.6289725463
H	-2.1611927220	0.3176275067	0.6289725463
H	0.8055228713	-2.0304615530	0.6289725463
P	0.0000000000	0.0000000000	-0.0049872942
H	0.0000000000	0.0000000000	1.3845965927

H	0.9299026005	1.2981484267	-3.5203790780
H	-1.5891808157	0.1562450617	-3.5203790780
H	0.6592782152	-1.4543934884	-3.5203790780
H	-0.3385499058	2.0159009074	-2.5430658993
H	-1.5765464444	-1.3011432726	-2.5430658993
H	1.9150963502	-0.7147576348	-2.5430658993
H	2.4684104849	1.3264282396	-1.6196115562
H	-2.3829257942	1.4744920671	-1.6196115562
H	-0.0854846906	-2.8009203067	-1.6196115562
H	1.6101283950	2.8468680693	-1.4879029605
H	-3.2705242667	-0.0290219412	-1.4879029605
H	1.6603958717	-2.8178461281	-1.4879029605

Cartesian coordinates for $FP[NH(CH_2)_2]_3N^+$:

N	0.0000000000	0.0000000000	-2.0936799629
C	0.4828723497	1.3396209812	-2.5184798028
C	-1.4015819760	-0.2516307689	-2.5184798028
C	0.9187096263	-1.0879902122	-2.5184798028
C	1.4797807884	1.7953802101	-1.4649538642
C	-2.2947352656	0.3838376497	-1.4649538642
C	0.8149544773	-2.1792178598	-1.4649538642
N	0.9064929223	1.3684182470	-0.2071985423
N	-1.6383314261	0.1008367756	-0.2071985423
N	0.7318385037	-1.4692550226	-0.2071985423
H	1.3113201789	1.7125219377	0.6378487559
H	-2.1387475921	0.2793756186	0.6378487559
H	0.8274274131	-1.9918975563	0.6378487559
P	0.0000000000	0.0000000000	-0.0834558373
F	0.0000000000	0.0000000000	1.4999931775
H	0.9030006116	1.2866815859	-3.5140316982
H	-1.5657992458	0.1386806763	-3.5140316982
H	0.6627986342	-1.4253622622	-3.5140316982
H	-0.3608926986	2.0130971060	-2.5330379150
H	-1.5629468848	-1.3190907981	-2.5330379150
H	1.9238395834	-0.6940063080	-2.5330379150
H	2.4641901227	1.3684971549	-1.6268511156
H	-2.4172483625	1.4498026685	-1.6268511156
H	-0.0469417602	-2.8182998235	-1.6268511156
H	1.5773365933	2.8720580907	-1.4847012446
H	-3.2759435643	-0.0700154852	-1.4847012446
H	1.6986069710	-2.8020426055	-1.4847012446

Cartesian coordinates for $ClP[NH(CH_2)_2]_3N^+$:

N	0.0000000000	0.0000000000	-2.0906634558
C	0.4906078599	1.3341865508	-2.5151919211
C	-1.4007433763	-0.2422144055	-2.5151919211
C	0.9101355165	-1.0919721454	-2.5151919211
C	1.4847401617	1.7806297870	-1.4587319851
C	-2.2844407112	0.3955078046	-1.4587319851
C	0.7997005494	-2.1761375916	-1.4587319851

N	0.8956164494	1.3805166811	-0.1948152409
N	-1.6433707408	0.0853682567	-0.1948152409
N	0.7477542914	-1.4658849377	-0.1948152409
H	1.2947845821	1.7589384195	0.6375017487
H	-2.1706776460	0.2418471308	0.6375017487
H	0.8758930639	-2.0007855502	0.6375017487
P	0.0000000000	0.0000000000	-0.0461992204
Cl	0.0000000000	0.0000000000	2.0334486637
H	0.9153272184	1.2794259487	-3.5090154020
H	-1.5656789831	0.1529836496	-3.5090154020
H	0.6503517646	-1.4324095983	-3.5090154020
H	-0.3473165629	2.0147318845	-2.5334562418
H	-1.5711507123	-1.3081509089	-2.5334562418
H	1.9184672753	-0.7065809756	-2.5334562418
H	2.4625444402	1.3342463094	-1.6049058700
H	-2.3867634189	1.4655028885	-1.6049058700
H	-0.0757810213	-2.7997491979	-1.6049058700
H	1.6019731962	2.8552008970	-1.4812576333
H	-3.2736631078	-0.0402509644	-1.4812576333
H	1.6716899116	-2.8149499326	-1.4812576333

Cartesian coordinates for $CH_2P[NH(CH_2)2]_3N$:

N	-0.0297411146	-0.0557743978	-2.6167062223
C	0.6714521667	1.1885712579	-2.7978214611
C	-1.4683984683	-0.0725170153	-2.6375248499
C	0.7083984830	-1.2906806024	-2.6032965599
C	1.4606807464	1.5818730225	-1.5521060405
C	-2.0561750570	0.5626452098	-1.3740886458
C	0.6537641536	-1.9904701302	-1.2485051293
N	0.6124224966	1.5480637016	-0.3693368097
N	-1.4984572114	-0.0005654769	-0.1620694867
N	1.0654838694	-1.0996083333	-0.1691373201
H	0.8978705635	2.2006453287	0.3297630568
H	-2.0641155511	-0.6397764915	0.3504570290
H	1.3607563385	-1.6289245357	0.6266390933
P	0.0555234061	0.1424893528	0.4036100332
C	0.0376404545	0.0727150491	2.0633429080
H	0.9421552448	-0.1817725832	2.5894742097
H	-0.6875526909	0.6645551915	2.5929710670
H	1.3464090708	1.1430067255	-3.6535098534
H	-1.8617919045	0.4407651648	-3.5165533388
H	0.3475761220	-1.9770082007	-3.3703767354
H	-0.0577546036	1.9615945929	-3.0099952784
H	-1.7957602564	-1.1044934812	-2.7031518014
H	1.7432206467	-1.0700078010	-2.8371010752
H	2.3221671020	0.9297060759	-1.4398752102
H	-1.8763599420	1.6300438890	-1.3847700971
H	-0.3443996003	-2.3923582765	-1.0825022436
H	1.8346458085	2.5944910999	-1.6692037113
H	-3.1318620308	0.4201503816	-1.3511923825

H	1.3352089486	-2.8350985778	-1.2591353700

Cartesian coordinates for $CH_3P[NH(CH_2)_2]_3N^+$:

N	0.0000000000	0.0000000000	-2.2288290435
C	0.4934392359	1.3306566604	-2.6029188189
C	-1.3991020896	-0.2379974167	-2.6029188189
C	0.9056628537	-1.0926592437	-2.6029188189
C	1.4498862645	1.7717333753	-1.5081602406
C	-2.2593092440	0.3697716500	-1.5081602406
C	0.8094229795	-2.1415050253	-1.5081602406
N	0.8307193129	1.4095101942	-0.2431274879
N	-1.6360312915	0.0146689313	-0.2431274879
N	0.8053119786	-1.4241791255	-0.2431274879
H	1.2588103779	1.8075599492	0.5665203439
H	-2.1947980238	0.1863817912	0.5665203439
H	0.9359876459	-1.9939417404	0.5665203439
P	0.0000000000	0.0000000000	0.0336775164
C	0.0000000000	0.0000000000	1.8565555224
H	-0.4266825806	0.9199970689	2.2404499331
H	-0.5833995428	-0.8295164885	2.2404499331
H	1.0100821233	-0.0904805803	2.2404499331
H	0.9632508166	1.3205016997	-3.5801795808
H	-1.6252134260	0.1739488276	-3.5801795808
H	0.6619626094	-1.4944505273	-3.5801795808
H	-0.3442355392	2.0122326346	-2.6386587658
H	-1.5705268103	-1.3042330392	-2.6386587658
H	1.9147623495	-0.7079995955	-2.6386587658
H	2.4237349506	1.3053313634	-1.6180190498
H	-2.3423175964	1.4463503576	-1.6180190498
H	-0.0814173542	-2.7516817210	-1.6180190498
H	1.5917667635	2.8436432267	-1.5401724961
H	-3.2585506553	-0.0433111593	-1.5401724961
H	1.6667838919	-2.8003320674	-1.5401724961

Cartesian coordinates for $NHP[NH(CH_2)_2]_3N$:

N	-0.0119822488	0.0072339323	-2.5526407821
C	0.6363121559	1.2877594240	-2.6751394754
C	-1.4496734598	-0.0712397943	-2.6255710965
C	0.7721154240	-1.1925468222	-2.6996900089
C	1.4327066579	1.6065831269	-1.4103060946
C	-2.0954146907	0.3841243294	-1.3187366717
C	0.7285071223	-2.0363243268	-1.4301807807
N	0.6068745056	1.4100284028	-0.2355505476
N	-1.5077874730	-0.3233773575	-0.1935462769
N	1.0643838575	-1.2248256409	-0.2657202661
H	0.6330820185	2.1295865057	0.4529723634
H	-2.1173299967	-0.4128966352	0.5936371655
H	1.3768518058	-1.7937699185	0.4948182217
P	0.0415199164	-0.0392404868	0.3813212175
N	-0.0785761020	-0.0599972921	1.9269556454

H	0.7650190069	0.0485085751	2.4535570201
H	1.2897156098	1.3294048355	-3.5475502035
H	-1.8427121093	0.5183862874	-3.4544505346
H	0.4392424710	-1.7915257881	-3.5480299048
H	-0.1262360889	2.0459122160	-2.8094417730
H	-1.7260488554	-1.1029854912	-2.8075411941
H	1.7991190063	-0.9071607320	-2.8938510299
H	2.3214028990	0.9846409001	-1.3661315371
H	-1.9982034309	1.4619754545	-1.2133073252
H	-0.2500653692	-2.4964287759	-1.3240754647
H	1.7626373185	2.6401647376	-1.4295598743
H	-3.1563858695	0.1577624302	-1.3416260540
H	1.4580580210	-2.8367599438	-1.5034041445

Cartesian coordinates of $NH_2P[NH(CH_2)_2]_3N^+$:

N	0.0081838189	-0.0158630182	-2.1366693293
C	0.5280032446	1.2781349722	-2.6020205721
C	-1.4026262813	-0.2344968431	-2.4895210264
C	0.8851339991	-1.1457025564	-2.4791840985
C	1.5368126110	1.7377718190	-1.5639803325
C	-2.2318463495	0.4748063546	-1.4279671843
C	0.7686772180	-2.1599835622	-1.3550978290
N	0.9630300617	1.4099835054	-0.2726841604
N	-1.5846550525	0.2212648508	-0.1561764010
N	0.7667986738	-1.4103109719	-0.1096225199
H	1.4045010581	1.8229359070	0.5205786392
H	-2.1590737937	0.0432669786	0.6388772710
H	0.6880814790	-1.9782394957	0.7089547695
P	0.0422241367	0.0754691289	0.0663620562
N	0.0218052766	0.0890849821	1.7448747058
H	0.8648565056	-0.1548499606	2.2244293280
H	-0.4391808880	0.8557963290	2.1918258355
H	0.9575359463	1.1968480408	-3.5937152583
H	-1.6154609385	0.1188080139	-3.4919216031
H	0.6245302064	-1.5682133618	-3.4426095968
H	-0.2896838350	1.9829222392	-2.6430945027
H	-1.6062826737	-1.2949984360	-2.4534094827
H	1.9024068013	-0.7858667072	-2.5325127155
H	2.5009667395	1.2590492865	-1.7020586938
H	-2.3041266171	1.5390307801	-1.6227873408
H	-0.1319628239	-2.7580658715	-1.4539369445
H	1.6870982357	2.8068748514	-1.6316498614
H	-3.2377209003	0.0785776900	-1.4055869377
H	1.6142455136	-2.8345053906	-1.3700897079

Cartesian coordinates of $OP[NH(CH_2)_2]_3N$:

N	0.0000000000	0.0000000000	-2.4896795864
C	0.6191941336	1.2938848140	-2.6514688406
C	-1.4301341853	-0.1107045574	-2.6514688406
C	0.8109400517	-1.1831802566	-2.6514688406

C	1.3889805035	1.6643060245	-1.3876151253
C	-2.1358215486	0.3707393891	-1.3876151253
C	0.7468410452	-2.0350454136	-1.3876151253
N	0.5319006410	1.4837605098	-0.2275632920
N	-1.5509246151	-0.2812407875	-0.2275632920
N	1.0190239741	-1.2025197223	-0.2275632920
H	0.7888516616	2.0492412466	0.5556225254
H	-2.1691208088	-0.3414550445	0.5556225254
H	1.3802691472	-1.7077862021	0.5556225254
P	0.0000000000	0.0000000000	0.3460683624
O	0.0000000000	0.0000000000	1.8137914214
H	1.2797336539	1.3248886161	-3.5179797982
H	-1.7872540257	0.4458375464	-3.5179797982
H	0.5075203717	-1.7707261624	-3.5179797982
H	-0.1593683886	2.0294472439	-2.8126922834
H	-1.6778686746	-1.1527406950	-2.8126922834
H	1.8372370632	-0.8767065489	-2.8126922834
H	2.2940575548	1.0671162448	-1.3130306125
H	-2.0711785542	1.4531539978	-1.3130306125
H	-0.2228790006	-2.5202702426	-1.3130306125
H	1.6893990886	2.7058683678	-1.4311102618
H	-3.1880502901	0.1101283439	-1.4311102618
H	1.4986512015	-2.8159967117	-1.4311102618

Cartesian coordinates of $OHP[NH(CH_2)_2]_3N^+$:

N	0.0043561017	0.0002057001	-2.0973254272
C	0.4788225377	1.3332687549	-2.5229959802
C	-1.4036526772	-0.2476003174	-2.4771433693
C	0.9117144314	-1.0850406388	-2.5239024748
C	1.5013509872	1.7788989483	-1.4891458064
C	-2.2662157020	0.3949975179	-1.4024485528
C	0.8131860516	-2.1757614845	-1.4717175307
N	0.9859842320	1.3290233366	-0.2141106199
N	-1.5990738214	0.1082152689	-0.1512337841
N	0.7587319211	-1.4870204696	-0.1963404879
H	1.2139891184	1.8565824853	0.6001173590
H	-2.0990680304	0.2693916087	0.6976173024
H	0.6794429096	-2.0798379976	0.6038158437
P	0.0375306243	-0.0036648279	-0.0038868657
O	0.0018196511	0.0091131364	1.6116668299
H	0.8332897254	-0.1185297871	2.0529803040
H	0.8792049909	1.2938445545	-3.5283510686
H	-1.6045961672	0.1381096084	-3.4687277697
H	0.6544768579	-1.4334873055	-3.5162102123
H	-0.3611480977	2.0119973242	-2.5144868660
H	-1.5723524901	-1.3141091381	-2.4832713019
H	1.9191354324	-0.6963718501	-2.5477859167
H	2.4837206189	1.3644770342	-1.6877797906
H	-2.3807962704	1.4623117539	-1.5630740443
H	-0.0609176799	-2.8007404301	-1.6239170052

H	1.5927737751	2.8564006508	-1.4914973455
H	-3.2538286262	-0.0457946957	-1.4033128053
H	1.6861173293	-2.8132057516	-1.5110222051

REFERENCES

1.a. Boatz, J.A.; Gordon, M.S.; Sita, L.; *J. Phys. Chem.*, **1990**, *94*, 5488.
b. Gordon, M.S.; Nguyen, K.A.; Carroll, M.T.; *Polyhedron*, **1991**, *11*, 1247.
c. Nguyen, K.A.; Carroll, M.T.; Gordon, M.S.; *J. Am. Chem. Soc.*, **1991**, *113*, 5998.
d. Gordon, M.S.; Carroll, M.T.; Jensen, J.H.; Davis, L.P.; Burggraf, L.W.; Guldry, R.M.; *Organometallics*, **1991**, *10*, 2657.

2.a. Lensink, C.; Xi,S.K.; Daniels, L.M.; Verkade, J.G.; *J. Am. Chem. Soc.*, **1989**, *111*, 3478.
b. Schmidt, H.; Lensink, C.; Xi, S.K.; Verkade, J.G.; *Z. Anorg. Allg. Chem.*, **1989**, *578*, 75.
c. Xi, S.K.; Schmidt, H.; Lensink, C.; Kim, S.; Wintergrass, D.; Daniels, L.M.; Jacobson, R.A.; Verkade, J.G.; *Inorg. Chem.*, **1990**, *29*, 2214.
d. Laramay, M.A.H.; Verkade, J.G.; *J. Am. Chem. Soc.*, **1990**, *112*, 9421.
e. Laramay, M.A.H.; Verkade, J.G.; *Z. Anorg. Allg. Chem.*, **1991**, *605*, 163.
f. Tang, J.S.; Laramay, M.A.H.; Young, V.; Ringrose, S.; Jacobson, R.A.; Verkade, J.G.; *J. Am. Chem. Soc.*, **1992**, *114*, 221.
g. Verkade, J.G. US Patent 5,051,533, 1991; *Chem. Abstr*, **1992**, *116*, 50379q.
h. Tang, J.S.; Verkade, J.G.; *J. Am. Chem. Soc.*, **1993**, *115*, 1660.
i. Tang, J.S.; Dopke, J.; Verkade,J.G.; *J. Am. Chem. Soc.*, **1993**, *115*, 5015.
j. Tang, J.S.; Verkade, J.G.; *Angew. Chem. Int. Ed. Engl.*, **1993**, *32*, 896.

3.a Kirkwood,J.G.; *J. Chem. Phys.*, **1934**, *2*, 351.
b. Onsager,L.; *J. Am. Chem. Soc.*, **1936**, *58*, 1486.
c. Tapia, O.; Goscinski,O.; *Mol. Phys.*, **1975**, *29*, 1653.
d. Karelson,M.M.; Katritzky,A.R.;Zerner,M.C.; *Int. J. Quantum Chem.*, **1986**, *20*, 521.
e. Wong,M.W.;Frisch,M.J.;Wiberg,K.B.; *J. Am. Chem. Soc.*, **1991**, *113*, 4776.
f. Szafan,M.;Karelson,M.M.;Katritzky,A.R.;Koput,J.; Zerner,M.C.; *J. Comput. Chem.*, **1993**, *14*, 371.

4. Roothaan,C.C.J.; *Rev. Mod. Phys.*, **1951**, *23*, 69.

5.a. Hehre,W.J. Ditchfield,R. Pople,J.A. *J. Chem. Phys.*, **1972**, *56*, 2257-2261.
b. Francl,M.M.;Pietro,W.J.;Hehre,W.J.;Binkley,J.S.

Gordon,M.S.;DeFrees,D.J.; Popel,J.A. *J.Chem.Phys.* **1982**,77,3654-3665.
c. Gordon,M.S. *Chem.Phys.Lett.* **1980**,*76*,163-168.
d. Ditchfield,R.;Hehre,W.J.;Pople,J.A. *J. Chem. Phys.*, **1971**, *54*, 724-728.
e. Hariharan,P.C.;Pople,J.A. *Theor. Chim. Acta*, **1973**, *28*, 213-222.

6. Schmidt,M.W.;Baldridge,K.K.;Boatz,J.A.;Elber,S.T.; Gordon,M.S.;Jensen,J.H.;Koseki,S.;Matsunaga,N.;Nguyen, K.A.;Su,S.;Windus,T.L.;Dupuis,M.;Montgomery,J.A. Jr. accepted *J. Comp. Chem.*

7. Windus,T.L.;Schmidt,M.W.;Gordon,M.S.; *Chem. Phys. Lett.*, accepted

8. Harrison,R.J.; version 4.0.2, available in directory /pub/tcgmsg from host ftp.tcg.anl.gov.

9.a. Bader, R.F.W.; Nguyen-Dang, T.T.; Tal, Y.; *Rep. Prog. Phys.*, **1981**, *44*, 893
b. Bader, R.F.W.; Nguyen-Dang, T.T.; *Adv. Quant. Chem.*, **1981**, *14*, 63
c. Bader, R.F.W.; *Accts Chem. Res.*, **1985**, *18*, 9

10. Private communication with Professor John Verkade.

Table I: Changes in P-N distance and energetics for $YP[NH(CH_2)_2]_3N + X^+ \rightarrow XYP[NH(CH_2)_2]_3N^+$.

P-Y	X±	$\Delta r(P\text{-}N_a)$[a]	$\Delta r(P\text{-}Y)$[a]	$\Delta r(P\text{-}N_e)$[a,b]	ΔE[c]
P	H	-1.030 (2.122)[d] [2.078][f]		-0.059 (1.656)[d]	-267.3 (-258.2)[e]
P	F	-1.142 (2.010)[d]		-0.068 (1.646)[d]	-347.4
P	Cl	-1.107 (2.080)[d]		-0.062 (1.652)[d]	-214.8
$P\text{-}CH_2$	H	-0.766 (2.263)[d]	+0.162 (1.823)[d]	-0.027 (1.659)[d]	-304.7
P-NH	H	-0.730 (2.205)[d]	+0.128 (1.679)[d]	-0.026 (1.656)[d]	-281.8
P-O	H	-0.742 (2.094)[d]	+0.148 (1.652)[d]	-0.025 (1.652)[d]	-252.2

a. Δr(Å) measures the bond length change upon addition of X^+.
b. Based on average of the three $P\text{-}N_e$ distances.
c. ΔE(kcal/mol) measures the energy change upon addition of X^+.
d. Bond distance in angstroms for the cationic product.
e. ΔH_o in kcal/mol, including zero point vibrational energy scaled by 0.89.
f. Experimental distance from reference 2.d.

Table II: Density at critical point between P and N_a.

P-Z	ρ_c	index[a]
P	0.0116	2
P-CH_2	0.0137	1
P-NH	0.0154	1
P-O	0.0184	2
P-H^+	0.0756	2
P-F^+	0.0934	2
P-Cl^+	0.0883	2
P-CH_3^+	0.0585	2
P-NH_2^+	0.0648	2
P-OH^+	0.0796	2
P-N_e [b]	0.184	2

a. The index is the number of negative curvatures of the electron density at the critical point. 1 corresponds to a ring critical point and 2 corresponds to a bond critical point.
b. The average density at the bond critical points between P and N_e.

Table III: Changes in energies and dipoles for $YP[NH(CH_2)_2]_3N + H^+ \rightarrow HYP[NH(CH_2)_2]_3N^+$ in gas phase and at two different cavity radii.

	gas phase		radius=4.60Å		radius=4.00Å	
P-Y	ΔE^a	ΔD^b	ΔE^a	ΔD^b	ΔE^a	ΔD^b
P	267.3	-0.10	302.6	-0.10	307.9	-0.17
		(0.64)[c]		(0.76)[c]		(0.76)[c]
$P-CH_2$	304.7	-3.72	338.9	-4.07	343.4	-4.54
		(0.17)[c]		(0.22)[c]		(0.25)[c]
P-NH	281.8	-3.72	315.7	-4.41	320.1	-4.88
		(0.28)[c]		(0.31)[c]		(0.33)[c]
P-O	252.2	-2.87	285.8	-3.38	289.9	-3.72
		(2.13)[c]		(2.44)[c]		(2.64)[c]

a. Change in energy in kcal/mol.
b. Change in the dipole in debyes.
c. Dipole in debyes for the cationic species.

Table IV: Relative reaction energies for $YP[NH(CH_2)_2]_3N + H^+ \rightarrow HYP[NH(CH_2)_2]_3N^+$ in gas phase and at two different cavity radii.

	gas phase	radius=4.60Å	radius=4.00Å
P-Y	$\Delta\Delta E^a$	$\Delta\Delta E^a$	$\Delta\Delta E^a$
P	0.0	0.0	0.0
$P-CH_2$	37.4	36.3	35.5
P-NH	14.5	13.1	12.2
P-O	-15.1	-16.8	-18.0

a. Relative energies in kcal/mol.

Table V: Changes in P-N distance and energetics for $YP[NH(CH_2)_2]_3N + H^+ \rightarrow HYP[NH(CH_2)_2]_3N^+$ using solvent cavity radius of 4.3 Å.

P-Y	X±	$\Delta r(P\text{-}N_a)$[a]	$\Delta r(P\text{-}Y)$[a]	$\Delta r(P\text{-}N_e)$[a,b]	ΔE[c]
P	H	-1.024 (2.117)[d] [2.078][e]		-0.058 (1.656)[d]	-305.1
$P\text{-}CH_2$	H	-0.688 (2.273)[d]	+0.151 (1.822)[d]	-0.020 (1.664)[d]	-340.9
P-NH	H	-0.667 (2.205)[d]	+0.125 (1.679)[d]	-0.024 (1.656)[d]	-317.4
P-O	H	-0.694 (2.077)[d]	+0.147 (1.622)[d]	-0.024 (1.653)[d]	-287.6

a. Δr(Å) measures the bond length change upon addition of X^+.
b. Based on average of the three $P\text{-}N_e$ distances.
c. ΔE(kcal/mol) measures the energy change upon addition of X^+.
d. Bond distance in angstroms for the cationic product.
e. Experimental distance from reference 2.d.

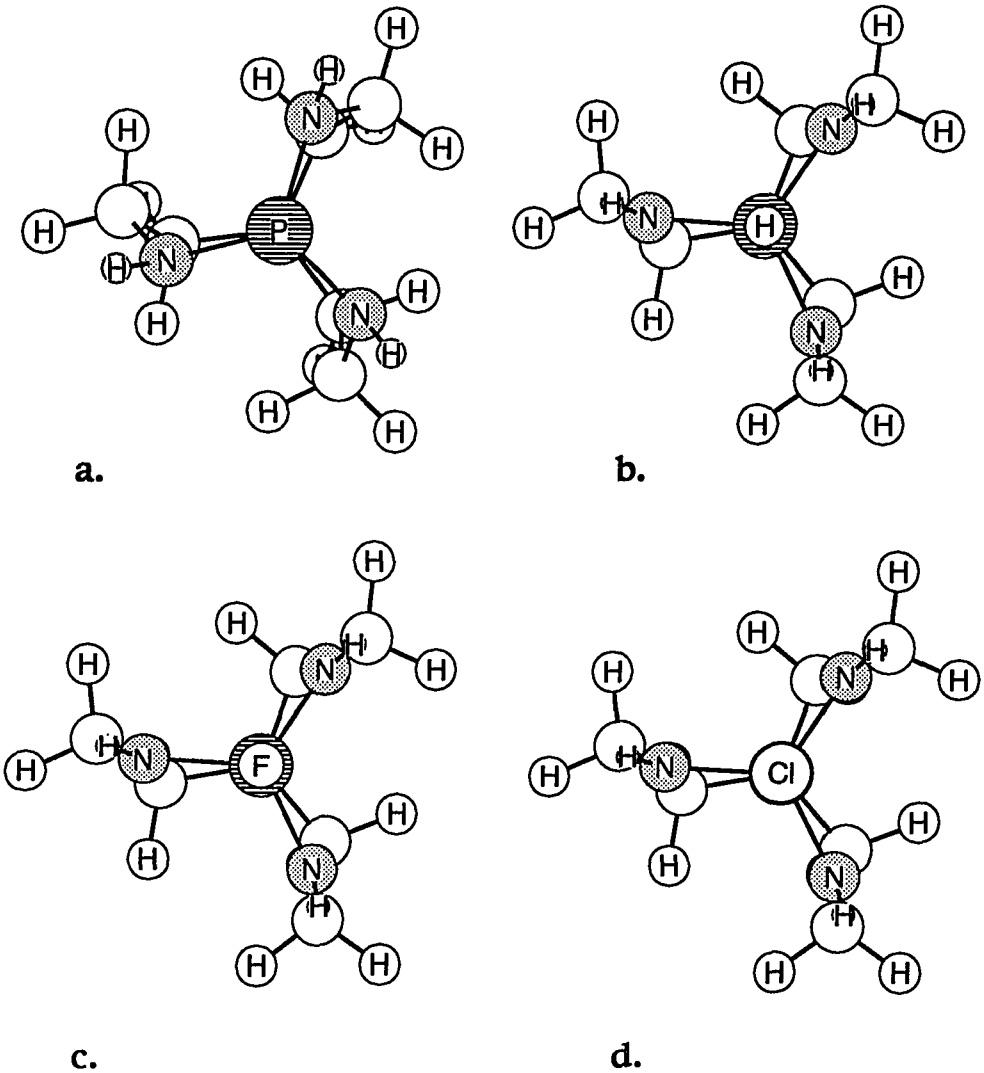

Figure 1: Top views of a. $P[NH(CH_2)_2]_3N$, b. $HP[NH(CH_2)_2]N^+$, c. $FP[NH(CH_2)_2]_3N^+$, d. $ClP[NH(CH_2)_2]_3N^+$, e. $CH_2P[NH(CH_2)_2]_3N$, f. $CH_3P[NH(CH_2)_2]_3N^+$, g. $NHP[NH(CH_2)_2]_3N$, h. $NH_2P[NH(CH_2)_2]_3N^+$, i. $OP[NH(CH_2)_2]_3N$, j. $OHP[NH(CH_2)_2]_3N^+$

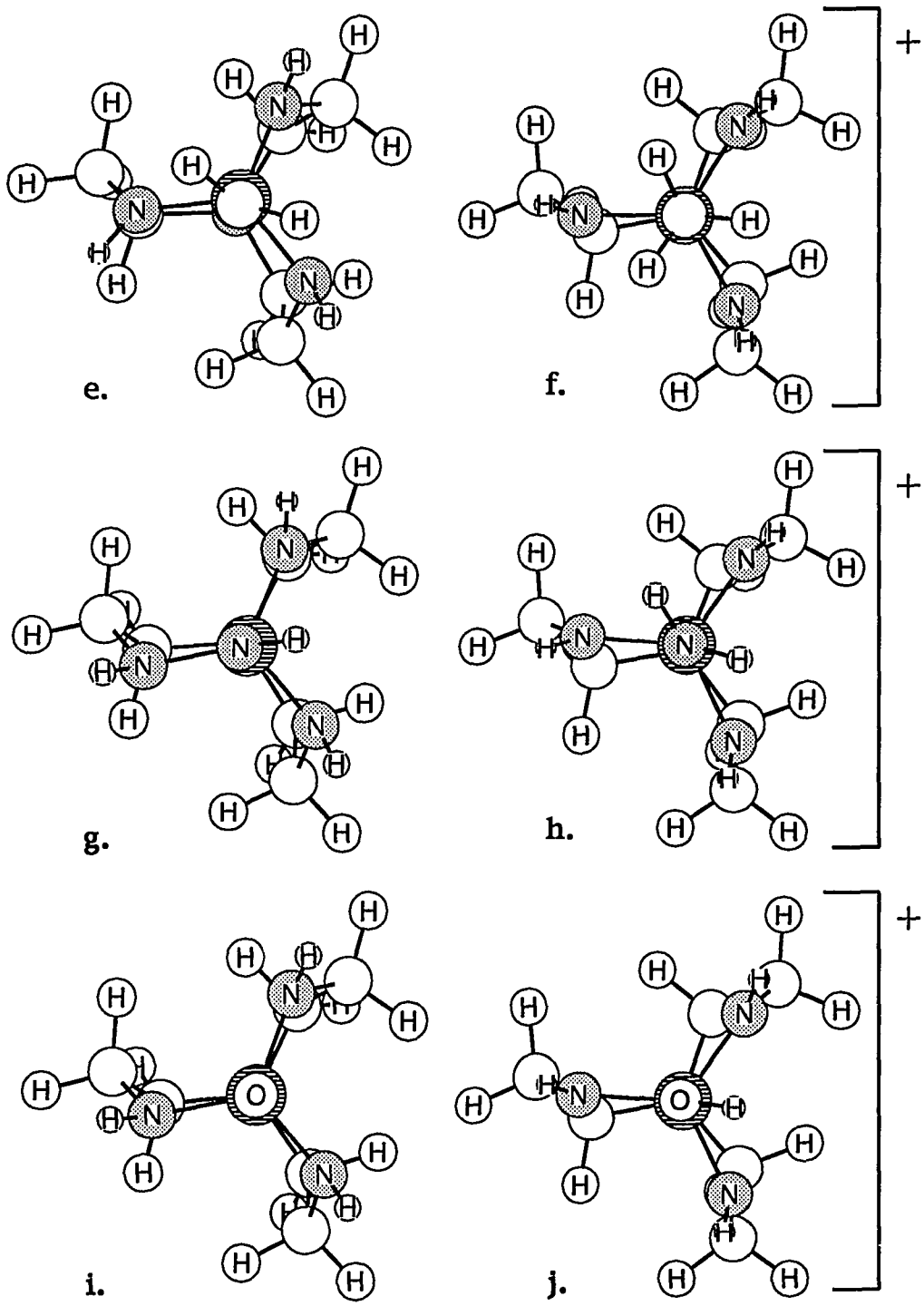

Figure 1: (cont.)

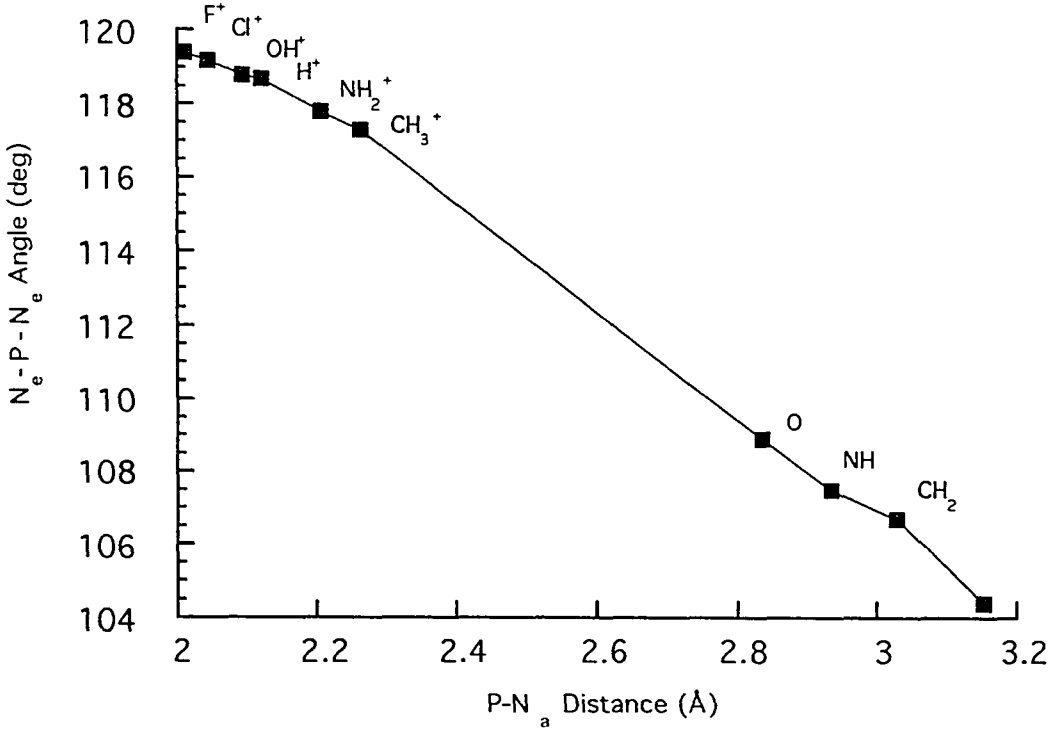

Figure 2: P-N $_a$ versus N_e-P-N_e for $ZP[NH(CH_2)_2]_3N$.

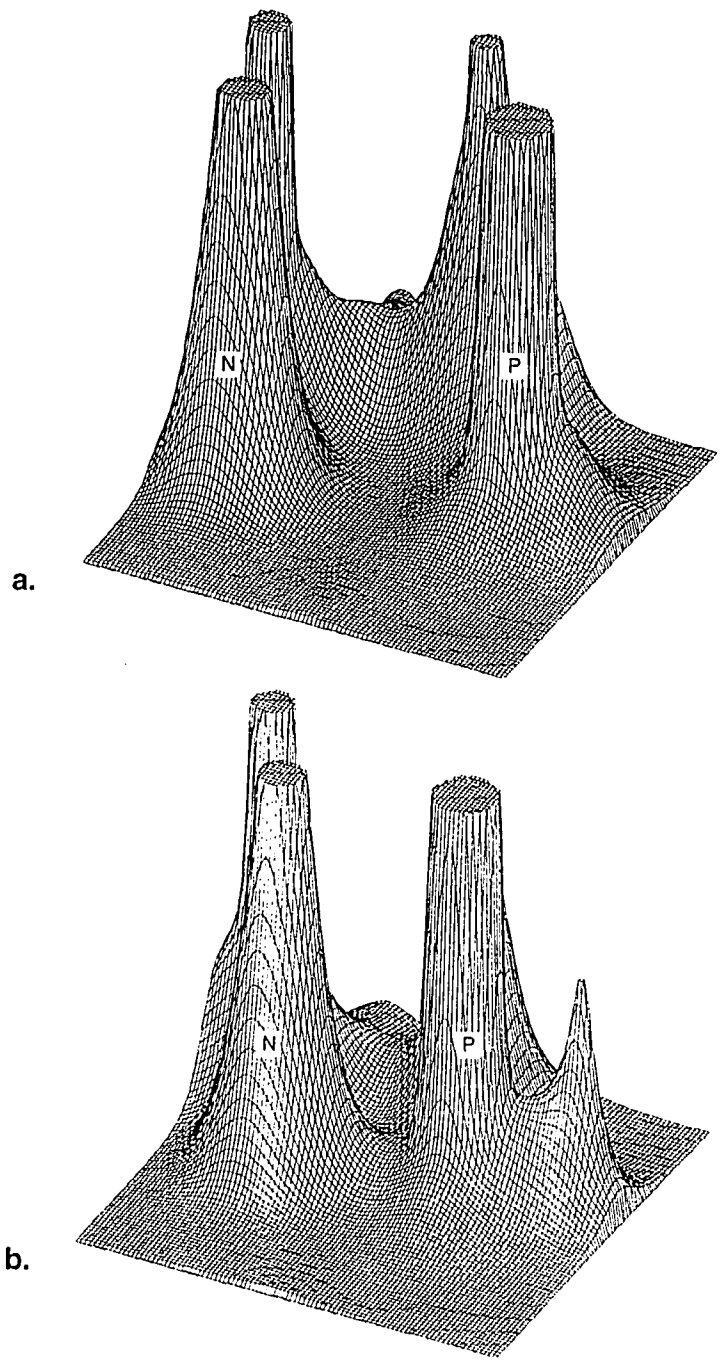

Figure 3: Total electron density plots of a. the parent base and b. its conjugate acid.

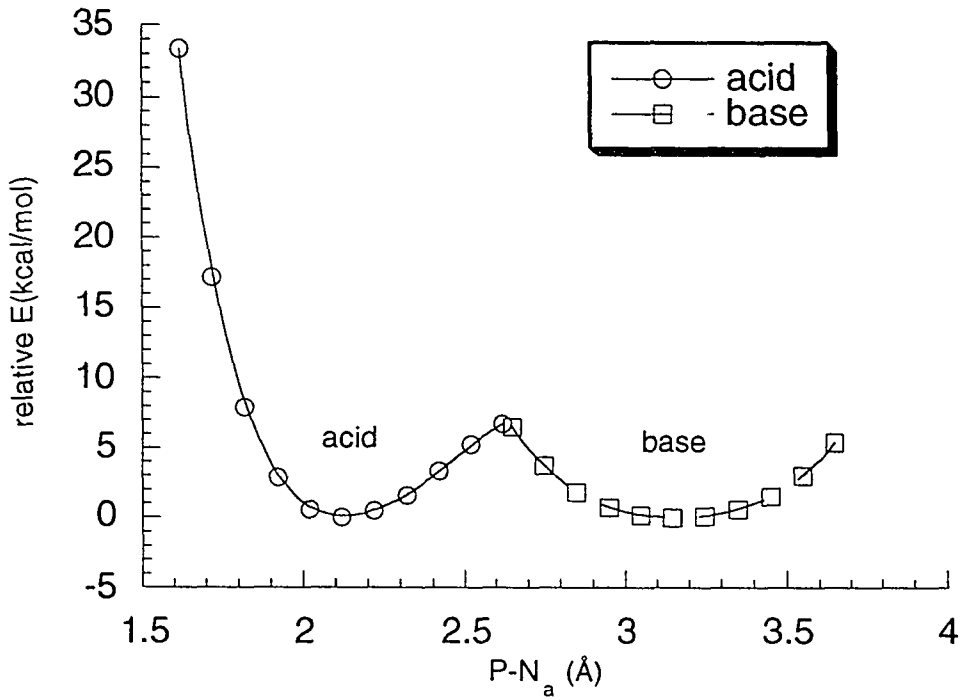

Figure 4: P-N_a distance versus relative energy for the parent base and the conjugate acid in C_3 symmetry.

PAPER 7: PARALLEL ALGORITHMS FOR SCF ANALYTIC HESSIANS I. SMALL SCALE ALGORITHM

Parallel Algorithm for SCF Analytic Hessians I. Small Scale Algorithm

Theresa L. Windus, Michael W. Schmidt, and Mark S. Gordon
Department of Chemistry
Iowa State University
Ames, Iowa 50011

accepted in *Chem. Phys. Lett.*

ABSTRACT

A novel parallel algorithm for the calculation of SCF analytic hessians is presented for use on a few compute nodes. This algorithm is most useful for a small laboratory with access to several workstations, since the calculation is ultimately dominated by the CPU intensive four-label transformation. Parallelization of the one- and two-electron hessian integrals is presented, and a timing example is included.

1. INTRODUCTION

The importance of parallel computers in increasing the size and complexity of chemical systems that can be treated using theoretical chemistry is gaining increased recognition [1,2]. Techniques for the parallelization used in the self-consistent field (SCF) energy and gradient calculations have been known for some time [1]. Several types of correlated wavefunctions have been examined for their potential to be used effectively on parallel computers [2].

We have previously reported details of the parallelization of the SCF and gradient portions of GAMESS (General Atomic and Molecular Electronic Structure System) [3]. This includes restricted Hartree-Fock (RHF), unrestricted Hartree-Fock (UHF), restricted open shell Hartree-Fock (ROHF) and generalized valence bond (GVB) wavefunctions and gradients. The parallel gradient algorithm allows geometry optimizations, transition state searches, intrinsic reaction path (IRC) following, and numerical hessian calculations to be performed in parallel.

The parallelization of GAMESS is accomplished through the use of the message passing toolkit, TCGMSG [4]. This package allows GAMESS to run on many types of platforms, including an Ethernetwork of UNIX workstations (possibly multiplatform), distributed memory multiprocessor computers (such as the Intel Touchstone Delta), and shared memory

multiprocessor computers, by using the best communication available. Since the number of different parallel calls used from TCGMSG is small (12), we have written FORTRAN routines emulating TCGMSG to facilitate the port of GAMESS to the Thinking Machine CM-5 with very little work.

A major problem associated with correlated wavefunctions, as well as analytic molecular orbital hessian calculations, is the transformation from the atomic orbital (AO) basis to the molecular orbital (MO) basis. Several workers have presented parallel algorithms intended to address this problem [5], but because of the large disk and memory requirements these have been difficult to implement efficiently on current distributed memory machines.

Since a parallel AO to MO transformation has not yet been implemented into GAMESS, we have devised a simple alternate parallel algorithm for calculating SCF analytic hessians. Since this algorithm is general, it can be easily implemented into most quantum chemistry codes where the single-program model is in use. This method is intended for use on systems with just a few compute nodes, and it assumes that one of the nodes has a large amount of memory and disk storage.

An integral (no pun intended) part of this discussion is the efficient parallelization of the one- and two-electron hessian integrals.

2. ALGORITHM

Analytic hessian calculation in the MO basis involves several steps: 1) calculation of the atomic integrals and the desired wavefunction, 2) calculation of the one-electron second derivative (hessian) integrals, 3) calculation of the two-electron hessian integrals [6], 4) transformation of the atomic integrals into molecular integrals (includes sorting the atomic integrals in our current method), and 5) solution of the coupled perturbed Hartree-Fock (CPHF) equations in the MO basis [7].

The bottleneck (most time consuming step) for this calculation is formally the transformation step. This step requires $O(N^5)$ operations, where N is the number of basis functions. However, because there are so many two-electron hessian integrals (the coefficient for this $O(N^4)$ calculation is large), step 3 generally requires as much or more time than the transformation, step 4.

Since steps 2, 3, and 4 are independent of one another, each one of these steps could conceptually be sent off to different processors. However, since step 2 (calculation of the one-electron hessian integrals) is not as time consuming as steps 3 and 4, this could result in a large load imbalance. Therefore, we have chosen to let all of the processors work in parallel on the one-electron hessian integrals and then split off steps 3 and 4 to separate

processors.

A flowchart of the basic algorithm is given in Figure 1. In this algorithm there are two different types of nodes. One is a master node (node 0) and the others are slave nodes. All nodes calculate the wavefunction in parallel [3] before the transformation begins. The SCF stage of the calculation can be run using local disks to hold integrals or in direct mode if the slave nodes do not have enough disk to hold their share of the atomic integrals. Then, all of the nodes calculate the one-electron hessian integrals in parallel.

We use two different algorithms for the parallelization of integrals [3], one based on static load balancing (LOOP) and the other based on dynamic load balancing (NXTVAL). These algorithms are represented in Figure 2 showing the parallelization scheme for the one-electron hessian integral calculation. The LOOP method is implemented at the innermost DO loop of the integral calculation and is intended for use when the nodes are of approximately the same speed and work load. Implementation at this loop helps to ensure that each node works on many relatively small integral packets that are about the same size and therefore, that the load will be balanced among all of the nodes.

The NXTVAL method is implemented at the first DO loop of the integral calculation and is intended for use when the nodes are not of the same speed and/or work capacity. The NXTVAL algorithm involves communication to increment a shared

counter that keeps track of which loops have been assigned. The estimated cost of communication is approximately 0.05 seconds per call on most UNIX machines using TCGMSG [4]. Implementation at the first DO loop balances the cost between communication and sending packets which are too large, insuring that load imbalance will not occur.

Before the calculation of the one-electron integrals, each node must have the density, the orbitals and the orbital energies. This is read off the disk by the master and broadcast to the slaves. The amount of I/O is the same as for a sequential run, but there is added communication cost to broadcast the information.

After each node is finished calculating all of its one-electron hessian integrals, a global sum is performed to accumulate the one-electron integral derivative contributions to the gradient, **g**, the nuclear hessian, **H**, the Fock derivative matrix, **F´**, and the derivative overlap matrix, **S´**. Every processor will have the full one-electron integral derivative contributions to **g**, **H**, **F´**, and **S´**. At this point, the master node writes these quantities to disk and requires no additional I/O than the sequential version.

After the one-electron hessian integrals have been calculated by all nodes, the master and slave nodes perform different computational tasks (Figure 1).

The *master* calculates all two-electron energy integrals so that it has all of the integrals on local disk. This must

be done for two reasons; the more important of these is that since the SCF calculation was performed in parallel, the master node will only have a partial list of the integrals. This partial list won't be enough to perform the transformation. Second, our current transformation works without symmetry. So, if the molecule has any symmetry, the full atomic integral list would still not be available from the SCF which does use symmetry.

Next, the integrals are sorted and transformed into the molecular orbital basis. This, of course, requires that the master node have as much disk and memory as would be required in a sequential calculation.

Simultaneously, the *slave processors* are calculating the two-electron hessian integrals. Since they do not participate in the transformation step, their disk and memory usage is much less than that of the master. This part of the calculation can be several times longer than the transformation step, so several processors can be employed in this step without resulting in a significant "wait" time for the slaves. However, if the master completes the transformation before the hessian integrals are finished, the master can join in the computation of the hessian integrals.

Since the master may or may not be involved in the calculation of the two-electron hessian integrals, only dynamic load balancing (NXTVAL) is used in this step. If LOOP balancing was chosen initially, the program will switch

to NXTVAL balancing for this part of the calculation. The NXTVAL load balancing is implemented at the second DO loop level of the four shell loops necessary to calculate the two-electron hessian integrals. This placement balances integral packet size and communication costs.

When the transformation is parallelized, the LOOP algorithm will be implemented at the innermost DO loop. This is the same algorithm that is used for the two-electron integrals and two-electron gradient integrals. From those calculations, this type of static load balancing is very efficient for nodes of the same speed.

Before the two-electron hessian integrals can be calculated, the master must read and broadcast the one-electron contributions to **g**, **H**, and **F'**. These quantities must be scaled by 1/(number of processors) so that the global sum after the two-electron contributions have been added will result in the correct results.

After steps 3 and 4 are complete, a synchronization (global sum) must occur to allow the two-electron hessian information to be shared between the processors so that all nodes (including the master node) have all the hessian information. This information consists of **g**, **H**, and **F´**. Then, the master solves the CPHF calculation by itself, since only this processor has all of the information needed for this step.

3. TEST CALCULATIONS

Since the current transformation does not utilize molecular symmetry but the hessian integral calculation does, the choice of a C_S symmetry test case was made to provide a "fair" compromise between the two. The puckered, C_S molecule 5-aza-2,8-dioxa-1-stibabicyclo[3.3.0]octa-2,4,6-triene [8] (**1**), referred to as

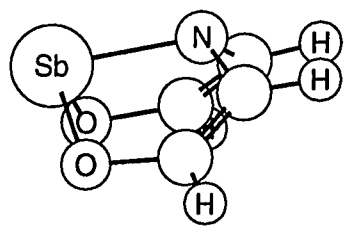

1

ADSbO, has been chosen as a test case. Using the 3-21G* basis set [9], this calculation has 110 basis functions and requires only 750 MB of disk for the master node. Since the disk space required by the preliminary SCF calculation was available on the slave nodes (100 MB, 50 MB, or 34 MB respectively on 1, 2, or 3 nodes), the SCF calculation was not run in direct mode.

The memory requirements for this calculation are 11.5 MB for the master node and 2.5 MB for the slave nodes. This does not include the 6 MB of memory required on each node to hold the executables.

These calculations were performed on three IBM RS6000/350s dedicated to the test. The communication is via an Ethernet segment which was not dedicated to these three computers and therefore, had to contend with other communication requests.

All times quoted in Table I are CPU times from the master node. As can be seen in Table I, only 2 processors can be effectively used in the parts of the calculation that are unique to the hessian calculation for this example. At 2 nodes (a master plus one slave), the master still does a small part of the calculation (84 seconds) on the two-electron hessian integrals. Addition of the third node effectively removes all of the two-electron hessian integral calculation from the master. The time saved by adding the third CPU probably does not warrant its use in this particular case. The ideal number of slave nodes is that which brings the master's two-electron hessian time near zero.

Several factors would make the analytic hessian calculation usable with more processors. First, when the molecule has low or no symmetry, there are relatively more two-electron hessian integrals to be computed in parallel. Second, if the slave nodes happen to be slower processors, relatively more of them can be brought to bear on the problem. Finally, the apparent parallel content of any program will be increased by decreasing the time spent in the

residual sequential-only sections. In the present case, this would mean speeding up the sequential integral transformation. Two ways of doing this, working from an unordered AO integral list and incorporating the use of point group symmetry, are currently being implemented.

4. CONCLUSIONS

A method of parallelizing the SCF analytic hessian calculation using only a few nodes has been presented. The master node must have enough memory and disk to perform the transformation sequentially. This algorithm is most useful to a "small" laboratory with access to several workstations (possibly from different vendors), only one of which needs to have large amounts of memory and disk to play the role of master.

The parallelization of the one- and two-electron hessian integrals has been presented. The four-index transformation (the bottleneck for this calculation) will be addressed in future work.

While the algorithm presented here does not scale to *massively* parallel machines, it represents a *simple* means to extract some parallel speedup from an existing analytic hessian code. Thus, this can serve as a bridge while the much more extensive changes needed for a large-scale parallel analytic hessian code are being implemented.

ACKNOWLEDGMENTS

This work was supported by a grant from the Air Force Office of Scientific Research (93-1-0105) and with the assistance of the Advanced Research Projects Agency. The IBM RS6000 workstations were generously provided by Iowa State University.

REFERENCES

[1.a.] M. Dupuis and J.D. Watts, Theor. Chim. Acta 71 (1987) 91.

[1.b.] M.F. Guest, R.J. Harrison, J.H. van Lenthe and L.C.H. van Corler,Theor. Chim. Acta 71 (1987) 117.

[1.c.] R. Ernenwein, M.M. Rohmer and M. Benard, Comput. Phys. Comm.58 (1990) 305.

[1.d.] M.M. Rohmer, J. Demuynck, M. Bénard, R. Wiest, C. Bachmann,C. Henriet and R. Ernenwein, Comput. Phys. Comm. 60 (1990) 127.

[1.e.] R.J. Harrison, R.A. Kendall, Theor. Chim. Acta 79 (1991) 337.

[1.f.] M.D. Cooper and I.H. Hillier, J. Computer-Aided Molecular Design 5 (1991) 171.

[1.g.] S. Kindermann, E. Michel and P. Otto, J. Comp.Chem. 13 (1992) 414.

[1.h.] H.P. Lüthi, J.E. Mertz, M.W. Feyereisen and J.E. Almlöf, J. Comput.Chem. 13 (1992) 160.

[1.i.] M. Feyereisen and R.A. Kendall, Theor. Chim. Acta.

[2.a.] J.D. Watts and M. Dupuis, J. Comput. Chem. 9 (1988) 158.

[2.b.] R.J. Harrison, J. Chem. Phys. 94 (1991) 5021.

[2.c.] R.J. Harrison and E. Stahlberg, CSCC Update 13 (1992) 5.

[2.d.] A. P. Rendell, T.J. Lee and R. Lindh, Chem. Phys. Letts. 194 (1992) 84.

[2.e.] M. Schüler, T. Kovar, Hans Lischka, R. Shepard and R.J. Harrison, Theor. Chim. Acta 84 (1993) 489.

[2.f.] See the entire issue of Theoret. Chim. Acta 84 (1993) 255ff.

[3] M.W. Schmidt, K.K. Baldridge, J.A. Boatz, S.T. Elbert, M.S. Gordon, J.H. Jensen, S. Koseki, N. Matsunaga, K.A. Ngyen, S. Su, T.L. Windus, M. Dupuis, and J.A. Montgomery, Jr., J. Comput. Chem. 14 (1993) 1347.

[4] R.J. Harrison, Argonne National Laboratory, version 4.0.2, available by anonymous ftp in directory /pub/tcgmsg from host ftp.tcg.anl.gov.

[5.a.] R.A. Whiteside, J.S. Binkley, M.E. Colvin and H.F. Schaefer III, J. Chem. Phys. 86 (1987) 2185.

[5.b.] L.A. Covick and K.M. Sando, J. Comput. Chem. 11 (1990) 1151.

[5.c.] R. Wiest, J. Demuynck, M. Bénard, M.M. Rohmer and R. Ernenwein, Comput. Phys. Comm. 62 (1991) 107.

[6.a.] M. Dupuis and H.F. King, in: Geometrical Derivatives of Energy Surfaces, NATO ASI Series C: Vol.166, eds, P. Jorgenson and J. Simon (D. Reidel,Dordrecht,1986) p. 167.

[6.b.] T. Takada, M. Dupuis, and H.F. King, J. Chem. Phys. 75 (1981) 332

[7.a.] H.F. King and A. Komornicki, in: Geometrical Derivatives of Energy Surfaces, NATO ASI Series C: Vol.166, eds, P. Jorgenson and J. Simon (D. Reidel,Dordrecht,1986) p. 207.

[7.b.] Y. Osamura, Y. Yamaguchi, P. Saxe, D.J. Fox, M.A. Vincent, and H.F. Schaefer III, J. Mol. Struct. 103 (1983) 183.

[7.c.] M.Duran, Y. Yamaguchi, and H.F. Schaefer III, J. Phys. Chem. 92 (1988) 3070.

[8.a.] A.J. Arduengo III, C.A. Stewart, F. Davidson, D.A. Dixon, J.Y. Becker, S.A. Culley, and M.B. Mizen, J. Am. Chem. Soc. 109 (1987) 627.

[8.b.] C.A. Stewart, R.L. Harlow, and A.J. Arduengo III, J. Am. Chem. Soc. 107 (1985) 5543.

[9.a.] J.S. Binkley, J.A. Pople, and W.J. Hehre, J. Am. Chem. Soc. 102 (1980) 939.

[9.b.] K.D. Dobbs and W.J. Hehre, J. Comput. Chem. 7 (1986) 359.

Table I: Timing (in seconds) for the C_S molecule AdSbO using 110 basis functions. NXTVAL balancing is used.

nodes	1	2	3	
setup	0.58	0.78	0.84	
one-electron int	1.12	0.86	0.84	
orbital guess	15.77	16.46	16.96	
two-electron int	133.90	62.14	39.48	
SCF	190.87	103.82	66.25	
properties	1.61	2.44	2.78	
one-electron hess	28.62	17.05	14.74	
two-electron int	206.23	211.29	213.38	(M)
ordering	147.75	154.67	155.52	(M)
transformation	1733.30	1747.48	1742.40	(M)
two-electron hess	3367.57	83.93	12.41	
CPHF	1653.75	1673.50	1664.48	(M)
finish	0.57	0.54	0.63	
total	7481.69	4075.05	3930.85	

(M) means master only

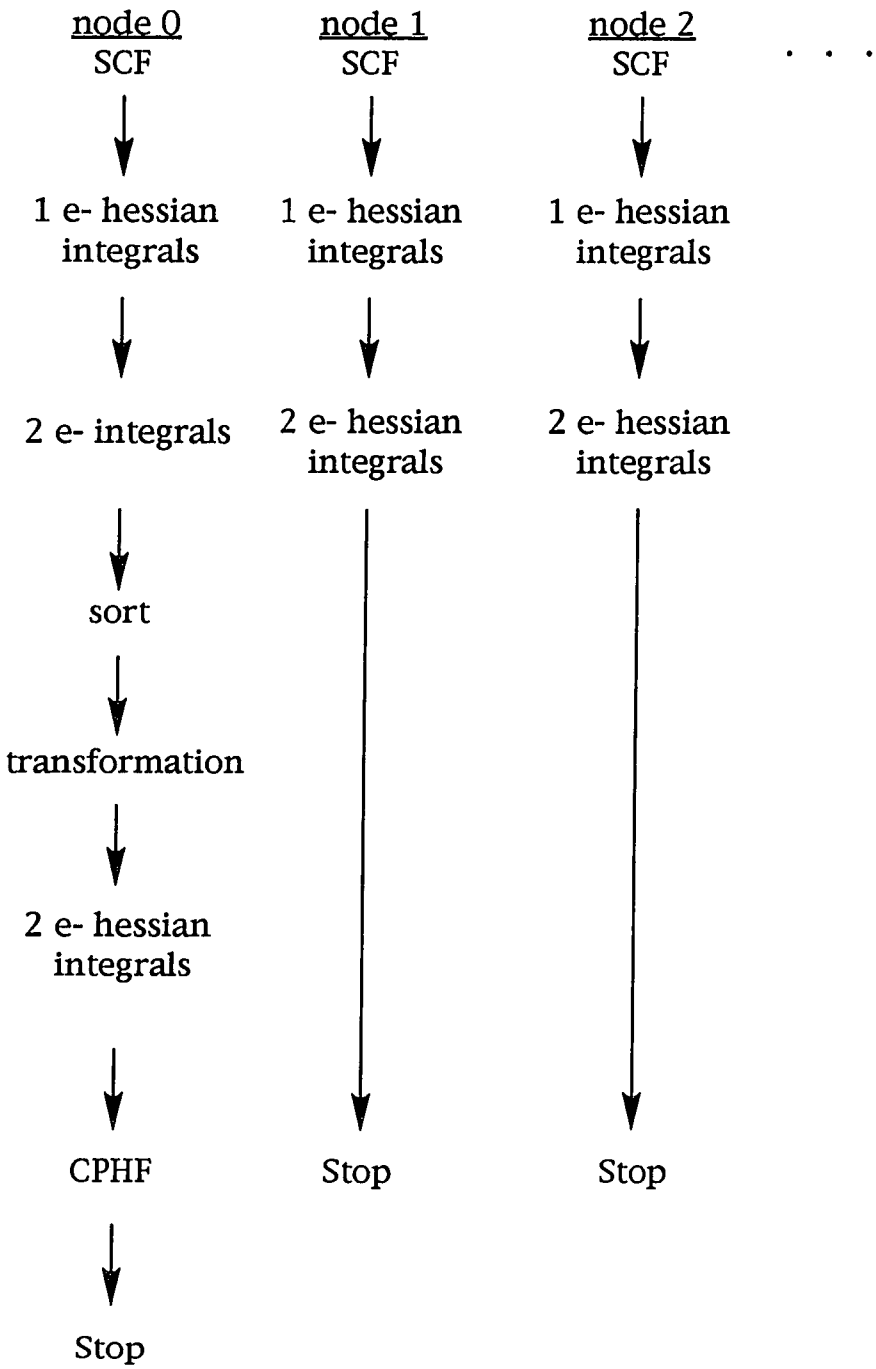

Figure 1: Flowchart of Analytic Hessian Calculation.

```
      SUBROUTINE DDONE
C
C     ME = this processor's ID number
C     NPROC = number of processors
C
C     initialize parallel work
C
      IPCOUNT = ME-1
      NEXT = -1
      MINE = -1
C     begin the loops over shell sets I and J
      DO 100 I =
         IF (NXTVAL balancing AND PARALLEL) THEN
          MINE = MINE + 1
          IF (MINE.GT.NEXT) NEXT=NXTVAL()
          IF (NEXT.NE.MINE) GO TO 100
         END IF
         .
         .
         DO 200 J =
            IF (LOOP balancing AND PARALLEL) THEN
              IPCOUNT = IPCOUNT + 1
              IF (MOD(IPCOUNT,NPROC).NE.0) GO TO 200
            END IF
            .
            .
C     Generate integrals <I|h|J>', <I|h|J>'', <I|J>', and
C        <I|J>''
C     Form contributions to g, H, F', and S'
            .
 200     CONTINUE
 100  CONTINUE
      .
C     Global sum g, H, F', and S'
      END
```

Figure 2: Pseudocode for One-Electron Hessian Integral Parallelization.

PAPER 8: PARALLEL ALGORITHM FOR INTEGRAL TRANSFORMATIONS AND GUGA MCSCF

Parallel Algorithm for Integral Transformations and GUGA MCSCF

Theresa L. Windus
Michael W. Schmidt
Mark S. Gordon

Department of Chemistry
Iowa State University
Ames, Iowa 50011

to be submitted

ABSTRACT

An algorithm for the parallelization of the atomic to molecular integral transformation and the subsequent steps in a GUGA based MCSCF calculation is presented. Timing data shows that the transformation and diagonalization steps are well parallelized and that several of the other portions of the MCSCF code are moderately parallel. Remaining sequential bottlenecks are identified.

INTRODUCTION

Over the last seven years, several papers have appeared that present algorithms for the parallelization of the self-consistent field (SCF) portions of ab initio electronic structure codes [1,2]. However, parallel implementation of correlated (post Hartree-Fock) methods have only recently been explored. Second-order Moller-Plesset perturbation theory (MP2) [3], coupled cluster [4], and multi-reference configuration interaction (MRCI) [5] methods have all been examined for parallel content.

A computational bottleneck common to all post Hartree-Fock methods is the transformation of the integrals in the atomic orbital (AO) basis into the molecular orbital (MO) basis. Several stand alone parallel transformation programs have been considered [6], but these were not incorporated into a practical application. Watts and Dupuis have presented a parallel transformation algorithm for shared memory machines which was used to parallelize MP2 calculations [3].

In this paper, we describe a parallel transformation algorithm that scales as the number of processors and the application of this algorithm to the parallelization of the graphical unitary group approach (GUGA) multi-configurational SCF (MCSCF) method [7]. This parallel algorithm has been

implemented into the General Atomic and Molecular Electronic Structure System (GAMESS) [2] quantum chemistry code.

PARALLEL ALGORITHM AND IMPLEMENTATION

In the full optimized reaction space (FORS) [8] and complete active space SCF (CASSCF) [9] approach to an MCSCF calculation, one partitions the molecular orbitals into several subspaces. These include the core orbitals (occupied with a fixed occupancy of two electrons), partially occupied orbitals, and empty virtual orbitals. The fractionally occupied valence orbitals are referred to as the "active space". Once these spaces have been chosen by the user, an MCSCF energy can be calculated.

The steps which must be performed by GAMESS in order to obtain an MCSCF energy are shown schematically in Figure 1. (For specific details regarding the GUGA method, the reader is referred to reference [7].) The basic steps are: 1) Obtain an initial guess for the molecular orbitals (MOs) (these are usually obtained from an SCF calculation, but do not have to be). 2) Calculate the integrals in the atomic orbital (AO) basis. 3) Generate the distinct row table which contains information describing the configuration state functions (CSFs) used in the MCSCF wavefunction. 4) Transform the AO integrals into the current MO basis. 5) Sort the transformed integrals (only those with all indices in the core and active spaces) into an order needed by step 6. 6) Calculate contributions (GUGA loops) to the CI Hamiltonian matrix, **H**. 7) Diagonalize **H** to obtain the CI

eigenvectors, **C**. 8) Calculate the 1 and 2 electron density matrices. 9) Form the orbital gradient (Lagrangian) and orbital hessian. 10) Form the augmented orbital hessian (the orbital hessian augmented by the orbital gradient). 11) Solve the Newton-Raphson equations to improve the orbitals. 12) Repeat steps 4 through 11 until the desired convergence is achieved.

In our algorithm, we try to parallelize as much of the steps in Figure 1 as possible without **major** revisions of the code.

The single-program multi-data (SPMD) model has been adopted for GAMESS [2]. In this model each node performs all of the tasks (the "peer" model), executes essentially the same code, and needs to have most (if not all) of the information (basis set, geometry, orbitals, etc.) necessary for the calculation. The major exception to the peer model is that only one node (the "master") reads the input and writes the output. The master broadcasts information from the input file to all of the nodes. The majority of this broadcasting is performed in the initial setup part of the calculation.

The SPMD model has been very useful in that it is relatively easy for a new section of code to be run in parallel. In fact, the current algorithm requires only about thirty lines of parallel code (not including code that was initially modified for the SCF).

To perform the parallel communication, we use the message passing library TCGMSG [10] developed by Robert Harrison. TCGMSG uses the best communication available for the particular architecture being used. It works on distributed memory machines (such as the Intel Delta), shared memory machines (such as an Alliant), and an Ethernetwork of UNIX workstations (possibly with different platforms). This portability is the main reason we chose TCGMSG to perform the communications.

We use two different methods to perform load balancing. One is a static model (loop) and the other is a dynamic model (nxtval). The loop model essentially assigns every nth loop in a DO loop to the nth processor. No communication is required in this type of load balancing and it generally works well when each loop has about the same amount of work and/or there are many loops. This method also works best on processors of equal speed and work load.

The nxtval method uses a shared counter to distribute the work. TCGMSG keeps track of the counter (generally on the master node) and increments it each time a processor calls for more work. This, of course, requires communication. Therefore, this model works best when the amount of work in each loop is fairly large (i.e. the communication is a small fraction of the compute time). This is the model that we use when the processors are not of the same speed and/or work load.

Before discussing the parallel steps needed for each iteration of the MCSCF energy, the first three steps of the energy calculation must be discussed. Step 1, the initial guess, is usually reading in orbitals from a previous calculation. Generally, the starting orbitals are obtained from an SCF calculation or a previous MCSCF calculation. If the orbitals are read from an input stream, the master reads and broadcasts them to the other nodes. This step is only performed once in the calculation and does not require much time (as will be shown in the timing examples).

Step 2, calculation of integrals in the AO basis, is also only performed once in the energy calculation. In the previous implementation of parallel SCF [2] this step was shown to be highly parallel. However, in this implementation, it is necessary for all of the nodes to have a complete list of atomic integrals available (the reason for this will be explained in the integral transformation discussion below) and therefore, the AO integrals are calculated sequentially on each node. Since this sequential step is performed only once and is approximately of order N^4 (where N is the number of basis functions), the overall cost is minimal compared to the repeated N^5 integral transformations. If there is not enough disk space available on each node to hold the atomic integrals, they are recalculated each time they are needed in the integral transformation step (in a direct method).

Generation of the distinct row table (DRT), step 3, is also performed just once in the energy calculation. Each node builds the table and stores all of the information into a local disk file. This information is needed throughout the rest of the calculation; therefore, it is necessary for each node to have the complete DRT. An alternative would be to let only the master node build the table and then broadcast the DRT data when it is needed. However, to avoid as much communication as possible during the iterative steps, we chose to allow each node to calculate and store the information needed.

The first three steps discussed above are sequential, but they can be considered to be setup for the MCSCF iterations, since they are only performed once. The next steps are executed during each MCSCF iteration and have been parallelized as much as possible.

A schematic of the parallel algorithm for the integral transformation (step 4) is given in Figure 2. We have currently incorporated a new transformation algorithm from Hondo 8.4 [11] into our code. This transformation can use an unsorted list of AO integrals and make use of the molecular symmetry (Abelian groups only). A key feature of this algorithm is that it calculates only those transformed integrals that are needed in the MCSCF. These are the <ij|kl>, <aj|kl>, <ab|kl>, <aj|lb> and <aj|bl> integrals,

where i, j, k, l are MOs in the core and active spaces and a, b are MOs in the virtual space.

One option for performing the transformation consists of passes over the complete list of atomic integrals, where each pass generates a subset of the required molecular integrals. A pass consists of generating all ij index pairs for a given subset of kl. Since each node has a complete list of integrals, this option is perfect for parallelization. The number of passes can be chosen to be evenly divisible by the number of processors, ensuring load balance. Each node then ends up with only a subset of the transformed integrals on its disk. The beautiful part of this algorithm is that there is no communication involved (unless nxtval balancing is used) and it is very easy to implement (as shown in Figure 2). Note that only the master node transforms the one-electron integrals.

The next task is to make each of the subsequent MCSCF steps work with the distributed molecular integrals and to parallelize where possible. Step 5 (sorting of the transformed integrals) is generally performed in memory since no integrals involving virtual MOs are needed and thus, memory for this step is usually available. First, the array that holds the sorted integrals is zeroed. (This ensures a correct global sum of the sort array.) Then, each node sorts its subset of the integrals into the appropriate position in the sort array. After all of the nodes have completed the

sort, a global sum is performed on the sorted array. Thus, all nodes end up with the identical complete list of occupied MO integrals which they store onto disk.

The global sum of the sorted integrals is essential for the next step (6). The sorted integrals are used to calculate contributions (GUGA loops) to the CI Hamiltonian matrix, **H**. Since several integrals can contribute to the same loop, it is convenient for all of the nodes to have all of the necessary integrals.

The GUGA loop generation part of the code is not easy to parallelize. This part of the code can use a large amount of CPU time (see examples below), but more importantly it can also require considerable disk space to store the generated loops. Ideally, we would like to make sure that 1) each node performs only the calculations needed to evaluate its assigned loops (i.e. distribute the CPU time evenly across the nodes) and 2) each node ends up with about the same number of loops stored on disk (i.e. distribute the loops evenly across the nodes). Unfortunately, many parts of the code have data dependencies that we have been unable to avoid. Parallelization at a higher level in the subroutine results in very poor load balance in both time and disk space. Therefore, we have opted to put the parallel calls around the subroutine that actually completes each loop's computation and writes it to disk. This means that the disk space needed to store loops is very evenly distributed, but

there is hardly any savings (or parallel content) in the CPU time needed to calculate the GUGA loops. The distribution of the disk space means that problems that would not fit on one node because of disk space limitations can be run on several nodes where the combined disk space is enough to hold all of the loops. Additional improvement in the parallel nature of this part of the code will probably require a total rewrite of the loop generation algorithm to evenly distribute the computational time.

The next step is to diagonalize **H** to obtain the CI eigenvectors. This step, 7, involves reading in the loops from disk to form **HC**, where **C** is the CI eigenvector. Formation of this matrix vector product is by far the most time consuming step in an iterative Davidson diagonalization [12] procedure. Each iteration requires an exact matrix diagonalization in an iterative subspace (of dimension less than 30, typically). This and other steps in the Davidson diagonalization are negligible compared to the formation of **HC**, and are therefore run sequentially.

Since the loops are distributed across the nodes, each node evaluates its partial contribution to **HC** and then a global sum is performed. Because the loops were evenly distributed across the nodes by the previous step, this step is essentially perfectly parallel.

During the CI diagonalization setup, loops contributing to the diagonal elements are processed to form the total

contribution to the diagonal of **H**. Unit vectors corresponding to the lowest diagonal element(s) is (are) generated as the initial approximation to **C**. Diagonal elements of **H** are then retained in memory to avoid the need to process the diagonal loops again. Their contribution to **HC** during the Davidson iterations is made correct by scaling each diagonal element by 1/p, p = number of processors. The final global sum of **HC** over p processors thus includes diagonal terms only once.

Step 7 actually shows very nice speed-ups as will be demonstrated below, even though the diagonalization step has not been parallelized.

Upon finishing the CI diagonalization step, each node has the CI vectors and eigenvalues. The CI vectors are then used to generate the 1 and 2 electron density matrices (step 8). This step works in a manner similar to that of step 6. The CI vectors are used to generate loops which in turn contribute to the density matrices. The loops are actually generated by the same subroutine that generates the loops in step 6 and the comments on load balance from that discussion also apply here. The main parallelization of the loops is to distribute the disk space needed for the loops over all of the nodes. The largest difference between this step and step 6 is that the number of loops needed to generate the density is generally less than the number of loops needed to generate **H**. After the loops are generated, they are read in, labeled,

and sorted into a form needed by step 9. Since each node has only a subset of the loops, a global sum of the density is performed after the sorting step. This results in each node having the complete density. This sort and global summation is similar to that in step 5 (sorting of the transformed integrals into an order the CI needs).

The next step (9) is the formation of the orbital gradient (Lagrangian) and orbital hessian (hessian). The Lagrangian and hessian are formed by combining the transformed integrals with elements of the density matrix. This is generally the part of the MCSCF calculation that requires the greatest amount of memory (to simultaneously hold the hessian and two-electron density in memory). In our current implementation, each node needs as much memory as it would to run sequentially. Each node reads the complete density matrix into memory from disk. Then, each node reads buffer loads of its partial list of transformed integrals and computes its partial contribution to the Lagrangian and hessian.

As mentioned earlier, only the master node has the one-electron transformed integrals, so that node evaluates the one-electron contributions to the Lagrangian and hessian. After all nodes have completed their contributions, global sums are performed on the Lagrangian and hessian, resulting in each node having the complete Lagrangian and hessian.

The next two steps, formation of the augmented orbital hessian [13] and solution of the Newton-Raphson (NR) equations for improving the orbitals, are sequential steps. Solution of the NR equations amounts to finding the lowest eigenvector of the augmented hessian, and is curently performed sequentially by each node. Timing results presented in the next section reveal that this is an obvious place for future improvements in the parallel algorithm.

Once the orbital improvements are made, convergence is checked. If the wavefunction (and energy) is not converged, steps 4 through 11 are then repeated.

TIMING EXAMPLES

One of the interesting aspects of MCSCF is that different types of calculations cause different parts of the code to be the primary bottleneck. For example, a calculation with many core orbitals and a relatively small active space will have the integral transformation and NR orbital improvement as its bottleneck. On the other hand, a calculation with only a few occupied orbitals but a relatively large active space will have its bottleneck at the CI diagonalization step. To illustrate this large variation in the computational bottleneck, three different types of examples are used for the timing tests. These examples are indicative of the range of MCSCF calculations performed with GAMESS.

All of the tests were performed on RS/6000 model 350s connected by an Ethernet. The machines were dedicated for these tests, but the network was not isolated. Therefore, other packets on the network could interfere with the TCGMSG communications. Since all of the nodes are of the same speed and load, only the loop (static) balancing was used in these examples. Also, all of the examples use C_1 symmetry. Even though we are able to use symmetry in each step of the MCSCF energy calculation, C_1 symmetry is used to provide a fair comparison between the different types of test examples and

to make one iteration long enough for timing information to be meaningful.

The first example is Ge_2F_4 using a 3-21G [14] basis set totaling 82 basis functions. The active space consists of four electrons in four orbitals which generates only 20 configuration state functions (CSFs). There are 48 core orbitals; therefore, the integral transformation and NR steps are the bottlenecks for the calculation. This example requires 3.8 MW of memory and approximately 63 MB of disk on one node. The disk usage is 7 MB for the two electron atomic integrals, 33 MB for the transformed integrals, and 0.065 MB for the loops. The remainder of the disk usage is for holding temporary information and the CI vectors. The memory requirement does not decrease when more processors are used, but the amount of disk used does (e.g., for five nodes, (5*7) + (33/5) + (0.065/5) MB for disk).

Table I shows the timing results for one iteration of the MCSCF energy on one to five nodes. The times reported are from the master node. Sequential steps are marked as such in the table. The one node timing shows that indeed the transformation and NR solution are the bottlenecks for this example. The transformation step (4) has speedups (time on one processor/time on n processors) of 2.3, 3.7, 6.2, and 7.6 for 2, 3, 4, and 5 nodes, respectively. While this seems strange (the speedups are actually larger than the number of nodes), the timing results given in the table are for the

master only. The slave nodes are taking more work than the master; this imbalance results in speedups that appear to be greater than the theoretical 100% efficiency. One way to try to rectify this imbalance is to make the number of passes larger, but this would also require the atomic integrals to be read in or calculated (if using the direct option) more times than necessary. Thus, this is not a very attractive option. Since the load imbalance is not large, we have decided to implement the algorithm as described above.

It is interesting that several steps (the sorting, density generation, and the transformed one-electron integrals - steps 5, 8, and 9) actually increase in time from 1 to 3 nodes, instead of decreasing as would be expected. Since the time for these steps is small sequentially, the time required to perform the large global sums is actually a significant percentage of each step. The large number of core orbitals gives relatively many occupied MO integrals needed in the sort (step 5) and many density elements in the density matrix generation (step 8) and increases the size of the orbital hessian (step 9). For example, the global sum operates on 614,916 double precision elements in step 5. To send such a long data set across the network and sum uses a non-trivial amount of CPU time. Of course, the more nodes involved, the larger the number of additions. Fortunately, the global summation time seems to level off after about 3 nodes. TCGMSG employs a clever algorithm to diminish the

number of operations and communication required for a global sum. For details, the reader is referred to reference [10]. As will be seen in the next two examples, the global summation of the orbital hessian (step 9) is always large, but the other two steps (5,8) are smaller when small numbers of core orbitals are used.

The transformed two-electron integral contributions to the Lagrangian and orbital hessian show only small time decreases when more nodes are applied. Since each node must read in the density from disk and put it into memory, this is a sequential part of the calculation that cannot be avoided. However, there may be other contributions to the poor scalability of this step.

A large bottleneck in this example is the formation of the augmented orbital hessian and the solution of the NR equations. When more than two nodes are used in this particular example, the NR step is the most time consuming portion of the calculation. This is obviously a part of the code that will need to be improved in the future.

The overall efficiencies for the iteration (steps 4 through 11) are reasonable only up to about 3 nodes. The time consuming, sequential NR step is the reason for the poor scalability beyond this point.

The second example is $Si_2H_4Ti^+$ in the quartet state [15]. Using a double-zeta basis set for Si and H [16] and effective core potentials (ECPs) with double-zeta valence for

Ti [17] produces 62 basis functions. The number of core orbitals is fourteen and the active space is seven electrons in ten orbitals (the reference consists of two doubly occupied, three singly occupied with alpha spin, and five unoccupied orbitals for the active space). There are 9,240 CSFs for this example. 1.1 MW of memory and approximately 120 MB of disk are needed. The main disk usage is 11 MB for atomic integrals, 6 MB for transformed integrals and 73 MB for loops (5 MB for diagonal loops and 68 for off-diagonal loops). Again, the memory requirement will be the same for each node, the AO integral list is duplicated on each node, but the transformed integral and loop disk space is evenly distributed across all of the nodes.

Timing information is given in Table II. The ECP integrals are calculated in parallel [2]. This example has several bottlenecks: formation of the GUGA loops, diagonalization of **H**, and formation of the density matrices (steps 6, 7, and 8, respectively). Steps 6 and 8 involve formation of loops which have only a small amount of parallel content. This is seen in the modest decrease in time when more nodes are applied to the problem. Certainly, the formation of loops will require attention in the future. Notice that since the number of elements involved in these steps is smaller than those of the first example (23,911 sorted integrals in the current example as compared to

614,916 in the previous example) and since the total time is larger in this example, the global summations do not dominate the timing results.

Step 7, on the other hand has very good speedups of 1.9, 2.8, 4.0, and 4.7 for 2, 3, 4, and 5 nodes, respectively. As noted in the algorithm section, these speedups are from the parallel formation of the matrix product **HC** and NOT from the small diagonalization during each iteration. The latter requires 24 iterations to converge.

The transformation step (4), although far from being a bottleneck in the calculation, still shows essentially perfect speedups. The transformed two-electron contributions to the Lagrangian and orbital hessian (step 9) still show poor speedup and the one-electron contributions still increase with the number of nodes. The orbital hessian is still very large for this example, and the global sum is certainly the cause for the increase in time.

Again, this example only scales to about 3 nodes. However, this time it is the generation of loops which constitutes the sequential bottleneck.

The third and final example is bicyclobutane, C_4H_6, using the 6-31G(d) basis set [18] giving 72 basis functions. There are 10 core orbitals and the active space is 10 electrons in 10 orbitals which generates 19,404 CSFs. 1.3 MW of memory and approximately 380 MB of disk are required. The major disk usage is 39 MB for atomic integrals, 13 MB for

transformed integrals and 294 MB for the loops (10 MB for diagonal loops and 284 for off-diagonal loops).

Timing information for this example is given in Table III. In this example, the bottleneck is clearly the CI diagonalization step and it remains the bottleneck even up to five nodes. The speedups for this step are 1.9, 2.7, 3.4 and 4.2 for 2, 3, 4, and 5 nodes, respectively giving an 84% efficiency (100*speedup/number of nodes) at 5 nodes.

Steps 6 and 8 (involving loop generation) again suffer from the problem of having only minimal parallelization in the CPU time. The advantage, of course, is that the GUGA loop disk files are evenly distributed across all of the nodes.

The transformation step shows very good efficiencies in this example as it has in the other two examples. Even though it does not represent a large part of the calculation, parallelization of each step is important to achieve good overall speedups. In the same vein, since steps 10 and 11 are sequential they decrease the overall speedups even though they are not a large portion of the calculation.

The overall efficiencies for this example are quite good even up to 5 nodes. Obviously, to get better speedups larger test cases can be used. However, the real key to future improvement is to make the portions that are only minimally parallel (steps 6, 8, 10, and 11) more efficient.

CONCLUSIONS

Techniques for the parallelization of the integral transformation and the subsequent steps of the GUGA MCSCF calculation are presented. The transformation and diagonalization steps show very good speedups. Other parts of the calculation (sorting of the transformed integrals, calculating the second order density, and forming the Lagrangian and orbital hessian) show only minimal speedups. Solution of the Newton-Raphson equation for the orbital improvement step has been identified as a sequential bottleneck.

Future improvements will involve obtaining more parallel content from the loop generation steps and to parallelize the Newton-Raphson step. Each of these will improve the overall scalability of the MCSCF iterations.

ACKNOWLEDGMENTS

This work was supported by a grant from the Air Force Office of Scientific Research (93-1-0105), a Department of Education GAANN fellowship to TLW and through the assistance of the Advanced Research Projects Agency. The IBM RS6000 workstations were purchased by Iowa State University.

REFERENCES

1. Dupuis M, Watts JD (1987) Theor.Chim.Acta 71:91
Guest MF, Harrison RJ, van Lenthe JH, van Corler LCH (1987) Theor.Chim.Acta 71:117
Ernenwein R, Rohmer MM, Benard M (1990) Comput.Phys.Comm.58:305
Rohmer MM, Demuynck J, Bénard M, Wiest R, Bachmann C, Henriet C, Ernenwein R (1990) Comput.Phys.Comm. 60:127
Harrison RJ, Kendall RA (1991) Theor.Chim.Acta 79:337.
Cooper MD, Hillier IH (1991) J.Computer-Aided Molecular Design 5:171
Kindermann S, Michel E, Otto P (1992) J.Comp.Chem. 13:414.
Lüthi HP, Mertz JE, Feyereisen MW, Almlöf JE (1992) J.Comput.Chem. 13:160.
Brode S, Horn H, Ehrig M, Moldrup D, Rice JE, Ahlrichs R (1993) J.Comput.Chem. 14:1142.
Also see (1993) Theor.Chim.Acta 255ff (No. 4-5)

2. Schmidt MW, Baldridge KK, Boatz JA, Elbert ST, Gordon MS, Jensen JH, Koseki S, Matsunaga N, Ngyen KA, Su S, Windus TL, Dupuis M, Montgomery JA, Jr., (1993) J. Comput. Chem. 14:1347.

3. Watts JD, Dupuis M (1988) J.Comput.Chem. 9:158.

4. Rendell AP, Lee TJ, Lindh R (1992) Chem.Phys.Lett. 194:84.

5. Harrison RJ (1991) J.Chem.Phys. 94:5021.
Harrison RJ, Stahlberg E (1992) CSCC Update 13:5.
Schuller M, Kovar T, Lischka H, Shepard R, Harrison RJ (1993) Theoret.Chim.Acta 84:489.

6. Whiteside RA, Binkley JS, Colvin ME, Schaefer III HF. (1987) J.Chem.Phys. 86:2185.
Covick LA, Sando KM (1990) J.Comput.Chem. 11:1151.
Wiest R, Demuynck J, Bénard M, Rohmer MM, Ernenwein R. (1991) Comput.Phys.Commun. 62:107.

7. Brooks B, Schaefer HF (1979) J.Chem.Phys. 70:5092.
Brooks B, Laidig W, Saxe P, Handy N, Schaefer HF (1980) Physica Scripta 21:312.

8. Ruedenberg K, Schmidt MW, Gilbert MM, Elbert ST (1982) Chem.Phys. 71:41.
Ruedenberg K, Schmidt MW, Gilbert MM, (1982) Chem.Phys. 71:51.
Ruedenberg K, Schmidt MW, Gilbert MM, Elbert ST

(1982) Chem.Phys. 71:65.

9. Lengsfield III BH (1980) J.Chem.Phys. 73:382 and references therein.

10. Harrison RJ, Argonne National Laboratory, version 4.0.2, available by anonymous ftp in directory /pub/tcgmsg from host ftp.tcg.anl.gov.

11. Dupuis M, Chin S, Marquez A "CHEM-Station and HONDO", in "Relativistic and Electron Correlation Effects in Molecules and Clusters", GL Malli Editor, NATO ASI Series, Plenum Press, New Yord (1992).

12. Davidson ER (1975) J.Comp.Phys. 17:87.

13. Yarkony DR (1981) Chem.Phys.Lett. 77:634.

14. Binkeley JS, Pople JA, Hehre WJ (1980) J.Am.Chem.Soc. 102-939.
Dobbs KD, Hehre WJ (1986) J.Comput.Chem. 7:359.

15. Moc J, Gordon MS unpublished results.

16. Dunning Jr. TH, Hay PJ Chapter 1 in "Methods of Electronic Structure Theory", HF Schaefer III, Ed, Plenum Press, NY (1977).
Binning Jr. RC, Curtiss LA (1990) J.Comput.Chem. 11:1206.

17. Stevens WJ, Basch H, Krauss M (1984) J.Chem.Phys. 81:6026.
Stevens WJ, Basch H, Krauss M, Jasien P (1992) Can.J.Chem. 70:612.

18. Ditchfield R, Hehre WJ, Pople JA (1971) J.Chem.Phys. 54:724.
Hehre WJ, Ditchfield R, Pople JA (1972) J.Chem.Phys. 56:2257.

Table I: Timing information from the master node in seconds for Ge_2F_4 for 1 to 5 nodes.

step[a]	1	2	3	4	5
1.guess[b]	6.4	6.7	7.1	7.2	7.1
2.AO int[b]	21.7	21.7	21.9	21.8	21.8
3.DRT[b]	1.4	1.4	1.5	1.5	1.5
4.trans	237.9	104.4	63.6	38.4	31.4
5.sort	9.3	14.9	22.6	23.0	21.1
6.GUGA loops	1.0	0.7	0.8	0.7	0.8
7.diag	0.1	0.1	0.1	0.1	0.1
8.DM2	30.1	39.3	48.1	48.1	48.2
9.Lag+hess					
2 e^- [c]	51.4	37.0	30.2	26.9	23.9
1 e^- [d]	10.4	24.7	27.4	27.7	27.6
10+11.NR[b]	100.0	100.4	100.2	100.1	100.3
iter.[e]	441.2	321.3	292.8	264.0	253.4
eff.[f]		67%	50%	42%	35%

a. The steps correspond to: 1) obtaining the initial guess, 2) calculating the atomic integrals, 3) generating the distinct row table, 4) transforming into the MO basis, 5) sorting the transformed integrals, 6) calculating GUGA loops 7) diagonalizing **H**, 8) calculating the electron density matrices, 9) forming the Lagrangian and the orbital hessian, and 10) forming the augmented orbital hessian and solving the NR equations.
b. This is a sequential step.
c. Transformed two-electron integral contribution.
d. Transformed one-electron integral contribution plus global sum of Lagrangian and the orbital hessian.
e. One iteration time - the sum of steps 4 through 11.
f. The efficiency (speedup/number of processors) based on steps 4 through 11.

Table II: Timing information from the master node in seconds for $Si_2H_4Ti^+$ for 1 to 5 nodes.

step[a]	1	2	3	4	5
1.guess[b]	2.8	3.1	3.0	3.3	3.3
ECP	18.9	9.1	5.7	5.7	3.1
2.AO int[b]	46.0	45.9	45.8	45.9	45.8
3.DRT[b]	1.0	1.0	1.0	1.0	1.0
4.trans	42.8	21.8	12.5	10.0	8.4
5.sort	1.2	1.0	1.3	1.2	1.1
6.GUGA loops	179.1	159.3	152.2	149.1	146.3
7.diag	330.0	175.2	118.8	82.6	70.0
8.DM2	148.5	136.1	131.7	128.9	127.6
9.Lag+hess					
2 e^- [c]	33.6	28.0	25.8	25.2	24.8
1 e^- [d]	4.5	9.9	15.5	16.0	15.5
10+11.NR[b]	22.8	22.9	22.8	22.8	22.8
iter.[e]	762.5	554.2	480.6	435.8	416.5
eff.[f]		69%	53%	44%	37%

a-f. See Table I for notes.

Table III: Timing information from the master node in seconds for bicyclobutane for 1 to 5 nodes.

step[a]	1	2	3	4	5
1.guess[b]	0.8	1.0	1.3	1.3	1.3
2.AO int[b]	69.4	69.7	70.1	69.0	69.0
3.DRT[b]	1.0	0.9	1.0	1.0	1.1
4.trans	118.0	57.9	48.8	27.6	22.8
5.sort	2.0	1.2	1.2	1.1	0.9
6.GUGA loops	336.3	300.9	276.2	264.7	256.6
7.diag	1904.0	1003.9	705.4	558.1	455.8
8.DM2	303.5	270.1	256.5	249.7	241.7
9.Lag+hess					
2 e^- [c]	74.3	59.0	57.44	50.0	49.3
1 e^- [d]	4.1	10.1	16.4	16.5	16.5
10+11.NR[b]	83.1	83.2	83.2	83.1	83.1
iter.[e]	2825.3	1786.3	1445.1	1250.8	1126.7
eff.[f]		79%	65%	56%	50%

a-f. See Table I for notes.

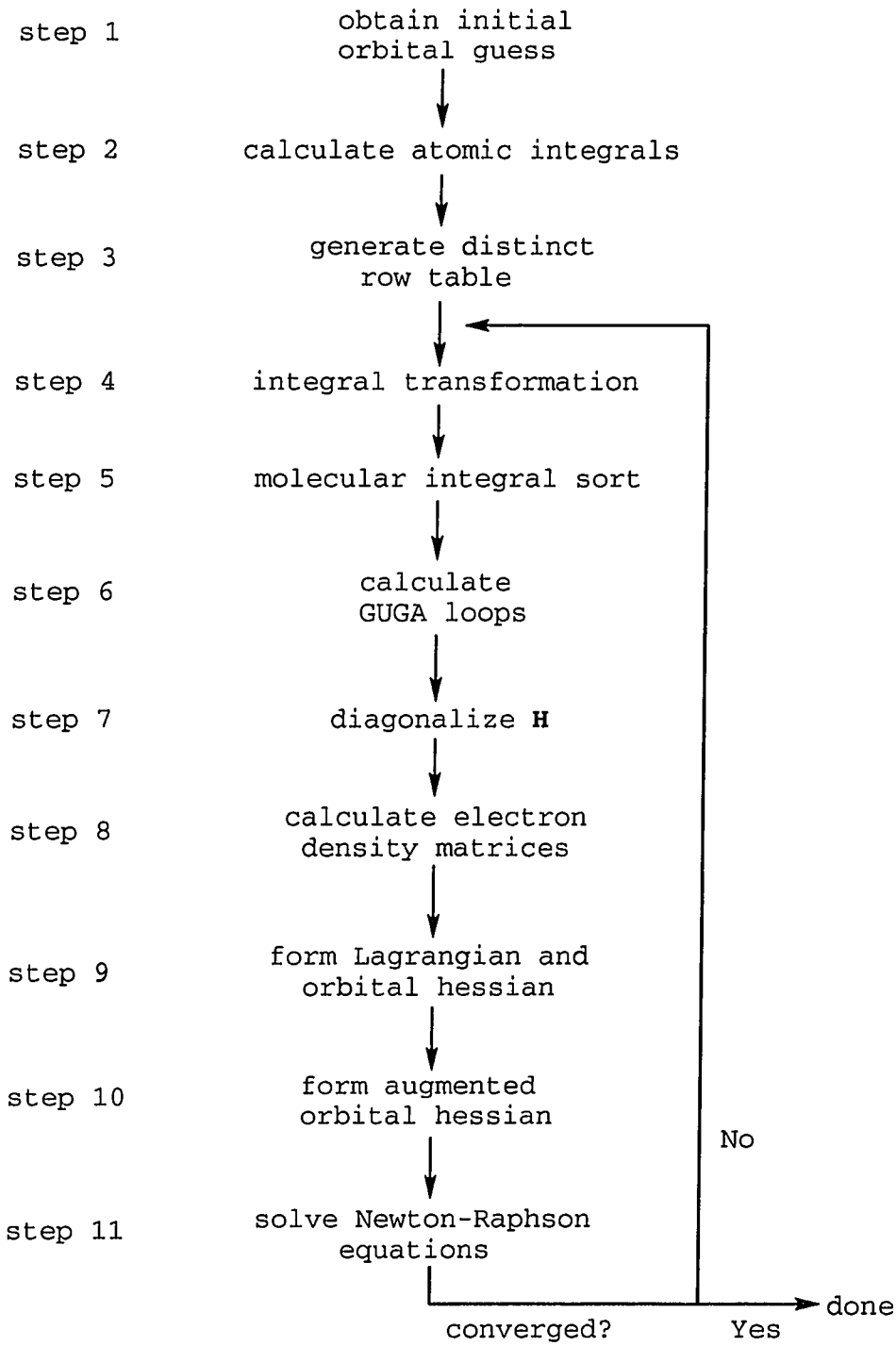

Figure 1: Schematic of the GUGA MCSCF steps.

```
      SUBROUTINE TRANSFORM
C
C     ME = the processor's ID number
C     NPROC = number of processors
C
C     initialize parallel
C
      IPCOUNT = ME -1
      NEXT = -1
      MINE = -1
C
C     Code here to determine number of passes.
C
      .
C
C     Begin passes over the atomic integrals to form subsets
C     of the transformed integrals (IJ/KL).
C
      MINKL = 1
   10 MAXKL = MINKL + SIZE_OF_PASS
         IF (PARALLEL) THEN
            IF (NXTVAL) THEN
               MINE = MINE + 1
               IF (MINE.GT.NEXT) NEXT = NXTVAL()
               IF (NEXT.NE.MINE) GO TO 20
            ELSE
C
C     If loop balancing ...
C
               IPCOUNT = IPCOUNT + 1
               IF (MOD(IPCOUNT,NPROC).NE.0) GO TO 20
            END IF
         END IF
         CALL SUBTRANS()
   20    CONTINUE
         IF (MAXKL.EQ.NUMKL) THEN GO TO 30
C
C     NUMKL = maximum number of KL indices
C
         MINKL = MAXKL + 1
         GO TO 10
   30 CONTINUE
      END
```

Figure 2: Schematic of parallel integral transformation.

CONCLUSIONS

Since each paper has a conclusion of its own, only a global summary of the results will be presented here.

While there is still a lot to be learned about the addition mechanisms involving silicon and phosphorus, this thesis sheds some light on the part of the potential energy surface involving the pentacoordinated silicon and phosphorus intermediates. Many of the systems investigated undergo Berry pseudorotation (or a variant thereof), but several of the systems with only a few heavy element ligands behave very differently. Specifically, part of the SiH_4F^- and PH_4F potential energy surfaces exhibit behavior where a minimum is connected to a transition state through a minimum energy path which in turn is connected to another transition state through a second minimum energy path.

The investigation of π-bonding used two different methods to determine π-bond strengths. The results of the two different methods were very similar and compared well with known experimental values. Also, contrary to previous work, $SnCH_4$ was shown to be a planar molecule.

This thesis has also shown that parallel processing is a very valuable tool for theoreticians to interact with experimentalists in a timely manner. The proton affinities, geometries and solvent effects for the azaphosphatrane series have been determined. Two of the substituted bases were

predicted to be stronger bases than the parent base. The ylide type structure (predicted to be the strongest base in the series) is currently being investigated experimentally.

The parallelization of analytic hessians and MCSCF energies has been presented. The parallel analytic hessian is scalable only to a few nodes using the idea of sending separate tasks to different sets of processors. The parallelization of the hessian integrals was also presented in this work.

Parallelization of the integral transformation and subsequent GUGA MCSCF steps was presented. The integral transformation which involves no communication scales well as the number of processors is increased. Parallelization of the MCSCF steps show minimal parallelization except for the diagonalization step which scales to at least 5 nodes for a "medium" sized problem. Future work will involve parallelization of the loop generation and the Newton-Raphson codes.

REFERENCES

1. M.W. Schmidt, K.K. Baldridge, J.A. Boatz, S.T. Elbert, M.S. Gordon, J.H. Jensen, S. Koseki, N. Matsunaga, K.A. Ngyen, S. Su, T.L. Windus, M. Dupuis, and J.A. Montgomery, Jr., J. Comput. Chem. accepted.

2. E. Schroedinger, Ann. Physik 81 (1926) 109.

3.a. E. Schroedinger, Ann. Physik 79 (1926) 361,489.
3.b. E. Schroedinger, Ann. Physik 80 (1926) 437.

4. For a detailed discussion of this problem the reader is referred to I.N. Levine, Quantum Chemistry, Allyn and Bacon, Inc., Newton (1983) Chapter 3 or almost any other graduate text on quantum chemistry.

5.a. B.T. Sutcliff, Fundamentals of computational quantum chemistry, in Computational Techniques in Quantum Chemistry, G.H.F. Diercksen, B.T. Sutcliff, and A. Veillard (Eds.), Reidel, Boston (1975) 1.

6. A. Szabo, N.S. Ostlund Modern Quantum Chemistry, Introduction to Advenced Electronic Structure Theory, McGraw-Hill (1982).

7. Many examples of basis sets are given in the chapters of the dissertation.

8. C.C.J. Roothaan, Rev. Mod. Phys. 23 (1951) 69.

9. J.A. Pople, R.K. Nesbet, J. Chem. Phys. 22 (1954) 571.

10.a. R.McWeeny, G. Diercksen, J. Chem. Phys. 49 (1968) 4852.
10.b. M.F. Guest, V.R. Saunders, Mol. Phys. 28 (1974) 819.
10.c. J.S. Binkley, J.A. Pople, P.A. Dobosh, Mol. Phys. 38 (1974) 1423.
10.d. E.R. Davidson, Chem. Phys. Lett. 21 (1973) 565.
10.e. K. Faegri, R. Manne, Mol. Phys. 31 (1976) 1037.
10.f. H. Hsu, E.R. Davidson, R.M. Pitzer, J. Chem. Phys. 65 (1976) 609.

11.a. J.A. Pople, J.S. Binkley, R. Seeger, Int. J. Quantum Chem. S10 (1976) 1
11.b. P. Carsky, B.A. Hess, L.J. Schaad, J. Comp. Chem. 5 (1984) 280.

12. R. Krishnan, M.J. Frisch, J.A. Pople, J.Chem.Phys. 72 (1980) 4244.

13. For FORS MCSCF see the following and references therein:
13.a. K. Ruedenberg, M.W. Schmidt, M.M. Gilbert, S.T. Elbert, Chem.Phys. 71 (1982) 41.
13.b. K. Ruedenberg, M.W.Schmidt, M.M. Gilbert, Chem.Phys. 71 (1982) 51.
13.c. K. Ruedenberg, M.W. Schmidt, M.M. Gilbert, S.T. Elbert, Chem.Phys. 71 (1982) 65.

14.a. J. Cizek, J. Chem. Phys. 45 (1966) 4256.
14.b. J. Cizek, Adv. Chem. Phys. 14 (1969) 35.

15.a. L.H. Thomas, Proc. Camb. Phil. Soc. 23 (1927) 542.
15.b. E. Fermi, Z. Phys. 48 (1928) 73.
15.c. P. Hohenberg, W. Kohn, Phys. Rev. 136 (1964) B864.